NOVA SCHOOL OF SCIENCE & TECHNOLOGY

DEPARTAMENT OF CHEMISTRY

BENZOPYRYLIUM (FLAVYLIUM) BASED DYES FOR REVERSIBLE THERMOCHROMIC SMART LABELS

MARIA ANGELA SPIRACHE

MSc in Environmental Engineering

DOCTORATE IN CHEMISTRY

NOVA University Lisbon

September, 2024

DEPARTAMENT OF CHEMISTRY

BENZOPYRYLIUM (FLAVYLIUM) BASED DYES FOR REVERSIBLE THERMOCHROMIC SMART LABELS

MARIA ANGELA SPIRACHE

MSc in Environmental Engineering

Adviser: António Jorge Dias Parola
Full Professor, Faculdade de Ciências e Tecnologia da Universidade NOVA de Lisboa

Co-advisers: César António Tonicha Laia
Associate Professor, Faculdade de Ciências e Tecnologia da Universidade NOVA de Lisboa

Philippe Marrec
PhD, LCR/TMC Hallcrest UK

Examination Committee:

Chair: João Carlos dos Santos Silva e Pereira de Lima,
Full Professor, Faculdade de Ciências e Tecnologia da Universidade NOVA de Lisboa

Rapporteurs: Raquel Gavara Castell,
Assistant Professor, Facultad de Ciencias, Universidad Autónoma de Madrid

Paulo Jorge dos Santos Coelho,
Associate Professor with Habilitation, Universidade de Trás-os-Montes e Alto Douro

Adviser: César António Tonicha Laia,
Associate Professor, Faculdade de Ciências e Tecnologia da Universidade NOVA de Lisboa

Members: João Carlos dos Santos Silva e Pereira de Lima,
Full Professor, Faculdade de Ciências e Tecnologia da Universidade NOVA de Lisboa

Maria Madalena Alves Campos de Sousa Dionísio Andrade,
Associate Professor with Habilitation, Faculdade de Ciências e Tecnologia da Universidade NOVA de Lisboa

Sandra Maria Nunes Gago,
Researcher, Faculdade de Ciências e Tecnologia da Universidade NOVA de Lisboa

DOCTORATE IN CHEMISTRY

NOVA University Lisbon
September, 2024

Benzopyrylium (Flavylium) Based Dyes for Reversible Thermochromic Smart Labels

This document was created with Microsoft Word text processor and the NOVA thesis Word template [1].

To my father.

ACKNOWLEDGMENTS

I would like to express my gratitude to several people. First and foremost, I want to thank my supervisor, Professor Jorge Parola, for giving me the chance to work on such an intriguing research project. His unwavering guidance and support have been invaluable to me. I also want to extend my thanks to my co-supervisor, Professor César Laia. His constructive criticism, input, and encouragement have been instrumental in helping me complete this thesis.

I also want to thank Dr. Philippe Marrec for always being available when I needed assistance. His prompt availability made our collaboration very effective. I am also grateful to him for providing me with the opportunity to meet all the wonderful people from LCR Hallcrest. In this regard, I want to extend special thanks to Simon and Kevin. Simon, thank you for all your help while I have been in the UK and back in Portugal, and I apologize if I sometimes bother you too much with my work.

Additionally, I want to express my gratitude to all the members of the CHARISMA team. It has been a blessing to work with each and every one of you. In this regard, I would like to extend special thanks to my colleagues Alberto and Sunil. Alberto, thank you for all the reports and emails we wrote together and for all the time we spent outside of the lab working. Sunil, I appreciate all the insightful talks and enjoyable lunches we had together.

I would also like to extend a special thanks to Dr. María Teresa Viciosa, who is currently a researcher at the Technical University of Lisbon, Portugal. Our collaboration was very fruitful to me and was of great help in shaping Chapter 4 of this thesis.

I would also like to express my gratitude to the entire Photochemistry group, and in particular to Dr. Nuno Basílio, Dr. Artur Moro, Dr. Claudia Pereira, Dr. Ambrósio Camuenho, and Dr. Mani Outis. I would also like to extend my thanks to the numerous PhD students, including Hanieh, Liliana Gomes, Joana Martins, Miriam Colaço, Ana Pinheiro, André Seco, Daniele, Kevin, Pingin, and Adi. Special thanks to Rita Anastacio - it has been a pleasure to meet and work with you in the lab for a while and thank you for being such a great trip adviser.

Last but not least, I would like to express my heartfelt gratitude to my family, especially to my husband, Marcel, and my sister, Oana. I truly appreciate your endless support and encouragement, which have meant so much to me over these years.

ABSTRACT

Given the global need to monitor temperatures during storage and distribution of many products, including food, medicines, blood and other temperature-sensitive products, access to cheap and disposable smart labels would be a breakthrough technology to minimise waste and as well health hazards. CHARISMA, an innovative training network funded by the European Union's Horizon 2020 program, aims to develop applied reversible/irreversible chromogenic systems that display a coloured message when encountering a specific thermal, chemical or redox stimulus. The CHARISMA smart labels were thought to be thin and flexible taking virtually no space, and thus printable on any surface by means of the ongoing printed electronics revolution.

In this research project, we aim to contribute to the development of these smart labels by two different approaches: (a) benzopyrylium-based spirolactone dyes with suitable developers and solvents to be exploited as reversible or irreversible thermochromic systems, and (b) benzopyrylium dyes for use with thermoresponsive polymers as reversible thermochromic systems.

The thermochromism of spirolactone dyes was evaluated in ternary systems composed of dye-developer-solvent. On the other hand, the thermochromism of benzopyrylium dyes with a CH-acidic aryl group at the α-methylene position was investigated in Pluronic® F127 three-block thermoresponsive copolymers. Both types of systems exhibited reversible thermochromism when appropriate conditions were met.

Finally, the ternary systems based on spirolactone flavylium dyes were microencapsulated by an *in-situ* polymerisation method, and the resulting microcapsule dispersion was converted into water-based inks and screen printed on a self-adhesive matt inkjet paper to evaluate the colour change properties.

The best performing indicator clears at +10°C on the heating cycle and fully recolours at +4°C on the cooling cycle, showing thermal and colour change stability. The colour change can be read with the naked eye without the need of an external reader. The engineered thermochromic smart label is a tiny (Ø×L×W=0.8×2.1×2 cm) and flexible device that can be applied onto various surfaces. Moreover, the developed label is also printable and paper-based, and most importantly, the printing ink is scalable.

Keywords: flavylium, leuco dyes, spirolactones, colour formers, colour developer, reversible thermochromic systems, smart labels

RESUMO

Dada a necessidade global de monitorizar as temperaturas durante o armazenamento e distribuição de numerosos produtos, incluindo alimentos, medicamentos, sangue e outros produtos sensíveis à temperatura, o acesso a etiquetas inteligentes baratas e descartáveis seria uma tecnologia inovadora para minimizar os resíduos e os riscos para a saúde. A CHARISMA, uma rede de formação inovadora financiada pelo programa Horizonte 2020 da União Europeia, visa desenvolver sistemas cromogénicos reversíveis/irreversíveis aplicados que exibem uma mensagem colorida quando encontram um estímulo térmico, químico ou redox específico. As etiquetas inteligentes CHARISMA foram concebidas para serem finas e flexíveis, ocupando praticamente nenhum espaço e, por consequência, podendo ser impressas em qualquer superfície através da atual revolução da eletrónica impressa.

Neste projeto de investigação, pretendemos contribuir para o desenvolvimento destas etiquetas inteligentes através de duas abordagens diferentes: (a) corantes de espirolactona à base de benzopirílio com desenvolvedores e solventes adequados para serem explorados como sistemas termocrómicos reversíveis ou irreversíveis, e (b) corantes de benzopirílio para utilização com polímeros termoresponsivos como sistemas termocrómicos reversíveis.

O termocromismo dos corantes de espirolactona foi examinado em sistemas ternários compostos por corante-desenvolvedor-solvente. Por outro lado, o termocromismo dos corantes de benzopirílio com um grupo aril CH-ácido na posição α-metileno foi investigado em copolímeros termoresponsivos de três blocos Pluronic® F127. Ambos os tipos de sistemas exibiram termocromismo reversível quando as condições adequadas foram cumpridas.

Por fim, os sistemas ternários baseados em corantes de espirolactona flavílio foram microencapsulados por um método de polimerização *in situ* e a dispersão de microcápsulas resultante foi convertida em tintas à base de água e impressa num papel de jato de tinta mate autoadesivo para avaliar as propriedades de mudança de cor.

O indicador com melhor desempenho clareia a +10°C no ciclo de aquecimento e volta a colorir completamente a +4°C no ciclo de arrefecimento, mostrando estabilidade térmica e de mudança de cor. A mudança de cor pode ser lida a olho nu, sem necessidade de um leitor externo. A etiqueta inteligente termocrómica concebida é um dispositivo minúsculo (Ø×L×W=0.8×2.1×2 cm) e flexível que pode ser aplicado em várias superfícies. A etiqueta desenvolvida é também imprimível e baseada em papel e, mais importante ainda, a tinta impressa é escalável.

Palavras chave: flavílio, corantes leuco, espirolactonas, formadores de cor, reveladores de cor, sistemas termo-crómicos reversíveis, etiquetas inteligentes

CONTENTS

LIST OF FIGURES

LIST OF TABLES

ACRONYMS

TS	Thermochromic Systems.
CVL	Crystal Violet Lactone.
PDA	Poly(diacetylene).
PT	Poly(thiophene).
PPV	Poly(phenylenevinylene).
TLC	Thin-Layer Chromatography.
NMR	Nuclear Magnetic Resonance.
HRMS	High Resolution Mass Spectrometry.
DCM	Dichloromethane.
THF	Tetrahydrofuran.
EtOAc	Ethyle Acetate.
CT	Charge Transfer.
HOMO	Highest Occupied Molecular Orbital.
LUMO	Lowest Unoccupied Molecular Orbital.
TICT	Twisted Intramolecular Charge Transfer.
LE	Local Excited-State.
SS	Stokes' Shift.
TEA	Triethylamine.
DIPEA	N,N-diisopropylethylamine.
TT	Transition Temperature.
PPO	Poly(propylene oxide).
PEO	Poly(ethylene oxide).
CST	Critical Solution Temperature.
UCST	Upper Critical Solution Temperature.
LCST	Lower Critical Solution Temperature.
PF-127	Pluronic® F127.
CF	Colour Former.
CD	Colour Developer.
IPP	Isopropyl Palmitate.
DLS	Dynamic Light Scattering.
SEM	Scanning Electron Microscopy.
TEM	Transmission Electron Microscopy.

PI	Polydispersity Index.
FTIR	Fourier Transform Infrared Spectroscopy.
EA	Elemental Analysis.
TGA	Thermogravimetric Analysis.
DSC	Differential Scanning Calorimetry.
HSM	Hot Stage Microscopy.
C_8	Caprylic Acid.
C_{10}	Capric Acid.
f	Free System.
c	Encapsulated System.
p	Printed Material.
R	Encapsulation Ratio.
E	Encapsulation Extent.
T_g	Glass Transition.
CIELAB	Colour Space.
PP	Polypropylene
RFID	Radio Frequency Identification.
IoT	Internet of Thing.
ESR	Early-Stage Researcher.

SYMBOLS

λ	Wavelength.
ε	Molar absorptivity coefficient.
f	Oscillator strength.
Φ	Fluorescence quantum yield.
χ	Mole fraction.
ΔE*	Contrast difference (CIELAB colour space).
Δ*H*	Enthalpy.
L*	Lightness (CIELAB colour space).
a*	Red-green colour component (CIELAB colour space).
b*	Yellow-blue colour component (CIELAB colour space).
Ø	Diameter.
L	Length.
W	Width.

1

LITERATURE REVIEW

1.1 Chromogenic materials and thermochromism

Chromogenic materials modify their optical properties due to changes in absorption, reflection or scattering of incident light in response to an external stimulus. Various stimuli, such as light, temperature and electric fields, are commonly used to evaluate the chromogenic characteristics of materials. For example, when the alteration of optical properties are due to the action of heat, the materials are termed as thermochromic. [1–3] The change of colour can occur gradually or abruptly. Gradual modification is known as continuous thermochromism, whereas abrupt transformation is referred to as discontinuous thermochromism. Continuous thermochromism develop across a temperature range, whereas discontinuous thermochromism occurs at the transition temperature of a material due to a structural change. [1] Thermochromism was first discovered in bianthrones at the beginning of the 20th century [4] and since then it was reported in various inorganic and organic materials, organometallic compounds, polymeric and sol-gel materials. [5]

1.2 Inorganic thermochromic materials

In *inorganic materials*, the thermochromism has often been reported in metal iodides, double salts, transition metal compounds, metal alloys, metal chlorides, etc. The colouration mechanism was related with solid-to-solid transition, which produces changes in the crystal lattice, ligand geometry or coordination number around the metal center due to loss or gain of crystallised water. For example, Cu_2HgI_4 and Ag_2HgI_4 change their colour during the crystalline transition from positive tetrahedral structure at low temperature to cubic structure upon heating. [6,7] Another well-known inorganic thermochromic material is vanadium dioxide (VO_2). Vanadium (IV) oxide is a promising thermochromic material in the production of smart windows due to reversible metal-to-insulator transition temperature at 68°C, which can be easily shifted to room temperature by doping metal ions (such us tungsten and magnesium) into the crystal lattice. VO_2 is in the semiconducting phase at low temperatures and has low infrared absorption with a transparent state. In contrast, at high temperature it is in its metallic phase with high infrared reflectance and a rutile-like crystal structure and a more blocking state.

Elemental vanadium has a high affinity for oxygen and can easily form metals with oxidation states +5, +4, +3 and +2. During synthesis with a strong oxidising agent such as O_2, tetragonal VO_2 is readily converted to thermodynamically stable V_2O_5 with V_6O_{13} and V_3O_7 as intermediates. [8,9]
Inorganic thermochromic materials based on metal complexes find use in the production of fast response code carriers, smart windows, security markings for banknotes and government documents, temperature sensors for security and quality control applications, optically writable/recordable data storage, thermal printing, and novelty items such as cutlery and colour-changing clothing. [10]
The colour transition of inorganic materials ranges from 70 to 500°C, and those with a colour transition around 70°C are of great interest for their future applications in building construction to make them more energy efficient. They are stable above 200°C and maintain stable chromatics, mechanical durability and storage stability for their stable crystalline symmetry, as required for a reversible thermochromic effect. However, the high-temperature thermochromism and toxicity of many of them limit their applications range. [11]

1.3 Organic thermochromic materials

In *organic materials*, the thermochromism has been frequently reported in liquid crystals, *leuco* dyes systems based on triphenylmethane and xanthene derivatives, spiroheterocyclic compounds such as spiropyrans and spirooxazines, Schiff bases, bianthrones and overcrowded ethenes, conjugated polymers, and miscellaneous compounds. The colour change mechanism can be a result of a physical transformation (due to mesophase formation like in liquid crystals), a molecular rearrangement (resulting from the cleavage of covalent bonds as in spiropyrans), changes in molecular stereoisomerism (due to the exchange between stereoisomers like in bianthrones), and the development of macro- and supra-molecular systems (resulting from the formation of covalent and noncovalent bonds between constituent units as in conjugated polymers). [12–14]

1.4 Liquid crystals

A liquid crystal is considered the forth state of matter and combines properties of both liquids and solid crystals. [15] Mechanical properties such as fluidity, inability to support shear, formation and coalescence of droplets are characteristics inherited from liquids. While electrical, magnetic, and optical properties are characteristics of solid matters. [16] Molecules with liquid crystalline properties are usually referred to as calamitic or discotic. Calamitic molecules have large length-to-breadth ratio and reassemble into a rod-like shape, while discotic reassemble into a disc-like shape due to their aromatics core and alkyl branches as outer part, **Figure 1.1**. Usually, thermotropic liquid crystals are calamitic molecules, and the type of mesophase is defined by molecular symmetry and arrangement. [12,17,18]

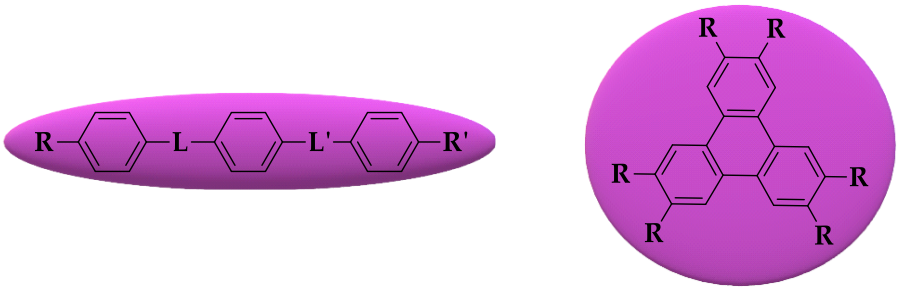

a) calamitic (rod-like shape) b) discotic (disc-like shape)

R & R': alkoxy chains, OH, CN, NO_2, etc (terminal units)
L: C=N,N=N, C=C, etc (linking units)

Figure 1.1 — Skeleton and shape of calamitic and discotic liquid crystal. [17]

The optical properties of thermochromic liquid crystals change in a predictable, repeatable, and precise manner, making them materials of great interest for applications where small temperature changes need to be detected. However, their fairly high cost and the need for a black background to maximise the colour contrast somehow narrow their range of applications. [19,20] Colour change is observed because liquid crystals selectively reflect light when temperature changes are detected. Temperature fluctuations induce molecular reorganisation or twisting which are marked by colouration or discoloration effects. [19]
The liquid crystalline phase, often referred to as mesophase, can be induced by a thermal stimulus that gives raise to thermotropic liquid crystals, or by the effect of solvents resulting in lyotropic liquid crystals. [21] For thermotropic liquid crystals, temperature is the only thermodynamic parameter involved in the formation of the liquid crystalline phase. They can arrange into nematics, smectics, cholesterics, and columnar mesophases, see **Figure 1.2**. [17,18]

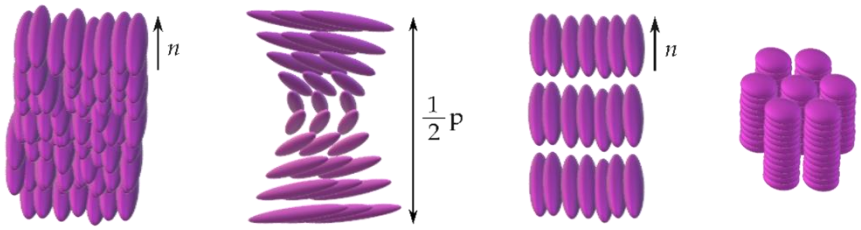

Figure 1.2 — Illustration of possible molecular arrangements in thermotropic liquid crystalline mesophases.

The liquid crystalline state occurs within a specific temperature range that starts at the melting point of the crystalline material and ends at the clearing point, which is when the liquid crystalline order disappears as it converts into an isotropic liquid, **Figure 1.3**. [17,18] The bandwidth (defined by the activation and clearing temperature range) can be of 1°C to 20°C and can change colour from red to blue. Often, the beginning of colouration is marked by red (lower clearing point) with yellow and green in the middle and blue at the highest clearing point. [19,22]

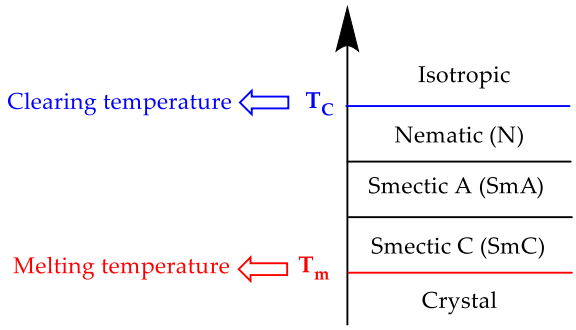

Figure 1.3 — Diagram with the generic phase sequence of thermotropic calamitic liquid crystals. The vertical axis corresponds to the main thermodynamic control parameter, temperature. The liquid crystalline region is bounded by the melting point T_m and the clearing point T_c. [18]

The *nematic mesophase* is the least ordered mesophase among others, as it only exhibits orientational order with a preference for alignment along the long axes. The molecules in a nematic mesophase are capable of rotating around their long axes, and the preferred direction can change through the medium. This preferred direction is known as the director, abbreviated *n*, and represents the average direction of the principal symmetry axis of the building blocks. Materials exhibiting nematic mesophase are of great technological importance and are widely used in the manufacturing of various types of displays. [21,23]
Cholesteric mesophase, also known as the helical twisted nematic phase, generally occurs when the liquid crystal molecule possesses a chiral center. The optical properties of cholesteric liquid crystals can change when the length of the helical pitch is altered by thermal, electrical, or magnetic stimuli. The periodicity of the cholesteric phase is given as ½ due to the head-tail molecule symmetry. Changes in the chemical composition and flow of the corresponding cholesteric liquid crystal can also affect the length of the pitch. Colouration is observed in cholesteric liquid crystals due to the physical phenomenon of Bragg reflection of light from the liquid crystal plane. The wavelength of generated light is typically several hundred nanometers, which is comparable to the wavelength of visible light. [21,23,24] Nowadays, cholesteric liquid crystals are used to manufacture various products; gas, thermochromic and humidity sensors are one of these products. They are also used in the production of super twisted nematic LCDs, tunable band-pass filters and rewritable colour recordings, thermal printable e-paper, polariser-free reflective displays, laser applications and prototypes of reflective smart windows. [24]
In *smectic mesophases* the molecules have both orientational and positional order, and it had found scarce commercial applications. *Columnar mesophases* arise when the aromatic core is stacking up as in piles of coins. The piles are usually arranged in a hexagonal or close to a hexagonal shape. Columnar mesophases are often formed by disc-shaped molecules of triphenyl derivatives. [21,23]

1.5 Leuco dyes

Leuco dyes are organic chromophores with indirect thermochromism. The colour alteration in indirect organic thermochromic materials is a response to environmental changes caused by heat around the chromophore. These materials are known as thermochromic systems (TSs) or composites and are typically composed of at least three components: a colour former, a colour developer, and a solvent. The colour former is a spirolactone *leuco* dye sensitive to pH changes,

the colour developer generally is a weak acid that interacts with the spirolactone dye to induce colouration, and the solvent is usually a long-chain alkyl alcohol, ester or acid that defines the transition temperature at which the colour begins to develop. Typically, these systems undergo a reversible colour change due to the opening and closing of the spirolactone ring. Interaction of the dye with strong or Lewis acids leads to irreversible colouration. During this transition, the electronic state of spiro-carbon change from sp^3 hybridisation to sp^2 and facilitates conjugation between previously isolated systems, **Scheme 1.1**. [13]

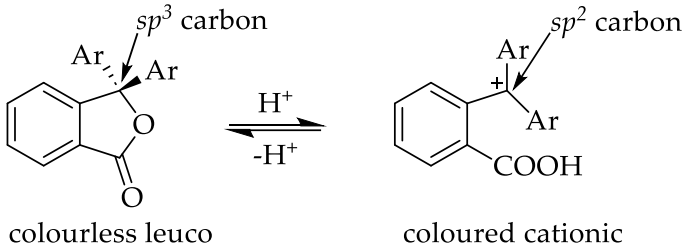

Scheme 1.1 — Mechanism of colour development in spirolactone systems.

F. Fu and L. Hu argued that "electron transfer theory" can be used to explain thermochromism in these types of systems. Therefore, they explained that thermochromism in such systems is favoured because the oxidation-reduction potential between the acceptor (colour former) and donor (colour developer) is similar; however, when the surrounding temperature changes, the oxidation-reduction potential is distinct for each, which allows the direction of the redox reaction to change with the alteration in temperature. The oxidation-reduction reaction promotes a proton transfer reaction between the dye and the developer that produces a rearrangement of the molecular structure, which is indicated by a turn in colour. [25]
Triphenylmethane (or diarylphthalide) [26–32] and xanthene [33–37] dyes, commonly referred to as crystal violet lactone (CVL) and fluoran dyes, are the most prevalent pH-sensitive *leuco* dyes used in the design of such composites, and recently an example of benzopyrylium (flavylium) based *leuco* dye was reported as an alternative. [38] When the temperature of the system changes, their lactone ring opens to produce the coloured dye, and their structural modification/functionalisation produces a wide range of colours. Reversible thermochromic systems are generally produced by mixing the dye and developer with a suitable solvent which interacts with the dye in the liquid state and pulls away when the system solidifies. [2] Phenol derivatives [2] are the most used colour developers, however, coumarins and 1,2,3-triazole compounds [14] have recently been reported as alternatives. Moreover, an example of liquid crystal colour developer (1-benzyl-3-methylimidazolium chloride) was explored in thermochromic composites based on xanthene derivatives. [39]

1.5.1 Triphenylmethane *leuco* dyes

Crystal violet lactone (6-(dimethylamino)-3, 3-bis[p-(dimethylamino)phenyl]phthalide) is a type of phthalide derivative that is widely explored for its use as a colour former in multicomponent thermochromic systems. In its *leuco* state, the lactone ring is closed, and the dyes appear to have low colour density with a π-π^* transition and a maximum wavelength (λ_{max}) at 280 nm. An appropriate colour developer opens the lactone ring and develop a dye with high

colour density due to extended conjugation, reduced energy of the π-π* transition, and a shift in the λ_{max} to 620 nm, **Scheme 1.2**. [40]

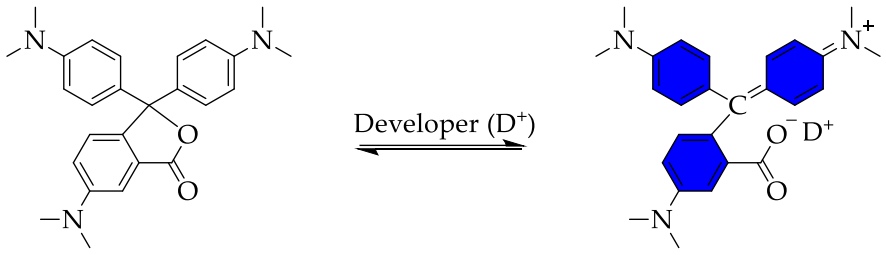

Scheme 1.2 — The developer opens the lactone ring to form coloured triphenylmethane-type system.

The first CVL synthesis is illustrated in **Scheme 1.3** and was described as a condensation reaction between a benzhydrol and a benzoic acid derivative in 90% sulfuric acid. The reaction product was an intermediate phthalide derivative, which was then oxidised to its *leuco* homologue with lead dioxide in dilute mineral acid. Subsequently, the reaction conditions and reagents were varied to find the most feasible conditions to produce CVL. Condensation in dilute mineral acid was shown to improve both the yield and the quality of the *leuco* CVL intermediate. Also, the particle size of the benzhydrol reagent has been found to be important in the reaction run. [41]

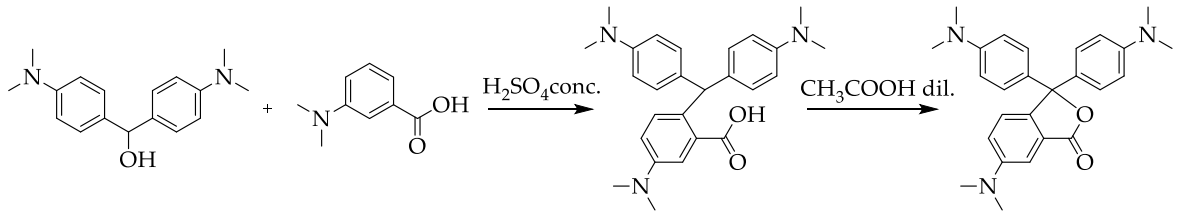

Scheme 1.3 — The first synthetic route used to develop CVL dye.

Alternative oxidising agents have been reported to be potassium permanganate, potassium persulfate, potassium ferricyanide or chloranil when using a metal complex as a catalyst. However, it was stated that the method of choice involved the use of hydrogen peroxide in a basic solution, catalysed by copper or cobalt complexes, chromium, iron, manganese or vanadium salts, and iron or manganese chelates. Moreover, the oxidation was also carried in the presence of air or oxygen with catalysts such as cobalt or manganese complexes, acetic acid or iron, copper or cobalt salts in acidic media. [41]

Despite the various reported synthetic alternatives, it was ultimately argued that the most versatile and elegant route for obtaining CVL dyes remains the one described by Haller and Guyot in 1899, and which was used for the development of well-known Malachite Green lactone. Through this method, the condensation reaction was performed in acetic anhydride between a benzaldehyde and a benzoic acid derivative to produce the corresponding intermediate phthalide. Then, the *leuco* product was formed with acetic anhydride as a catalyst and dimethylaniline as a reagent, **Scheme 1.4**. [41]

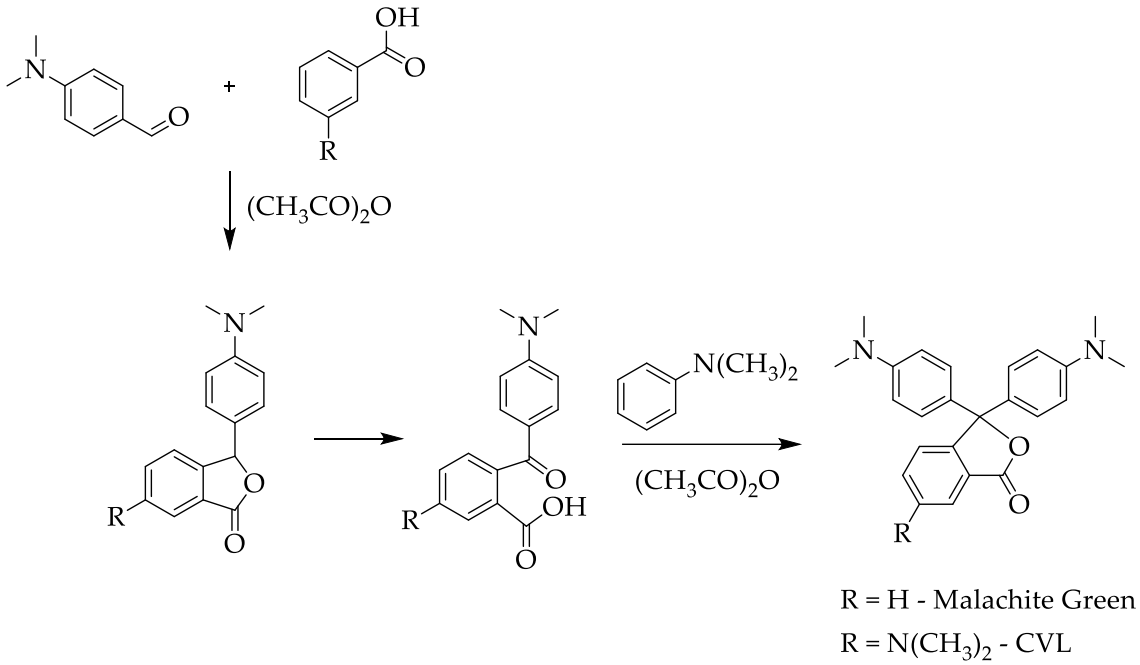

Scheme 1.4 — Alternative synthetic route that can be used to develop CVL *leuco* dyes.

Low solubility in organic solvents and poor lightfastness of parent CVL had led to the synthesis of numerous derivatives. A few examples of these derivatives are presented in **Figure 1.4**. And it has been claimed that CVL of type 1 and 2 presented good solubility in organic solvents, while CVL of type 3 possess excellent light-resistance. [41]

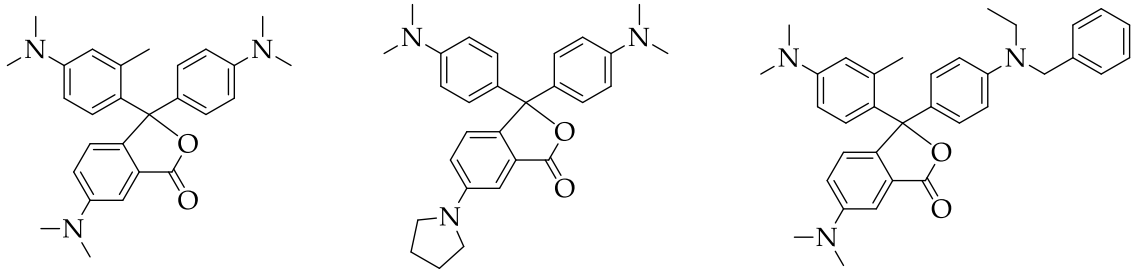

(1) (2) (3)

Figure 1.4 — CVL derivatives with good solubility in organic solvents (1, 2) and high light fastness resistance (3).

Over the years, different thermochromic systems based on CVL and its derivatives have been designed to be used in various applications or simply for elucidating their colour change mechanism. For example, Haiyue Yang *et al.* [42] prepared a reversible thermochromic system based on CVL colour former, bisphenol A developer and 1-tetradecanol solvent to be used in the construction sector after its impregnation into delignified wood by vacuum-assisted impregnation method. The impregnated delignified wood underwent a reversible colour change on heating, from dark blue to light blue and then to off-white, due to the slow melting of the solvent. The liquid state breaks the dye-developer interactions and decreases the colour density. The low colour density in the liquid state was explained to be due to the interruption of the conjunction in the dye molecules. Wenbo Li *et al.* [29] also prepared a thermochromic

system based on CVL colour former, bisphenol A developer and tetradecanol solvent for coating of a metal substrate after being microencapsulated.
Shixiong Yi *et al.* [43] developed a reversible thermochromic system based on bromocresolpurple CVL derivative (colour former), boric acid (developer) and tetradecyl alcohol (solvent) to be used in the production of thermochromic and thermoregulating textile materials. Prior to fabric addition, the TS was embedded in silicone gel network (to avoid leakage or other unwanted reaction), and the resulted powder was mixed with an acrylate adhesive to obtain a suitable paste for the coating process. After heating, the coated fabric underwent a reversible colour change from yellow to pink between 25 and 50°C within 1 minute. The colour change was attributed to a lactone tautomerism mechanism. The proton transfer reaction led to a molecular rearrangement that produced a new chromophore with extended conjugated π systems, **Scheme 1.5.** It was also mentioned that the tautomerisation reaction was possible due to acidic properties of lactone colour former and tetradecyl alcohol solvent.

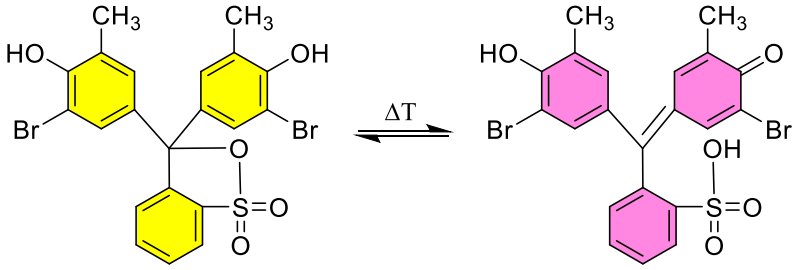

Scheme 1.5 — Temperature induces molecular rearrangement in bromocresolpurple CVL derivative.

Danfei Liu *et al.* [44] also reported a reversible thermochromic system based on CVL, boric acid and hexadecyl alcohol. In this system, CVL was the colour former, boric acid the developer, and hexadecyl alcohol the solvent. The system exhibited remarkable reversible thermochromism with a colour change from blue-green to colourless and the authors claimed that such a system can be used in anti-counterfeiting applications for smart packaging and smart sensors.
Haisheng Liu *et al.* [45] developed reversible thermochromic microcapsules containing CVL, bisphenol AF and methyl stearate mixture as the core material to prepare a reversible thermochromic anti-counterfeiting mark. In the core system, CVL was the colour former, bisphenol AF was the developer and methyl stearate worked as a solvent. The developed microcapsules exhibited a unique reversible thermal memory function and a strong colour contrast between cooling and heating conditions, enabling information encryption.
He Liu *et al.* [46] prepared a reversible thermochromic system composed of CVL colour former, bisphenol A developer, and dodecanol solvent to develop a portable patch that can be used as a temperature indicator in electronics to indicate overheating. With such a patch, overheating can be observed when the colour changes from deep blue to colourless after 70°C. The discolouration process is a result of dye-developer dissolution in liquid dodecanol. The fluid state disrupts dye-developer interactions and leads to a colourless system. On the other hand, the colouration step is a result of the temperature drop in the system, which induces a phase transition from liquid to solid. The solid state induces solvent precipitation and allows dye-developer interactions.

Alexander N. Bourque and Mary Anne White [32] investigated the chromism of twelve developer/solvent combinations with CVL as colour former. Four alkyl gallate derivatives were selected as developers and three long-chain alcohols as a solvent. The focus was on evaluating how alkyl chain length of the developers and solvents affected the thermochromism of the systems. They found that, when the solvent and developer alkyl chains had a similar length, melt-darkened thermochromism occurred, especially when the difference was two carbon atoms or less. On the other hand, melt-lightened thermochromism was observed when the solvent and developer alkyl chains differed in length. Hong Tang *et. al.* [31] also reported a thermochromic system based on CVL that promoted colouration of the molten state, when using lauryl gallate as developer and tetradecanol as a solvent. In the same paper, they also presented a CVL-lauryl gallate-hexadecanol thermochromic system that showed colouration just below the solvent's freezing point, which faded after further cooling. The presence of polymorphic material in the used solvent led to this type of colour change behaviour. The colour was developed in the α disorder phase and vanished in β and γ ordered phases.
Alina Raditoiu *et al.* [28] investigated how the ratio between colour former (CVL) and developer (phenolphthalein) affects their thermochromic properties in 1-tetradecanol solvent. They concluded that the reversibility of systems with a colour change from blue to colourless was ensured at 1:2.5/dye:developing agent. They also noted that it is essential to ensure sufficient solvent to allow complete dissolution of the molten components due to the hydrogen bonds established between the components in the solid state.

1.5.2 Xanthene *leuco* dyes

Xanthene dyes, commonly known as fluoran dyes, consist of two different π-systems. One is represented by a xanthene fragment and the other by a phenyl moiety with a carboxyl group at the 2-position, which acts as a stimulus-responsive site (see **Figure 1.5**). The crystallographic analysis has showed that the two π-systems arrange themselves perpendicular to each other due to the weak interactions between the electron clouds. However, the geometry changes in solution due to the free rotation of the phenyl unit. [39] The carboxyl group attached to the phenyl unit makes fluorans to behave like a *leuco* dye through a lactone ring-opening and ring-closing reaction under the influence of various stimuli such as heat, UV light, pressure and changes in pH (see **Scheme 1.6)**. These stimuli cause C_{spiro}-O cleavage, resulting in a colour change due to molecular rearrangement in the xanthene fragment. It has been observed that basic conditions favour the *leuco* and zwitterionic forms, whereas strong acidic conditions stabilise the cationic dye. [39,47,48]

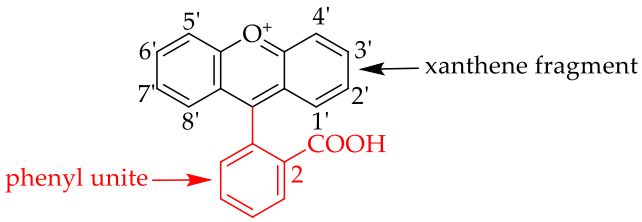

Figure 1.5 — The constituent units of a typical fluoran dye.

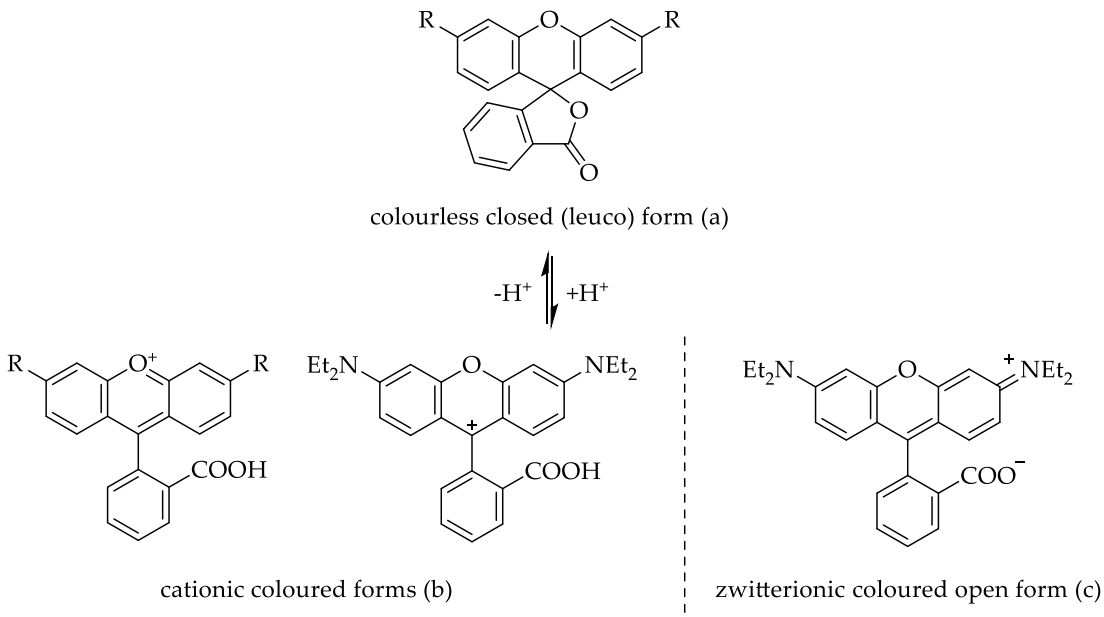

Scheme 1.6 — The *leuco* fluoran dye (a) can be converted into a cationic (b) and zwitterionic (c) coloured form under the action of heat, UV light or changes in pH. The coloured form may be stabilised by a proton transfer reaction or by physical interaction with an appropriate developer or a polar solvent.

Fluoran is the conventional name for spiro[isobenzofuran-1,9'-xanthen]-3-one (structure 1, **Figure 1.6**), and when a benzene ring is fused to the 1'- and 2'-positions of the xanthene moiety, the dye is referred to as benzo[a]fluoran (structure 2, **Figure 1.6**). Fusion at the 3'- and 4'-positions gives benzo[c]fluoran (structure 3, **Figure 1.6**). [41]

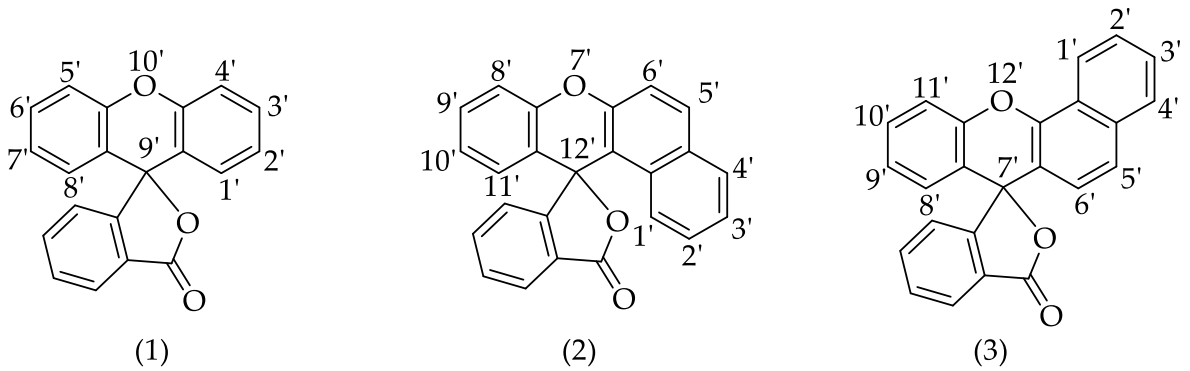

Figure 1.6 — Fluoran *leuco* dyes of type 1-3.

Fluorans are known as the class of dyes that can cover a wide range of colours. The colour is usually adjusted by changing the nature of the substituents on the xanthene moiety or by fusing benzene units at certain positions. Also, substituents on the phthalide moiety can impact the colour. **Figure 1.7** shows the structure of some fluoran dyes that presented different colours. For example, fluoran (5) gives a black colour when mixed with red fluoran and this combination is still used today in carbonless copy paper and inorganic co-reactants. In addition, fluoran (6) gives a singly black colour that is difficult to achieve with other classes of *leuco* dyes. It has been mentioned that the steric hindrance of a methyl group at the 3' position contributes greatly to the development of the black hue. All black fluoran dyes marketed today

are derivatives of (6) and each has individual properties that make them suitable for use in specific applications, such as thermosensitive recording paper. [41]

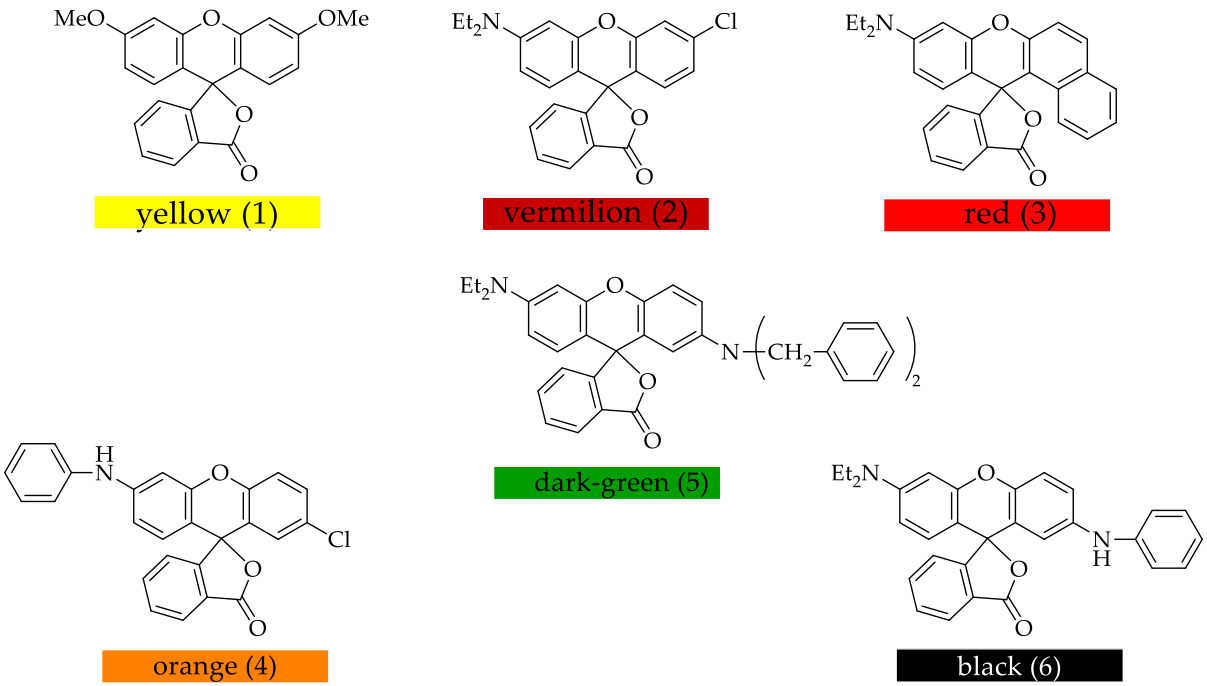

Figure 1.7 — The nature of substituents defines the colour in fluoran *leuco* dyes.

The reaction of keto acids with a wide range of phenols yields 3'-aminofluoranes derivatives that develop colours ranging from orange to red, **Scheme 1.7.** 3'-Aminofluoranes can also be synthesised by reacting 3'-chlorofluoranes with a variety of primary amines such as alkylamines, cycloalkylamines, aralkylamines and arylamines, as well as cyclic secondary amines such as piperidine, morpholine, etc. However, the typical example describes the reaction of 3'-chlorofluoranes with cyclohexylamine to give 3'-cyclohexylaminofluoranes, **Scheme 1.8**. [41]

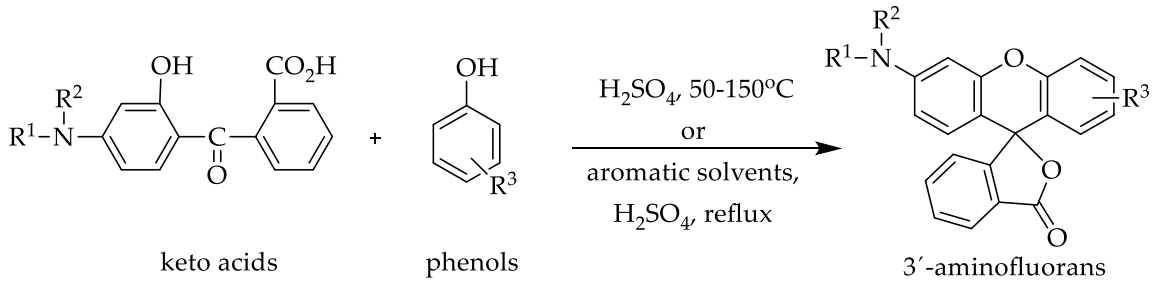

Scheme 1.7 — Reaction of keto acids with phenols gives 3′-aminofluorans.

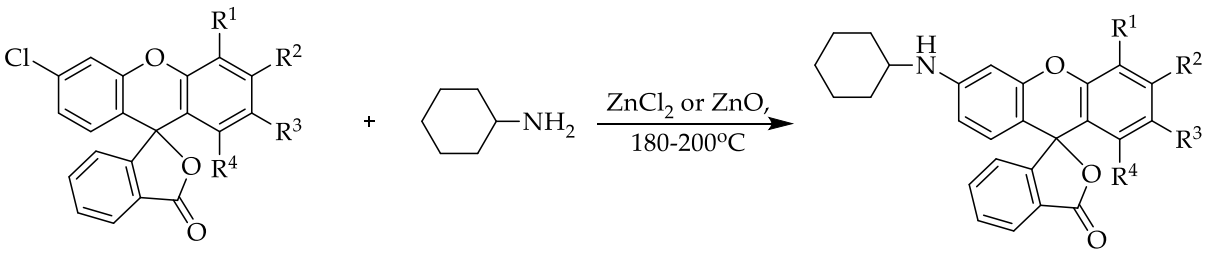

3′-chlorofluorans amines 3′-aminofluorans

Scheme 1.8 — Reaction of 3′-chlorofluoran with primary amines gives 3′-aminofluorans.

Keto acids also react with aminophenols or aminoanisoles to give diaminofluoranes, **Scheme 1.9**. To obtain satisfactory results, it is recommended to carry out the reaction in concentrated sulphuric acid below 60°C. [41]

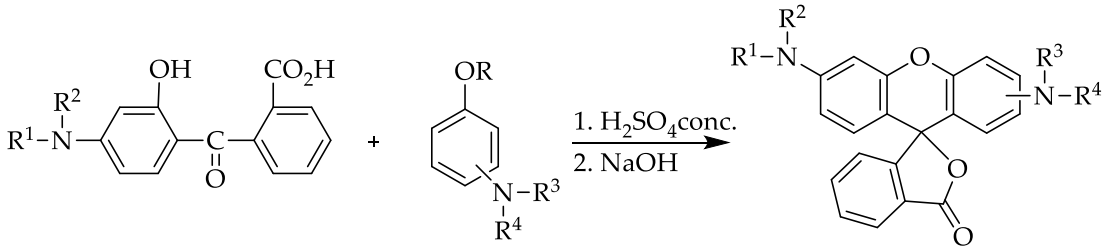

keto acids

R = H, aminophenols
R = CH3, aminoanisoles

diaminofluorans

Scheme 1.9 — Reaction of keto acids with aminophenols or aminoanisoles gives diaminofluorans.

For developing green or black fluoran dyes, the reaction of keto acids with 4-alkoxy-diphenyl-amines, **Scheme 1.10**, is recommended. This reaction is carried out in concentrated sulphuric acid to give phthalide intermediates which are then treated with base to give 2'-anilino-6'-aminofluoranes. In addition, if 4-alkoxydiphenylamines (R = CH_3, C_2H_5) are replaced by 4-hydroxydiphenylamines (R = H), the fluoran dye is obtained directly. [41]

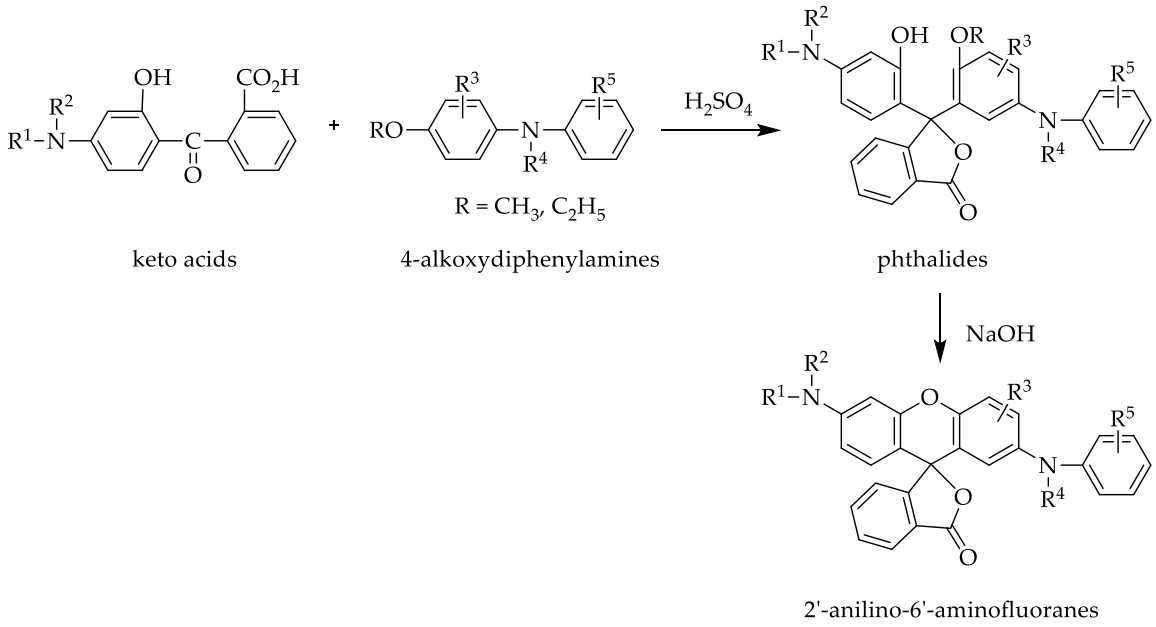

keto acids 4-alkoxydiphenylamines phthalides

2'-anilino-6'-aminofluoranes

Scheme 1.10 — Reaction of keto acids with 4-alkoxydiphenylamines gives green and black fluorans.

Fluorans with near-infrared absorption were synthesised by reaction of unsubstituted amino keto acids with 3-alkoxydiphenylamines, **Scheme 1.11**. This reaction led to the synthesis of 3′-anilinofluorans. [41]

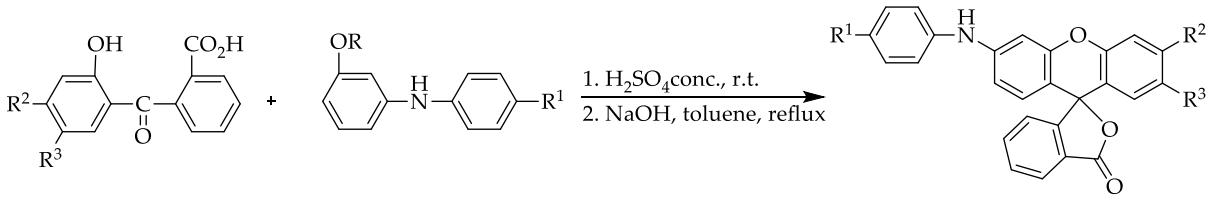

keto acids 3-alkoxydiphenylamines 3′-anilinofluorans

Scheme 1.11 — Reaction of keto acids with 3-alkoxydiphenylamines gives 3′-anilinofluorans.

Reaction of 2'-diaralkylaminofluorans with aralkyl halides gives 2'-diaralkylaminofluorans which develop only red or green colours, **Scheme 1.12.** This reaction is carried out in isopropanol or toluene under reflux and in the presence of potassium carbonate or sodium carbonate catalyst. [41]

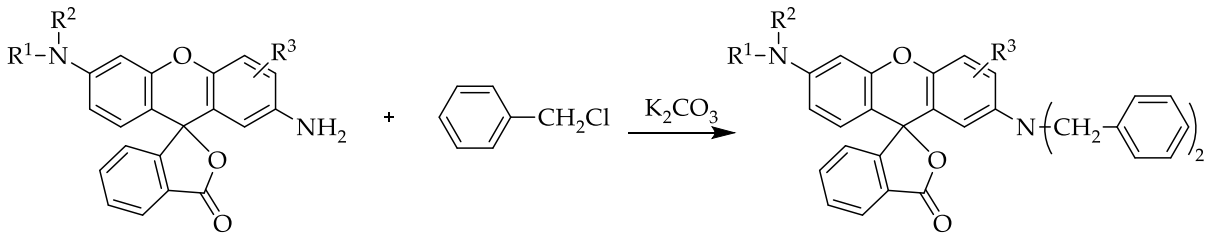

2′-aminofluorans aralkyl halides 2′-diaralkylaminofluorans

Scheme 1.12 — Reaction of 2'-diaralkylaminofluorans with aralkyl halides gives red or green 2'-diaralkylaminofluorans.

Along the years, fluoran dyes have found applications in various industries, including the industry manufacturing thermal indicators, heat-sensitive recording paper, carbonless paper, printed circuit boards, writing materials, textile finishing, and so forth. [41]
Generally, fluoran-based thermochromic systems consist of at least three components: colour former, developer and solvent, and these systems are known to change colour in a reversible manner. However, Bartłomiej Potaniec *et al.* [39] have reported recently, two-component thermochromic systems based on fluoran dye used as colour formers and a liquid crystal (1-benzyl-3-methylimidazolium chloride, [BMIm][Cl]) which worked as a colour developer. These systems developed an irreversible colour change from colourless to yellow/orange-red at high temperatures, with greater colour intensity in fluorans with electron-donating substituents. The colour change mechanism was attributed to a lactone ring-opening reaction via intermolecular association between the ionic liquid and the spironolactone moieties, **Scheme 1.13.** The authors had also mentioned that such systems might find applications as sensors for the detection of overheating, defrosting, and so forth.

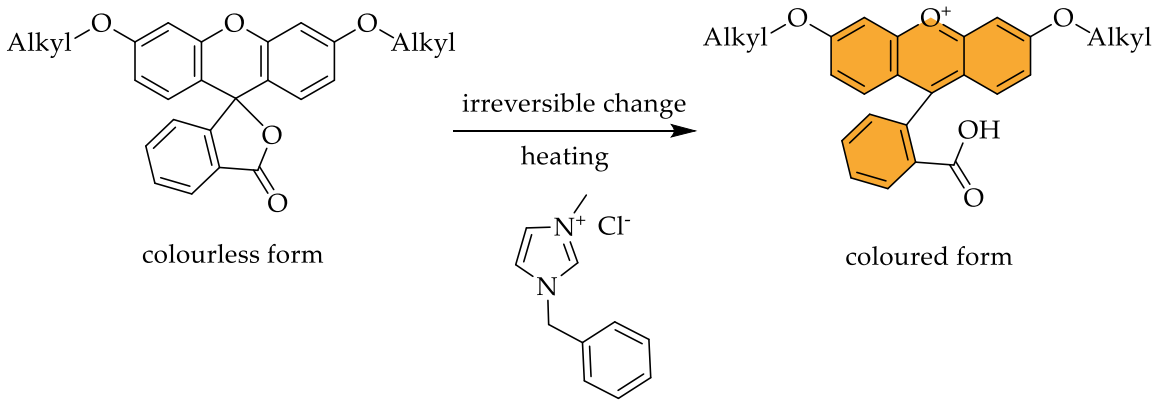

Scheme 1.13 — Reaction of fluoran dyes with liquid crystal-based developer induces an irreversible colouration.

1.6 Spiropyrans and spirooxazines

Spiropyrans are organic compounds that are well known for their photochromic properties, but they can also exhibit halochromism, solvatochromism and thermochromism. [49] Spiropyran skeleton is constituted of two aromatic (Ar) rings that are interconnected through a spiro carbon (C_{spiro}) with a sp^3 hybridisation, **Figure 1.8**. Aromatic moieties such as thiophenol, anthracene, benzene, indoline, and naphthalene can be employed in the functionalisation of the its skeleton. [49,50]

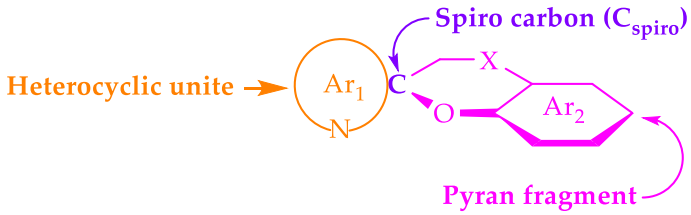

Ar_1, Ar_2 = thiophenol, anthracene, benzene, indoline, and naphthalene

X = N = spirooxazine

Figure 1.8 — The skeleton of spiropyrans and spirooxazines.

Thermochromism in spiropyrans was detected in 1926, when three independent reports of di-β-naphospiropyran derivatives appeared simultaneously. It was noted that its initial colour reversibly changed upon heating, and since then, thermochromism was commonly found in naphtho- and indoline-derivatives such as the ones illustrated in **Figure 1.9**. [49,51]

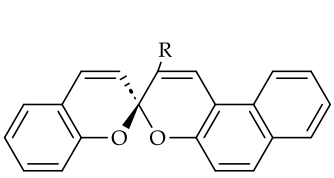

Benzo-b-naphthospiropyran
R = H: coloured upon heating
R = alkyl: colourless

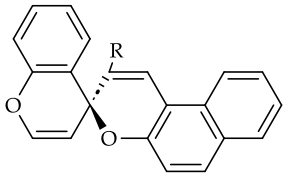

Benzo-b-naphthaisospiropyran
R = H: coloured upon heating

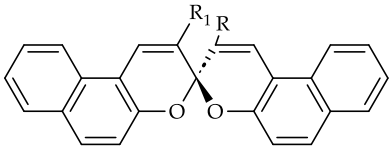

Di-b-naphthaisospiropyran
R or R_1 = H: coloured upon heating
R = R_1 = alkyl, C_6H_5: colourless

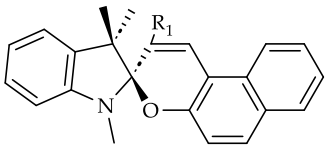

Indolino-b-naphthaisospiropyran
R_1 = H: coloured upon heating

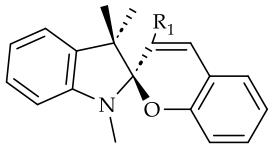

Indolinobenzospiropyran
R = H, CH_3: coloured upon heating

Figure 1.9 — Thermochromic spiropyrans constructed from naphtho- and indoline-derivatives.

The colour transition mechanism is attributed to the cleavage of C_{spiro}-O bond. During this cleavage, the colourless ring-closed form, known as the spiropyran form (SP), is converted into a coloured ring-open species that is usually referred as the merocyanine counterpart (MC), **Scheme 1.14**. [49,51]

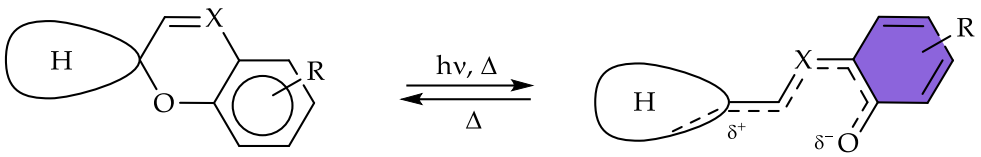

Spiropyran
(ring-closed coloureless form)

Merocyanine
(ring-open coloured form)

X = CH; spiropyrans, X = N; spirooxazines, and H = heterocycle

Scheme 1.14 — Colourless spiropyran form (SP) and its coloured merocyanine species (MC) resulted after the breaking of C_{spiro}–O bond of the corresponding thermochromic spiropyrans and spirooxazines.

The merocyanine form can adopt various conformations, which are influenced by factors such as nature of solvent, the specific substituents on the pyran ring, and the heterocycle type. Among these, the zwitterionic and quinoidal forms are the most frequently observed isomers, **Scheme 1.15**. [51]

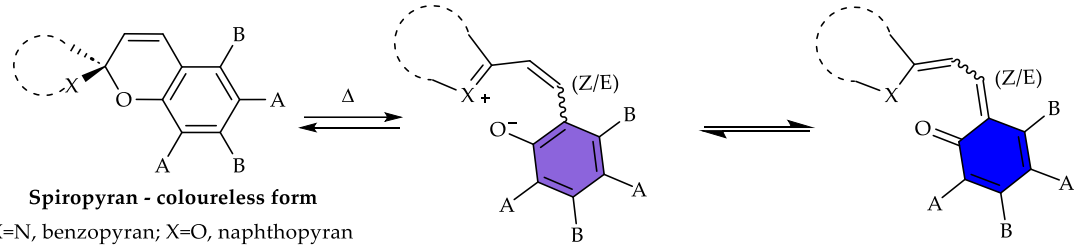

Spiropyran - coloureless form

(X=N, benzopyran; X=O, naphthopyran for thermally accessible ring opening)

Zwitterionic form of merocyanine

(predominant form when A=electron withdrawing)

Quinoidal form of merocyanine

(predominant form when B=electron donating)

Scheme 1.15 — Conformations adopt by thermochromic spiropyrans with different substituents at the pyran ring; electron withdrawing substituents at the positions A, stabilises the zwitterionic form, and electron donating groups at the positions B, stabilise the quinoidal form.

Thermochromic spiropyrans can also exhibit a consecutive alteration in colour through specific bis-spiropyrans. An example of such spiropyrans is depicted in **Scheme 1.16.** As illustrated, when a *n*-propanol solution of colourless bis-spiropyran, **Scheme 1.16a**, is heated to 60°C, it switches to a red hue because of the mono-merocyanine formation, **Scheme 1.16b**. Upon further heating to 70°C, it changes to blue, indicating the conversion to bis-merocyanine, **Scheme 1.16c**. [52]

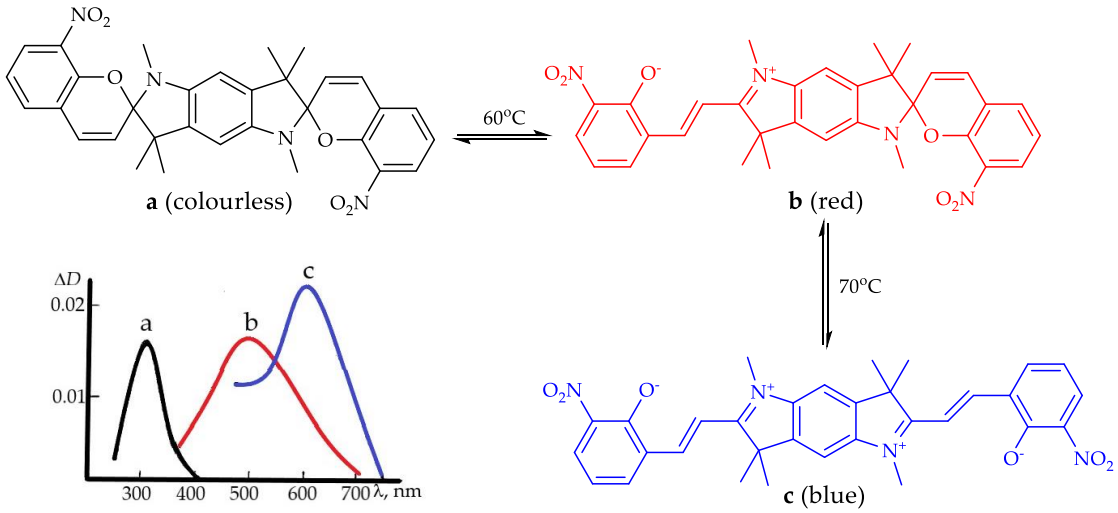

Scheme 1.16 — Reaction products of sequential thermal colouration of a bis-spiropyran and their absorption spectra of bis-spiropyran (a), mono-merocyanine (b) and bis-merocyanine (c) in *n*-propanol.

1.7 Schiff bases

A Schiff base (also referred as imine or azomethine) is a derivative of aldehydes or ketones in which the carbonyl group (C=O) is replaced by an imine or azomethine (>C=N—) and can be synthesised by condensing carbonyl compounds (aldehydes or ketones) with primary amines, **Scheme 1.17**. [53–56]

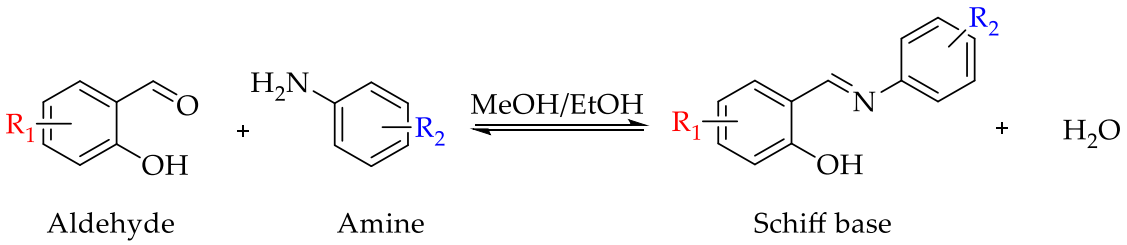

Scheme 1.17 — General procedure of aromatic Schiff base synthesis. [55,56]

Thermochromism in Schiff bases is a result of the keto-enol equilibrium reaction. At appropriate temperature, the intramolecular tautomerisation reaction reversibly induces an electronic rearrangement that is flagged by a colour change due to the extending of the π-bonding system, **Scheme 1.18**. [57,58] The tautomerisation reaction involved an intramolecular proton transfer from the hydroxylic oxygen to the imino nitrogen in the ground state via six-membered ring producing keto species, **Scheme 1.19**. Often, the enolic form is the most stable species and the keto tautomer can only be accessed at low temperatures. [59,60]

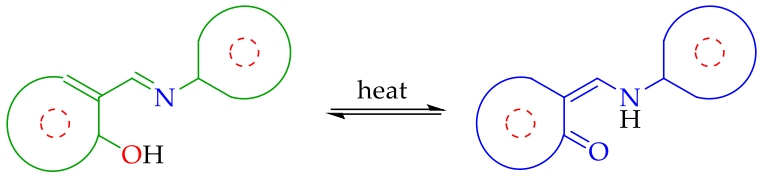

enol-imine keto-enamine

Scheme 1.18 — Temperature triggers the tautomerisation reaction to convert the enol to a keto species of *ortho*-hydroxy Schiff bases. Cyclic moiety can be represented by different aromatic units. [57]

Schiff bases made up with derivatives of salicylaldehyde and anilines (anils) have been classified as being both photochromic and thermochromic. According to the X-ray interpretation, a thermochromic crystal would have the salicylaldimine group locked by an intramolecular H-bond (**Scheme 1.19**), planar molecular organisation with π···π intermolecular interactions and short interplanar distance (3.5 Å), **Figure 1.10a**. On the other hand, the photochromic crystal would have the aniline ring rotated by 50° with respect to the plane (preventing close contact in the crystal lattice) and the latter planar moiety with intramolecular H-bonds, **Figure 1.10b**. [60]

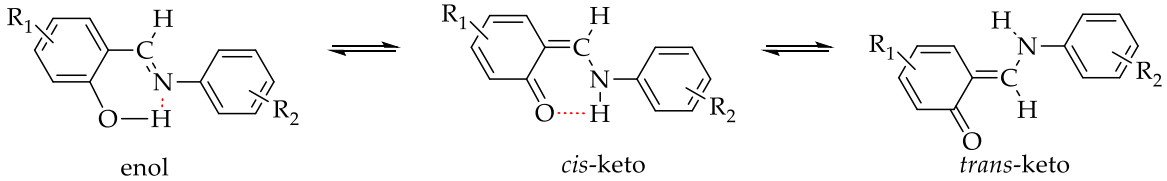

Scheme 1.19 — Reversible thermochromism in anils.

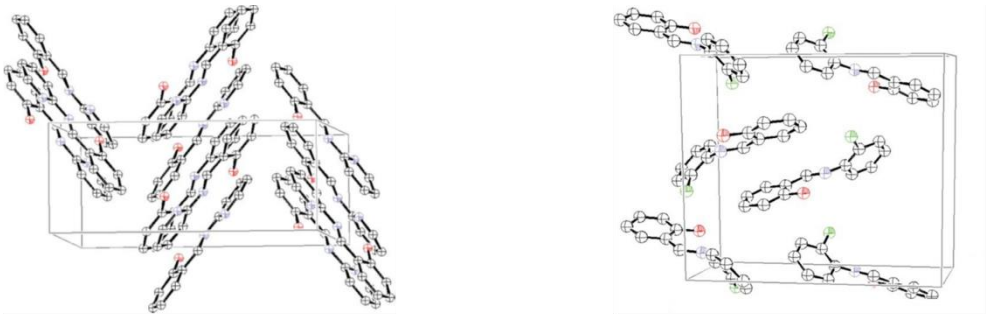

(a) **thermochromic** *N-salicylidene-2-aminopyridine* (b) **photochromic** *N-salicylidene-2-chloroaniline*

Figure 1.10 — Example of the 3D organisation of thermochromic (a) and photochromic (b) aniles. Thermochromic molecules generally adopt a closer packing, while photochromic molecules adopt a more open organisation.

Subsequent investigations have shown that planar organisation is not a primary factor for the thermochromic behaviour of a Shiff base, but it is indeed essential for its photochromism. The crucial factor for thermochromism in Schiff bases is regarded with the electron density of the imine N-atom. For example, when a CH_2 spacer group was placed between the aldimine and phenyl groups in the nonplanar N-salicylidene-benzylamines, in addition to photochromism, the Schiff base also exhibited thermochromism, **Figure 1.11**. It was concluded that the phenyl ring of the benzylamine disrupted the conjugation of the system and therefore increased the electron density on the lone pair of the imino nitrogen. [60–63]

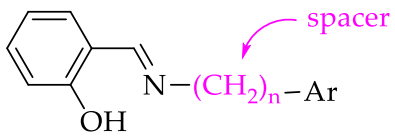

n = 1, 2
Ar = phenyl, pyridyl, thienyl

Figure 1.11 — Nonplanar Schiff base with CH_2 spacer is thermochromic. [63]

1.8 Bianthrones & Overcrowded Ethenes

Bianthrones and overcrowded ethene are chromogenic materials capable of reversibly changing their colour under the action of light (photochromism), pressure (piezchromism) and heat (thermochromism). The general structure of bianthrones is described by two tricyclic moieties (anthrone units) connected through a central carbon-carbon double bond also referred as "pinch", **Figure 1.12a**. The type of atoms from 10, 10' positions define whether the bianthrone molecule is *homomeric* (X = Y, **Figure 1.12a**) or *heteromeric* (X ≠ Y, **Figure 1.12a**) in nature. The overcrowding in bianthrones causes out-of-plane deformations to mitigate unfavourable steric interactions between the nonbonded atoms in the *fjord* regions, and a more realistic conformations are presented in **Figure 1.12b**. [64–66]

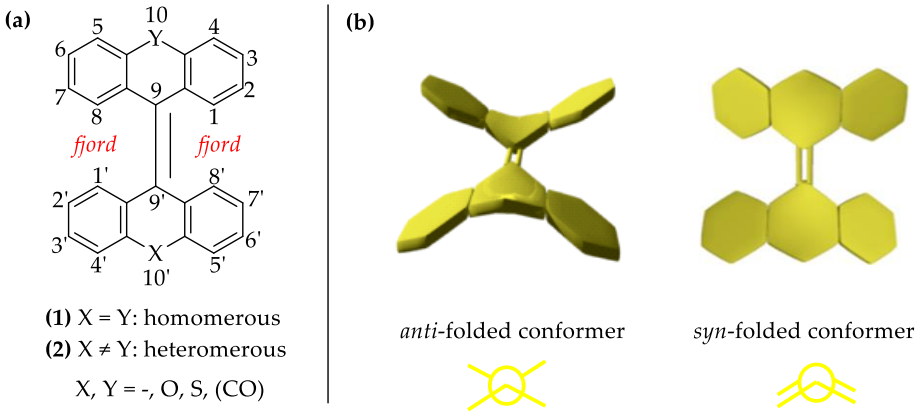

Figure 1.12 — The general structure of bianthrones with atom labeling (a) and *anti*- and *syn*-folded conformers (b).

Thermochromism of bianthrones was first discovered in 1906 by Meyer, where it was reported that 10-[10'-oxo-9'(10'H)-anthracenylidene]-9(10H)-anthracenone (bianthrones 2 in **Figure 1.13**) underwent a colour change in solution from yellow to dark green upon heating. [64] The reaction responsible for the chromic effect in bianthrones describes an equilibrium between two distinct and interconvertible A and B isomers, **Scheme 1.20**. Isomer A is the yellow (or colourless) ground state species with a *folded* conformation, while isomer B is the dark purple (or green) thermochromic species with absorption in the 600-700 nm visible region and a *twisted* conformation. Under the action of an external stimuli (e.g., heat) *folded* A conformer is reversible transformed into a *twisted* B species. The molecular twist decreases the π overlap and causes a visible red shift of the spectrum. [4,64–66] Some reports have concluded that the

bulky substituents in the *ortho* position relative to the central bond cancel thermochromic properties of bianthrones (while retaining the photochromic effect) due to steric interactions in the vicinity of the "pinch". [4] It was also showed that the voluminous substituents in the 1, 1' positions also inhibit the thermochromic effect. The bulky hydrogen group would prevent twisting of the molecule to reach the thermochromic species B. [67–70]

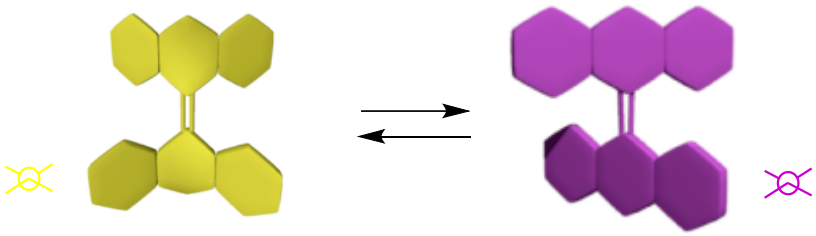

folded A conformer *twisted* B conformer

Scheme 1.20 — A and B conformers identified often in bianthrones.

Over the years, three types of conformational behaviour have been identified in bianthrones**.** Bianthrones of *Type 1* are thermochromic only if the energy between *anti*-folded **a** (or unevenly *anti*-folded **au**) room temperature A conformer is sufficient small (e.g., less than 30 kJ/mol according to DFT determinations) to access the twisted B conformer. Structures **1** and **2**, **Figure 1.13,** are example of bianthrones of *Type 1*. Bianthrones of *Type 2* also adopt *anti*-folded conformations as global minima; however, they are not thermochromic because the *syn*-folded **s** conformation is usually more stable than the twisted one. Structure **3**, **Figure 1.13,** is an example of *Type 2* bianthrones. In *Type 3* bianthrones, the global minimum belongs to twisted conformations. These conformers are present at all temperatures and are responsible for the deep colour in bianthrones. Structure **4** from **Figure 1.13** is an example of *Type 3* bianthrones. [64,71]

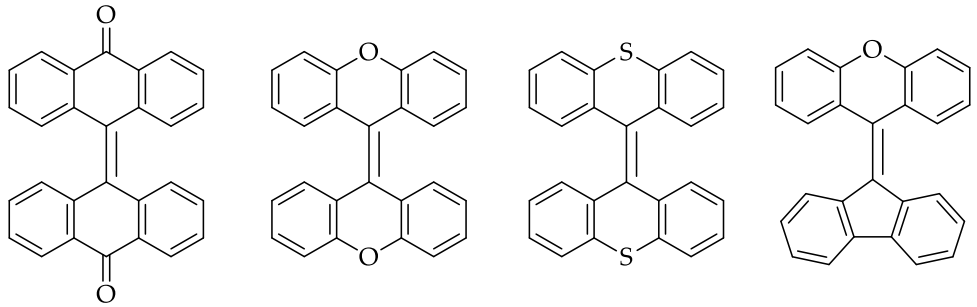

(1) **(2)** **(3)** **(4)**

Figure 1.13 — Bianthrones structures that can display one of *Type 1-3* conformational behaviours.

1.9 Conjugated polymers

Conjugated polymers have also been reported as thermochromic materials, and this property was often reported in poly(diacetylene)s (PDAs), poly(thiophene)s (PTs) and poly(phenylene-vinylene)s (PPVs). The thermochromic response occurs due to a conformational change in the polymer backbone as a result of modification in conjugation length or physical interactions. [2,72]

Poly(diacetylene)s is the most relevant class of polymers with reversible and irreversible thermochromism both in solution and solid state and a colour transition from blue to violet, red or orange. The structure of a common PDA is built from an yne-ene conjugated backbone and alkyl side chain containing some functional groups in terminal position. The crosslinking of the monomer is typically achieved by topotactic polymerisation, which is characterised by the formation of a metastable thermodynamic state with a blue colour. [2,73–77] The colour change is usually attributed to intra- and intermolecular interactions within PDA assemblies and can be triggered by heat, exposure to near-infrared light, mechanical stress, presence of acids, bases, biomolecules and surfactants, **Scheme 1.21**. [73]

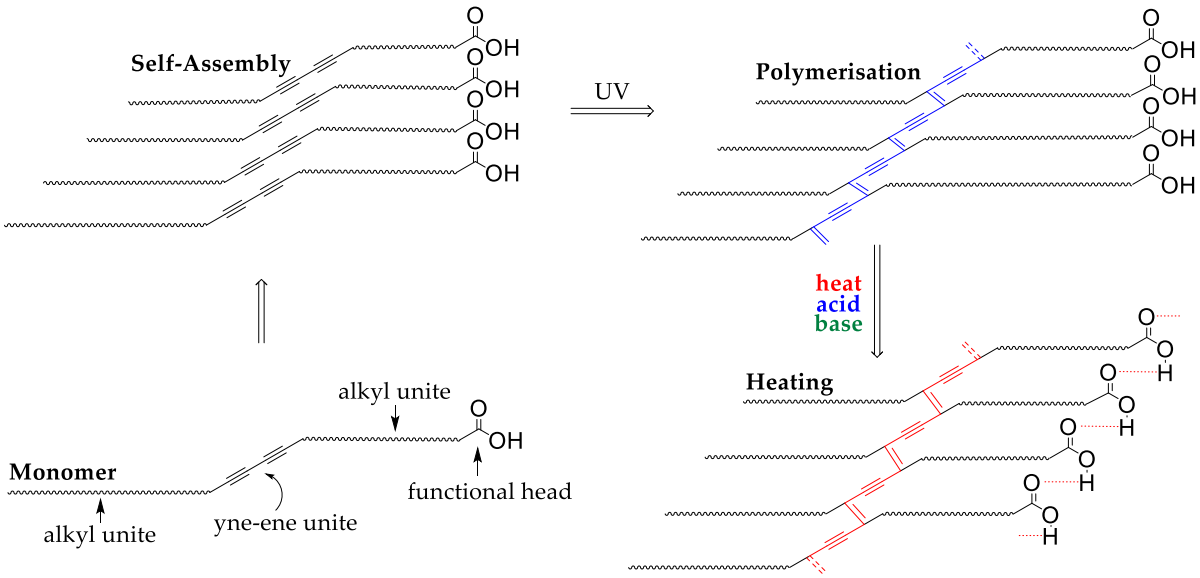

Scheme 1.21 — Schematic illustration of self-assembly, topotactic polymerisation and formation of intramolecular interactions of polydiacetylene monomer. The scheme was adapted after reference [77].

PDAs's reversibility is usually controlled by structural modifications of head group, alkyl side and addition of foreign materials (e.g., polymers, cations, and metal oxide nanoparticles) to improve interactions within PDA assemblies. [73,74] On the other hand, by mixing PDAs with diacetylene precursor via suspension polymerisation, materials with irreversible thermochromism are obtained. [2]

Excellent reversible thermochromism has also been reported in bis-polydiethylene connected via an intermediate *p*-phenylene group (Bis-PCDA-Ph). The synthesis of Bis-PCDA-Ph monomer was achieved in two steps, and it is illustrated in **Scheme 1.22**. In the first step, the precursor 10, 12-pentacosadiynoic acid (PCDA, commercially available) was treated with oxalyl chloride, and then, the resulted product was reacted with *p*-hydroquinone to generate Bis-PCDA-Ph in 90% yield. Subsequent UV treatment for 30 s of the self-assembled Bis-PCDA-Ph in water resulted in the formation of the blue coloured Bis-PCDA-Ph polymer, **Scheme 1.23.** At elevated temperatures, the colour change shifted from clear blue to red, attributed to unique interactions between hydrophobic alkyl chains and π-π aryl units. Moreover, the polymerised Bis-PDA-Ph was then mixed with polyethylene oxide (matrix polymer) to develop Bis-PDA-Ph-based electrospun fibers for use as a thermochromic sensor material. As shown in **Figure 1.14,** the embedded polymer fiber underwent a striking reversible colour change from 20 to 120°C. [78]

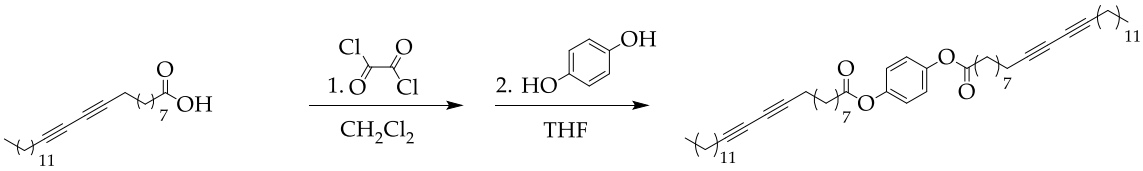

10, 12-Pentacosadiynoic acid (PCDA) — Bis-PCDA-Ph (monomer)

Scheme 1.22 — Synthesis of Bis-PCDA-Ph monomer.

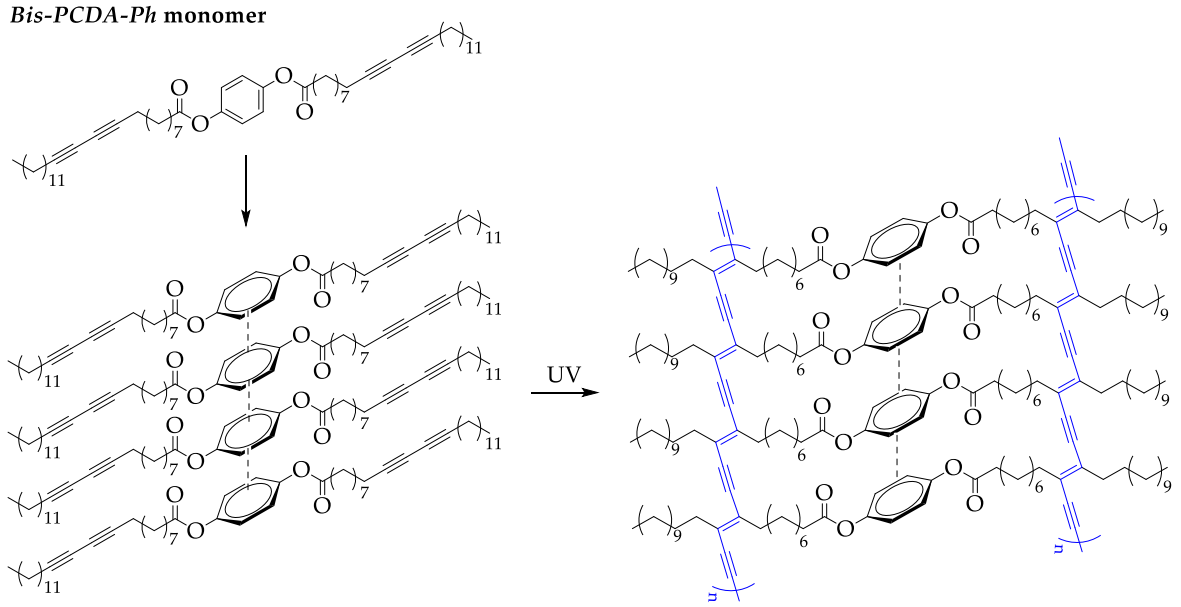

Scheme 1.23 — Bis-PCDA-Ph monomer undergoes a self-assembly and polymerisation reaction under the action of UV light in aqueous solution. The scheme was adapted after reference [78].

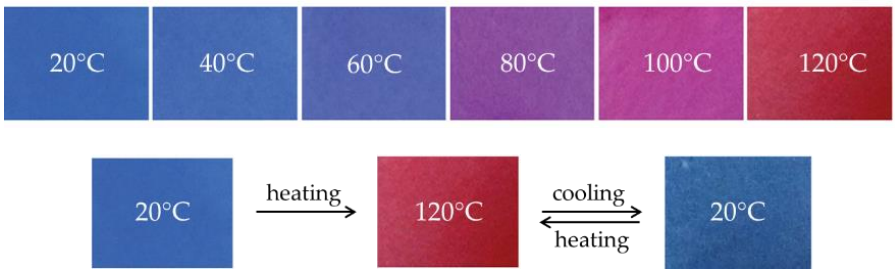

Figure 1.14 — Temperature promotes reversible colour change in Bis-PDA-Ph based electrospun fibers. The figure was adapted after reference [78].

Poly(thiophene)s is the second most relevant class of conjugated polymers that display thermochromism with a general colour transition from violet to yellow due to a decrease in conjugation. [2] The functionalisation of the 3- and/or 4-positions of the thiophene rings (see **Figure 1.15** for structure) with various substituents, develops polyconjugate polymers with desired optical and processing properties. For example, introducing flexible side chains in the polymer backbone improves polythiophene solubility. Oxidative polymerisation with $FeCl_3$ as catalyst

(first reported by Using Sugimoto et al.) has been widely used to develop various substituted polythiophenes, such as those containing alkyl, fluoroalkyl and ether groups. [72]

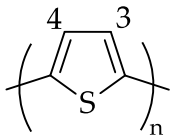

Figure 1.15 — Polythiophene.

The chain length of alkyl substituents is a major characteristic influencing the thermochromic properties. By increasing chain length, the absorption maxima are marked by a large shift accompanied by a decrease in the transition temperature range. These modifications are a result of steric effect which is characterised by a twisting phenomenon of the polymer backbone with fluctuations in temperature. [2] The π-π^* bandgap in most of conjugate PTs structures is relatively small and characterised by a strong absorption bond in the visible region. [79] **Scheme 1.24** illustrates an example of thermochromic PT polymer with a reversible chromic effect from red-violet (20°C) to red-orange (190°C). [80]

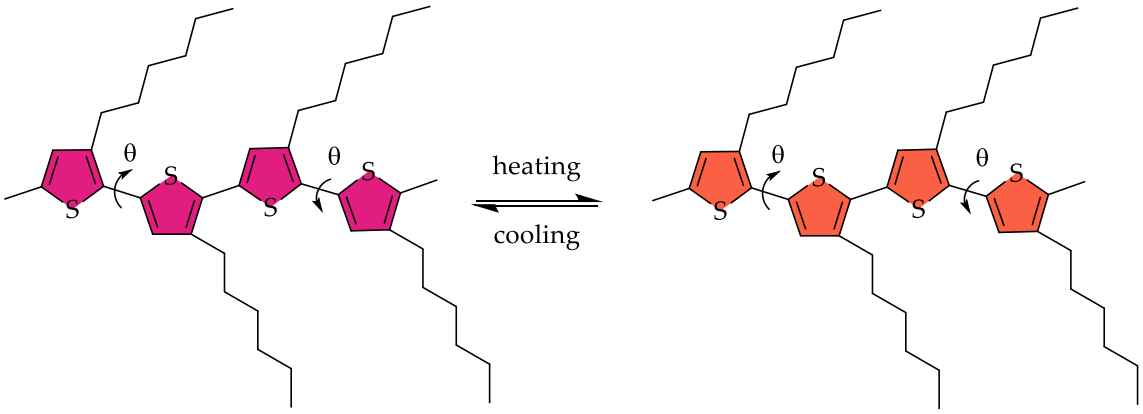

red-violet at 20°C **red-orange at 190°C**

Scheme 1.24 — Reversible colour changes of poly(3-alkylthiophene) with a hexyl group under the action of heat.

Poly(phenylenevinylene)s have also been reported as thermochromic materials with thermochromism depending on the conformational state of the polymer. Polymers of this type display a gradual colour change on heating due to a loss of conjugation. [2] Poly{2,5-bis[3-(N,N-diethylamino)- 1-oxapropyl]-1,4-phenylenevinylene} is an example such a polymer that exhibits its gradual colour transition from 10 to 100°C under the action of heat, and which can be observed under the UV light at 360 nm, **Figure 1.16**. [81] Furthermore, poly[2-(3,7-dimethyloctoxy)-5-methoxy-1,4-phenylene vinylene) was also reported as thermochromic PVA derivative, and its chromism was assigned to reduction of the chain order and the dissolution of polymer aggregates. At gel-to-sol transition in benzene, the polymer went from red to yellow by heating above 35°C. [2,82]

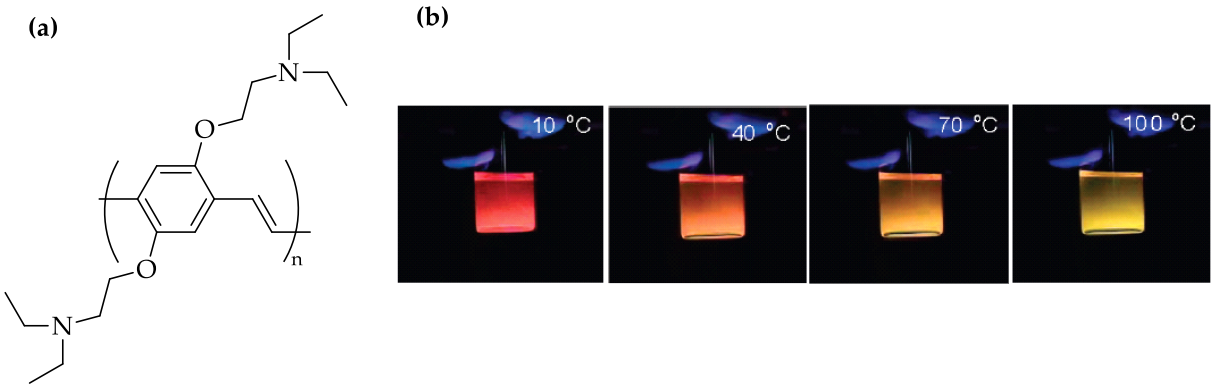

Figure 1.16 — (a) Chemical structure of thermochromic poly{2,5-bis[3-(N,N-diethylamino)- 1-oxapropyl]-1,4-phenylenevinylene}, DAO-PPV. (b) Temperature induced photoluminescence colour changes in a toluene solution of DAO-PPV under UV (360 nm) illumination. Adapted with permission from *J. Phys. Chem. B 2009, 113, 50, 16110–16117*. Copyright 2009 American Chemical Society.

1.10 Miscellaneous compounds

Thermochromism has also been noticed in some indano[l,2-*b*]aziridines. Compounds of this type can undergo a colour change due to the cleavage of aziridine C-C bond to reach the valence azomethyl ylides tautomer through 1,3-dipolar additions, **Scheme 1.25**. As described, l-cyclohexyl-6-(cyclohexylimino)-1a-phenylindano[l,2-b]aziridine (1) undergoes thermal conversion to the tautomeric isoquinoline imine (2). Thermochromism proceeded after rapid heating of **1** in toluene or xylene at 135°C. The compound developed a strong red colour that disappears upon cooling. Moreover, it was also observed that compound **2** is also sensitive to UV light/oxygen exposure, addition of trace quantities of base/acid, and the presence of electron deficient olefins/acetylenes, as the bleaching of the red coloured solution was observed under the action of these constituents. [83–86]

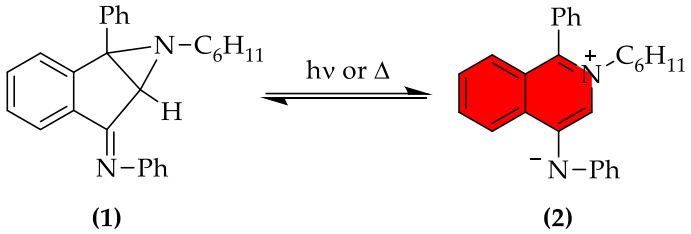

Scheme 1.25 — Reaction responsible for reversible thermochromism and photochromism in aziridines.

4,6,7-tri(alkoxy-substituted phenyl)-l,2,5-thiadiazolo[3,4-c]pyridines (**Figure 1.17**) was also reported to be thermochromic. By grinding its yellow crystals, the material turned into an orange amorphous solid. Then heating and washing process (with a suitable solvent) restored his original state. [83,87]

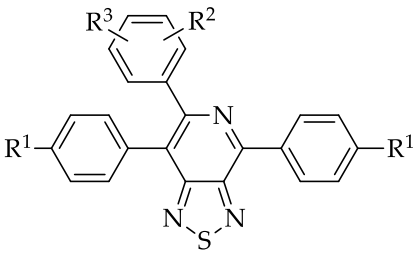

$R^1 = OCH_3, OC_2H_5, OC_4H_9$

$R^2, R^3 = H, OCH_3$

Figure 1.17 — Structure of 4,6,7-tri(alkoxy-substituted phenyl)-l,2,5-thiadiazolo[3,4-c]pyridines.

Thermochromism was also found in *semibullvalenes* and *barbaralanes* both in solution and in solid state. Thermochromism has been associated with different surface energy shapes of ground (shallow double minimum) and excited state (narrow, steep minimum). Semibullvalenetetracarboxylates (1), dicyanosemibullvalene (2), semibullvalene-dicarbonitrile (3) 2,4,6,8-tetraphenylbarbaralane (4) and dicyanodiphenylbarbaralane (5) are the known thermochromic structures belonging to these classes of compounds**, Figure 1.18**. [83,88–90] For example, the thermochromism of **3** from **Figure 1.18** was reported as a reversible colour change from intense red to orange on cooling. [89]

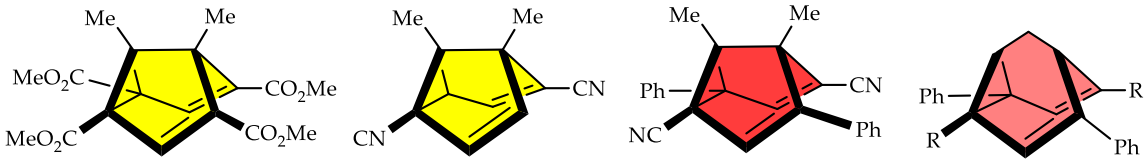

(1) **(2)** **(3)** **(4):** R = Ph; **(5):** R = CN

Figure 1.18 — Thermochromic semibullvalenes (1-3) and barbaralanes (4-5) and their characteristic colours at room temperature.

Thermochromism was also reported in sterically hindered amino-substituted cyclohexadienones, **Scheme 1.26.** The chromic effect was attributed to the C_{spiro}—N bond cleavage and O → N proton transfer. The intramolecular bonding between the hydroxy group and the amino groups leads to a decrease of the C_{spiro}—N bond strength and makes possible its cleavage under the action of heat. 2,6-Di-tert-butyl-4-morpholino-4-(2-hydroxyphenyl)cyclohexadien-2,5-one **(1, Scheme 1.26)** and 4-dimethylamino derivative **(2, Scheme 1.26)** are examples of reversible thermochromic compounds belonging to these derivatives. For example, the absorption of **1** (**Scheme 1.26**) in heptane will reveal maxima at 393 nm and 500 nm on heating. [83,91–93]

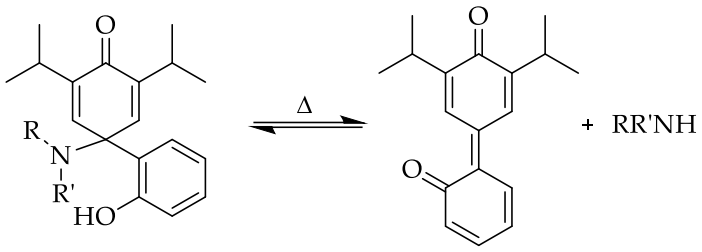

(1): R, R' = -$(CH_2)_2O(CH_2)_2$-

(2): R = R = CH_3

Scheme 1.26 — Thermochromism in hindered amino-substituted cyclohexadiones.

Mannich bases (1) were also reported as thermochromic (and photochromic) materials due to their reversible dissociation into compounds identified as methylenequinones (2) and well known morpholine (3), **Scheme 1.27**. [83,92] The effect is observed only in protic solvents, which demonstrates the participation of the solvent during the proton transfer that occurs before morpholine elimination. Moreover, it was also observed that substituents define the ratio of the two species in ethanol at room temperature. [83]

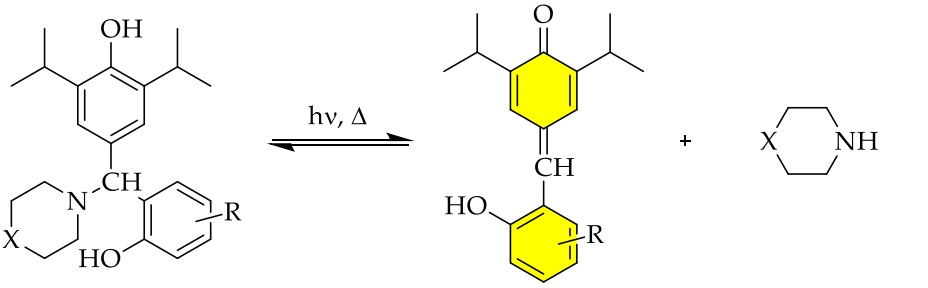

Mannich bases **(1)** methylenequinones **(2)** morpholine **(3)**

X = O, CH_2; R = benzo, Cl, Br

Scheme 1.27 — Thermochromic and photochromic Mannich bases.

2

REVERSIBLE THERMOCHROMIC SYSTEMS BASED ON A NEW LIBRARY OF FLAVYLIUM SPIROLACTONE LEUCO DYES

Abstract

The aim of this work was the design, synthesis, and characterisation of new chromogenic spirolactone dyes based on a 2-phenyl-1-benzopyrylium (flavylium) backbone for further development of thermochromic smart labels. The influence of electron-donating and electron-withdrawing groups on the five synthesised dyes was studied in terms of colour modification, acid-base behaviour and thermochromic properties. By using UV-Vis absorption and emission spectroscopies, molar absorptivity, oscillator strength, Stokes shift, and fluorescence quantum yield were determined for each dye to evaluate the impact on colour and excited state properties of the designed structures. The acid-base behaviour and the ability to evolve towards *leuco* species was assessed by titrations with triethylamine and *N*,*N*-diisopropylethylamine in non-polar and polar aprotic solvents such as acetonitrile and octan-1-ol. In addition, the reversibility of the colour was also evaluated by titrations with polar protic solvents (water and ethanol) and Lewis acids (gallic acid and iron(III) chloride). The numbers of equivalents of base/acid required to reach the *leuco* product and then to reverse the colour were determined by representing the absorption maximum as a function of added base/acid in acetonitrile (water content less than 0.01-v/v). Finally, the thermochromic properties were evaluated in the presence of long-chain organic amines and water-insoluble solvents with melting points close to room temperature. The synthesised compounds can switch between two species if the appropriate conditions are used. Moreover, the tests carried out to assess their thermochromic behaviour concluded that all dyes display thermochromism to some extent. The dyes that have electron-withdrawing groups attached, such as cyano, display stronger chromogenic effects useful for future applications.

2.1 Introduction

Spirolactone dyes are organic compounds that are well-known for their thermochromic properties and are widely used in industry because of their low-cost manufacturing process. They are generally used for displaying applications due to their high colour contrast on different surfaces, and their availability in a broad range of colours. [94] These dyes are often used to produce dynamic colours in products such as mugs, t-shirts, magazines, or toys, but not only. They are also used as sensors (if the temperature accuracy is not so crucial), warning messages, security elements for tickets, smart cards, erasable pens, and documents, or as temperature indicators for products such as beverages, ice-cream, and others. [95–97] The most common thermochromic dyes of spirolactone type are fluorans, crystal violet lactone, spiropyrans and fulgides (**Figure 2.1**), and are the colour formers in a multi-component system. [14]

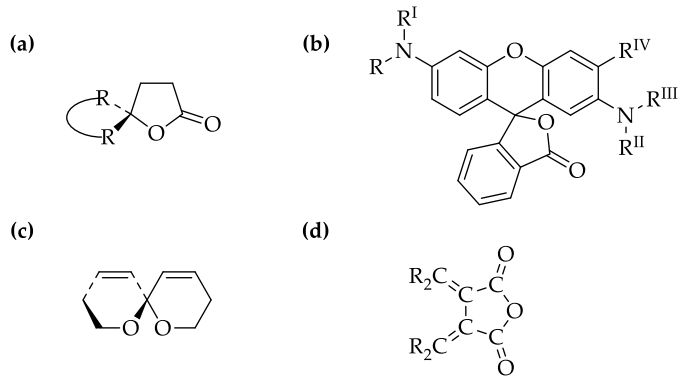

Figure 2.1 — Typical *leuco* dyes; (a) spirolactones, (b) fluorans, (c) spiropyrans, and (d) fulgides.

Sensitive to the changes in pH, the *leuco* dye molecules are alternating between two chemical species, where one is coloured and the other one colourless. The reversible colouration/discolouration of a *leuco* dye system results from the alternate predominance of two competing interactions: one between the *leuco* dye and the colour developer (acid-base reaction), and the other between the colour developer and the solvent (non-covalent interactions). The former usually predominates at lower temperatures, when the solvent solidifies, and the latter in the liquid state, when the colour developer is interacting with the solvent. Typically, the melting point of the solvent controls the temperature at which the colour of the thermochromic composite changes. [95,98–102]

Specifically, spirolactone dyes do not undergo these reactions by themselves, they rather change colour because of a change in pH. In solution, the coloured (protonated) species exists when the pH is more acidic (usually around 4), and the uncoloured (deprotonated) species predominates when the pH is more alkaline. The temperature is only used to shift the equilibrium. [103]

A thermochromic material based on a three-component system capable of changing colour after a phase transition was reported by Raquel Gavara *et al.* in 2010. [38] The system was developed by introducing a flavylium cation with a 2-carboxyphenyl group in position 4 as a new family of *leuco* dyes (as colour former), an organic amine and a suitable solvent (acetonitrile or *n*-pentadecanonitrile). The colour change effect was taking place due to protonation/deprotonation of the carboxylic group upon changing from liquid to solid state, **Scheme 2.1**. The deprotonation reaction was favoured in the liquid state because the solvation entropy

increases, making the proton transfer process to the amine easier. This was a reversible process because once the solid state was reached, the proton returns to the carboxylic moiety stabilising the coloured flavylium cation. [38,104]

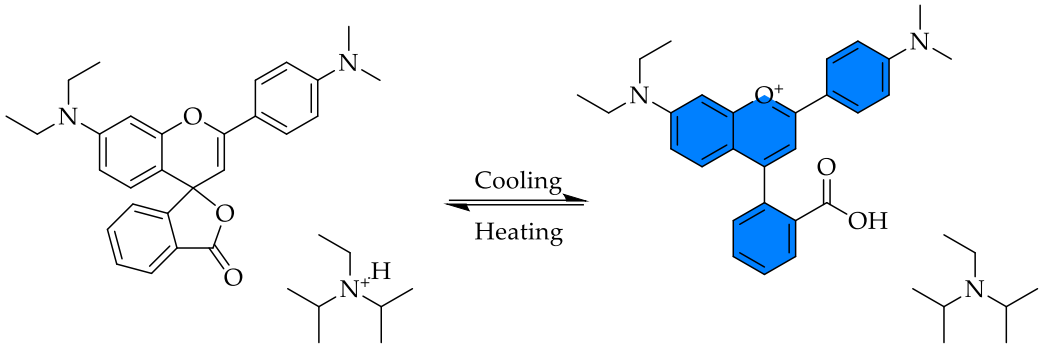

Scheme 2.1 — Phase-change thermochromic system based on a flavylium dye. [38]

As can be seen in **Scheme 2.1**, the above studies were carried out with a flavylium cation having 2 amino substituents attached which developed a blue colour. To our knowledge, it was a first system where a weak base colour developer was used. Yet there were some barriers that hamper applications, namely:

a) the solvents used are not water insoluble or are rather expensive.
b) the study was done only with one compound, limiting greatly the colour palette.
c) it remained unanswered of other flavylium dyes could be used in 3 component thermochromic systems.

Therefore, inspired by the example mentioned above, we have proposed to further study this system by designing a small library of flavylium dyes with electron-donating and electron-withdrawing substituents to evaluate their impact on colours. In addition, we have also proposed to evaluate their thermochromic behaviour in water-insoluble solvents and long-chain organic amines, commonly used in industry [105], that can be further encapsulated and used in the development of thermochromic smart labels.

Here we show that materials composed of dyes with electron-withdrawing groups, such as cyano, exhibited most pronounced colour change effect with a clear transition from colourless to coloured state in other organic solvents, and not restricted to nitriles. [38] For those containing electron-donating groups, such dimethylamine, the switch was not so obvious outside nitrile solvents, as the transition was between two coloured states that exhibited almost the same hue.

2.2 Experimental

2.2.1 Materials and methods

All solvents and chemicals were reagent grade and used as received. Ultrapure Millipore grade water was used, and acetonitrile was dried over molecular sieves, 4 Å. Thin-layer chromatography was run on pre-coated TLC sheets ALUGRAM® Xtra SIL G/UV$_{254}$ or pre-coated TLC sheets ALUGRAM® RP-18W/UV$_{254}$, purchased from Macherey-Nagel. The reverse phase

column was run by using a LiChroprep® RP-18 silica gel (40-63 μm) from Merck. The deuterated solvents (CD_3CN, DMSO-d_6 and DCl) were purchased from Eurisotop. The NMR spectra at 298 K were obtained on a Bruker AMX400 operating at 400 MHz (^1H) and 100 MHz (^{13}C), deuterated solvent signals were used as an internal reference. HR ESI MS analyses were performed on a Bruker maXis UHR ESI-Qq-TOF mass spectrometer in the positive ion mode. Absorption spectra were recorded with a Shimadzu UV-2501PC/Varian Cary 100 Bio spectrophotometer, and fluorescence spectra on a HORIBA iHR320 SPEX Fluorolog 3-22. As for the thermochromic studies, the spectra were recorded on a Cary 5000i coupled to a Varian Peltier temperature controller. A quartz cuvette with a 2 mm optical pathway was used to obtain suitable absorptions from the solid samples. For the thermochromic systems with the transition temperature/colour below room temperature, an DankamHT E995F (DTU6005-0027-SN) with an aluminum plate was used.

2.2.2 Synthesis

*General experimental procedure of compounds **1-5*** :

Syntheses of compounds **1-5** were carried out by heating a solution of 2-[4-(dibutylamin)-2-hydroxybenzoyl] benzoic acid (2.5 mmol) with a corresponding acetophenone (2.5 mmol) in concentrated sulfuric acid (7 mL), at 100°C. The reactions were kept under stirring between 4-8 hours, and the conversion of the reagents was checked by TLC (DCM:MeOH = 9:1). After cooling, the acidic mixture was poured onto an ice bath, and the raw material was isolated by filtration. The final products were obtained either by recrystallisation from mineral acids or separation through reverse phase chromatography (MeOH:H_2O = 1:1) in an overall yield of 25-89%.

*4-(2-Carboxyphenyl)-7-(dibutylamino)-2-(4-(dimethylamino)phenyl) chromenylium perchlorate (**1**)*

^1H NMR 400 MHz, DMSO-d_6, δ (ppm): 88.33 (2H, d, J = 8.9 Hz), 8.16 (1H, d, J = 7.8 Hz), 7.94 (1H, s), 7.84 (1H, t, J = 7.7 Hz), 7.75 (1H, t, J = 7.8 Hz), 7.53 (1H, d, J = 7.5 Hz),7.28 (1H, d, J ~ 2 Hz), 7.15 (1H, dd, J = 7.2 Hz, J ~2 Hz), 7.10 (1H, d, J = 7.2 Hz), 6.93 (2H, bt, J = 9.0 Hz), 3.56 (4H, d, J = 8.4 Hz), 3.19 (6H, s), 1.59 (4H, m), 1.38 (4H, m), 0.94 (6H, t, J = 7.4 Hz). ^{13}C NMR 126 MHz, DMSO-d_6, δ (ppm): 166.76, 166.19, 161.07, 157.33, 154.79, 154.38, 135.96, 132.54, 131.12, 130.63, 130.43, 130.18, 129.88, 128.74, 115.94, 114.87, 114.24, 112.48, 108.88, 96.42, 50.56, 39.53, 29.01, 19.50, 13.81. HRMS: calcd. for $C_{32}H_{37}N_2O_3^+$: 497.2799; found: 497.2796. Yield: (1.24 g), 86%.

*4-(2-Carboxyphenyl)-7-(dibutylamino)-2-(p-tolyl) chromenylium chloride (**2**)*

^1H NMR 400 MHz, DMSO-d_6 plus DCl, δ (ppm): 8.82 (1H, d, J = 7.7 Hz), 8.71 (2H, d, J = 8.0 Hz), 8.38 (1H, t, J = 7.6 Hz), 8.31 (2H, t, J = 7.6 Hz), 8.28 (1H, s), 8.04 (2H, d, J = 8.0 Hz), 7.97 (1H, d, J = 7.5 Hz), 7.88 (1H, d, J = 9.4 Hz), 7.78 (1H, dd, J = 9.4 Hz, J ~2 Hz),7.75 (1H, bs, J ~2 Hz), 4.15 (4H, t, J = 7.9 Hz), 3.02 (3H, s), 2.31 – 2.18 (4H, m), 1.98 (4H, m), 1.53 (6H, t, J = 7.4 Hz). ^{13}C NMR 126 MHz, CD_3CN plus DCl, δ (ppm): 180.33, 167.21, 165.80, 164.57, 160.25, 157.47, 146.70, 136.90, 133.68, 132.16, 131.27, 130.76, 130.46, 128.60, 127.94, 111.13, 97.21, 52.47, 29.93, 21.73, 20.52, 13.96. HRMS: calcd. for $C_{31}H_{34}NO_3^+$: 468.2533; found: 468.2534. Yield: (0.35 g), 25%.

*4-(2-Carboxyphenyl)-7-(dibutylamino)-2-(4-nitrophenyl) chromenylium perchlorate (**3**)*

^{1}H NMR 400 MHz, CD_3CN plus DCl, δ (ppm): 8.44 (2H, d, J = 8.8 Hz), 8.38 (2H, d, J = 8.9 Hz), 8.26 (1H, d, J = 7.8 Hz), 7.84 (1H, t, J = 7.5 Hz), 7.77 (1H, t, J = 7.6 Hz), 7.71 (1H, s), 7.42 (1H, d, J = 7.5 Hz), 7.33 (1H, d, J = 9.6 Hz), 7.25 (1H, dd, J = 9.5 Hz, J = 2.4 Hz), 7.19 (1H, d, J = 2.4 Hz), 3.62 (4H, t, J = 9.4 Hz), 1.69 (4H, m), 1.44 (4H, m), 0.99 (6H, t, J = 7.3 Hz). ^{13}C NMR 126 MHz, CD_3CN plus DCl, δ (ppm): 167.09, 160.94, 160.33, 157.93, 151.18, 136.64, 134.16, 132.07, 131.68, 131.17, 130.44, 129.81, 129.30, 125.50, 120.33, 112.59, 97.53, 52.79, 29.99, 20.63, 14.08. HRMS: calcd. for $C_{30}H_{31}N_2O_5^+$: 499.2227; found: 499.2229. Yield: (0.70 g) 47%.

*4-(2-Carboxyphenyl)-2-(4-cyanophenyl)-7-(dibutylamino)chromenylium perchlorate (**4**)*
^{1}H NMR 400 MHz, CD_3CN plus DCl δ (ppm): 8.29 (2H, d, J = 8.4 Hz), 8.27 (2H, d, J = 7.8 Hz), 8.04 (2H, d, J = 8.3 Hz), 7.84 (1H, t, J = 7.6 Hz), 7.77 (1H, t, J = 7.6 Hz), 7.74 (1H, s), 7.42 (1H, d, J = 7.5 Hz) 7.33 (1H, d, J = 9.6 Hz), 7.24 (1H, dd, J = 9.5 Hz, J = 2.4 Hz), 7.20 (1H, d, J = 2.4 Hz), 3.62 (4H, t, J = 6.5 Hz), 1.70 (4H, m), 1.44 (4H, m), 0.98 (6H, t, J = 7.3 Hz). ^{13}C NMR 126 MHz, CD_3CN plus DCl, δ (ppm): 168.42, 167.20, 163.20, 160.28, 157.65, 138.80, 133.72, 133.31, 132.01, 131.40, 130.89, 130.32, 130.15, 129.36, 128.27, 119.88, 118.26, 111.81, 97.19, 52.49, 29.75, 20.45, 13.90. HRMS: calcd. for $C_{31}H_{31}N_2O_3^+.H_2O$: 497.2435; found: 497.2432. Yield: (1.29 g), 89%.

*4-(2-Carboxyphenyl)-7-(dibutylamino)-2-(4-fluorophenyl) chromenylium hydrogensulfate (**5**)*
^{1}H NMR 400 MHz, CD_3CN plus DCl, δ (ppm): 8.30 (2H, m), 8.26 (1H, d, J = 7.9 Hz), 7.82 (1H, t, J = 7.6 Hz), 7.76 (1H, t, J = 7.6 Hz), 7.71 (1H, s), 7.40 (3H, m), 7.33 (1H, d, J = 9.6 Hz), 7.23 (1H, bd, J = 9.8 Hz), 7.20 (1H, bs), 3.60 (4H, t, J = 8.0 Hz), 1.68 (4H, m), 1.42 (4H, m), 0.97 (6H, t, J = 7.3 Hz). ^{13}C NMR 126 MHz, CD_3CN plus DCl, δ (ppm): 179.33, 173.11, 167.90, 167.26, 165.88, 164.17, 160.37, 157.70, 136.81, 133.70, 132.20, 131.45, 131.39, 131.32, 130.91, 130.48, 130.43, 127.32, 127.30, 119.81, 111.39, 97.27, 52.55, 20.53, 13.96. HRMS: calcd. for $C_{30}H_{31}FNO_3^+$: 472.2282; found: 472.2283. Yield: (0.76 g), 64%.

2.3 Results and discussions

2.3.1 Synthesis

The synthesis of compounds **1-5** was adapted after reference [106], and the general experimental pathway is described **Scheme 2.2.** The dyes were synthesised by carrying out different condensation reactions using an equimolar ratio between the corresponding benzophenone (A) and acetophenone (B). The reactions were run between 4-8 hours in the presence of concentrated sulfuric acid, at 100°C. The final products were isolated either by recrystallisation or by purification through reverse phase chromatography in an overall yield of 25-89%.
Different colours were achieved by attaching to the R position of the B-ring, electron-donating or electron-withdrawing groups, **Table 2.1.** Strong and weak activating/deactivating groups, such as dimethylamine, methyl, nitro, cyano and fluorine were used. Furthermore, various anions like perchlorate (compound 1, 3 and 4), chloride (compound 2) and hydrogensulfate (compound 5) ensured the neutrality of the molecules, the anion's nature was defined by synthetic and purification procedures.

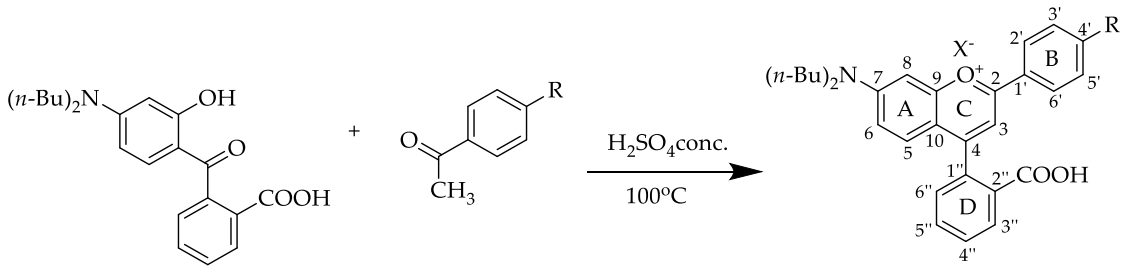

(A) (B) **1-5**

Scheme 2.2 — General experimental pathway used to obtain the spirolactone dyes based on flavylium backbone, compounds 1-5.

Table 2.1 — The attached substituents, compounds 1-5.

Compound	R	X^-	Colour
1	$N(CH_3)_2$	ClO_4^-	blue
2	CH_3	Cl^-	light magenta
3	NO_2	ClO_4^-	purple
4	CN	ClO_4^-	dark magenta
5	F	HSO_4^-	light magenta

2.3.2 Spectrophotometric data

Spectrophotometric characterisation was performed by using absorption and emission spectrophotometry. The data were collected in acidic methanolic solutions at room temperature, for both absorption (**Figure 2.2**) and emission (**Figure 2.3**). Methanol was selected for these measurements because all dyes showed good solubility in polar protic solvents. The acid was added to ensure that all carboxylic moieties were protonated, and the dyes were in their coloured (cationic) form. The spectra show a blue shift of *circa* 70 nm on going from strong (compound 1) to weak (compound 2) donor groups attached on ring B, **Figure 2.3a**. This shift has a visible impact on the colour, as it changes from blue (compound 1) to magenta (compound 2). On the other hand, when strong electron-withdrawing groups like nitro and cyano (compounds 3 and 4) were replaced by a weaker electron-withdrawing group like fluorine (compound 5) the blue shift was smaller, *circa* 14 nm, **Figure 2.3b**. And in this case, the colour changed from purple (compound 3) to various shades of magenta (compounds 4 and 5).
In terms of photophysical parameters, **Table 2.2,** there are substantial differences across the five dyes. Fluorescence quantum yield is high for compound **1**, but low for the other compounds. It is also remarkable that the presence of the amino group at position 4' drastically increases the oscillator strength, making the colour more intense.

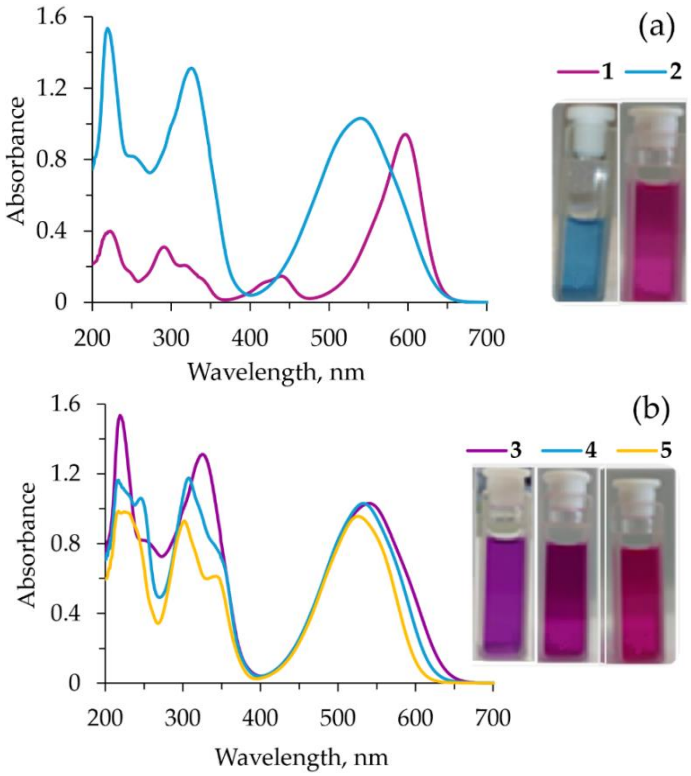

Figure 2.2 — Absorption spectra recorded in acidic methanolic solutions, compounds 1-5. Molar concentration: [1]=1.5×10^{-5} mol dm^{-3}; [2]=7.3×10^{-5} mol dm^{-3}; [3]=6.51×10^{-5} mol dm^{-3}; [4]=6.3×10^{-5} mol dm^{-3}; [5]= 6.43×10^{-5} mol dm^{-3}.

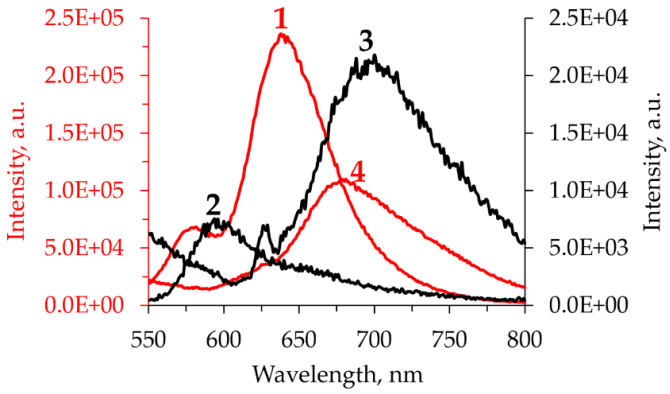

Figure 2.3 — Emission spectra recorded in acidic methanolic solutions, compounds 1-5. Excitation wavelength: 1=525 nm, 2-5=500 nm.

Compounds **3** and **4** display a large Stokes shift, highlighting a high variation of the dipole moment during the electronic transition, expected for a push-pull compound. This is compatible with a charge transfer from ring A (with the amine donor group) to ring B (with an electron acceptor group) during the electronic transition. The oscillator strengths are higher when compared with compound **2** (mainly a typical π,π* transition with no particular CT character). Furthermore, the absorption band is rather broad. For compound **5** a similar trend was noticed, but it was not fluorescent, and the Stokes shift could not be measured.

We observed that amino groups, due to their electron donating properties, increase the oscillator strength and shift the absorption spectra into the red decreasing the HOMO-LUMO energy difference. This also gives rise to high fluorescent quantum yields, since the impact of

non-radiative processes is smaller due to the high oscillator strength (which impacts the radiative rate constant as well). [38] Electron withdrawing groups gives rise to charge-transfer states and resemble the so-called TICT states. [104] TICT molecules are known for their low fluorescence quantum yields in polar solvents such as methanol since the charge transfer excited state is non-fluorescent. The HOMO-LUMO energy difference will be due to a local excited-state (LE), and is essentially π,π* transition that undergoes charge-transfer in the excited state explaining the large Stokes shift. [104] The final result is that compounds **3**, **4** and **5** have basically the same colour and extinction coefficients due to the local π,π* transition, and large Stokes shift and low fluorescent quantum yields due to charge transfer processes in the excited states (absent on compound I). Compound **2** displays only π,π* transitions, small Stokes shifts and low fluorescent quantum yields since the absence of an electron donor/acceptor ring B leads to negligible resonance between ring A and B increasing non-radiative twisting processes in the excited state.

Table 2.2 — Molar absorptivity coefficient (Ɛ), oscillator strength (f), Stokes' shift (SS) and fluorescence quantum yields (Φ) in acidic methanolic solutions, compounds I-V.

Compound	R	λ_{abs}^{max} (nm)	ε (M^{-1} cm^{-1})	f	λ_{em}^{max} (nm)	SS (cm^{-1})	Φ (%)
1	$N(CH_3)_2$	597	83006	0.70	640	1154	88.5
2	CH_3	532	13448	0.21	595	2061	0.7
3	NO_2	540	21568	0.39	698	4192	2.8
4	CN	533	22675	0.39	682	4099	12.4
5	F	526	22778	0.37	—	—	—

2.3.3 Acid-basic behaviour

To evaluate the ability of the synthesised spirolactone dyes to switch between two species (e.g., to move from cationic/coloured species to *leuco*/colourless species) by deprotonation or protonation of carboxylic group [38], **Scheme 2.3**, titrations were performed under various conditions.

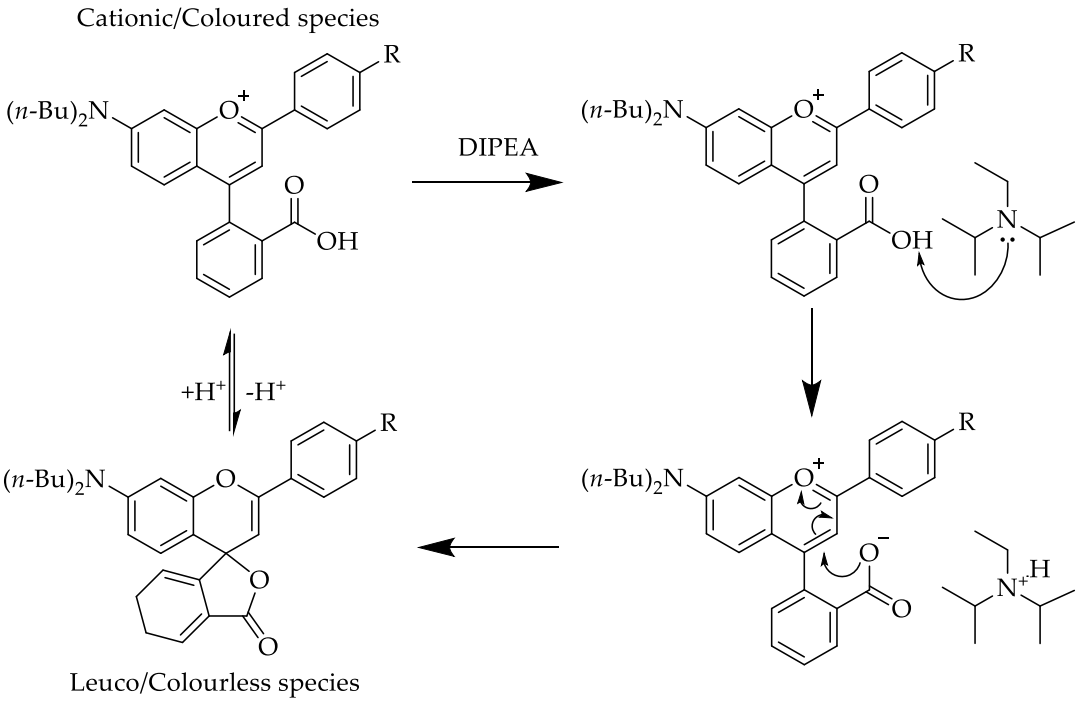

Scheme 2.3 — Proposed acid-basic mechanism of newly flavylium-based dyes in the presence of an organic amine.

In particular, the acid-basic behaviour of dye **1** was checked by performing titrations with different organic bases such as triethylamine (TEA) and *N*,*N*-diisopropylethylamine (DIPEA) in non-polar protic solvent (octan-1-ol) and polar aprotic solvent (acetonitrile, water content 0.01-v/v). Therefore, when titrations were performed in acetonitrile as a function of added TEA, the dye was completely decolourised, **Figure 2.4a**. In contrast, when acetonitrile was replaced with a non-polar protic solvent such as octan-1-ol, the cationic species are strongly stabilised, **Figure 2.4b**. This behaviour may be due to physical interactions through the formation of hydrogen bonds between the carboxyl group of the dye and the hydroxyl group of the solvent or between the hydroxyl group of the solvent and the nitrogen atom of the amine, which prevent the transfer of protons to the amine and thus the formation of the lactone.

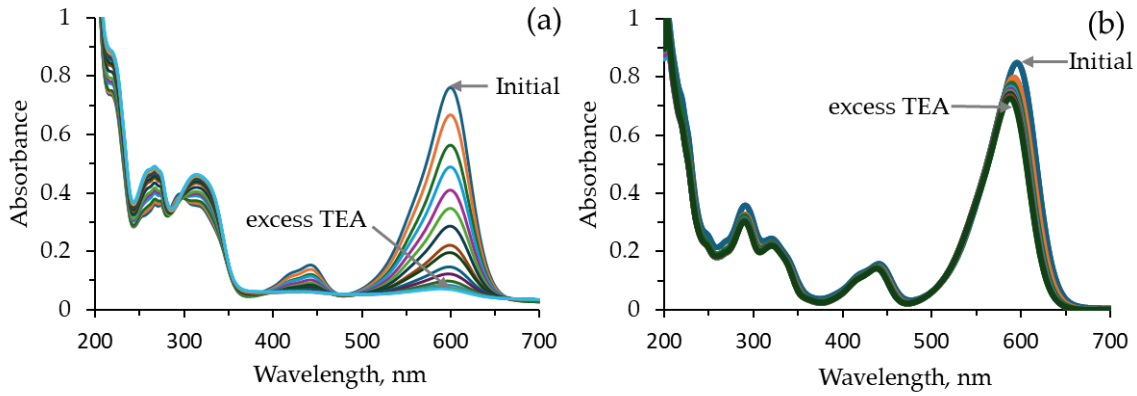

Figure 2.4 — Absorption spectra recorded in acetonitrile (a) and octan-1-ol (b) as a function of added TEA, compound 1.

When TEA was replaced by DIPEA keeping acetonitrile as solvent, the same discolouration effect was observed and, in addition, the presence of a clear isosbestic point appears, **Figure 2.5a**. This point highlights a process involving two species in equilibrium, possibly between the cationic and *leuco* species. By using the data collected in acetonitrile and DIPEA the number of equivalents of base required to fully reach the *leuco* species were determined by representing the maximum absorption of the lowest energy transition as a function of added DIPEA, **Figure 2.5b**. The number of equivalents required to reach the *leuco* species was less than one, **Table** 2.3. This behaviour can be assigned to the slightly basic nature of acetonitrile [107] and therefore, to its ability to behave as a proton acceptor to some extent, therefore an equilibrium between *leuco* and colour species already exists. These results also show the influence of substituents on the lactonisation process, because by having a methyl group as substituent it is much easier to reach the *leuco* species. An amount of 0.7 equivalents of base (compound 2) was enough for a complete conversion process to the uncoloured form.

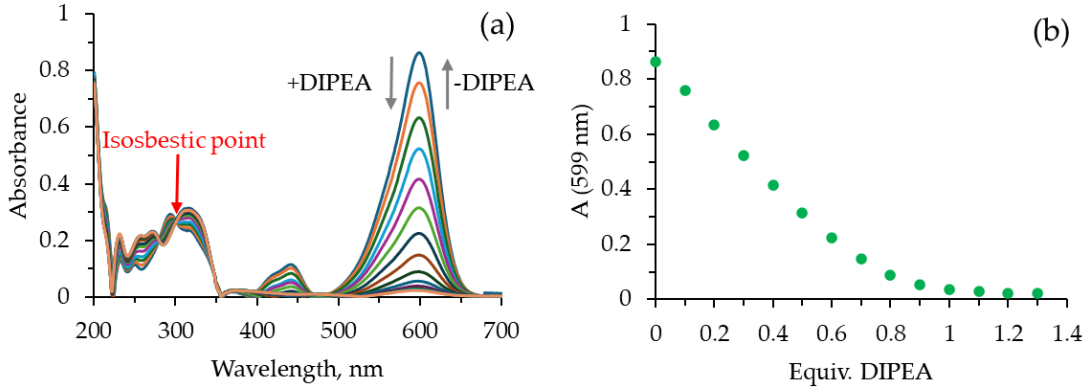

Figure 2.5 — Absorption spectra of compound 1 in acetonitrile as a function of added DIPEA (a); Absorption at λ_{max} as a function of the number of equivalents of added DIPEA (b).

Table 2.3 — Equivalents of added DIPEA in acetonitrile, compounds 1-5.

Compound	R	Absorption (nm)	Equiv. DIPEA
1	$N(CH_3)_2$	599	1.1
2	CH_3	531	0.7
3	NO_2	542	0.9
4	CN	534	0.8
5	F	528	0.8

After reaching the colourless species, various tests were performed to assess the reversibility of the colour changes. Polar protic solvents such as water and ethanol, and acids such as gallic acid and iron(III) chloride (Lewis acid) have been tested, **Figure 2.6**. The colour was reversed completely in the presence of water (Fig. 2.6a) and partially in the presence of ethanol (2.6b). This behaviour is compatible with the higher acidity of water when compared to ethanol. On the other hand, Lewis acids such as iron(III) chloride are also capable to fully reverse the colour (2.6c), while weak acids such as gallic acid only partially revert colour (2.6d). Therefore, Lewis acids are suitable to be used as colour developers for further development of thermochromic systems. As well, for this study by using the data recorded in the presence of iron(III) chloride, **Figure 2.7a**, the equivalents of acid used to fully reverse the colour were determined as an example of a Lewis acid colour developer. The equivalents of used acid were determined by representing the absorption maximum as a function of added iron(III) chloride, **Figure 2.7b**. And according to the data, all dyes required an excess of iron(III) chloride to completely reverse the colour, see **Table 2.4**. This highlights the fact that association equilibrium constants between Fe(III) and these dyes are not high. Previously it was shown that for Crystal Violet Lactone there is a two-step mechanism in which $FeCl_3$ must first dissociate to form $FeCl_2^+$. [108] This step has a rather unfavourable equilibrium constant, which hinders the interaction with the dye to give rise to coloured species. Still, the association constant in the second step is high, and we can effectively use $FeCl_3$ as a colour developer even if we need a molar excess of this reagent.

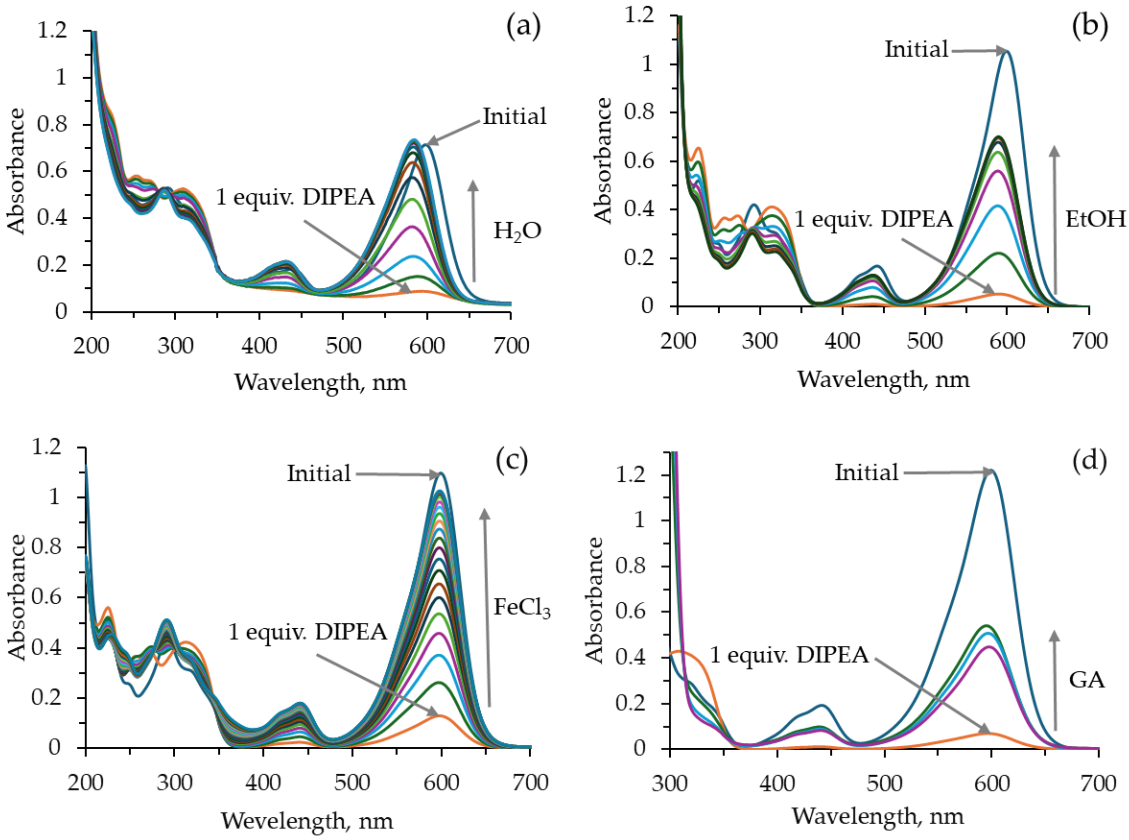

Figure 2.6 — Absorption spectra of compound 1 in acetonitrile and DIPEA, as a function of added water (a), ethanol (b), iron(III) chloride (c), and gallic acid (d).

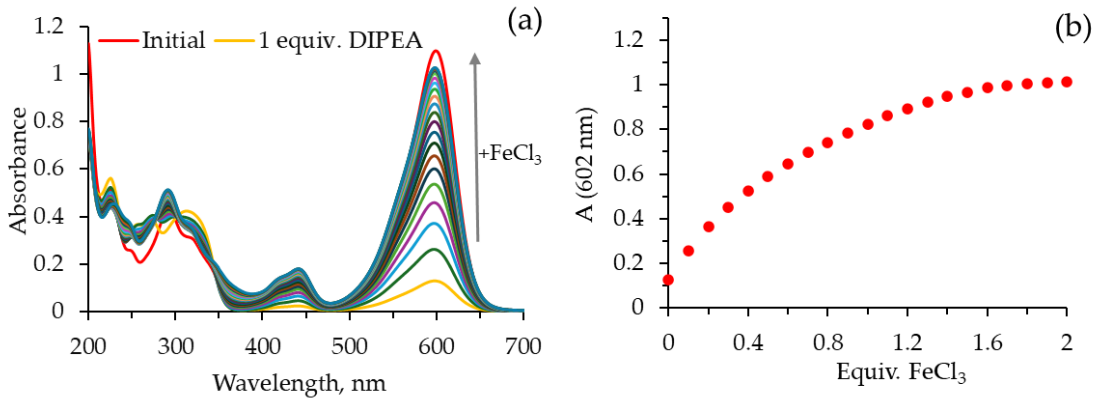

Figure 2.7 — Absorption spectra of compound 1 in acetonitrile and DIPEA (1 Equiv.), as a function of added $FeCl_3$ (a); Absorption at λ_{max} as a function of the number of equivalents of added $FeCl_3$ (b).

Table 2.4 — Equivalents of added acid in acetonitrile, compounds 1-5.

Compound	R	Absorption (nm)	Equiv. $FeCl_3$
1	$N(CH_3)_2$	602	1.6
2	CH_3	529	2.25
3	NO_2	552	3.25
4	CN	529	2.25
5	F	552	3.25

2.3.4 Thermochromic behaviour

The thermochromic behaviour of dyes **1-5** was evaluated by developing a three-component system containing the spirolactone dye, an organic amine, and a suitable solvent. Colour switching was gradual, with an initial colour transition at -11°C and a stronger colour contrast at -20°C when the cooling rate was kept constant at 1°C/min. And as can be seen in **Figure 2.8**, all dyes exhibited to some extent reversible thermochromic behaviour.

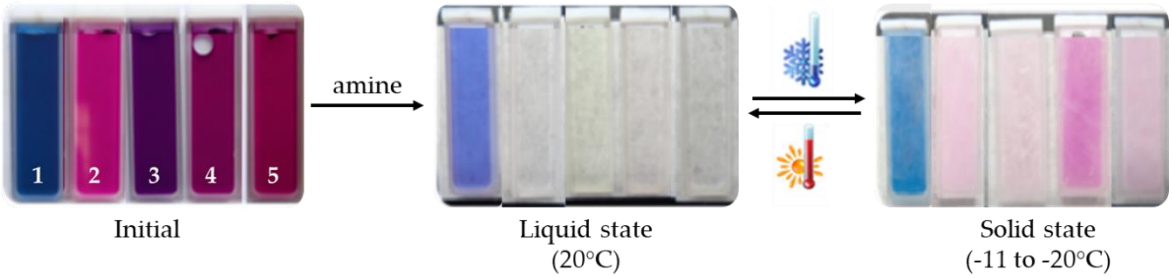

Figure 2.8 — Reversible thermochromic behaviour of compounds 1-5 (~0.07 wt.-%) in acetophenone and N,N-dimethyldodecylamine (1 equivalent).

The initial assessment of thermochromism was performed by using acetophenone (m.p. 20.2°C) as solvent and *N,N*-dimethyldodecylamine as a base, and then, to cover a broad range of switching temperature, other solvents with melting points close to room temperature such as nitrobenzene (5.7°C), acetonaphthone (55-56°C), cinnamonitrile (19-22°C) and benzoyl cyanide (28-31°C) were also used. In the second case, the most balanced properties were obtained for compound **4** when the ratio dye:base was 1:0.5, **Figure 2.9**. Also, for these systems the colour switching was gradual, and the temperatures displayed for the solid state (**Figure 2.9**, bottom side) show the temperature at which the strongest colour contrast was observed. In all the cases the colour transition started with 2, 3°C before the full contrast was displayed. The thermochromic effect took place, because once the solid state is reached, the thermodynamic equilibrium favours the transfer of the proton from the conjugated acid of the amine to the lactone, yielding the coloured opened form, **Scheme 2.4**. [104] Since **4** has the cyano group, this finally points out that thermochromic materials are easier to achieve with the presence of electron-withdrawing groups (push-pull effect), that favour a more labile equilibria between *leuco* and coloured forms. It is also worth noting that the thermochromic behaviour of *leuco* dye system is a complex phenomenon and depends on various factors such as the chemical structure, solvent and developer used. Acetonitrile has already shown similar thermochromic behaviour for all dyes when tested, but this experiment was not presented in the paper as it was not part of the objective of the work. As for compound **4**, we have also tried to explain this peculiar

behaviour by comparing the Hammett constants and Kamlet-Taft parameters between nitrobenzene and benzonitrile, but since the differences were insignificant, we could not draw a clear conclusion. However, we can point out that these small details can make the difference in a such complex system.

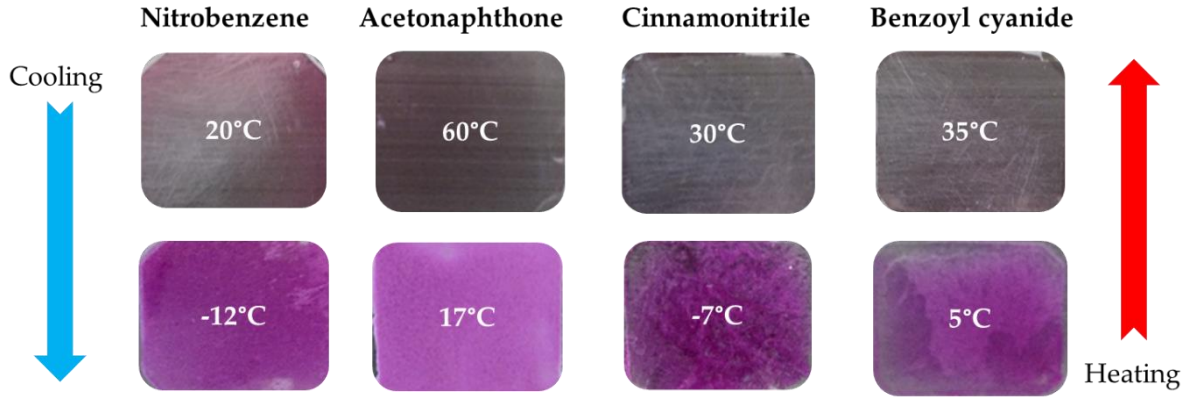

Figure 2.9 — The reversible thermochromic behaviour of compound 4 (~0.05 wt.-%) in nitrobenzene, acetonaphthone, cinnamonitrile and benzoyl cyanide plus N,N-dimethyldodecylamine (0.5 equivalents).

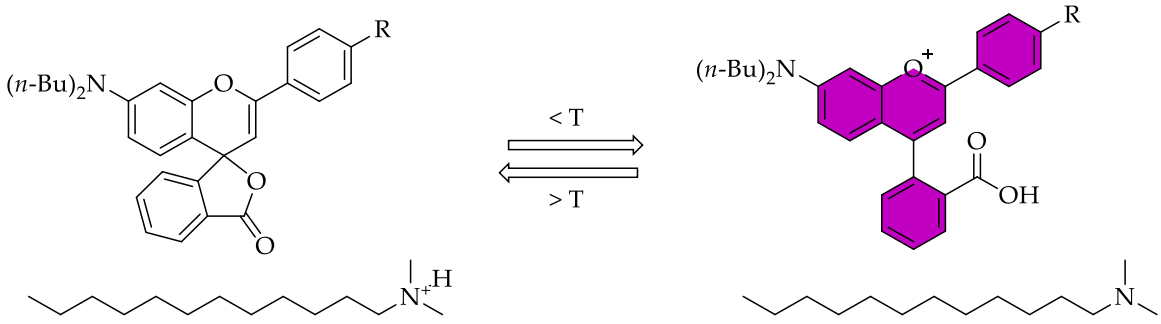

Scheme 2.4 — Schematic molecular representation of the thermochromic spirolactone system based on phase transition.

Furthermore, by using transmittance spectrophotometry the transition temperature and response time were determined for the thermochromic system formulated by compound **4** (0.05 wt.-%), N,N-dimethyldodecylamine (0.5 equivalents) and acetonaphthone. To determine the transition temperature, the absorption spectra were acquired as a function of temperature (**Figure 2.10**) on cooling cycle when going from 60°C to 15°C and the stabilisation time was 5 minutes for every degree. Then, by representing the ΔA:

$$\Delta A = A_{\lambda=550nm} - A_{\lambda=750nm}$$

which accounts for the amount of colour developed subtracting the baseline measured at 750 nm as a function of temperature, the transition point was displayed, **Figure 2.11**.

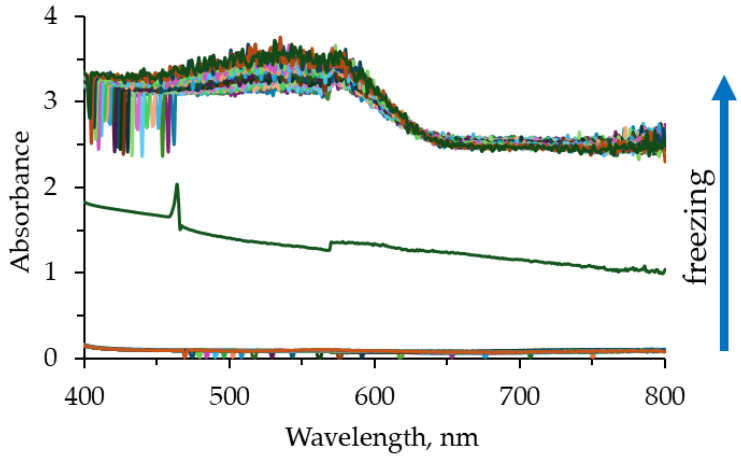

Figure 2.10 — Absorption spectra of compound 4 (~0.05 wt.-%), N,N-dimethyldodecylamine (0.5 equivalents) and acetonaphthone as a function of temperature. The absorption spectra were acquired as a function of temperature on melting and cooling cycle going from 60 to 15°C. The stabilisation time was 5 minutes for every degree.

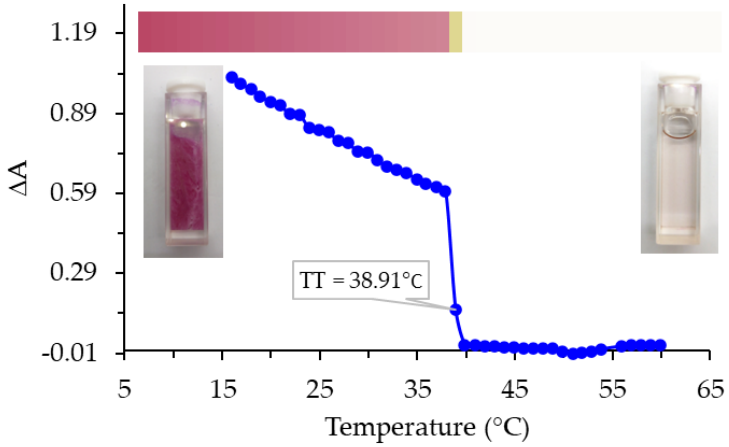

Figure 2.11 — The transition temperature (TT) of thermochromic system formulated by compound 4 (0.05 wt-%), N,N-dimethyldodecylamine (0.5 equivalents) and acetonaphthone. The photos show the material at 20°C and 60°C while the colour bar are the colours calculated from the absorption spectra converted to CIELAB colour co-ordinates.

As for the response time, the transmittance was acquired as a function of time at 530 and 750 nm on both freezing and melting when the temperature was hold at 20°C and 60°C, **Figure 2.12**. At 750 nm we can detect the solvent phase transition (which occurs at 39°C) while at 530 nm we also detect the colour change. The time difference between these two effects was determined to be *circa* 2 minutes for cooling and 0.5 minutes for heating. We give an estimative value for the response time because it is highly dependent of the working conditions. And in our case, it is important mentioning that a 1 cm quartz cuvette with a volume of 0.7 mL was used for data collection.

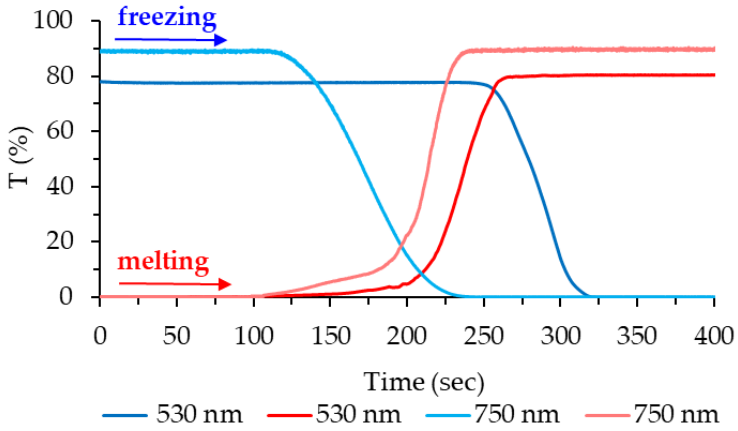

Figure 2.12 — Transmittance spectra of compound 4 (~0.05 wt.-%), N,N-dimethyldodecylamine (0.5 equivalents) and acetonaphthone at 530 and 750 nm on melting and freezing cycle.

Finally, we can point out that the above results showed the advantage of easily adjusting the transition temperature only by changing the solvent, without the need of any structural modification as for other thermochromic systems such as polydiacetylene [109–111], Schiff bases [59,60], bianthrones [4,112], and others [83]. Both solvents with melting points close to room temperature or well below 0°C are suitable to be used, as the colour contrast does not show to be affected in either case. In addition, the results also showed that, if appropriate conditions are used, the thermochromic effect can be quite strong, with a clear transition from colourless to coloured state. These results compare well with classical thermochromic systems [30,99,113] and have a huge potential to be used in industry, since affordable components were used in the design of the experiments. As for the switching time, it occurred in a narrow time range, but it should be pointed out that it highly depends on heat transfer processes not discussed in this work.

2.4 Conclusions

Five chromogenic dyes of spirolactone type based on flavylium backbone have been successfully synthesised, structurally and spectrophotometric characterised. The influence of substituents in position 4' of the flavylium skeleton was studied in terms of colour modification, acid-basic behaviour and thermochromic properties.

The compounds displayed distinct colours in acidic methanolic solutions, going from blue (compound 1)/purple (compound 3) to various shades of magenta (compound 2, 4 and 5). In addition, the photophysical parameters show that amino group, due their electron donor properties, raise the oscillator strength and shift the absorption spectra into the red. Electron-withdrawing groups give rise to charge-transfer states, but their impact on the final colour is much smaller. Furthermore, the spectrophotometric studies showed that all the dyes were able to switch to the *leuco* species when acetonitrile was used as a solvent and DIPEA as a base. Moreover, these results also showed the influence of substituents on the lactonisation process, since by attaching methyl groups it is much easier to reach the *leuco* species, with only 0.7 base equivalents (compound 2) required for a complete conversion process. Furthermore, the thermochromic studies pointed out that thermochromic materials are easier to achieve with the

presence of electron-withdrawing groups (push-pull effect), that favour a more labile equilibria between *leuco* and coloured forms.

3

THERMOCHROMIC SYSTEMS BASED ON A NEW LIBRARY OF 4-ARYLIDENE-SUBSTITUTED FLAVYLIUM DYES IN PLURONIC® F127 THERMORESPONSIVE POLYMERS

Abstract

The aim of this work was the design, synthesis, and characterisation of new chromogenic compounds based on 4-arylidene-substituted flavylium dyes with CH-acidic aryl group at the α-methylene position for further development of thermochromic systems based on Pluronic® F127. The influence of electron-donating and electron-withdrawing groups on the rigid flavylium skeleton (position 4 and 7) was studied in terms of colour modification, acid-base behaviour and thermochromic properties. Spectrophotometric characterisation was performed by absorption and emission spectrophotometry. Absorption spectra were collected in acidic solutions of dichloromethane, and emission in acidic solutions of acetonitrile. By using UV-Vis absorption and emission spectroscopies, molar absorptivity, oscillator strength, Stokes shift, and fluorescence quantum yield were determined for each dye to evaluate the impact on colour and excited state properties of the designed structures. pk_a values were determined by acid-base titration in a mixture of acetonitrile-water (7:3) solutions. Moreover, relying on the ability of Pluronics® F127 triblock thermoresponsive copolymer containing a central hydrophobic block of poly(propylene oxide)-PPO trapped between two hydrophilic parts of poly(ethylene oxide)-PEO, to self-assembly in micelles/gel at the transition temperature, thermochromic systems containing the synthesised 4-arylidene-substituted flavylium dyes were developed. Thermochromic studies show that the dyes with the donor group at position 7 and withdrawing substituent in position 4 exhibited fully reversible colouration.

3.1 Introduction

3.1.1 4-Subsituted flavylium compounds

The 4-substituted flavylium dyes are of great interest as they have shown good stability of the cationic coloured dye be less sensitive to nucleophiles, e.g. water. [114,115] Over the years, various methods have been developed for the synthesis of this type of compounds, but the most widely used was the one reported by Katrizky *et al*. [116,117] This method describes an indirect electrophilic substitution through which the pyrylium unit is customised with various aryl/alkyl functional groups at the 4-position, **Scheme 3.1**.

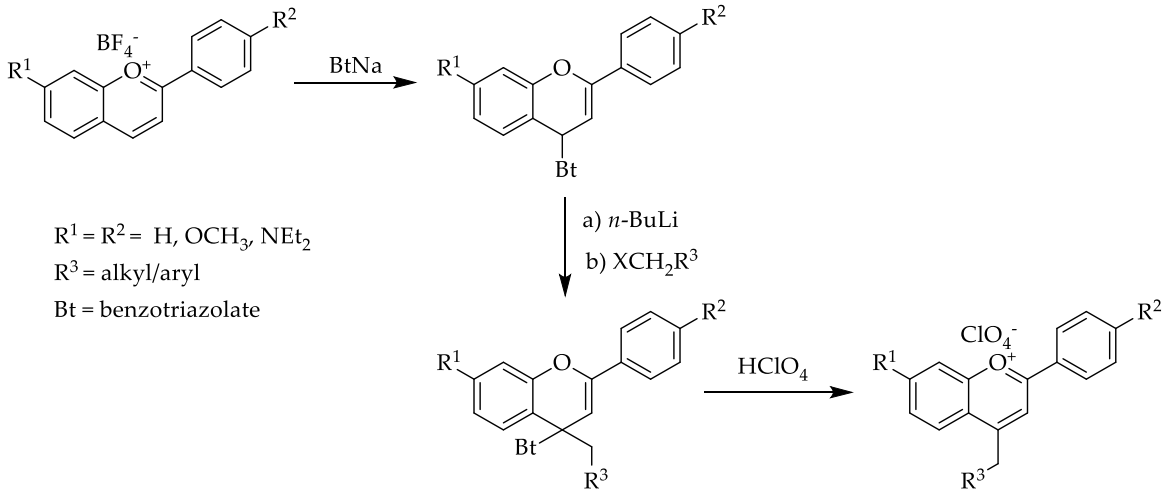

Scheme 3.1 — Synthetic route leading to 4-subsituted flavylium salts. [115]

According to McClelland and Gedge [118], unsubstituted flavylium can undergo various reactions under the action of UV light or pH changes, **Scheme 3.2**. As depicted, at acidic pH, the cationic coloured flavylium dye (AH^+) is the most thermodynamically stable species. Once the pH is brought into the range 5-7, the hydration reaction at the 2- and 4-positions leads to the formation of colourless hemiketals, B_2 and B_4. Then, B_2 species may undergo a tautomerisation reaction, establishing equilibrium with *cis*-chalcone (C_c) species. A slow isomerisation of the double bond transforms the C_c species into its thermodynamically stable *trans*-chalcone (C_t). At more basic pH, the equilibrium broadens by deprotonation of the C_c and C_t chalcones, forming the anion C_c^- and C_t^-, respectively, which can also be interconverted by isomerisation. [115,119]

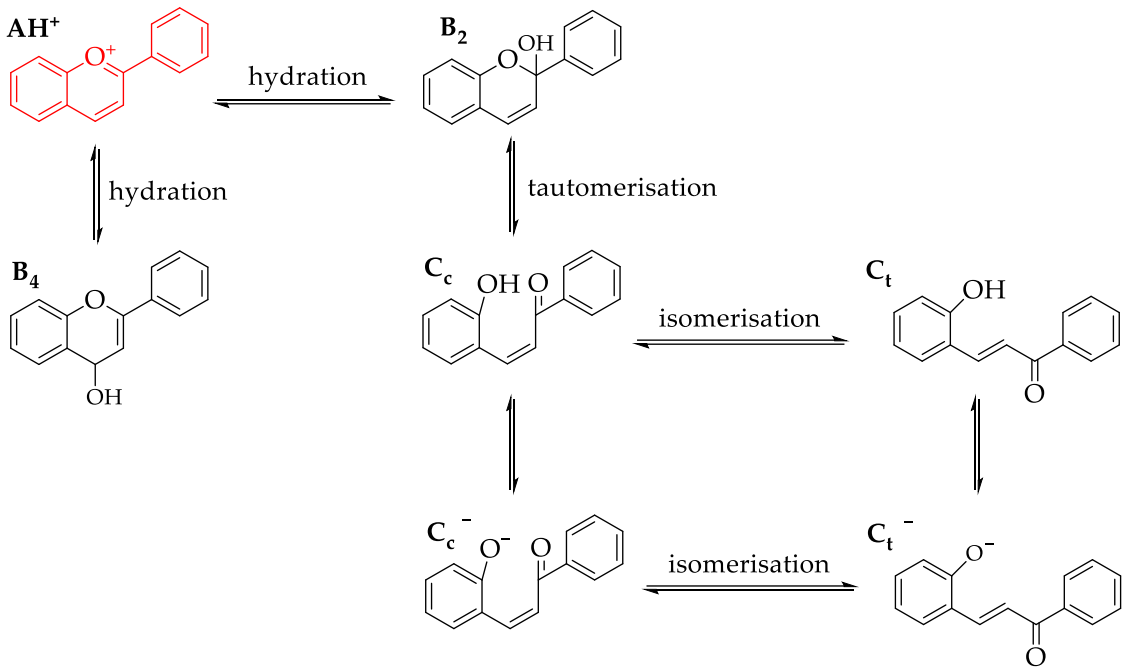

Scheme 3.2 — Structural transformation of unsubstituted flavylium compounds. Structure AH^+ is the cationic coloured flavylium, B_2 and B_4 are the colourless hemiketals, C_c/C_c and C_t/ C_t^- are the *cis*- and *trans*-chalcones along with their corresponding anions. [115,119]

Years later, Grummt and Czerney [120] concluded that an alkyl unit in position 4 leads to a new acid-base equilibrium, as shown in **Scheme 3.3**. This equilibrium describes the transformation of the cationic flavylium (AH^+) into a neutral ethylenic base (D). The alkyl group in 4-position did not prevent a subsequent nucleophilic attack at C_2. [115,121] However, future studies have shown that replacing the alkyl substituent with an aryl unit strongly stabilises the ethylenic base, allowing a resonance delocalisation between the substituent and the flavylium chromophore, which prevent the hydration reaction. [115,122] Furthermore, it was also shown that the hydroxy group in the 4'-position allows the formation of new anionic species (C_c^{2-} and C_t^{2-}) after subsequent deprotonation of the $C_c^-$and C_t^- isomers. [115,121]

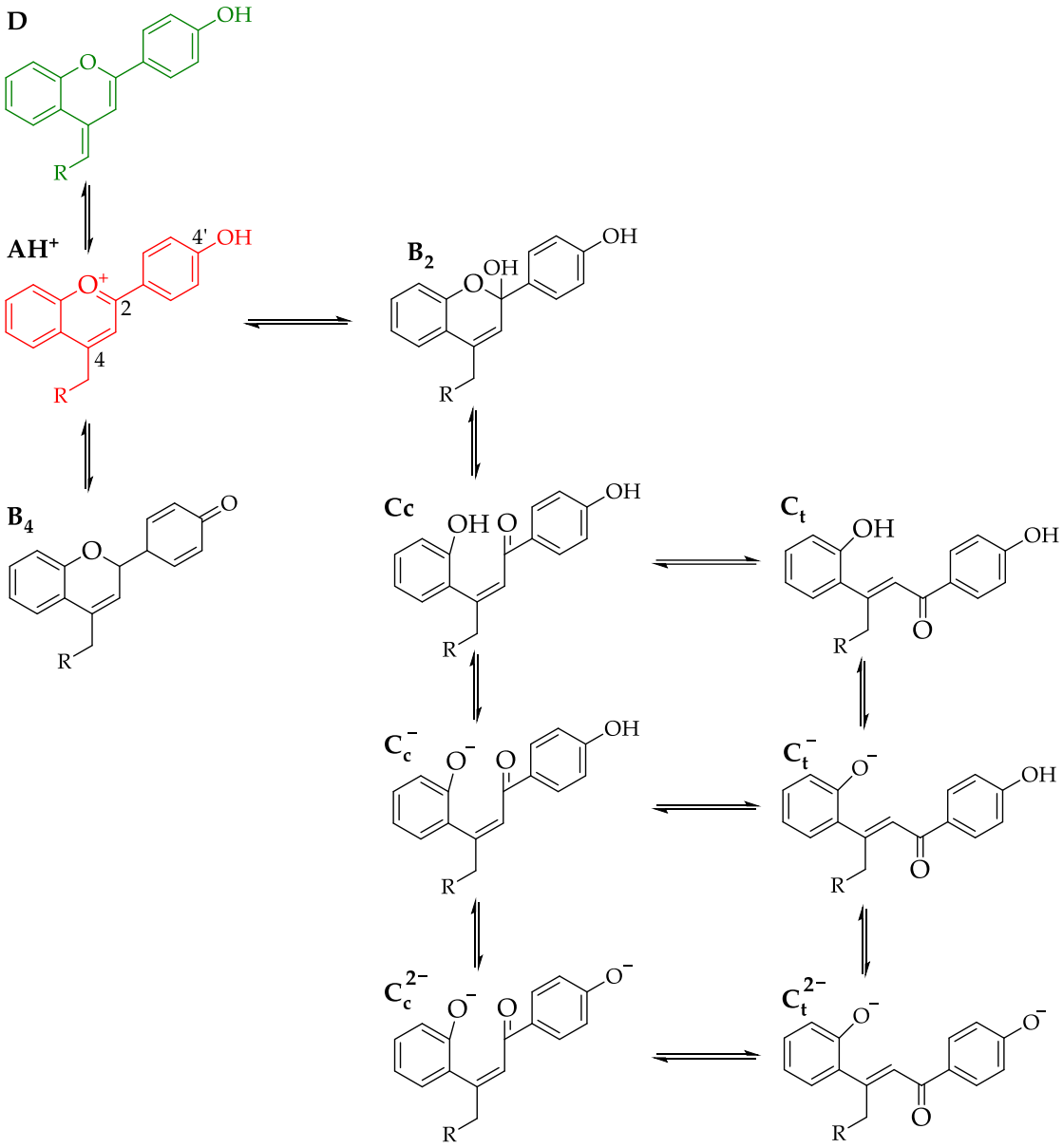

Scheme 3.3 — Structural transformation of 4, 4′ substituted flavylium, 4-alkyl-2-phenyl-4'-hydroxy-benzopyrylium. Structure AH^+ is the cationic coloured flavylium, D its corresponding ethylenic base, B_2 and B_4 are the colourless hemiketals, $C_c/C_c^-/C_t^{2-}$ and $C_t/C_t^-/C_t^{2-}$ are the *cis*- and *trans*-chalcones along with their corresponding anions. [115,119,121]

The ability of flavylium compounds to switch from one state to another under the action of different stimuli makes them excellent candidates for technological applications. [123,124] For example, flavylium systems that can change colour under the action of a thermal stimulus can find use in thermal analysis [125], laser marking [126], and in household appliances or urban engineering. [124,127,128]

3.1.2 Thermoresponsive polymers

Polymers that change their solubility with the environmental temperature are called thermoresponsive. The solubility changes due to the conformational alteration in the polymers structure. The temperature at which the polymeric structure or the solubility modifies is

known as critical solution temperature (CST). In addition, there are two groups of thermoresponsive polymers: either polymers with an upper critical solution temperature (UCST) or polymers with a lower critical solution temperature (LCST). Polymers possessing an UCST behaviour are insoluble in water below this temperature and become soluble above it. Polymers with a LCST are completely miscible in a solvent below the transition temperature and phase separation occurs above it. To date, the most studied thermoresponsive materials are described by poly(*N*-isopropylacrylamide), Pluronics® and poly-(*N*-vinylcaprolactam). [129] Pluronics®, also known as poloxamers, are synthetic tri-block copolymers containing a central hydrophobic block of poly(propylene oxide)-PPO trapped between two hydrophilic blocks of poly(ethylene oxide)-PEO, **Figure 3.1**. They are non-ionic and amphiphilic materials able to interact with hydrophobic surfaces. In aqueous dispersion above a critical micellar temperature (CMT), Pluronics® display self-assembly forming micelles, and when the volume fraction of the micelles is above a critical value, the micelles pack into a face-centered cubic gel, **Scheme 3.4**. [130,131]

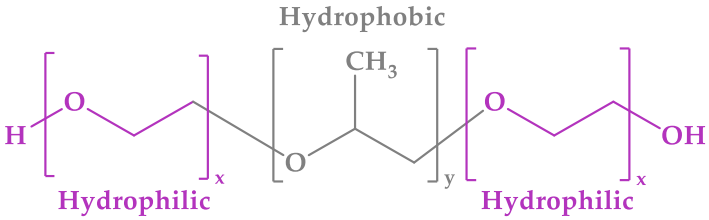

Figure 3.1 — The chemical structure of poloxamer is composed of PPO (y) and PEO (x) blocks. The PPO is poly(propylene oxide) fragment, and PEO are the poly(ethylene oxide) units.

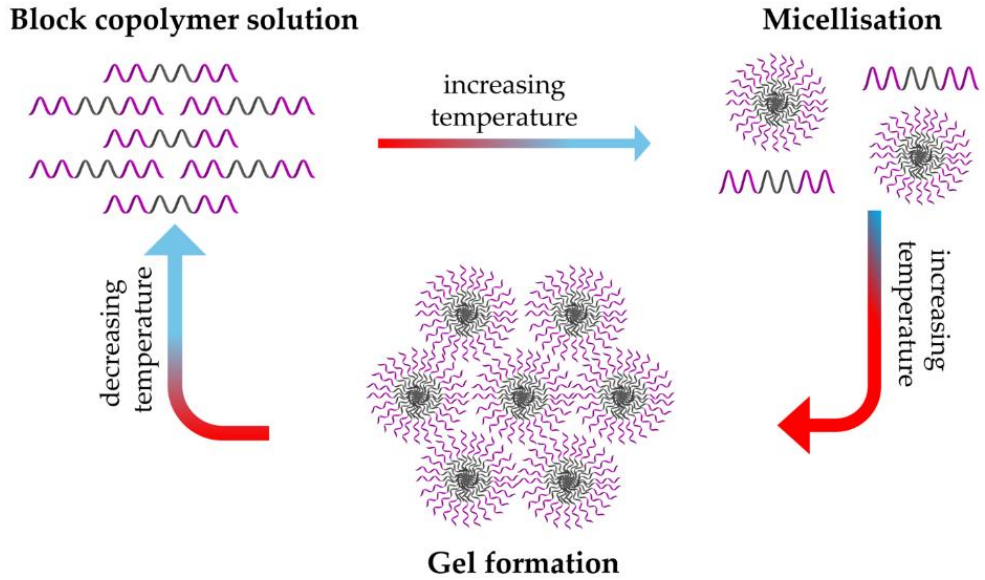

Scheme 3.4 — Self-assembled poloxamers in aqueous solution by increasing the temperature. The scheme was adapted after references [130,131].

The most widely used co-polymer is the commercially available Pluronic® F127 (PF-127). It has attracted much interest due to its reversible sol-gel transition behaviour in aqueous solution, switching from liquid to gel when warmed due to the formation of the micelles. The concentration required to achieve a sol-gel transition range between 15-20% (wt./wt.). Furthermore,

the LCST of PF-127 is at around 30°C, and it is more soluble in cold water (refrigeration temperature), since higher temperatures disrupt the hydrogen bonding (the hydrogen bonding between O from PF-127 and H from water). [129,132]
In 2011, J. Avó *et al.* [122] showed a phase transition thermochromism based on C-H acidity of 4-arylidene-substituted flavylium dyes in PF-127. The preferential partition of the neutral base to the micellar/gel phase allowed the generation of thermochromic systems based on acid-base reactions, characterised by a sharp transition associated with the polymer aggregation, **Scheme 3.4**. [133,134] However, the thermochromic behaviour of systems with other 4-arylidene substituents were not exploited, especially aryl bearing electron withdrawing groups.

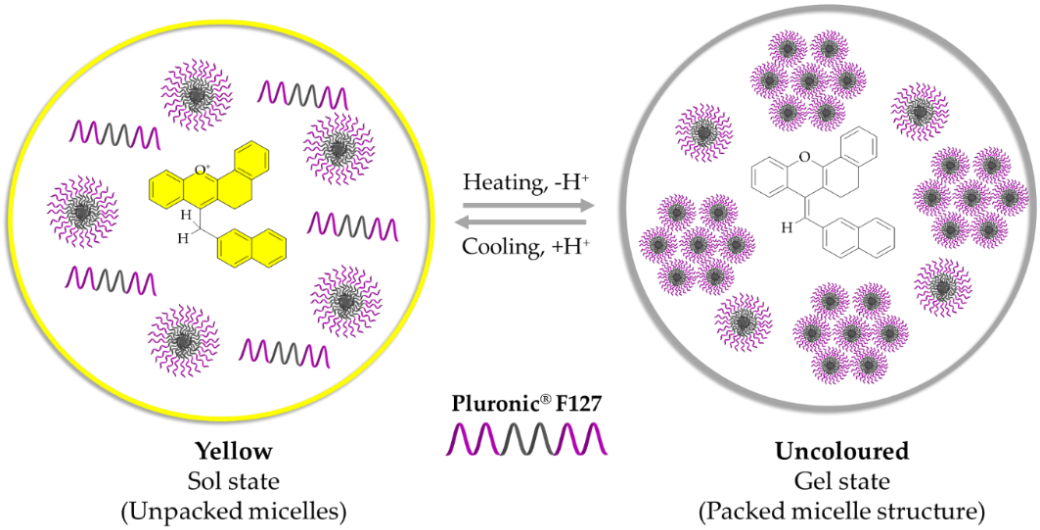

Scheme 3.5 — Proposed mechanism for the thermochromic behaviour of 4-arylidene flavylium dye in Pluronic® F127.

3.2 Experimental

3.2.1 Materials and methods

All solvents and chemicals were reagent grade and used as received. Ultrapure Millipore grade water was used, and acetonitrile was dried over molecular sieves, 4 Å. *n*-Butyllithium (1.6 M in hexane, Sigma Aldrich) was titrated before use with diphenylacetic acid to determine the actual concentration. Thin-layer chromatography was run on pre-coated TLC sheets ALUGRAM® Xtra SIL G/UV$_{254}$ or pre-coated TLC sheets ALUGRAM® RP-18W/UV$_{254}$, purchased from Macherey-Nagel. The deuterated solvents (CD_3CN, DMSO-d_6, CF_3CO_2D and DCl) were purchased from Eurisotop. The NMR spectra at 298 K were obtained on a Bruker AMX400 operating at 400 MHz (^1H) and 100 MHz (^{13}C), deuterated solvent signals were used as an internal reference. HRMS analyses were performed on a Bruker maXis UHR ESI-Qq-TOF mass spectrometer in the positive ion mode. Absorption spectra were recorded with a Shimadzu UV-2501PC/Varian Cary 100 Bio spectrophotometer, and fluorescence spectra on a HORIBA iHR320 SPEX Fluorolog 3-22. As for the thermochromic studies, the spectra were recorded on a Cary 5000i coupled to a Varian Peltier temperature controller. Aqueous solutions containing 20% (wt./wt.) of Pluronic® F-127 at a defined pH were utilised to investigate the thermochromic behaviour between 0°C and 50°C.

3.2.2 Synthesis

Experimental procedures of compounds ***6-10***

7-(3,5-bis(trifluoromethyl)benzyl)-N,N-diethyl-5,7-dihydro-6H-benzo[c]xanthen-10-amine ***(6)***

To a solution of 7-(1H-benzo[d][1,2,3]triazol-1-yl)-N,N-diethyl-5,7-dihydro-6H-benzo[c]xanthen-10-amine (0.518 g, 1.22 mmol) in dry THF (20 mL) at - 78°C, was added *n*-BuLi (0.763 mL, 1.22 mmol, 1.6 M in hexane), dropwise. The solution was stirred at - 78°C for 30 min before adding 3,5-bis(trifluoromethyl)benzyl bromide (0.375 g, 0.224 mL, 1.22 mmol) as a solution in dry THF (5 mL). The solution was warmed to room temperature and left under stirring in an inert atmosphere for 24 hours. Then a saturated aqueous solution of NH_4Cl (30 mL) was added, and the resulting mixture was extracted with diethyl ether (4x30 mL). The organic extracts were washed with brine (2x20 mL) and dried with anhydrous $MgSO_4$, and the solvent was removed by rotary evaporation. The resulting oil was dissolved in acetic acid (10 mL) and left under stirring for 30 minutes. After the addition of water (50 mL), the resulting suspension was extracted with diethyl ether (several times). The collected organic extracts were then washed with saturated aqueous solution of $NaHCO_3$ and deionised water and dried over anhydrous $MgSO_4$. The solvent was removed by rotary evaporation and the resulting oil was recrystallised from methanol to give an orange-red solid.

^{1}H NMR 500 MHz, CD_3CN plus DCl δ (ppm): 8.26 (1H, d, J = 7.8 Hz), 8.05 (1H, d, J = 9.8 Hz), 7.92 (1H, s), 7.75 (2H, s), 7.62 (1H, t, J = 7.5 Hz), 7.55 (1H, t, J = 7.6 Hz), 7.45 - 7.36 (2H, m), 7.21 (1H, d, J = 2.6 Hz), 3.69 (4H, q, J = 7.1 Hz), 3.01 (2H, t, J = 7.5 Hz), 2.90 (2H, t, J = 7.6 Hz), 1.30 (6H, t, J = 7.1 Hz). ^{13}C NMR 101 MHz, CD_3CN plus DCl, δ (ppm): 181.53, 164.00, 159.83, 157.02, 143.01, 140.85, 135.75, 132.98, 132.65, 130.32, 130.04, 129.34, 128.10, 127.05, 126.03, 123.26, 122.55, 120.19, 118.69, 97.25, 47.23, 27.53, 23.99, 13.07. ^{19}F NMR 376 MHz, CD_3CN plus DCl, δ (ppm): - 63.27. HRMS: calcd. for $C_{30}H_{26}F_6NO^+$: 530.1913; found: 530.1914. Yield: (0.06 g), 19%.

(E)-7-(3,5-bis(trifluoromethyl)benzylidene)-10-methoxy-5,7-dihydro-6H-benzo[c]xanthene ***(7)***

To a solution of 1-(10-methoxy-5,7-dihydro-6H-benzo[c]xanthen-7-yl)-1H-benzo[d][1,2,3]triazole (0.533 g, 1.39 mmol) in dry THF (20 mL) at - 78°C, was added *n*-BuLi (0.869 mL, 1.39 mmol, 1.6 M in hexane), dropwise. The solution was stirred at - 78°C for 30 min, before adding 3,5-bis(trifluoromethyl)benzyl bromide (0.428 g, 0.255 mL, 1.39 mmol) as a solution in dry THF (5 mL). The solution was warmed to room temperature and left under stirring in an inert atmosphere for 48 hours. A saturated aqueous solution of NH_4Cl (30 mL) was added, and the resulting mixture was extracted with diethyl ether (3x30 mL). The organic extracts were washed with brine (2x20 mL) and dried with anhydrous $MgSO_4$, and the solvent was removed by rotary evaporation. The resulting oil was dissolved in acetic acid (10 mL) and left stirring for 30 minutes. After the addition of water (50 mL), the resulting suspension was extracted with diethyl ether (5x50 mL). The collected organic extracts were then washed with saturated aqueous solution of $NaHCO_3$ and water and dried over anhydrous $MgSO_4$. The solvent was removed by rotary evaporation and the resulting oil was recrystallised from methanol to yield a crystalline-yellow solid.

^{1}H NMR 500 MHz, CD_3CN plus DCl, δ (ppm): 8.44 (1H, d, J = 7.9 Hz), 8.28 (1H, d, J = 9.4 Hz), 7.92 (1H, s), 7.82 (1H, d, J = 2.5 Hz), 7.78 (1H, t, J = 7.5 Hz), 7.74 (2H, s), 7.64 (1H, t, J = 7.7 Hz), 7.54 – 7.46 (2H, m), 4.12 (3H, s), 3.13 (4H, s). ^{13}C NMR 126 MHz, CD_3CN plus DCl, δ (ppm): 180.77, 169.59, 169.31, 164.58, 158.85, 145.02, 139.76, 137.70, 132.46, 132.19, 130.06, 129.91,

129.44, 129.37, 128.39, 128.30, 127.00, 125.19, 123.01, 121.23, 101.57, 58.24, 26.78, 24.13. ^{19}F NMR 376 MHz, CD_3CN plus DCl, δ (ppm): - 63.26. HRMS: calcd. for $C_{27}H_{19}F_6O_2^+$: 489.1284; found: 489.1286. Yield: (0.16 g), 26%.

(E)-7-(3,5-bis(trifluoromethyl)benzylidene)-5,7-dihydro-6H-benzo[c]xanthene ***(8)***

To a solution of 1-(5,7-dihydro-6H-benzo[c]xanthen-7-yl)-1H-benzo[d][1,2,3]triazole (1.55 g, 4.42 mmol) in dry THF (40 mL) at - 78°C, was added *n*-BuLi (2.95 mL, 4.42 mmol, 1.6 M in hexane), dropwise. The dark-blue solution was stirred at - 78°C for 30 minutes, before adding 3,5-bis(trifluoromethyl)benzyl bromide (1.36 g, 0.812 mL, 4.42 mmol) in dry THF (5 ml). The solution was warmed to room temperature and left under stirring and an inert atmosphere for 48 hours. A saturated aqueous solution of NH_4Cl (140 mL) was then added, and the solvent was removed by rotary evaporation. Subsequently, extractions with diethyl ether (3x90 mL) were carried out. The organic extracts were washed with saturated solution of brine (2x90 mL) and dried over anhydrous $MgSO_4$, and the solvent was removed by rotary evaporation. The resulting oil was dissolved in concentrated acetic acid (50 mL) and kept under stirring for 30 minutes. After the addition of water (240 mL) a yellow precipitate was filtered off. The final product was isolated as yellow needles from methanol.

^{1}H NMR 500 MHz, CD_3CN plus DCl, (δ ppm): 8.56 (1H, d, J = 8.0 Hz), 8.35 (2H, d, J = 8.75 Hz), 8.27 (1H, t, J = 7.65 Hz), 7.96 - 7.91 (2H, m), 7.86 (1H, t, J = 7.5 Hz), 7.76 (2H, s), 7.68 (1H, t, J = 7.7 Hz), 7.58 (1H, d, J = 7.7 Hz), 3.29 – 3.24 (2H, m), 3.20 (2H, m). ^{13}C NMR 101 MHz, CD_3CN plus DCl, δ (ppm): 180.15, 172.61, 165.34, 155.57, 146.82, 139.26, 139.16, 132.62, 132.29, 132.02, 131.34, 130.38, 130.01, 129.77, 129.67, 127.83, 126.91, 125.74, 122.36, 120.72, 26.79, 24.77. ^{19}F NMR 376 MHz, CD_3CN plus DCl, δ (ppm): - 63.65. HRMS: calcd. for $C_{26}H_{16}F_6O$: 458.1105; found: 458.1086. Yield: (0.87 g), 43%.

(E)-N,N-diethyl-7-(naphthalen-2-ylmethylene)-5,7-dihydro-6H-benzo[c]xanthen-10-amine ***(9)***

To a solution of 7-(1H-benzo[d][1,2,3]triazol-1-yl)-N,N-diethyl-5,7-dihydro-6H-benzo[c]xanthen-10-amine (0.560 g, 1.33 mmol) in dry THF (20 mL) at - 78°C, was added *n*-BuLi (0.83 mL, 1.33 mmol, 1.6 M in hexane), dropwise. The solution was stirred at - 78°C for 30 min, before adding 2-bromomethyl naphthalene (0.294 g, 1.33 mmol) as a solution in dry THF (5 mL). The solution was warmed to room temperature and left under stirring in an inert atmosphere for 48 hours. Then a saturated aqueous solution of NH_4Cl (30 mL) was added, and the resulting mixture was extracted with diethyl ether (4x50 mL). The organic extracts were washed with brine (2x20 mL) and dried over anhydrous $MgSO_4$, and the solvent was removed by rotary evaporation. The resulting oil was dissolved in acetic acid (15 mL) and left under stirring for 30 minutes. After the addition of water (50 mL), the resulting suspension was extracted with diethyl ether (5x100 mL). The organic extracts were then washed with saturated aqueous solution of $NaHCO_3$ and water and dried over anhydrous Na_2SO_4. The solvent was removed by rotary evaporation and the resulting oil was recrystallised from methanol to yield the final product as yellow-brown solid.

^{1}H NMR 500 MHz, CD_3CN plus DCl, δ (ppm): 8.26 (1H, d, J = 7.8 Hz), 8.13 (1H, d, J = 9.7 Hz), 7.86 (2H, m), 7.74 – 7.68 (1H, m), 7.61 (1H, t, J = 7.5 Hz), 7.57 – 7.50 (2H, m), 7.49 – 7.33 (6H, m), 3.67 (4H, q, J = 7.2 Hz), 3.00 (4H, s), 1.29 (6H, t, J = 7.1 Hz). ^{13}C NMR 126 MHz, CD_3CN plus DCl, δ (ppm): 180.84, 163.17, 162.17, 159.19, 156.32, 142.48, 135.09, 135.06, 134.33, 133.07, 129.89, 129.51, 129.41, 128.78, 128.37, 128.28, 127.66, 127.62, 127.52, 127.35, 126.96, 126.49, 122.87,

119.50, 119.42, 46.69, 27.08, 23.42, 12.58. HRMS: calcd. for $C_{32}H_{29}NO$: 443.2249; found: 443.2231. Yield: (0.199 g), 34%.

10-methoxy-7-(naphthalen-2-ylmethyl)-5,6-dihydrobenzo[c]xanthen-12-ium perchlorate ***(10)***
To a solution of 1-(10-methoxy-5,7-dihydro-6H-benzo[c]xanthen-7-yl)-1H-benzo[d][1,2,3]triazole (0.93 g, 2.44 mmol) in dry THF (20 mL) at - 78°C, was added *n*-BuLi (1.62 mL, 2.44 mmol, 1.6 M in hexane), dropwise. The solution was stirred at - 78°C for 30 min, before adding 2-bromomethyl naphthalene (0.54 g, 2.44 mmol) as a solution in dry THF (5 mL). Subsequently, the solution was warmed to room temperature and left stirring under in an inert atmosphere for 48 hours. Then a saturated aqueous solution of NH_4Cl (50 mL) was added, and the solvent was removed by rotary evaporation. The resulting mixture was then extracted with diethyl ether (5x50 mL). The organic extracts were washed with brine (2x40 mL) and dried with anhydrous $MgSO_4$, and the solvent was removed by rotary evaporation. The resulting oil was dissolved in acetic acid (30 mL) and left under stirring for 30 minutes. After the addition of water (100 mL), the resulting suspension was extracted with diethyl ether (3x100 mL) and the organic extracts were washed with saturated aqueous solution of $NaHCO_3$ and water and dried over anhydrous $MgSO_4$. The solvent was removed by rotary evaporation, and the resulting oil was first recrystallised from diethyl ether/methanol, and then from ethanol/$HClO_4$ 70% (*circa* 4 mL). Eventually, the final product was isolated as orange powder after washing with cold ethanol (carefully washed) and hexane (well washed).
^{1}H NMR 500 MHz, CD_3CN plus DCl, δ (ppm): 8.52 (1H, d, J = 8.0 Hz), 8.36 (1H, s), 8.16 (2H, s), 8.04 (1H, d, J = 8.3 Hz), 7.91 (2H, d, J = 9.4 Hz), 7.83 (1H, t, J = 7.6 Hz), 7.76 (2H, d, J = 8.6 Hz), 7.69 (1H, t, J = 7.8 Hz), 7.62 (1H, t, J = 7.6 Hz), 7.53 (1H, d, J = 7.9 Hz), 7.42 (1H, d, J = 9.4 Hz), 4.15 (3H, s), 3.17 – 3.09 (4H, m). ^{13}C NMR 126 MHz, CD_3CN plus DCl, δ (ppm): 192.98, 178.14, 171.44, 170.08, 161.31, 159.69, 145.78, 138.60, 137.74, 135.81, 133.39, 132.84, 131.51, 130.83, 130.67, 130.52, 129.78, 128.98, 128.71, 128.62, 127.03, 125.04, 123.78, 123.61, 101.83, 58.47, 26.76, 24.47. HRMS: calcd. for $C_{29}H_{23}O_2^+$: 403.1693; found: 403.1694. Yield: (0.41 g) 33%.

3.3 Results and discussion

3.3.1 Synthesis

The synthesis of compounds **6-10** was adapted after references [133,135], and the general experimental pathway is described in **Scheme 3.6**. As can be seen, functionalisation of the flavylium core with different aryl moieties in position 4 involved several steps. In step 1, condensation reactions between tetralone and the corresponding aldehydes were carried out to obtain the corresponding flavylium intermediate salts. Then, customisation of the 4-position was achieved by an indirect electrophilic substitution (step 2) that allowed the formation of a carbanion after lithiation at -78°C which subsequently triggered a nucleophilic attack on the corresponding alkyl halide (step 3). Finally, without isolation, the intermediates were treated with strong or weak mineral acids to induce removal of the benzotriazole moiety and to reach the target compounds in an overall yield of 19-43%. The structures of all isolated compounds were characterised by 1D, 2D NMR and HRMS analysis. ^{1}H NMR was also used to identify which one of dye species was isolated. A single proton to the 11-position confirmed the isolation of the ethylenic base, whereas two protons at α-methylene position showed the isolation of the cationic flavylium. Additionally, the proton (s) at the 11-position was observed in spectra

collected without DCl. When DCl was added to the sample, it facilitated the replacement of the H^{11} proton (s) with deuterium.

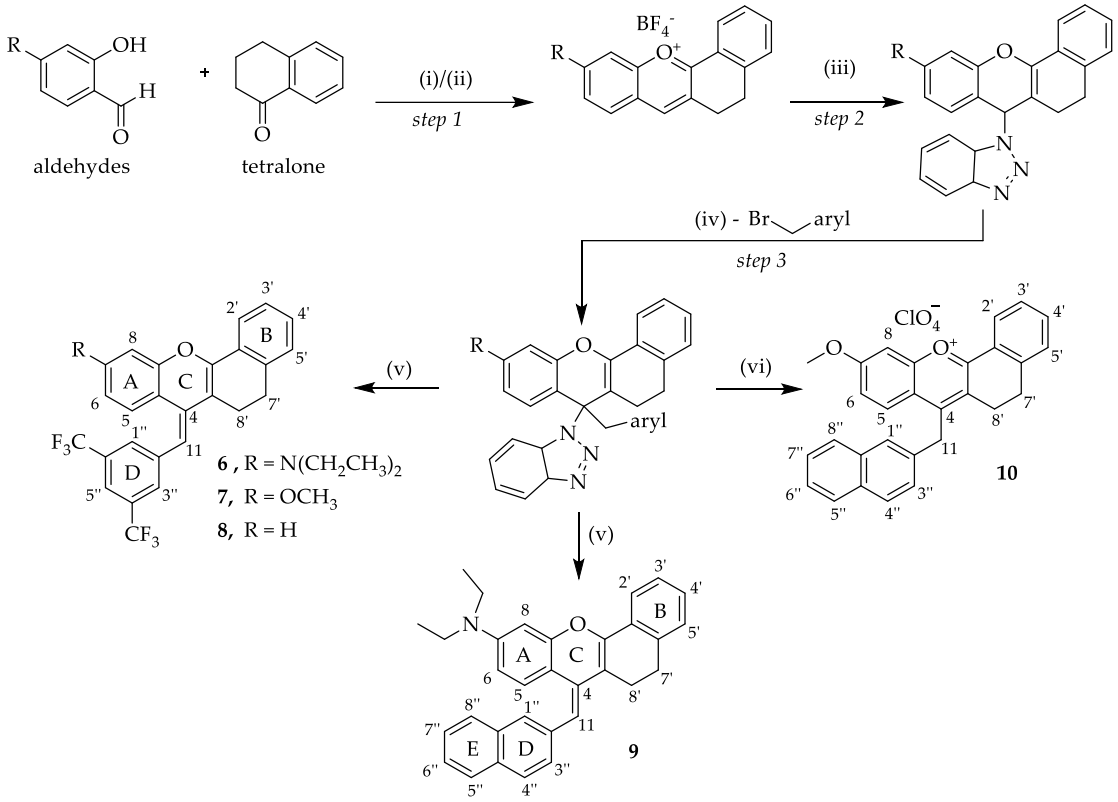

Scheme 3.6 — Synthesis of 4-arylidene-substituted flavylium derivatives: (i) acetic acid, HBF_4 48%; (ii) acetic acid, acetic anhydride and HBF_4 48%; (iii) benzotriazole, sodium hydride, THF_{dry}; (iv) *n*-butyl lithium, benzylic halide, THF_{dry}; (v) acetic acid/water; (vi) acetic acid, $HClO_4$ 70%. Compounds **6-10** were isolated in neutral ethylenic base species, and compound 10 as a cationic flavylium salt.

3.3.2 Spectrophotometric characterisation

The spectrophotometric characterisation was performed by absorption (**Figure 3.2**) and emission (**Figure 3.3**) spectrophotometry. Absorption spectra were collected in acidic solutions of dichloromethane, whereas emission in acidic solutions of acetonitrile. The HCl was added to ensure that the dyes were in their cationic form. Examination of the absorption spectra indicate that substituents at position 4 have minimal influence on the ultimate colours (see compounds 6+9 and 7+10, **Figure 3.2)**. Regarding the substituents of position 7, the spectra show a blue shift of *circa* 120 nm on going from strong (compound 6) to weak donor (compounds 8) groups, **Figure 3.2**. This change has a visible impact on the colour, as it changes from purple (compound 6) to yellow (compounds 7 and 8). A similar behaviour was observed for the dyes with methyl naphthalene unit at position 4. However, in this case the blue shift was smaller, *circa* 80 nm, and the shades were slightly different with a change from magenta (compound 9) to a bright yellow (compound 10). Moreover, the absorption of compounds 6 and 9 presented a particular behaviour, exhibiting two shoulders in the visible region at 543/570 nm (compound 6) and 536/563 nm (compound 9). All dyes showed low (or residual) emission (**Figure 3.2**), which typically is not characteristic for flavylium-based dyes. This effect might be caused by aryl substituents in the 4-position. Similar behaviour has been observed in other compounds,

where it was noted that the aryl group in the 4-position reduces the emission compared to the alkyl group. [115]

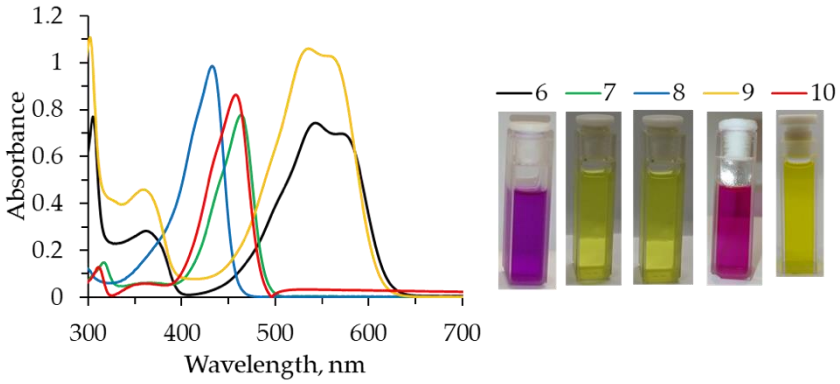

Figure 3.2 — Absorption spectra recorded in solutions of dichloromethane acidified with HCl, compounds 6-10. Molar concentration: [6]=2.46×10^{-5} mol dm^{-3}; [7]=8.8×10^{-6} mol dm^{-3}; [8]=3.09×10^{-5} mol dm^{-3}; [9]=4.22×10^{-5} mol dm^{-3}; [10]= 2.24×10^{-5} mol dm^{-3}.

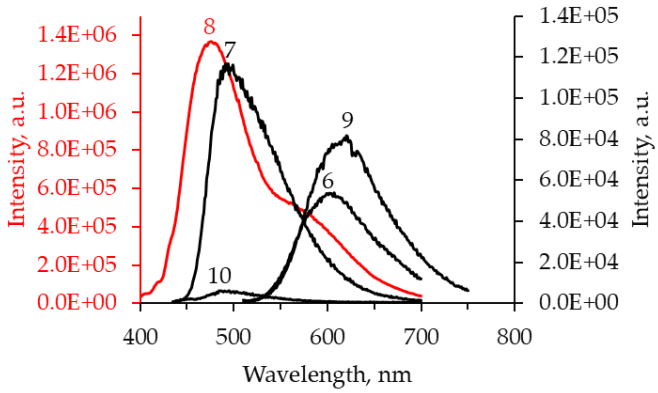

Figure 3.3 — Emission spectra were recorded in solutions of acetonitrile acidified with HCl, compounds 6-10. Excitation wavelength: 6,9=500 nm; 7,10=435; 8=382 nm.

Regarding the photophysical parameters (see **Table 3.1**), it can be observed methoxy group at position 7 (compounds 7 and 10) increases the oscillator strength and extinction coefficient, thereby producing the strongest colour in dyes 7 and 10. Moreover, it can be also noted that all the compounds exhibited a large Stokes shift (except 10, which was not emissive), highlighting a large dipole moment variation during the electronic transition, as expected for a push-pull compound.

Table 3.1 — Molar absorptivity coefficient (ε), oscillator strength (f), Stokes' shift (SS), and fluorescence quantum yields (Φ) in acidic solution of dichloromethane, compounds 6-10.

Compound	R	λ_{abs}^{max} (nm)	ε (M^{-1} cm^{-1})	f	λ_{em}^{max} (nm)	SS (cm^{-1})	Φ (%)
6	$N(CH_2CH_3)_2$	543	31151	0.42	604	3444	0.59
7	OCH_3	463	93334	0.83	499	2948	10.8
8	H	433	28743	0.39	476	5170	0.16
9	$N(CH_2CH_3)_2$	536	25634	0.35	624	3974	1.0
10	OCH_3	458	40931	0.43	—	—	—

3.3.3 Acid-base behaviour

To evaluate the ability of the synthesised dyes to switch between two species (e.g., to move from cationic to ethylenic base species, which is of high interest in terms of thermochromism) by deprotonation of *α*-methylene group of the attached substituents in position 4, **Scheme 3.7**, titrations in acetonitrile-water (7:3) were performed after 1h equilibration time at 20°C. A mixture of acetonitrile-water was used as a solvent due to poor solubility of the dyes in water or any other polar solvent.

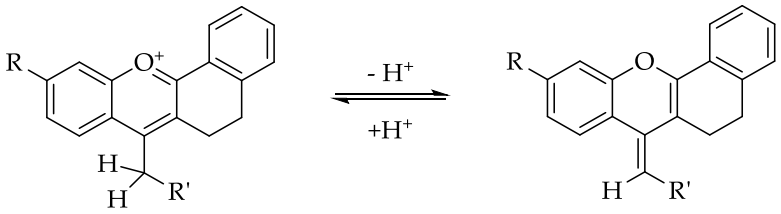

Cationic species Ethylenic base species

Scheme 3.7 — Acid–base equilibrium involving deprotonation of a C–H bond in flavylium compounds. [115,120,122]

All spectra showed a decrease in absorption maximum in the 400-600 nm and 250-300 nm regions as the pH increased. Which was accompanied by an increase in absorption maximum in the 300-400 nm region (refer to **Figure 3.4**). This behaviour can be explained by the reversible transformation of the strongly coloured cationic flavylium into the corresponding ethylenic base (see **Scheme 3.7**). This conversion is also supported by the presence of the clear isosbestic point, which emphasises the existence of an equilibrium between two species, probably an equilibrium between the cationic dye and its ethylenic base counterpart. [115,120] The latter being the main species at pH higher than 8.5, 5, 6.5 and 5 for compounds 6, 7, 9 and 10, respectively.

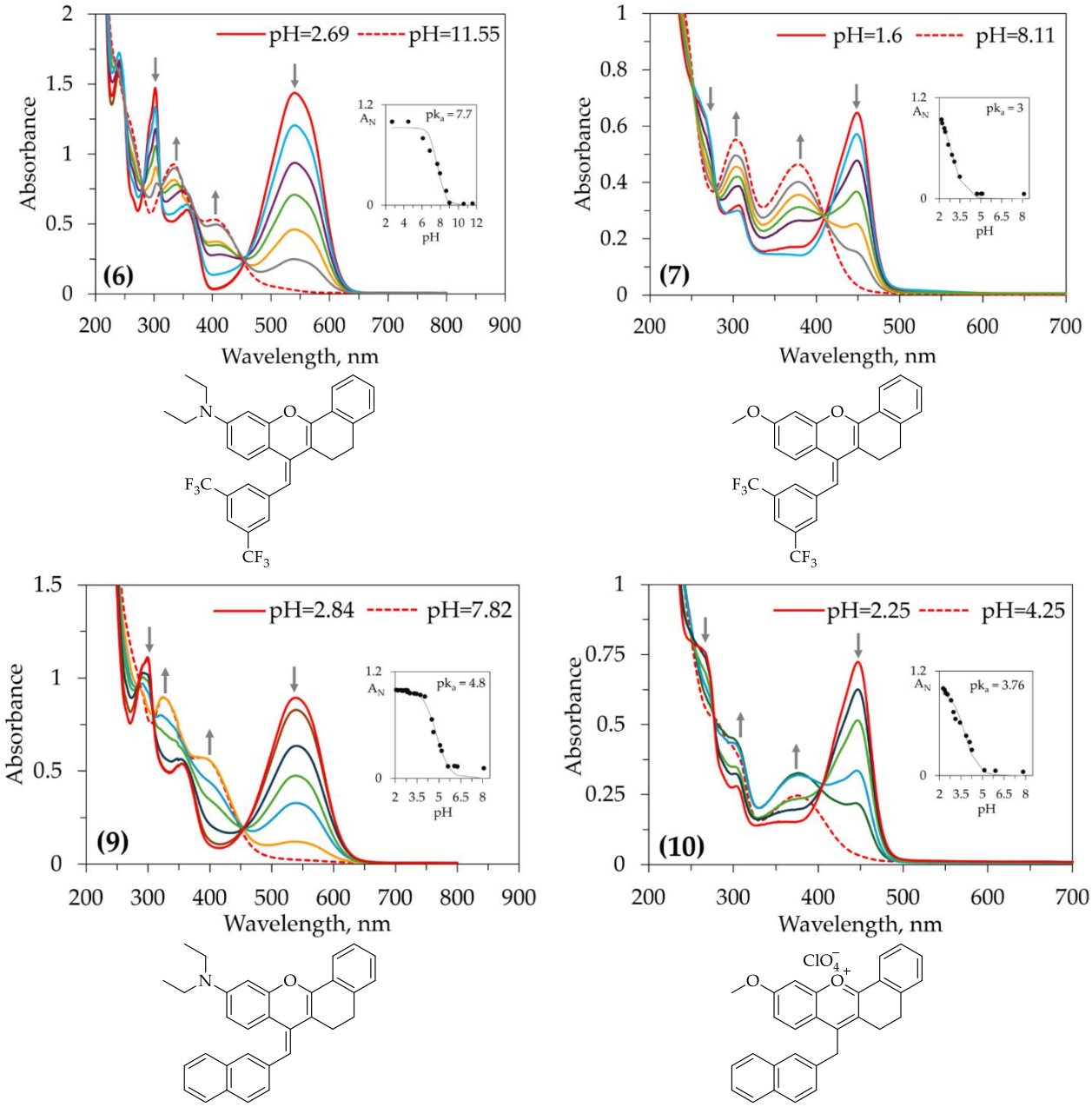

Figure 3.4 — Spectral modifications of compounds 6, 7, 9 and 10 as a function of pH, in acetonitrile-water (7:3). Molar concentration: [6]=5.25×10^{-5} mol dm^{-3}; [7]=2.97×10^{-5} mol dm^{-3}; [9]=4.8×10^{-5} mol dm^{-3}; [10]=3.48×10^{-5} mol dm^{-3}. The spectra were run after 1h equilibration time at 20°C. The traced line corresponds to the absorption spectrum of pure ethylenic base in the same solvent and concentration.

The titration data were also used to determine the pK$_a$ values of compounds **6-10** by fitting normalised absorbance at the absorption maximum (A_N) through equation 3.1, **Table 3.2**. In this equation, A_{max} is the absorption at λ_{max} in the most acidic solutions. Additionally, based on the obtained results, an approximate pK$_a$ for compound 8 was derived, as the experimental determination was challenging due to its low acidity. The acidity constant provides information about the thermodynamic stability of cationic flavylium in aqueous solutions. For example, a high pk$_a$ value suggests a stable cationic flavylium that can resist the nucleophilic attack by water at C_2 and addition of -OH group. [136] As such, based on the determined

values, we can conclude that compound **6** (pka=7) and compound **9** (pka=4.8) are the most likely dyes to resist nucleophilic attack. This is also supported by the titration curve showing that cationic flavylium is the unique species below pH 7 (compound 6) and pH 5 (compound 9), respectively.

$$A_N = \frac{A}{A_{max}} = \frac{[H^+]}{[H^+] + K_a} \qquad \text{Equation 3.1}$$

Table 3.2 — pK_a values of compounds 6-10.

Compound	R	λ_{abs}^{max} (nm)	pK_a
6	$N(CH_2CH_3)_2$	540	7.7
7	OCH_3	450	3
8	H	425	< 2
9	$N(CH_2CH_3)_2$	545	4.8
10	OCH_3	450	3.76

3.3.4 Thermochromism in Pluronic® F127

Relying on the capabilities of Pluronic® F127 [$(PEO)_{98}$-$(PPO)_{67}$-$(PEO)_{98}$] triblock thermoresponsive copolymers — composed of a central hydrophobic block of poly(propylene oxide)-PPO trapped between two hydrophilic parts of poly(ethylene oxide)-PEO — to self-assemble in micelles/gel at the transition temperature as illustrated in **Scheme 3.5**, the thermochromic properties of the synthesised 4-arylidene-substituted flavylium dyes were evaluated. The small difference in Gibbs free energy between the cationic flavylium and its ethylenic base makes it possible to shift the equilibrium by adjusting the pH of the medium. [120] Aggregation and disaggregation of micellar/gel phase by increasing or decreasing temperature induces a change in the polarity of the medium, consequently affecting the pH balance either towards the cationic dye or the neutral ethylenic species. Specifically, upon heating, the aggregation of Pluronic in a micellar/gel phase makes the medium less polar and stabilises the ethylenic base by lowering the pH due to deprotonation of the α-methylene position. Conversely, upon cooling, disaggregation of the gel/micellar phase into monomeric solution increases the polarity of the medium and stabilises the cationic flavylium and increases the pH by protonation of the α-methylene position of the dye.

Compounds **6** and **10** were the dyes exhibiting the most noticeable thermochromism, with their spectral and colour change effects depicted in **Figure 3.5** and **Figure 3.6**. The experiments were conducted in 20% (wt./wt.) Pluronic® F127 aqueous solutions at pH=2 for compound **6** and pH=1 for compound **10**. The defined pH ensured complete reversible colouration for compound **6** and partial colour reversibility for compound **10**. Compound **6** demonstrated reversible colour change due to the preferential partition of the neutral base to the micellar/gel phase allowing the generation of thermochromic systems based on acid/base reaction, **Scheme 3.5**. [133] On the other hand, the partial reversible colouration of compound **10** suggests that the cationic flavylium was not converted to its ethylenic base when elevating the temperature (as was the case for compound 6), but rather to a hemiketal species. This transformation is supported by the increasing of 255 nm maxima which takes place concomitant with the decreasing of 467 nm cationic flavylium maxima and 368 nm ethylenic base. Furthermore, the absence of

the isosbestic point also supports that the resulting species is not the ethylenic base. Finally, based on these observations, we may conclude that the hemiketal species led to partial reversible colouration, because the kinetic reaction from hemiketal to flavylium is smaller than that of the base to flavylium. [133]

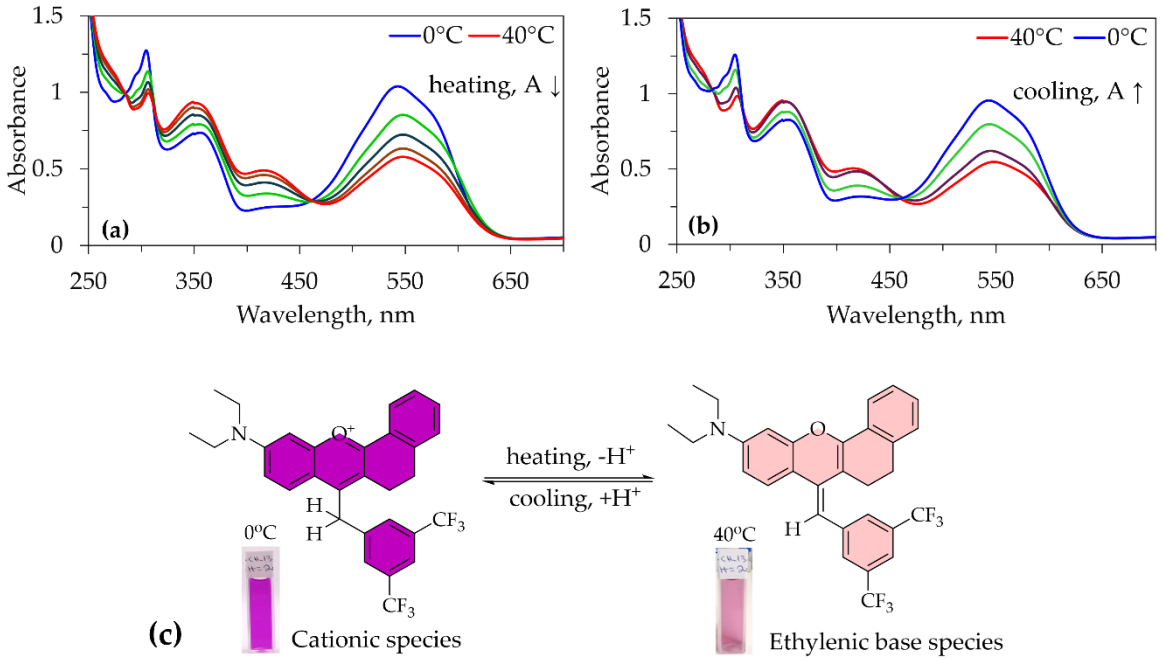

Figure 3.5 — Spectral modifications of 20% (wt./wt.) Pluronic® F127 aqueous solutions of compound 6 (M_C=5.71×10^{-5} mol dm^{-3}, pH=2) observed as a function of temperature during both heating (a) and cooling (b). The acid-base reaction that occurs during the colour change process (c).

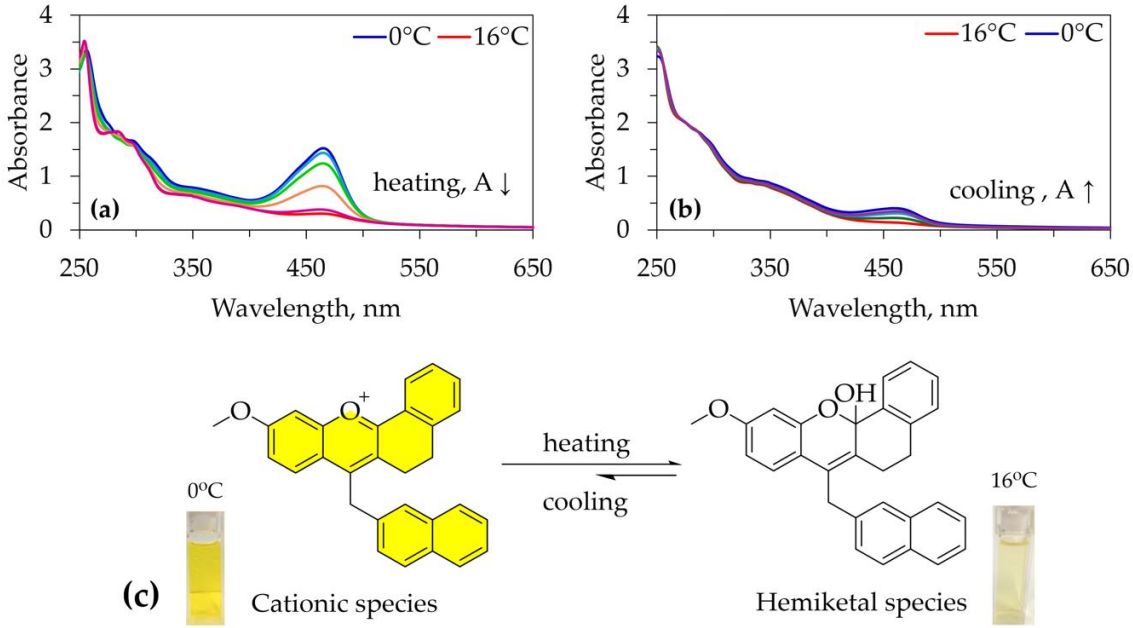

Figure 3.6 — Spectral modifications of 20% (wt./wt.) Pluronic® F127 aqueous solutions of compound 10 (M_C=10^{-4} mol dm^{-3}, pH=1) observed as a function of temperature during both heating (a) and cooling (b). The acid-base reaction that occurs during the colour change process (c).

3.4 Conclusions

Five chromogenic dyes compounds based on 4-arylidene-substituted flavylium dyes with CH-acidic aryl group at the α-methylene position have been successfully synthesised, structurally and spectrophotometric characterised. The influence of electron-donating and electron-withdrawing groups on the rigid flavylium skeleton (position 4 and 7) was studied in terms of colour modification, acid-base behaviour and thermochromic properties.

The compounds displayed shades of violet and yellow in acidic solutions of dichloromethane when going from strong to weak donating group in the 7-position. The absorption also revealed that the substituents of position-4 have little influence on the ultimate colour. Furthermore, the spectrophotometric studies showed that the dyes were able to change between two species by an alteration in pH, and the determined pk_a show their high stability against hydration rection that could lead to formation of various species. The compound with amine at the 7-position and 3,5-bis(trifluoromethyl) benzyl unit at the 4-position exhibited fully reversible thermochromism in 20% (wt./wt.) PF-127, pH=2, of interest for applications where a feature exhibiting a reversible switch is desired.

4

MICROENCAPSULATED THERMOCHROMIC SYSTEMS BASED ON FLAVYLIUM SPIROLACTONE LEUCO DYE COLOUR FORMER AND FATTY ACIDS DEVELOPERS

Abstract

This work focused on the microencapsulation of different ternary thermochromic systems to be subsequently used for the development of reversible thermochromic indicators with a colour transition close to the refrigeration temperature (about 8°C). A novel flavylium spirolactone dye, used as colour former (CF), was dissolved into isopropyl palmitate, a phase change material (m.p. 13.5°C), in the presence of caprylic and capric acid colour developers (CD). Each ternary system was microencapsulated into a water-based dispersion using *in-situ* polymerisation in O/W emulsion.

The isolation of flavylium spirolactone dye was confirmed through UV-Vis absorption spectrophotometry, IR/1H NMR spectroscopy and elemental analysis (EA). Dynamic light scattering (DLS) and scanning electron microscopy (SEM) provided indication on the morphology of the microcapsule and information on the particle size distribution in the dispersion. Differential scanning calorimetry (DSC) measurements were employed to evaluate the transition temperatures, determine the encapsulation ratio (R), encapsulation extent (E), and interpret interactions between the colour former and developer. Hot stage microscopy was also used to confirm the phase transitions.

Higher concentration of CF led to an increasing polydispersity index (PI), Z-Average, mean values and solids content. SEM images illustrated capsules with smooth surfaces, spherical shapes, and homogeneous distribution. DSC analysis revealed that crystallisation and melting is a multi-step process due to the formation of eutectic systems and the presence of

polymorphic components, and the transition temperatures are affected by the formation of the polymeric wall and by increasing colour developers' concentration.

4.1 Introduction

Thermochromic inks printed on a plastic or paper surface of a container or packaging give rise to thermochromic indicators. [137] This type of indicators are materials capable of changing colour in a reversible or irreversible manner when fluctuations in the surrounding temperature occur. Reversible thermochromic indicators can move from colourless to a coloured state or switch between colours. [30,137–139] Their functionality is generally based on a *leuco* dye system or a liquid crystal compound. [140] In most instances, the thermochromic system undergoes an encapsulation process to avoid undesired reactions that could impact its functionalities, characteristics and use. [141] Encapsulation leads to the synthesis of micro or nanocapsules assembled from a core and a shell material. [142] The *leuco* dye system is typically composed of a ternary mixture and is referred to as the core material. The core's components are the colour former, the colour developer and the solvent. During the colouration-discolouration reaction, the colour former acts as a proton acceptor (electron donor), the developer is the proton donor (electron acceptor), and the solvent is the component that defines the temperature at which the colour change start to develop. [138,143–145] Generally, the *leuco* dye based-system is coloured in the solid state and colourless or weakly coloured in its liquid phase due to the ring opening-closing reaction of the lactone dye, **Figure 4.1a**. As already mentioned in the introduction of chapter 1, colouration-discolouration effect is a result of two competing reactions; one between colour former and developer that prevails in the solid state, and the other between developer and solvent that predominant in the liquid state of the system, **Figure 4.1b**. [5,140]

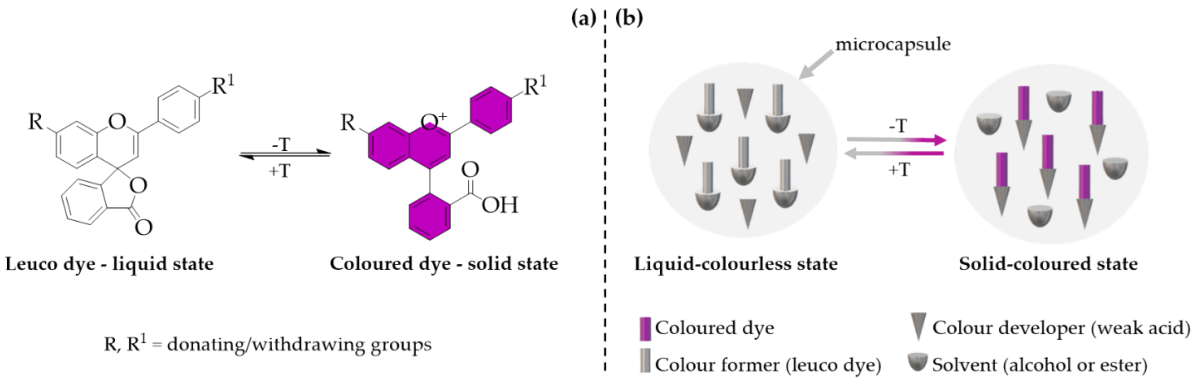

Figure 4.1 — Ring-opening and -closing reaction of a typical *leuco* dye (a). Schematic illustration of the interactions that trigger the colouration and discolouration reaction of microencapsulated ternary thermochromic *leuco*-dye systems when the colour develops in the solid state (b). [5]

Factors such as the acidity and polarity of the selected developers and solvents need to be considered to allow colouration and discolouration reactions to take place. If the acid is too strong or the solvent is too polar, discolouration does not proceed or is hardly noticeable. Also, the steric compatibility between the colour former and developer is a factor to be considered when colouration does not occur. [146]

The colour formers are *leuco* dye compounds [138] based on crystal violet lactone analogs, N-acylleucomethylene blue derivatives, fluorane dyes, diarylphthalyde counterparts, diphenylmethane counterparts, and spiropyrans counterparts. [26,28,30–32,113,139,140,144–157] However, to the best of our knowledge, no encapsulated ternary system reported flavylium lactone dyes as colour formers. Furthermore, frequently used colour developers are bisphenol A [113,139,146–155,158,159], dihydroxydiphenyl propane [156], propyl gallate [26,32], octyl gallate [26,32], dodecyl gallate [32], ethyl gallate [147], lauryl gallate [26,30,31,147,157], octadecyl gallate [32], benzyl 4-hydroxybenzoate [140], and phenolphthalein [28]. Nonetheless, systems in which fatty acids such as caprylic and capric acid act as colour developers in encapsulated ternary systems have not yet been reported. The solvent is a long-chain alkyl alcohol, ester, ketone, ether, or a fatty acid. [138,143–145]

Microcapsules can be generated through various physical, chemical, and physico-chemical methods. Among these, the most explored by researchers were the chemical methods, where the shell is formed around the core either by polymerisation or condensation of monomers, oligomers, or prepolymers. Moreover, the most used polymerisation methods are *in-situ* polymerisation, interfacial polymerisation, suspension polymerisation, and emulsion polymerisation. *In-situ* polymerisation is widely selected for the encapsulation of the thermochromic systems owing to its simplicity, feasibility, and eco-friendly components. [11,139,144,160] Melamine formaldehyde resin [161], urea-formaldehyde resin [162], poly (methyl methacrylate) [139,148], polyurethane [163], and polylactic acid [164] are one of the most used organic materials to construct the polymeric shell, refer to **Figure 4.2** for structures.

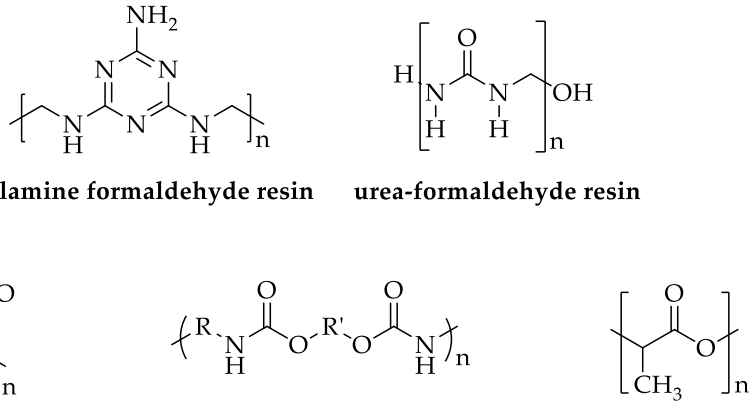

Figure 4.2 — Example of organic materials used to build the polymeric shell of microcapsules.

Several characterisation methods are commonly employed to comprehensively investigate and describe the characteristics of encapsulated thermochromic materials. These methods include UV-Vis spectroscopy, Fourier transform infrared spectroscopy (FTIR), dynamic light scattering (DLS), differential scanning calorimetry (DSC), thermogravimetric analysis (TGA), scanning electron microscopy (SEM), and transmission electron microscopy (TEM). These techniques enable a thorough examination of the materials' structural, microstructural, elemental, optical, chemical, and thermal functionalities. The CIELAB colour space, established by the International Commission on Illumination, offers an avenue to gather numerical data of the printed surfaces. [11]

In this work, caprylic and capric acid were investigated as colour developers in thermochromic ternary *leuco* dye systems. Furthermore, a novel synthesised flavylium spirolactone dye was tested as a colour former, while isopropyl palmitate was selected as a phase change material. DLS, SEM and solids content analyses were performed to characterised the microcapsule dispersion and dry contents. DSC measurements were performed to evaluate the encapsulation effect on the onset and crystallisation temperatures, determined the encapsulation ratio (R)/encapsulation extent (E) and to gain insight about the interactions of the colour former with the developer and solvent. The impact on the transition temperature was analysed before and after microencapsulation process using different concentrations of colour former and colour developer.
DLS and SEM data showed that higher concentration of CF led to an increasing Z-Average, PI and mean values. DSC analysis revealed that crystallisation and melting is a multi-step process due to the formation of eutectic systems and the presence of polymorphic components, and the transition temperatures are affected by the polymeric wall formation and by the increase in colour developer concentration. Encapsulation ration (R) and encapsulation extent (E) were found to be high for most systems.

4.2 Materials and methods

4.2.1 Materials and chemicals

Isopropyl palmitate - $CH_3(CH_2)_{14}COOCH(CH_3)_2$ (99% C_{16}, 0.5% C_{14}, Sigma-Aldrich), caprylic acid - $CH_3(CH_2)_6COOH$ (≥98%, Sigma-Aldrich), and capric acid - $CH_3(CH_2)_8COOH$ (99%, Alfa Aesar) were used without further purification. A Sokalan® product was used as a surfactant and melamine formaldehyde resin was selected as a polymeric shell material.

4.2.2 Methods

4.2.2.1 Lactone dye (colour former) characterisation

Absorption spectra were recorded with a Shimadzu UV-2501PC/Varian Cary 100 using reagent-grade acetonitrile. IR spectra recorded with an FT-IR Spectrometer, Perkin-Elmer-Spectrum Two, were collected in transmittance mode from 500 to 4000 μm. The samples were prepared with KBr powder. The ^1H NMR spectra at 298 K were obtained on a Bruker AMX400 operating at 400 MHz, and deuterated solvent signals were used as an internal reference. Elemental analysis was performed with a Thermo Finnigan-CE Instruments, Flash EA 1112 CHNS series, at 900°C reactor's combustion temperatures.

4.2.2.2 Microencapsulation

IKA Dispersers T25 digital ULTRA-TURRAX® was used as an emulsifier, at 20000 rmp stirring speed.

4.2.2.3 Microcapsules characterisation

4.2.2.3.1 Dynamic light scattering (DLS)

Dynamic light scattering analysis was performed with a HORIBA Scientific model SZ-also as a function of number in ultrapure deionised water at 25°C. Prior to sample preparation, the water was passed through a 0.45 μm PP syringe filter (FILTER-LAB®).

4.2.2.3.2 Scanning electron microscopy (SEM)

The surface morphology of the microcapsules was analysed by scanning electron microscopy with a Hitachi Regulus SU8220. The acceleration voltage was 5 kV, the working distance was around 9 mm, and the magnification was between 2 and 25 Kx SE(U). To obtain SEM images of undisrupted capsules, the corresponding slurry was dropped onto holey carbon support film and allowed to dry for about 5 minutes under vacuum. The dried samples were then coated with a thin film of 20 nm of Au/Pd (80:20 ratio) by sputtering in a Quorum QT150 ES. ImageJ was used to calculate the mean values for a number of 70 capsules or higher.

4.2.2.3.3 Solids content analysis

The solids content was recorded after the capsule dispersion was maintained at 100°C until a constant weight was displayed. An Adam AMB 50 Moisture Balance apparatus was used for the measurements.

4.2.2.3.4 Differential scanning calorimetry (DSC) and hot stage microscopy (HSM)

The phase transition temperatures of the free binary/ternary and encapsulated systems were analysed through differential scanning calorimetry with a DSC 131, Setaram, France Instrument, fitted with a liquid nitrogen cooling accessory under a dry high purity nitrogen atmosphere at a purge rate of 50 mL/min. The cooling/heating rate of the free systems was established at 10°C/min, whereas for the encapsulated materials to 18°C/min. An Olympus BX51-P Polarizing Light Microscope connected to a Linkam Scientific TMS94 32 Ramp Temperature Programmer was also used to confirm the phase transition temperatures. The cooling/heating rate for the microscopic measurements was set to 5°C/min.

4.3 Experimental

4.3.1 Isolation of lactone flavylium dye colour former (CF)

The cationic flavylium dye, *4-(2-carboxyphenyl)-2-(4-cyanophenyl)-7-(dibutylamino) chromenylium perchlorate*, synthesised following the experimental procedure outlined elsewhere, [5] was converted into its *leuco* form under the action of triethylamine in ethyl acetate. The resulting lactone dye was then isolated through several liquid-liquid extractions, and after solvent evaporation and vacuum drying, the final product was obtained as a brown precipitate, in a qualitative yield. **Scheme 4.1** depicts the conversion mechanism, where the cationic dye functions as a donor, triethylamine serves as an acceptor, and ethyl acetate as the solvent of the medium. The isolation of the *leuco* species was confirmed through UV-Vis absorption spectrophotometry (**Figure 4.3**), IR spectroscopy (**Figure 4.4**), elemental analysis (EA) and ^{1}H NMR spectroscopy (**Figure 4.5**).

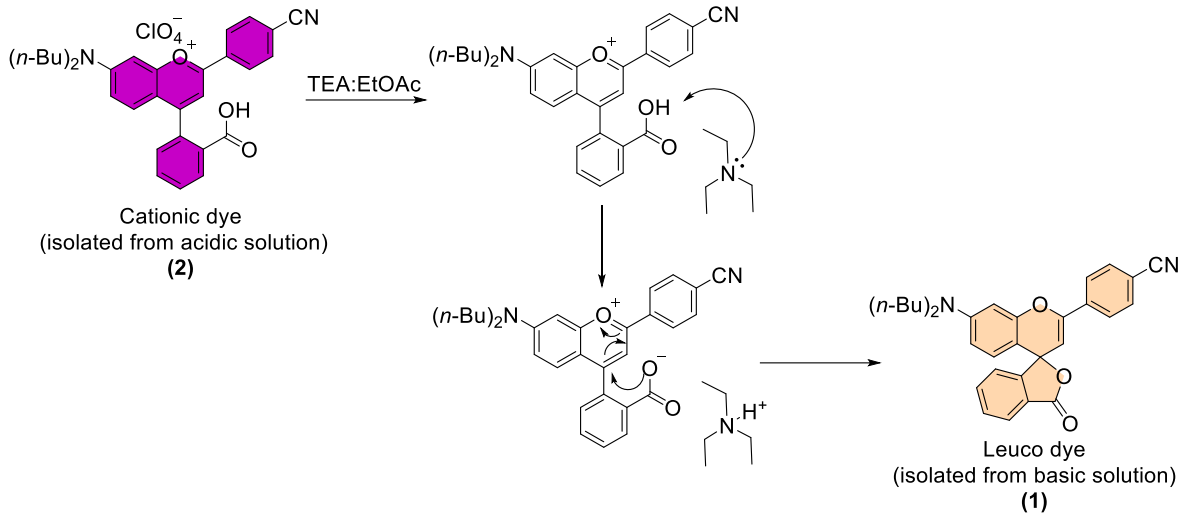

Scheme 4.1 — The conversion mechanism of cationic flavylium dye (2) into its leuco product (1). Triethylamine (TEA) was used as a proton acceptor, and ethyl acetate (EtOAc) as the solvent of the medium.

The UV-Vis spectrum of the lactone dye recorded in reagent-grade acetonitrile presented no bands in the visible region, **Figure 4.3-line 1**. After adding HCl into the acetonitrile solution, a new and intense band appeared in the visible region, with a maximum at 534 nm, **Figure 4.3-line 2**. The new band indicates the conversion of the isolated neutral *leuco* dye into its cationic species by opening the lactone ring, **Scheme 4.2**.

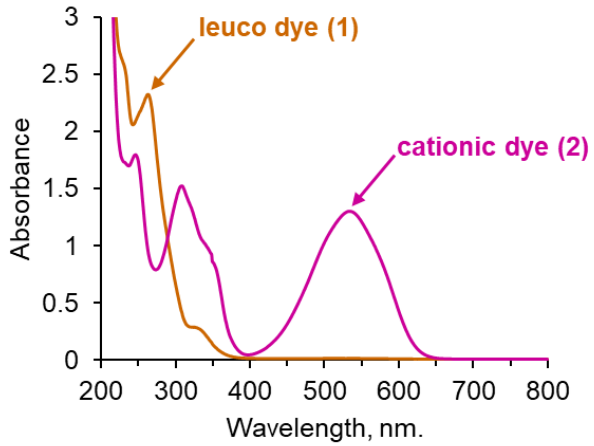

Figure 4.3 — UV-Vis spectra of cationic dye (2) and its *leuco* species (1). The spectrum of the *leuco* dye was recorded in pure acetonitrile, while the spectrum of the cationic dye was acquired after the addition of HCl to the acetonitrile solutions. Acetonitrile was used as the solvent of the medium, and HCl as a donor. The molar concentration of the dye was 5.6×10^{-5} mol dm^{-3}.

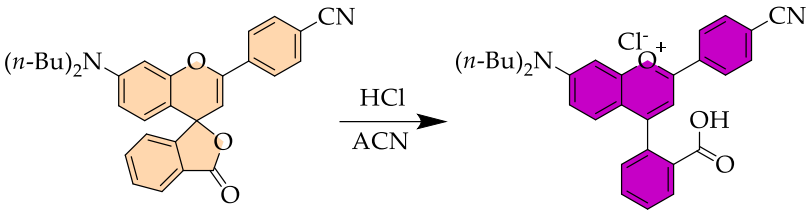

Leuco dye
(isolated from basic solution)

Cationic dye
(isolated from acidic solution)

Scheme 4.2 — Conversion of the lactone dye into its cationic product with hydrochloric acid (HCl) in acetonitrile (ACN). HCl was used as a donor, and ACN as the solvent of the medium.

Comparison between IR spectra of isolated *leuco* dye (1) and its corresponding cationic form (2), showed that the carbonyl stretching band ($\lambda_{C=O}$, 1755 cm^{-1}) of *leuco* species are blue shifted towards higher frequencies in respect to the band ($\lambda_{C=O}$, 1711 cm^{-1}) of their corresponding cationic flavylium dye, **Figure 4.4**. [38] Additionally, the band presented at 625 cm^{-1} by the cationic dye is hardly observed for its *leuco* product. The 625 cm^{-1} band corresponds to the bending vibration (δ_{Cl-O}) of ClO_4^- anion. [165,166] The IR analysis, showed that the predominant isolated species (from basic solutions) was the *leuco* product, however, within 2000-4000 region, the spectra showed no obvious changes that can be considered when comparing the cationic dye with its *leuco* counterpart. Both species showed bands in 3000-3600 region. The band exhibited by the *leuco* form in this region may be due to its strongly hygroscopic nature. Moisture can readily open the lactone ring by protonation of the carboxyl ring, **Scheme 4.2**. The presence of water molecules was also confirmed by elemental analysis; calcd. for $C_{31}H_{30}N_2O_3 \times 2.5H_2O$: C, 71.11; H, 6.74; N, 5.35; found: C, 71.61; H, 6.63; N, 5.12.

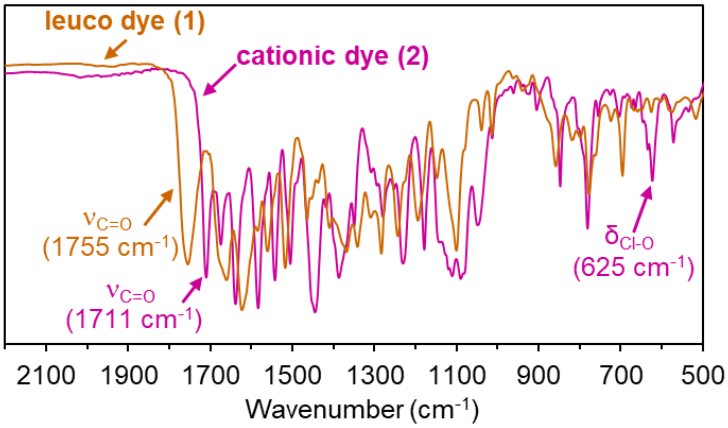

Figure 4.4 — IR spectra of isolated cationic flavylium dyes (2) and its *leuco* species (1), 500-2200 region. The spectra were collected in the transmittance mode, and KBr powder was used for sample preparation.

The isolation of lactone dye was also confirmed through ^1H NMR spectroscopy, **Figure 4.5** and **Table 4.1**. Comparison between ^1H NMR spectra of isolated *leuco* dye (1) and its cationic counterpart (2), showed upfield shifts of the lactone signals. The most affected proton is H^3, followed by protons $H^{3',5'}$, H^5, H^6 and H^8, which suggests that the isolated species is the lactone dye. [38]

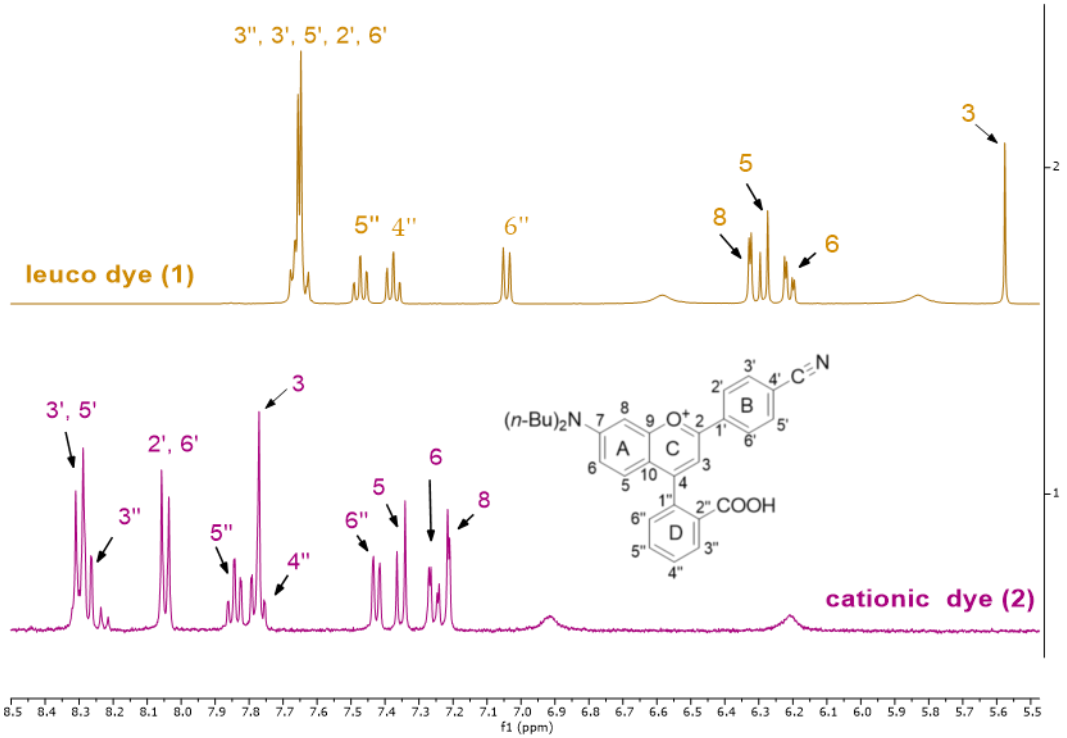

Figure 4.5 — ^{1}H NMR spectrum of *leuco* (1) and cationic (2) dye (CD_3CN, 298.0 K) at 400 MHz.

Table 4.1 — Assignment of ^{1}H NMR data for *leuco* (1) and cationic (2) dye (CD_3CN, 298.0 K) at 400 MHz.

Position	^{1}H δ /ppm (J/Hz)	
	***Leuco* dye (1)**	**Cationic dye (2)**
3′, 5′	7.90 (2H, d, J = 6 Hz)	8.29 (2H, d, J = 8.8 Hz)
3″	7.90 (1H, d, J = 6 Hz)	8.27 (1H, d, J = 7.2 Hz)
2′, 6′	7.90 (2H, d, J = 6 Hz)	8.05 (2H, d, J = 8.8 Hz)
5″	7.72 (1H, t, J = 7.6 Hz)	7.84 (1H, t, J = 7.2 Hz)
4″	7.63 (1H, t, J = 7.6 Hz)	7.78 (1H, t, J = 7.6 Hz)
3	5.83 (1H, s)	7.77 (1H, s)
6″	7.29 (1H, d, J = 7.6 Hz)	7.43 (1H, d, J = 7.2 Hz)
5	6.54 (1H, d, J = 8.8 Hz)	7.35 (1H, d, J = 9.6 Hz)
6	6.46 (1H, dd, J = 9.2 Hz, J = 2.4 Hz)	7.26 (1H, dd, J = 9.2 Hz, J = 2.4 Hz)
8	6.58 (1H, d, J = 1.2 Hz)	7.21 1H, d, J = 2.4 Hz)

4.4 Synthesis of microcapsules

Microencapsulation was carried out through oil in water emulsion *in-situ* polymerisation method in the presence of a surfactant emulsifier agent and a melamine formaldehyde resin used as a shell material. The mechanism of capsules formation is depicted in **Figure 4.6**.

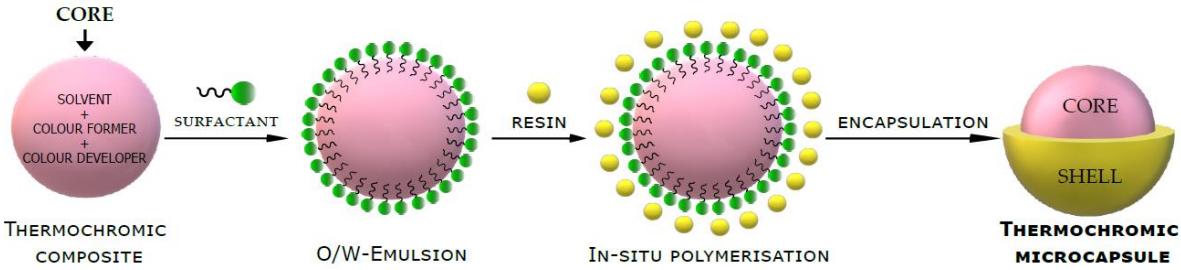

Figure 4.6 — Mechanism of microencapsulation process of a three-component thermochromic composite through *in-situ* polymerisation method by using a surfactant as emulsifier agent and melamine formaldehyde resin as shell material.

The emulsifier was dissolved in deionised water and activated with 1N NaOH solution. The core solution was prepared by mixing the colour former (*leuco* dye) with caprylic (C_8) or capric (C_{10}) acid developers in isopropyl palmitate (IPP). Prior to the emulsification process, the core materials were brought to temperatures equal to or above 70°C and left under stirring until the colour former was completely dissolved. Microcapsules were produced at 70°C after 1 hour and 30 minutes curing time. The concentration of both colour former and developers was adjusted to observe the impact on the transition temperatures and colour contrasts. The composition of core materials of prepared encapsulated systems is presented in **Table 4.2**. The emulsifier:core:shell ratio was set at 0.24:5:1 in all compositions.

Table 4.2 — Composition of core material in the free (f) and encapsulated (c) systems expressed as mass ratio, wt.-% and molar fraction (χ). Caprylic (C_8) and capric (C_{10}) acid were selected as colour developers (CD), and isopropyl palmitate as a solvent, and the isolated *leuco* dye **1** was used as a colour former (CF). In all the systems, the core:shell ratio was 5:1.

System	Sample	Ratio IPP:C_8/C_{10}:CF	CD (wt.-%)	χCD	CF (wt.-%)	χCF
C_8	$f_1 \rightarrow c_1$	8.82 : 1.1 : 0.08	11	0.20	0.8	0.005
	$f_2 \rightarrow c_2$	8.74 : 1.1 : 0.16			1.6	0.01
	$f_3 \rightarrow c_3$	7.72 : 2.2 : 0.08	22	0.37	0.8	0.005
	$f_4 \rightarrow c_4$	7.64 : 2.2 : 0.16			1.6	0.01
C_{10}	$f_5 \rightarrow c_5$	8.82 : 1.1 :0.08	11	0.18	0.8	0.005
	$f_6 \rightarrow c_6$	8.74 : 1.1 : 0.16			1.6	0.01
	$f_7 \rightarrow c_7$	7.72 : 2.2 : 0.08	22	0.33	0.8	0.005
	$f_8 \rightarrow c_8$	7.64 : 2.2 : 0.16			1.6	0.01

4.5 Results and discussions

4.5.1 Capsules characterisation

4.5.1.1 Dynamic light scattering (DLS) and solids content analysis

Dynamic light scattering analysis was performed to determine the Z-Average and polydispersity index (PI) as a function a number. The Z-Average and PI values show that the polydispersity of the samples increases by increasing CF's concentration, **Table 4.3**. These increases suggest an approach to the CF saturation point in the corresponding formulas. However, for c_2 and c_8 samples, the particle size could not be measured due to the high solids content of about 60%, which also increases slightly with CF's concentration, **Table 4.3**.

Table 4.3 — Z-average, polydispersity index (PI), mean and solids content of C_8 *(c_1, c_2, c_3, c_4)* and C_{10} *(c_5, c_6, c_7, c_8)* systems. Z-Average and PI were determined by DLS, while mean was determined by measuring the diameter of SEM capsules with ImageJ software. Z-Average and PI were determined as the average of four data sets. The SEM measurements were carried out on a number equal to or greater than 70 capsules.

System	Capsules (c)	CD (wt.-%)	CF (wt.-%)	DLS		SEM	Solids (%)
				Z-Average (μm)	PI (μm)	Mean (μm)	
C_8	c_1	11	0.8	2.3 ±0.07	0.38	1.1 ±0.5	48.22
	c_2		1.6	–	–	4.2 ±3.6	60.88
	c_3	22	0.8	1.02, ±0.2	0.19	0.9 ±0.4	45.28
	c_4		1.6	6.9, ±1.1	1.03	1.3 ±0.7	48.73
C_{10}	c_5	11	0.8	1.4, ±0.5	0.28	1.2 ±0.7	49.18
	c_6		1.6	5.8, ±0.3	0.96	3.5 ±1.4	53.56
	c_7	22	0.8	4.2, ±1.2	0.52	1.3 ±0.7	51.01
	c_8		1.6	–	–	3.9 ±2.6	61.26

4.5.1.2 Scanning electronic microscopy (SEM)

SEM images and particle size distribution graphs of C_8/C_{10} capsules are shown in **Figure 4.7**. The images illustrate that the resulting microcapsules are particles with smooth surfaces, spherical shapes, and homogeneous distribution. Measurements also showed microcapsules with a wall thickness between 50 and 200 nm that increases with the content of colour former for both C_8 and C_{10} systems, **Figure 4.8**. The mean values determined with ImageJ software showed capsules with particle size lower than 5 μm that increase in size with concentration of dye, **Table 4.3**. Moreover, the images reveal the presence of white particles on the capsules' surface. These particles are probably precipitated content of core material due to capsules' degradation (or self-polymerised prepolymer resin [167]), considering that the measurements were taken six months after the encapsulation process and some degradation of the capsules is expected.

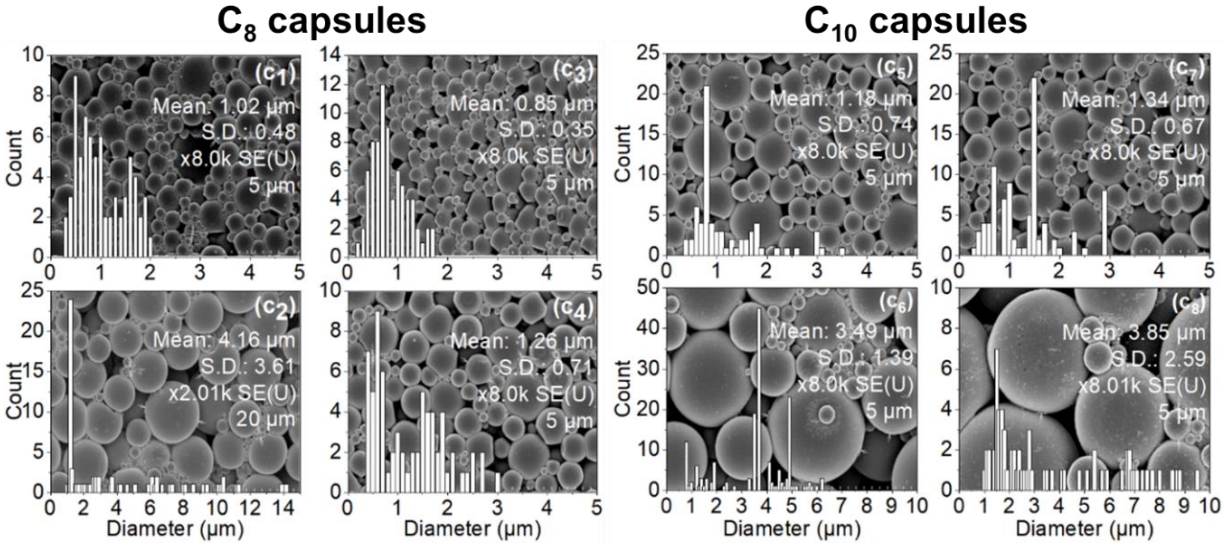

Figure 4.7 — Particle size distribution graphs and SEM images of C_8 *(c_1, c_2, c_3, c_4)* and C_{10} *(c_5, c_6, c_7, c_8)* capsules. The mean size was determined by measuring the diameter of SEM capsules with ImageJ software. The measurements were carried out on a number equal to or greater than 70 capsules.

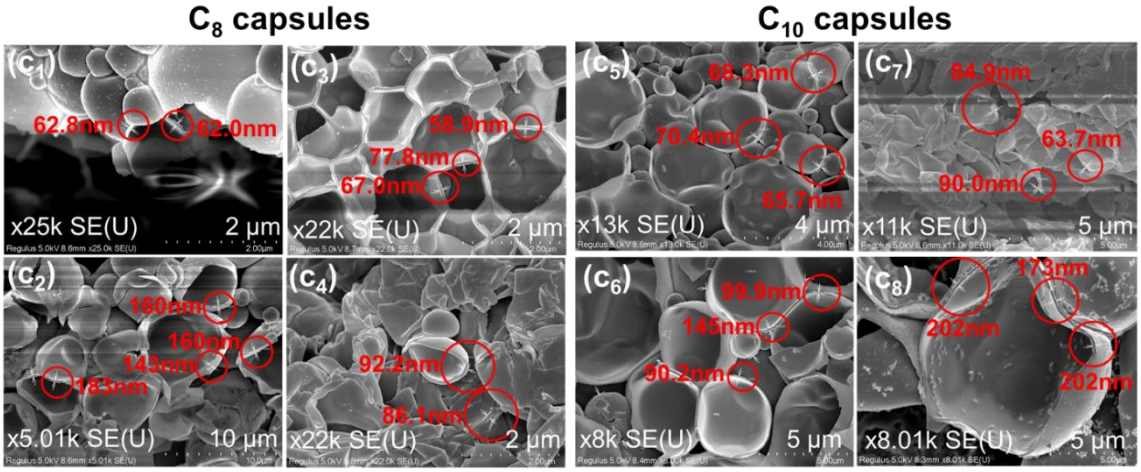

Figure 4.8. — SEM images showing the shell thickness of C_8 (c_1, c_2, c_3, c_4) and C_{10} (c_5, c_6, c_7, c_8) capsules.

4.5.2 Differential scanning calorimetry (DSC) and hot stage microscopy (HSM)

DSC measurements were performed to evaluate the encapsulation effect on the onset and crystallisation temperatures, determine the encapsulation ratio (R)/encapsulation extent (E), and to gain insight about the interactions of the colour former with the developer and solvent.

Before evaluating the encapsulation effect, the impact of the colour former on the IPP_C_8/C_{10} mixtures was analysed. In **Figure 4.9**, the thermogram taken on cooling for f_4/f_8 ternary samples of IPP:C_8/C_{10}:CF (see **Table 4.4** for compositions) shows multiple exothermal peaks, and the addition of CF makes the peaks to appear better resolved in both C_8 and C_{10} systems. Moreover, in C_8 systems, the peaks also intensify, and in C_{10} systems they are slightly shifted to lower temperatures, especially the peaks identified with **. From a detailed analysis presented in **subsection 4.5.3** in which bulk compounds have been also considered, it can be concluded that this peak is mainly related to the crystallisation of the eutectic composition. The other peaks are related to the polymorphic transformations occurring in the IPP-rich regions of the samples. Then, the differences observed due to the presence of the CF suggest that the dye is present in both regions and acts either as a nucleating agent or colour former, which leads to the intensification and better definition of the peaks.

The onset of crystallisation occurs at lower temperatures for C_8 relative to C_{10} binary systems and for both systems, this temperature shifts to lower values as C_8/C_{10} content increases. With the addition of the colour former no significant shifts are observed, which is somewhat to be expected given the small amount it represents in the whole sample (**Table 4.4**).

On heating, the thermograms show several endothermal and exothermal events meaning that besides the melting of the previous crystals formed on cooling, also another recrystallisation (and corresponding melting) is promoted (photos 2 and 3, **Figure 4.9a$_1$**). Given that cold-crystallisation is observed in bulk IPP (see photo 3 in **Figure 4.9a$_1$** and also **subsection 4.5.3** for more details), the observation of this phenomenon in the mixtures reinforces the idea of the existence of an IPP-rich domains.

When the ternary mixtures are encapsulated, the overall thermal response is significantly affected. The spatial confinement reflects in a broad and asymmetric band that hardly lets to resolve any of the multiple peaks previously observed in free systems (**Figure 4.9e/4.9e$_1$**). Due

to the absence of transitions related to the polymeric shell (T_g for similar polymers is higher than 150°C [168]) the calorimetric response must be associated completely to the encapsulated mixtures.

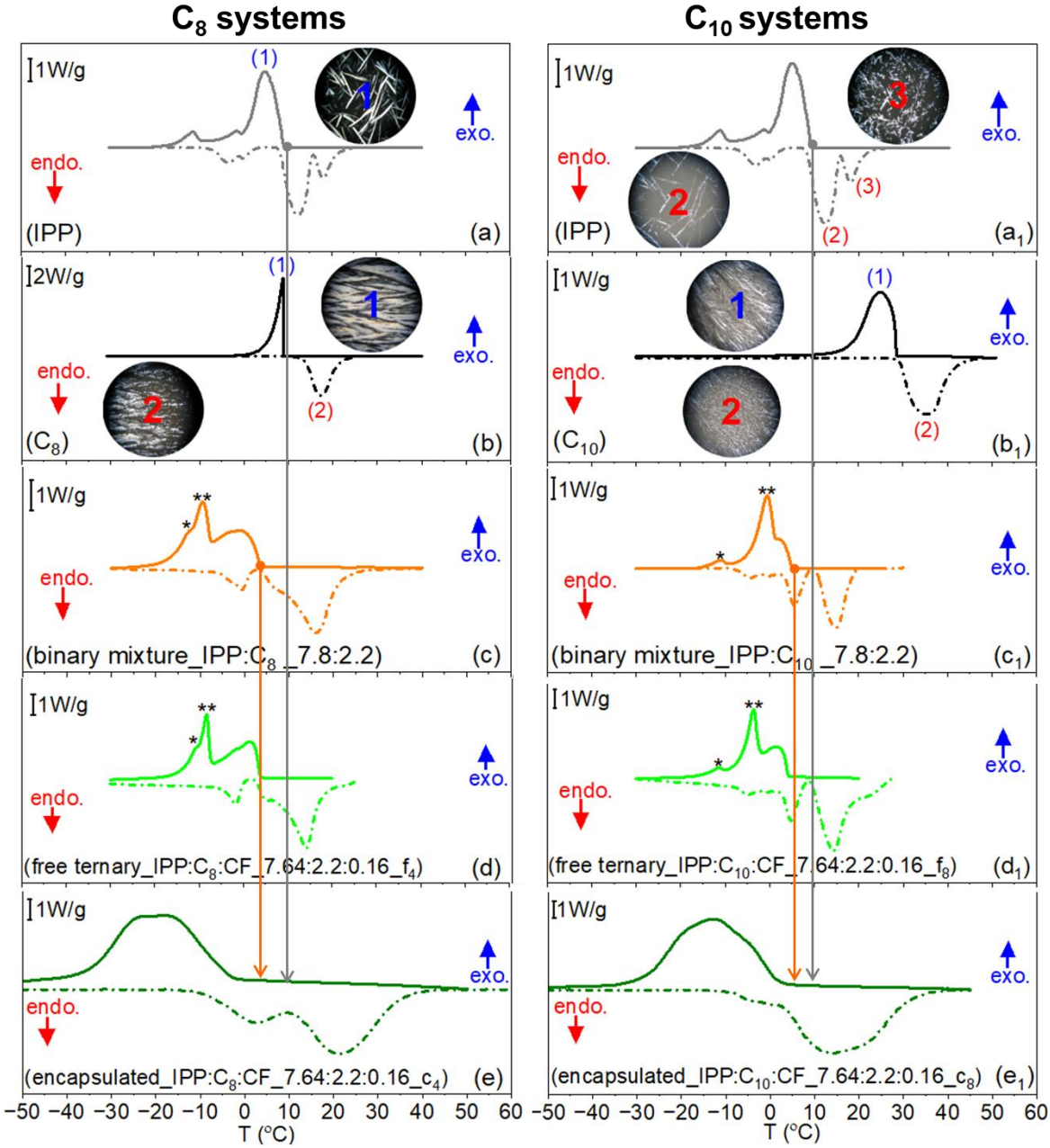

Figure 4.9 — Cooling and heating thermograms of bulk compounds (a/a1 and b/b1), binary mixtures (c/c1), ternary mixtures with composition 7.64:2.2:0.16 of IPP:C8/C10:CF (d/d1), and the corresponding ternary encapsulated mixture (e/e1). For bulk compounds, binary and ternary mixtures thermograms were collected at 10°C/min, while for encapsulated mixtures the scanning rate was set at 18°C/min. Microphotographs with 40x (C8) and 100x (IPP and C10) magnification were taken under 5°C/min cooling/heating rates around the indicated temperature.

Table 4.4 — Onset (T_{onset})/transition temperatures of crystallisation ($T_{L\text{-}S}$, $T_{S\text{-}S}$) of C_8/C_{10} binary (11%/22%), ternary (*f_1, f_2 … f_8*), and encapsulated (*c_1, c_2 … c_8*) systems.

Ratio	**C_8 systems**				**C_{10} systems**			
IPP:C_8/C_{10}:CF	**Sample**	**T_{onset} (°C)**	**$T_{L\text{-}S}$ (°C)**	**$T_{S\text{-}S}$ (°C)**	**Sample**	**T_{onset} (°C)**	**$T_{L\text{-}S}$ (°C)**	**$T_{S\text{-}S}$ (°C)**
	free binary systems							
8.9 : 1.1 : 0	**11% C_8**	6.9	3.7	-8.5	**11% C_{10}**	7.4	5.8	-1.1
7.8 : 2.2 : 0	**22% C_8**	3.7	1.5	-8.0	**22% C_{10}**	5.3	4.3	-1.3
	free ternary systems							
8.82 : 1.1 : 0.08	**f_1**	6.3	4.3	-8.9	**f_5**	7.4	5.4	-1.9
8.74 : 1.1 : 0.16	**f_2**	6.8	5.3	-8.9	**f_6**	7.0	4.1	-3.3
7.72 : 2.2 : 0.08	**f_3**	3.7	2.5	-8.4	**f_7**	5.1	4.2	-3.3
7.64 : 2.2 : 0.16	**f_4**	4.2	3.4	-7.5	**f_8**	4.4	3.6	-3.4
	encapsulated ternary systems							
8.82 : 1.1 : 0.08	**c_1**	1.5	-5.9	-20.5	**c_5**	4.4	-5.9	-18.1
8.74 : 1.1 : 0.16	**c_2**	7.1	-0.4	-15.3	**c_6**	4.9	-3.8	-19.0
7.72 : 2.2 : 0.08	**c_3**	-4.0	-11.7	-20.3	**c_7**	2.5	-8.8	-18.0
7.64 : 2.2 : 0.16	**c_4**	-1.7	-10.7	-24.2	**c_8**	4.3	-3.6	-14.2

The broadened and the loss of resolution of the underlying peaks suggest a higher overlapping of the multiple crystallisations. These changes could be related to a greater difficulty in diffusing heat from inner to outside the shell originating a temperature gradient inside the microparticles, and then coexistence of different crystalline structures. In fact, a "protective effect of the polymeric shell causing delayed temperature" has been referred by Li *et al.* [169] to explain the occurrence of heterogeneous nucleation inside capsules, different from which was found for the bulk compound. [167,169]

The crystallisation enthalpy of each system, free and encapsulated, was calculated by integrating the areas of the corresponding peaks considering an adequate baseline (**Table 4.5** in **subsection 4.5.3**).

To deep understanding the impact of the shell formation around the core components, it is usual to evaluate the encapsulation ratio, *R*, and the encapsulation extent, *E*, estimated from crystallisation enthalpy using the next equations [170]:

$$R = \frac{\Delta H_{c-encapsulated}}{\Delta H_{c-free}} \times 100\% \qquad \text{Equation 4.1}$$

$$E = \frac{R \times (m_{shell} + m_{core} + m_{emulsifier})}{m_{core}} \qquad \text{Equation 4.2}$$

where $\Delta H_{c\text{-}encapsulated}$ and $\Delta H_{c\text{-}free}$ are the crystallisation enthalpies of encapsulated and free systems respectively; m_{core} is the mass of the ternary system (IPP:C_8/C_{10}:CF), m_{shell} is the polymer mass and $m_{emulsifier}$ the emulsifier mass. It must be noted that crystallisation and not melting enthalpies were considered for these calculations due to the additional cold-crystallisation

observed on heating which made difficult the estimative of the melting enthalpy. The obtained *R* and *E* values have been included in **Table 4.5**. In general, a high encapsulation ratio is obtained for most of the systems analysed. However, attending to the *E* values, some of them are higher than the limit value of 100%. Possible reasons to explain these results can be related to:

(i) the fact that, during encapsulation, some fraction of the core material locates outside the shell, and the lack of the expectable crystallisation signal of this fraction suggests that molecules are highly dispersed;

(ii) the occurrence of some type of interactions between core and shell. In fact, some authors have reported that some of the core molecules may be "trapped" at the boundaries with the shell, either between the emulsifier [171,172] or in the polymer. In this situation, these molecules would not contribute to the overall crystallisation enthalpy;

(iii) the difference in the cooling rate applied in DSC measurements which for free mixtures was 10°C/min while for encapsulated was 18°C/min. This could lead to a higher overlap of the crystallisations and a different enthalpy value.

Table 4.5 — ΔH_{free} represents the crystallisation enthalpy of the free ternary mixtures (f_1, f_2 … f_8); $\Delta H_{encapsulated}$ is the crystallisation enthalpy of encapsulated system considering the (5:1) mass ratio of core/shell (c_1, c_2 … c_8); R and E are the encapsulation ratio and encapsulation extent calculated from equation 1 and 2.

System	Sample	Mass core ratio (IPP : C_8/C_{10} : CF)	ΔH_{free} (J/g)	$\Delta H_{encapsulated}$ (J/g)	R (%)	E (%)
C_8	$f_1 \rightarrow c_1$	8.82 : 1.1 : 0.08	156.7	148.5	75.9	94.8
	$f_2 \rightarrow c_2$	8.74 : 1.1 : 0.16	159.5	183.6	92.2	115.1
	$f_3 \rightarrow c_3$	7.72 : 2.2 : 0.08	154.5	143.3	74.3	92.7
	$f_4 \rightarrow c_4$	7.64 : 2.2 : 0.16	152.5	161.7	85.0	106.1
C_{10}	$f_5 \rightarrow c_5$	8.82 : 1.1 : 0.08	138.9	156.2	90.1	112.5
	$f_6 \rightarrow c_6$	8.74 : 1.1 : 0.16	157.3	109.0	55.5	69.3
	$f_7 \rightarrow c_7$	7.72 : 2.2 : 0.08	147.0	161.4	88.0	109.8
	$f_8 \rightarrow c_8$	7.64 : 2.2 : 0.16	148.8	162.7	87.6	109.4

4.5.3 Microscopic assignment of DSC crystallisation and melting transitions

To deeply understand the phase transitions of free and encapsulated systems, the calorimetric analysis was initialised by studying the bulk compounds, i.e. IPP, C_8 and C_{10}.

As it can be observed in **Figure 4.10a,** on cooling from room temperature, IPP shows an intense exothermal peak with onset at 10°C and maximum at 7.0°C, indicating the transition from the liquid to the solid crystalline state. Further cooling leads to two more exothermal events at 0.2 and -9.4°C (PM_1 and PM_2 in **Figure 4.10a**), that in accordance with Prado *et al.* correspond to two reversible enantiotropic solid-solid transformations. [173,174] The origin of the latter ones has been related to the greater intermolecular interference exerted by alkyl ester with isopropyl groups (more voluminous than methyl groups) on the ester bond interactions present in IPP. [174]

Microphotographs taken under 5°C/min rate allow visualising the formation of needle-like crystalline structures arising at ~10°C, in good agreement with the onset observed by DSC (see

photos 1 and 2 in **Figure 4.10a**). Crystallisation continues with further cooling until 7°C, from which no additional changes are visible that could be associated with polymorphic transformations indicated by DSC.
Thermograms obtained on heating present three well identified peaks that can be associated to the melting of previous crystalline structures formed; additionally, a more complex event is detected around 15°C that is related to the cold-crystallisation in another 3D structure and the corresponding melting. [173] The latter phenomenon is also followed by HSM which allows distinguishing the melting of needle-like crystals and the superposition of a growing different crystalline structure from around 12°C, and the corresponding melting ending up to 18°C (see photos 3 and 4 in **Figure 4.10a**).
C_8 and C_{10} exhibit a thermal profile simpler than IPP; on cooling, only one exothermal peak is detected at 8.9 and 26°C respectively (**Figure 4.10b** and **4.10c**), indicating that only one crystalline structure is formed. At the microscope, the complete crystallisation of the sample was observed in a very narrow temperature range (see photo 5 in **Figure 4.10b** and photo 7 in **Figure 4.10c**). Upon heating, C_8 melts in one step (one endothermal peak) at 17.6°C, while C_{10} displays a broad and asymmetric one. These melting profiles agree with those observed by HSM, in particular note that C_{10} starts melting around 27°C and only ends up to 37°C.

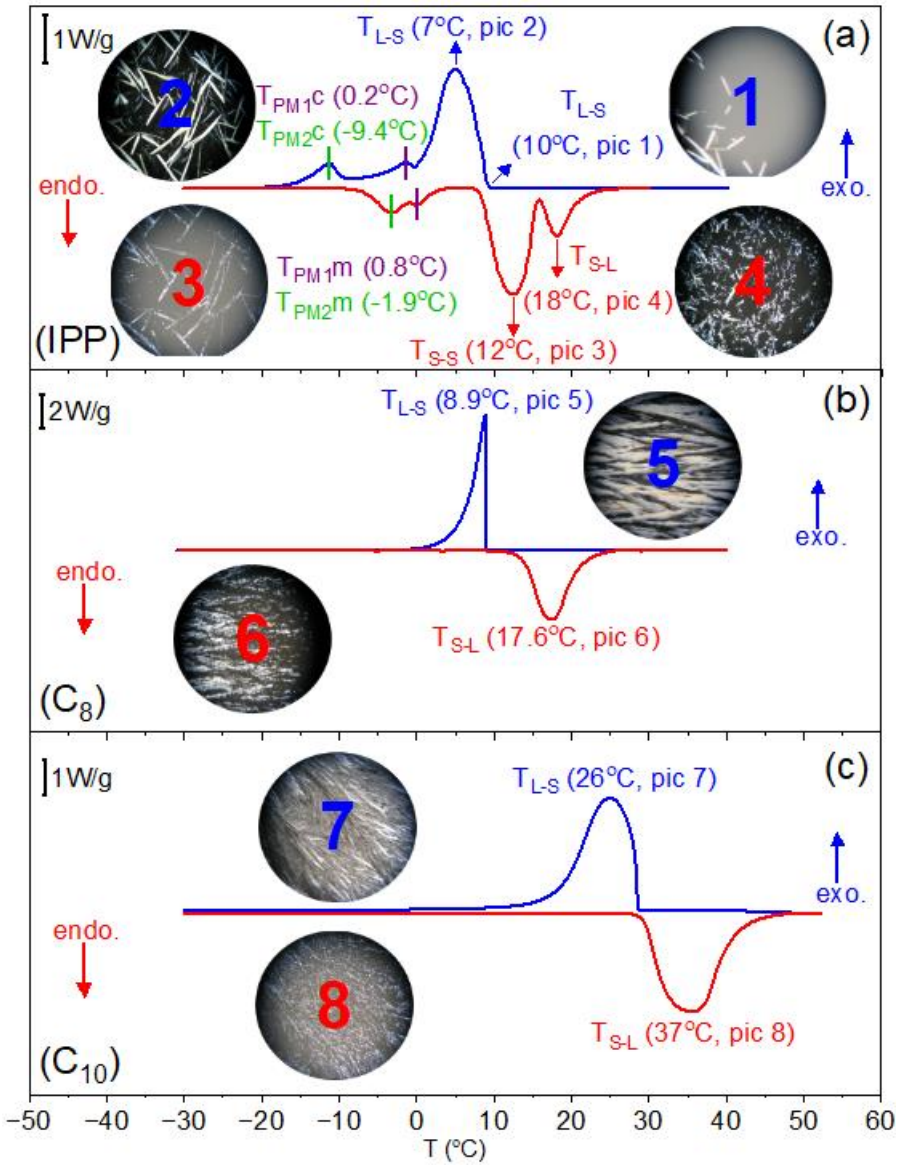

Figure 4.10 — Thermograms obtained at 10°C/min on cooling (blue) and on subsequent heating (red) for bulk: (a) isopropyl palmitate (IPP), (b) capric acid (C_8), and (c) caprylic acid (C_{10}). Microphotographs with 40x (C_8) and 100x (IPP and C_{10}) magnification were taken under 5°C/min cooling/heating rates around the indicated temperature. The liquid-to-solid transition was marked as T_{L-S}, the solid-to-solid transition as T_{S-S}, the solid-to-liquid transition as T_{S-L}, and the transitions of polymorphic materials as T_{PM1}, T_{PM2}.

Crystallisation and melting onset temperatures are nearly the same for C_{10}, and a difference of nearly 5 degrees was detected in C_8 (data are displayed in **Table 4.6**), indicating a certain degree of supercooling (for cooling/heating rates of 10°C/min). The global enthalpies of crystallisation are calculated from the area under the exothermal line relative to an arbitrary baseline also included in **Table 4.6**. For bulk IPP, the enthalpies values are lower, ~115 J/g [173–176], likely related to differences in the overlapping of the polymorphic phases as result of different cooling rates applied. These values are in good agreement with data reported in literature for C_8 [177–179] and C_{10} [180–182].

Table 4.6 — Onset and transition temperatures of crystallisation (T_c) and melting (T_m) of isopropyl palmitate (IPP), caprylic (C_8) and capric (C_{10}) acids and their corresponding C_8/C_{10} binary mixtures. The liquid-to-solid transitions were marked as $T_{L\text{-}S}$, the solid-to-solid transitions as $T_{S\text{-}S}$, the solid-to-liquid transitions as $T_{S\text{-}L}$, and the transitions of polymorphic transformations as T_{PM1} and T_{PM2}. ΔH_c is the global enthalpy of crystallisation.

Sample	Cooling						Melting				
	Phase transition					ΔHc (J g^{-1})	Phase transition				
	$T_{onset,c}$ (°C)	$T_{L\text{-}S,c}$ (°C)	$T_{S\text{-}S,c}$ (°C)	$T_{PM1,c}$ (°C)	$T_{PM2,c}$ (°C)		$T_{onset,m}$ (°C)	$T_{PM2,m}$ (°C)	$T_{PM1,m}$ (°C)	$T_{S\text{-}S,m}$ (°C)	$T_{S\text{-}L,m}$ (°C)
IPP	10.0	7.3	–	0.2	-9.4	156.2	9.3	-1.9	0.8	12	18
C_8	8.9	8.9	–	–	–	149.6	13.6	–	–	–	17.6
C_{10}	29.8	26.0	–	–	–	164.6	28.4	–	–	–	35.7
11% C_8	7	2	-9.4	–	-11.6	162.1	-6.9	–	–	-0.1	18.7
22% C_8	4.3	-0.1	-9.2	–	-12.8	151.9	-5.8	–	–	-0.5	16.3
11% C_{10}	7.6	4	-1.9	–	-11.6	152.1	-7.6	-4.1	-0.2	6.6	17.1
22% C_{10}	5.8	2.4	-0.2	–	-10.6	140.8	-7.8	-4.5	-0.1	5.5	14.8

In the binary C_8 and C_{10} systems, the overall thermal behaviour resembles that of bulk IPP, presenting multiple peaks, as well as in the different morphologies observed by HSM (see **Figure 4.11** and photos included in); however, some differences must be pointed out. Regarding the crystallisation onset, the dispersion of the acids in IPP leads to a shift toward lower temperatures, then extending the liquid temperature range. Additionally, this shift becomes more pronounced with the increases of C_8 or C_{10} content (see **Table 4.6**). This behaviour occurs because the addition of fatty acid esters causes a depression in the solvent's freezing point [183] as the C_8/C_{10}:IPP complex starts to form.

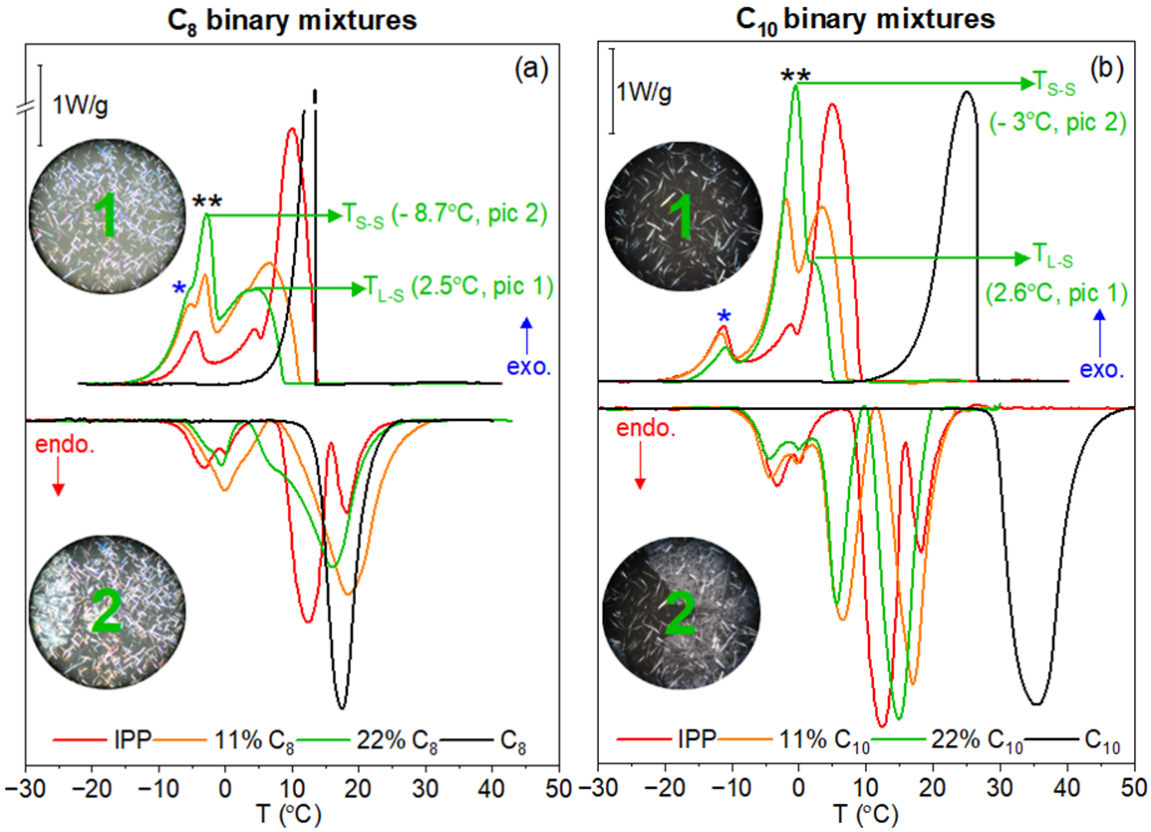

Figure 4.11 — Thermograms of C_8 and C_{10} binary mixtures obtained on cooling (exo.) and heating (endo.) at 10°C/min (for data processing the second cycle was considered). Sample masses between 7-23 mg. Microphotographs with 40x (22% C_8) and 100x (22% C_{10}) magnification were taken under 5°C/min cooling/heating rates around the indicated temperature. The liquid-to-solid transition was marked as $T_{L\text{-}S}$, and the solid-to-solid transition as $T_{S\text{-}S}$.

To clarify the origin of the multiple maxima, different compositions were additionally analysed for each of the mixtures. In **Figure 4.12**, the cooling (a, b) and subsequent heating (a_1, b_2) thermograms for the indicated compositions are represented.

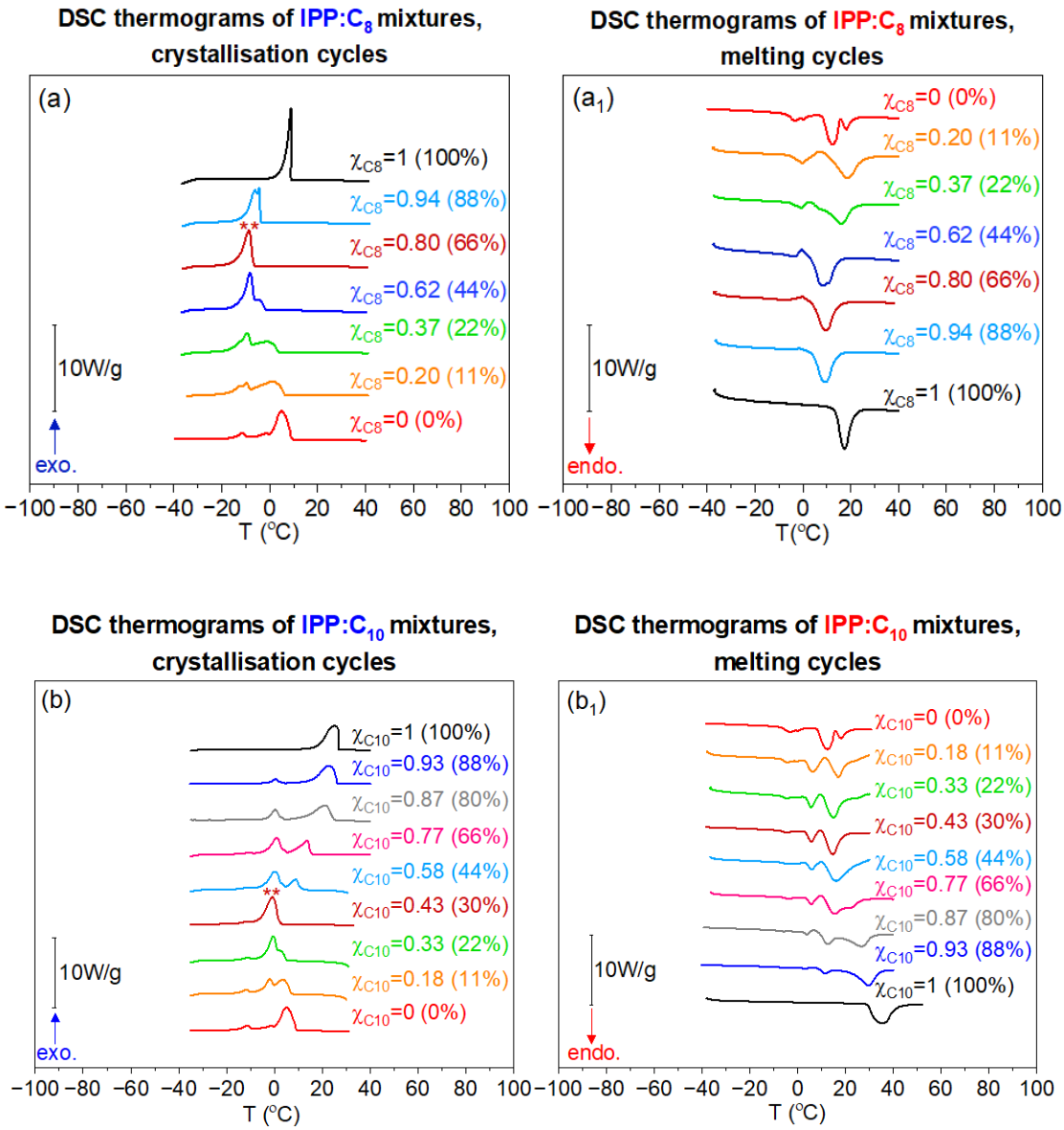

Figure 4.12 — Binary mixture thermograms obtained at 10°C/min on cooling, (a) and (b), and the subsequent heating, (a_1) and (b_1).

Taking the onset temperature of the crystallisation peaks from the cooling thermograms (**Figure 4.12a** and **4.12b**), it can be constructed the phase diagram for these mixtures, that are represented in **Figure 4.13**. For all compositions, the T_c is lower than that which would result from the linear combination of the T_c of the pure compounds, which means that both IPP:C_8 and IPP:C_{10} behave as eutectic mixtures. [184–187] For that with $\chi(C_8) = 0.80$ and $\chi(C_{10}) = 0.43$, only one crystallisation peak, indicated by (**), is observed meaning that the eutectic composition is close to these values. However, on heating, cold-crystallisation is still observed close below the more intense melting peak in C_8 mixtures, and it is even more evident in C_{10} ones. These features point to the high tendency of IPP for recrystallising on heating in the presence of fatty acids; however, when IPP is mixed with C_8 close to the eutectic composition (around $\chi(C_8) = 0.80$), this tendency is significantly reduced.

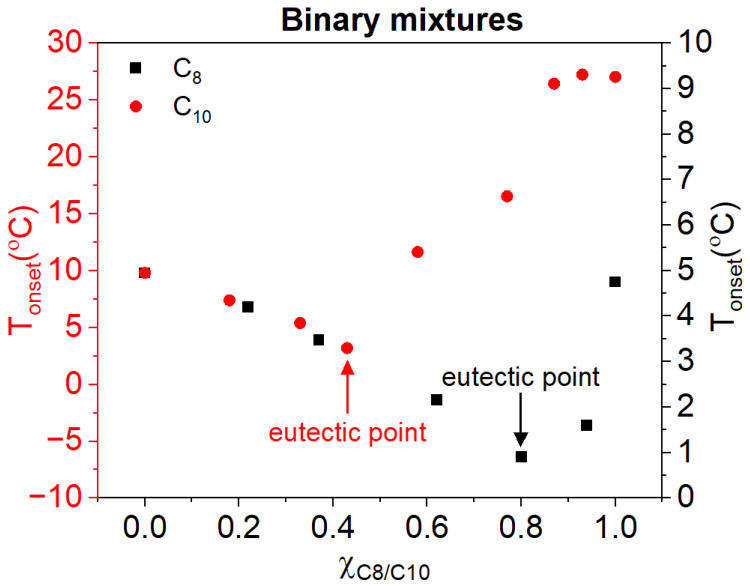

Figure 4.13 — Liquid-solid phase diagrams of IPP:C_8 and IPP:C_{10} mixtures (thermograms taken on cooling at 10°C/min).

With this information, focusing again on the binary mixtures for subsequent encapsulation, it is possible to identify in the thermograms the crystallisation peaks related to the eutectic compositions (marked with **) and those related to the "excess" of IPP corresponding to their polymorphic transformations (marked with *).

4.6 Conclusions

In this study, the microencapsulation of diverse thermochromic ternary systems, formulated with fatty acids as colour developers and a novel spirolactone dye as the colour former, were successfully achieved. The resulting microcapsules were characterised using dynamic light scattering (DLS), scanning electron microscopy (SEM) and differential scanning calorimetry (DSC) techniques. The data obtained from DLS and SEM demonstrated that the PI, Z-average and mean values increased in conjunction with the concentration of the colour former. The DSC analysis indicated that the crystallisation and melting processes are characterised by a multi-step mechanism, resulting from the formation of eutectic systems and the presence of polymorphic components. Additionally, the transition temperatures are influenced by the polymeric wall formation and the rise in colour developer concentration. The encapsulation ratio (R) and encapsulation extent (E) were found to be considerable for most of the systems.

5

CONSTRUCTION OF REVERSIBLE THERMOCHROMIC SMART LABELS. INKS FORMULATION, PRINTING PROCESS AND COLOUR CHARACTERISATION.

Abstract

The focus of this work was the construction process of reversible thermochromic smart labels. This process comprised several steps such as ink formulation, printing process, colour characterisation, and graphical design work for sketching the label's interface.

The inks were formulated by mixing microcapsule dispersion (developed in Chapter 4) with a water-based acrylic binder and then screen printed as a 24 μm wet film (*circa* 12 μm dry film) on a self-adhesive matte inkjet paper. Subsequently, the resulting indicators were delineated and placed on the label's interface, which had been previously sketched in PowerPoint and digitally printed on a polypropylene (PP) laminated paper substrate.

SEM analysis was used to visually assess prints' quality, microcapsule-binder homogeneity, and capsule integrity after the printing pressure. CIELAB measurements were carried out to observe the colour evolution, determine the onset/transition temperatures and colour contrast. SEM images revealed that the printing process does not affect the integrity of the capsules, and the inks have a good adhesion to the paper substrate. Colourimetric data showed that the contrast increases with the concentration of colour former, and both caprylic and capric acid act as good colour developers for the novel flavylium spirolactone dye. Remarkably, in the presence of capric acid a two steps colour transition mechanism was established. The best performing indicator clears at +10°C on the heating cycle and recolours fully at +4°C on the cooling cycle and shows thermal and colour switching stability.

5.1 Introduction

Labelling technologies have made massive advances in recent years, see **Table 5.1**. The rapid transition from barcode/QR-code labels to sensor-based displays (smart labels), makes them items with wide range of application options. [188] Barcode/QR code labels are inexpensive technologies as they can be applied on various surfaces by printing technique. However, the need to use a hand scanner for detection led the industry to move towards the development of radio frequency identification (RFID) tags. The RFID-tag utilises radio frequency waves and can wireless transfer information by simply passing the tag through a reader or gate without optical contact. Both barcode and RFID labels are data-carrying devices designed to store, distribute and track certain goods. [188]

Subsequent evolution led to more versatile labels and are nowadays referred to as smart labels. These labels are advanced devices with both identification and interactive functions. They can collect and communicate data in the Internet of Things (IoT) using various wireless technologies and interact with costumers through an energy-efficient display. [188,189] The interactive interface (display) of these types of labels can be activated by changes in temperature, UV light, humidity, electric power, or pH. For example, a display that changes its characteristics according to temperature fluctuations is referred to as a thermochromic display or thermochromic smart label.

Table 5.1 — Evolution of labelling technology over the years. The table was adapted after reference [188,189].

Identification technology			
line of sight	no line of sight		
no sensors		sensors	
no display			display
 Bar/QR-Code	 RFID-Tag	 RFID-Sensor-Tag	 Smart Label (e-Label)

Currently, in the global market, the dominant labels are plastic-based as they are durable, resistant to moisture and chemicals and flexible. However, the forecast presents that the paper-based labels will be expanding at a higher rate in the upcoming period. This growth is owing to its eco-friendly components, recyclability and biodegradability. Moreover, advances in printing technologies have improved the quality and durability of printing and hence spread their acceptance across various sectors. [190]

Thermochromic labels are projected to account for a market share of $USD 781.14 million by 2033, **Table 5.2**. This growth is influenced by advancement in technology and the implementation of smart packaging solutions. Their extensive use in the pharmaceutical sector to guarantee authenticity and improve the lifespan of medicines and healthcare products will significantly contribute to this growth. Additionally, the increasing need to efficiently manage food waste will lead to greater adoption of these labels in active and smart packaging. Smart labels will also be increasingly utilised as a security element to combat product counterfeiting. It is

also predicted their use in the food & beverages industry, cosmetic & personal care sector, and automotive market to ensure the integrity of some sensitive products. [191]

Table 5.2 — Forecast growth of Global Thermochromic Labels Market, 2023-2033. CAGR is the compound annual growth rate.

Attributes	Details
Thermochromic Labels Market CAGR (2023 to 2033)	6.3%
Thermochromic Labels Market Size (2023)	US$ 424.03 million
Thermochromic Labels Market Size (2033)	US$ 781.14 million

In 2022, irreversible labels had a share of around 80% of the thermochromic labelling market, but this is expected to lose significant ground due to re-usability issues. Therefore, this issue will drive the market for reversible thermochromic labels. [191]
Finally, based on the above information, it can be concluded that the reversible thermochromic smart label developed in this project has important characteristics that meet the market requirements. Firstly, it is constructed from biodegradable components, as it is paper-based and using recyclable polypropylene. Secondly, it has a reversible colour change, so it is reusable. And ultimately, the printing technology used to produce the indicators is already available and well-known. However, it should be noted that the recent limitation imposed by the European Commission on the use of microplastic may require replacing the melamine formaldehyde polymer with a more biodegradable one.

5.2 Materials and methods

5.2.1 Materials and chemicals

The screen binder was available from LCR Hallcrest (part of Spotsee) under the brand name LE-15 Water based screen binder. The inks were printed on self-adhesive matte inkjet paper. Polypropylene (PP) laminated paper substrates were used to digitally print the label's interface, and subsequently the best performing indicator (1.6 wt.-% leuco dye **1** and 22 wt.-% capric acid composition) was placed onto the PP-based card.

5.2.2 Methods

5.2.2.1 Ink formulation and printing process

The inks were formulated by mixing the microcapsule dispersions (see **Table 5.3** for microcapsules' composition used to produce the thermochromic inks) with a water-based acrylic binder, in 1:1 ratio (wt/wt), and then screen printed as a 24 μm wet (*circa* 12 μm dry film) on a self-adhesive matt inkjet paper substrate.

5.2.2.2 Characterisation of printed indicators

5.2.2.2.1 Scanning electron microscopy (SEM)

The printed indicators were characterised by scanning electron microscopy with a Hitachi Regulus SU8220. The acceleration voltage was 5 kV, the working distance was around 9 mm, and the magnification was between 2 and 25 Kx SE(U). Samples preparation was achieved by placing the printed surface on a holey carbon support film and coated with a thin film of 20 nm of Au:Pd (80:20 ratio) by sputtering in a Quorum QT150 ES.

5.2.2.2.2 CIELAB characterisation

The colour change of all the printed indicators was monitored using a DankamHT E995F (DTU6005-0027-SN) apparatus equipped with an aluminum plate. 1°C/min cooling/heating rate is used during all experiments. Photos were taken with a Sony Cybershot DSC-HX60 camera using standard mode settings. ImageJ was employed to extract the CIELAB colour coordinates of both printed and white surfaces. Furthermore, the colour change of the final label was monitored by placing the indicator on the back side of a cell holder connected to a VWR 1160S Heated Recirculating Chiller with PID/digital temperature control and LED temperature display. The temperature on the surface of the holder was measured with a Beizuu TM-902C Digital Thermometer equipped with a Thermocouple Needle Probe. The reflectance values were collected with Lovibond® spectrophotometer TR520, SN 950999, standards D65 light source at 10° observer angle, at 30°C and -5°C on cooling/heating cycles.

5.2.2.2.3 Cycling tests

For cycling tests, the colour change of the printed indicator was monitored by placing the indicator on the back side of a cell holder connected to a VWR 1160S Heated Recirculating Chiller with PID/digital temperature control and LED temperature display. The temperature on the surface of the holder was measured with a Beizuu TM-902C Digital Thermometer equipped with a Thermocouple Needle Probe. The lightness values were collected with Lovibond® spectrophotometer TR520, SN 950999, standards D65 light source at 10° observer angle, at 30°C and -5°C for 10 heating/cooling cycles.

5.3 Experimental

5.3.1 Printing process and SEM characterisation of printed indicators

Screen printing is a versatile printing technique as it can print on a variety of substrates such as paper, plastic, glass, metals and fabrics. Industries that make heavy use of screen-printing technology are those producing labels, stickers, signs, posters and textiles. The prints can display product-related information, brand names, security elements, and static or dynamic images for informative or promotional purposes. [192]

The screen-printing equipment is (a simplistic machine) made up of three main components: ink, a rubber blade (squeegee) and a mesh (screen), **Figure 5.1**. The screen is the image carrier, and the rubber blade is the tool used to squeeze the ink through the mesh. To develop a physical pattern or image, a stencil is projected onto the porous mesh. The mesh is then stretched over a frame that eventually resembles the well-known screen. The ink laid on the screen is then forced through the pores of the mesh with the squeezing tool to eventually form a design. The ink can be passed through the mesh manually or automatically with the help of a press. [192–194]

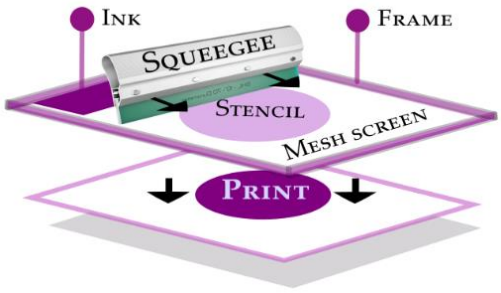

Figure 5.1 — Screen-printing technology.

Nowadays, screen printing technology is also widely used to print graphic images with thermochromic inks, which are smart materials made up of a dynamic ink that changes colour when exposed to different temperatures and can be formulated as water-based inks. For instance, printed thermochromic inks are used as thermal indicators in novelty items such as coffee cups and syrup bottles. Moreover, they are also used to print life indicators on batteries and temperature indicators on drinking containers. As mentioned in the introduction, thermochromic inks are usually *leuco* dye or liquid crystal based; however, *leuco* dye-based inks are preferred because they are cost-effective and easier to work with. These inks can be printed by lithography, letterpress, gravure, flexography or screen printing. However, for this work screen-printing was used because of its availability and simplicity. [192] The thermochromic ink used for printing was water-based and was prepared by mixing the microcapsule dispersion with a 1:1 by weight with water-based acrylic binder (see the **Table 5.3** for microcapsules' composition used to produce the thermochromic inks). After a good homogenisation of the samples, the ink was printed as a 24 μm wet film (*circa* 12 μm dry) on a self-adhesive matte inkjet paper substrate and analysed by SEM.

Table 5.3 — Composition of core material in encapsulated (c) systems used to produce the thermochromic inks and subsequently the prints (p). The composition is expressed as mass ratio and wt.-%. Caprylic (C_8) and capric (C_{10}) acid were selected as colour developers (CD), and isopropyl palmitate as a solvent, and the isolated leuco dye **1** was used as a colour former (CF). In all the systems, the core:shell ratio was 5:1.

System	Sample	Ratio IPP:C_8/C_{10}:CF	CD (wt.-%)	CF (wt.-%)
C_8	$c_1 \rightarrow p_1$	8.82 : 1.1 : 0.08	11	0.8
	$c_2 \rightarrow p_2$	8.74 : 1.1 : 0.16		1.6
	$c_3 \rightarrow p_3$	7.72 : 2.2 : 0.08	22	0.8
	$c_4 \rightarrow p_4$	7.64 : 2.2 : 0.16		1.6
C_{10}	$c_5 \rightarrow p_5$	8.82 : 1.1 :0.08	11	0.8
	$c_6 \rightarrow p_6$	8.74 : 1.1 : 0.16		1.6
	$c_7 \rightarrow p_7$	7.72 : 2.2 : 0.08	22	0.8
	$c_8 \rightarrow p_8$	7.64 : 2.2 : 0.16		1.6

5.3.1.1 Scanning electron microscopy (SEM) of printed indicators

SEM analysis was used to visually assess prints' quality, microcapsule-binder homogeneity, and capsule integrity after the printing pressure. **Figure 5.2** shows SEM images of C_8/C_{10} thermochromic printed indicators. These images display that the printing process does not affect the integrity of the capsules. It can also be observed that the inks have a good adhesion to the

paper substrate and the resulting printed film makes the paper surface smoother. Additionally, the images reveal that the capsules, except c_2 and c_6, have high compatibility with the binder, as they are evenly dispersed into the polymeric composition. The low compatibility of c_2 and c_6 capsules dispersion with the binder may be due to degradation of some capsules that release core components (i.e., non-polar isopropyl palmitate), which eventually leads to an inhomogeneous ink. This phenomenon may be caused by the difference of surface tension between the non-polar isopropyl palmitate and the polar acrylic binder (see references [47-49] for acrylic polymers structures). Furthermore, SEM analysis of the p_6-printed material showed regions with disrupted capsules, **Figure 5.3**, which support the above-mentioned.

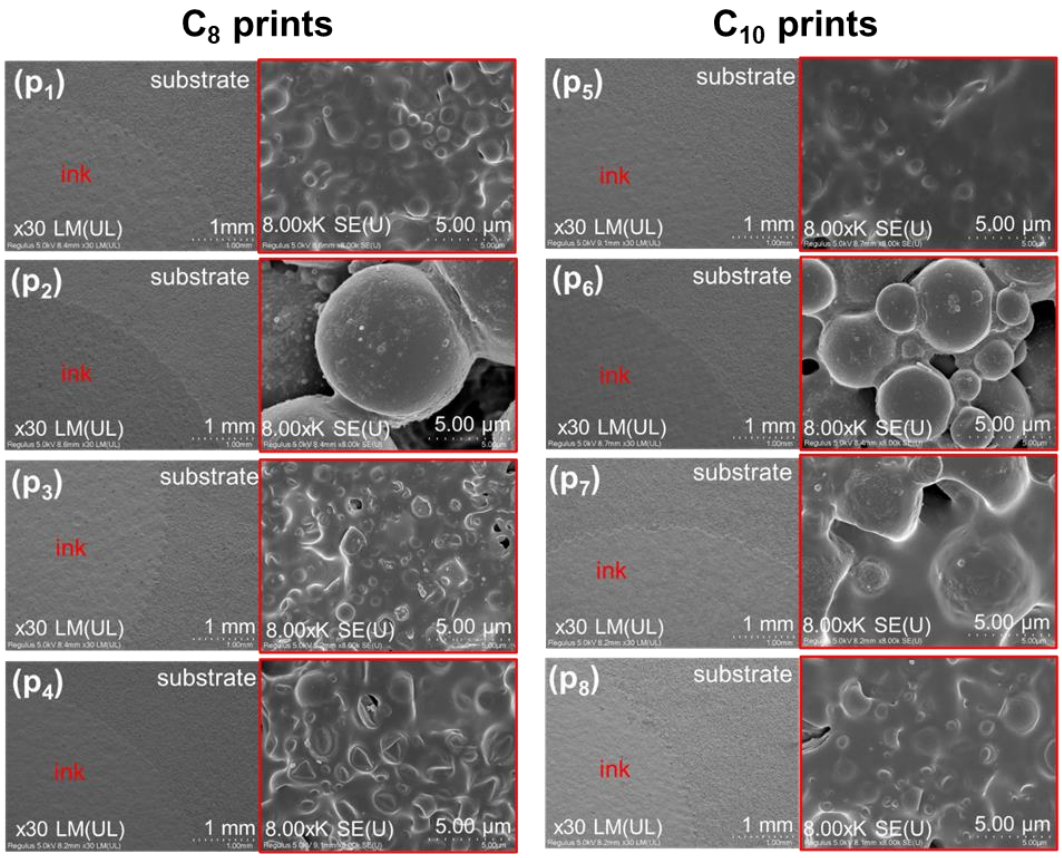

Figure 5.2 — SEM images of C_8 *(p_1, p_2, p_3, p_4)* and C_{10} *(p_5, p_6, p_7, p_8)* printed indicators. Photos were taken at x30 and 8xK magnification. The inks were formulated by mixing the microcapsule dispersion with a water-based acrylic binder, in 1:1 ratio (wt/wt), and then screen printed as a 24 µm wet (*circa* 12 µm dry film) on a self-adhesive matte inkjet paper substrate.

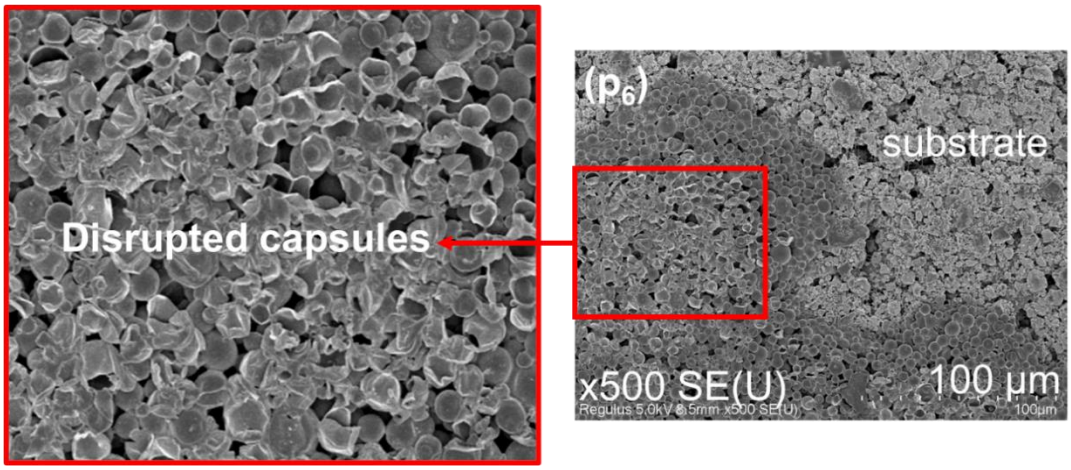

Figure 5.3 — SEM images of p_6 printed indicator showing a region with disrupted capsules. Photos were taken at x500 magnification. The ink was formulated by mixing the microcapsule dispersion with a water-based acrylic binder, in 1:1 ratio (wt/wt), and then screen printed as a 24 µm wet (*circa.* 12 µm dry film) on a self-adhesive matte inkjet paper substrate.

5.3.2 CIELAB colour characterisation

To observe the colour evolution, to determine the onset/transition temperatures of colouration and contrast difference (ΔE*), the printed indicators were photographed at 15°C, 12°C, and each degree from 10°C to -15/-5°C (C_8/C_{10} prints). The collected photographs were then processed with ImageJ software to extract Lab* coordinates for further used in the determination of ΔE* with the help of **equation 5.1**. Subsequently, the obtained numerical data were plotted as a function of temperature and fitted with a sigmoidal function defined by **equation 5.2**. [195]

$$\Delta E^* = \sqrt{(\Delta L^*)^2 + (\Delta a^*)^2 + (\Delta b^*)^2} \qquad \text{Equation 5.1}$$

$$\Delta E^* = \Delta E^*_{hot} + (\Delta E^*_{cold} - \Delta E^*_{hot}) \times \left(1 - \frac{1}{1 + e^{-x}}\right) \qquad \text{Equation 5.2}$$

in equation 5.1, L* is the lightness, a*, b* are red-green, respectively yellow-blue colour components; and in equation 5.2, ΔE^*_{hot} is the contrast at the beginning of colouration, while ΔE^*_{cold}, the contrast at the end of colouration. **Figure 5.4** displays the obtained graph, and **Table 5.4** the corresponding contrast values, onset and transition temperatures at which colouration starts (T_{onset}) and reaches 50% ($T_{T^{50}}$) and 75% ($T_{T^{75}}$) conversion level.

The obtained graphs show that the contrast increases as the systems starts to freeze (**Figure 5.4**). Colouration is a one step process in C_8 systems, whereas in C_{10} systems it occurs in two steps. Furthermore, **Table 5.4** shows that the contrast increases (both at the beginning and end of colouration) with CF's concentration, and 75% colouration is achieved in a relatively short range.

The contrast increases as the systems start to freeze, because the thermodynamic equilibrium favours the transfer of the proton from the acid to the lactone, yielding the coloured opened

form species. [104] Moreover, the two-step colouration behaviour in C_{10} indicators suggests that the dye is not exclusively confined to the C_{10}:IPP eutectic region (**Figure 4.9d$_1$, Chapter 4**), but it also extends into the IPP-rich part where certain CD molecules are present and capable of interacting with CF to produce the observed colouration. As for the one-step colouration behaviour observed for C_8 indicators, it suggests that colour transition occurs exclusively in the IPP-rich region. This could be due to the presence of the IPP polymorph in the IPP:C_8 region, which obstructs or weakens the interactions between CF and CD (**Figure 4.9d, Chapter 4**). As for the contrast observed before cooling, it may come from the CF units trapped in the microcapsule wall that interact with the polar parts of the acrylic binder. These interactions transform the *leuco* dye into its strongly coloured cationic form and generate the observed colour. [104]

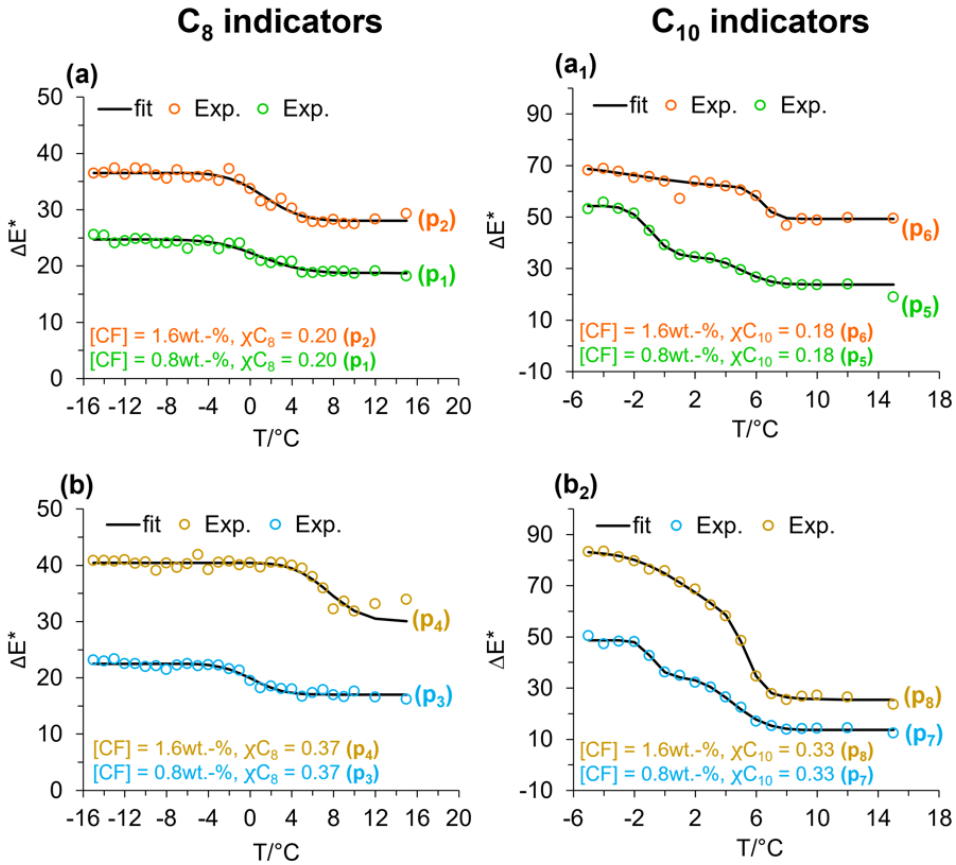

Figure 5.4 — ΔE* plotted as a function of temperature for C_8/C_{10} systems, cooling event. The molar fraction (χ) of C_8/C_{10} was set at 0.20 (a/a$_1$) and 0.37 (b/b$_1$), respectively. The concentration of colour former was set at 0.8wt.-% *(p_1, p_3, p_5, p_6)* and 1.6wt.-% *(p_2, p_4, p_7, p_8)*, and data were collected at 1°C/min scanning rate.

Table 5.4 — Contrast difference (ΔE*) at the beginning (ΔE^*_{hot}) and end (ΔE^*_{cold}) of colouration along with colouration onset temperatures (T_{onset}) and transition temperatures at which colouration reaches 50% (T_T^{75}) and 75% (T_T^{75}) conversion level.

System	Print (p)	CD (wt.-%)	CF (wt.-%)	ΔE^*_{hot}	ΔE^*_{cold}	T_{onset}	T_T^{50}	S.D.^{50}	T_T^{75}	S.D.^{75}
C_8	p_1	11	0.8	13.4	29.7	6.0	2.5	1.8	–	–
	p_2		1.6	42.5	58.1	8.6	6.9	0.9	–	–
	p_3	22	0.8	10.9	25.3	6.9	1.3	2.8	–	–
	p_4		1.6	35.3	48.2	1.5	-0.5	1.0	–	–
C_{10}	p_5	11	0.8	23.8	54.3	8.1	5.1	1.5	-0.9	1.1
	p_6		1.6	49.3	71.0	7.9	6.4	0.8	-1.7	4.6
	p_7	22	0.8	13.6	48.7	8.0	4.5	1.8	-0.9	0.7
	p_8		1.6	25.5	83.7	7.0	5.4	0.8	1.9	3.2

5.3.3 Temperature profile analysis of p_8 indicator

Figure 5.5 shows the colour change profile of the best performing indicator (1.6 wt.-% leuco dye **1** and 22 wt.-% capric acid composition). The thermochromic indicator shows reversible colouration with an onset colour transition at 7°C and a small hysteresis lag. It can also be observed that the colour change occurred gradually with a 95% colour transition at 4°C. These features highlight that the printed material can be used as a thermochromic indicator for products requiring storage at refrigeration temperatures.

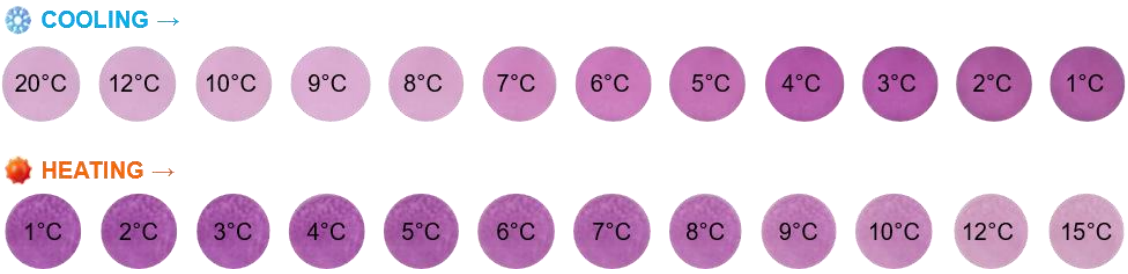

Figure 5.5 — Temperature profile of p_8 indicator recorded after ink formulation (screen binder:capsules dispesion=1:1 ratio) and screen-printing on a self-adhesive matte inkjet paper as a 24 μm wet film (*circa* 12 μm dry film). The indicator displayed a reversible colouration with an onset cooling temperature at 7°C and a small hysteresis lag.

The intensity of colour change against temperature (of p_8 indicator) was also measured by spectrophotometric measurements carried out with a Lovibond® TR520 spectrophotometer, SN: 950999. By using this apparatus, the changes in reflectance were recorded on both cooling and heating cycles. The reflectance was then converted to absorbance, and by plotting its maximum as a function of temperature, the graphs shown in **Figure 5.6** were obtained. According to these graphs, the absorbance gradually increases during cooling cycle and decreases on heating. Moreover, on heating cycle, between 2.5-10°C, the absorbance tends to increase because there is some light scattering generated by the condensation phenomena. Finally, the CIELAB measurements also confirmed that the developed thermochromic indicator shows a reversible and gradual colour change with a small hysteresis lag.

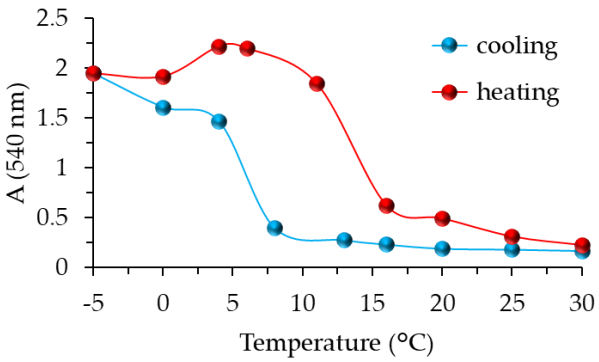

Figure 5.6 — Absorbance maximum as a function of temperature of p_8 indicator on both cooling and heating cycles. The data were recorded between 30°C and -5°C on cooling and heating cycles.

Figure 5.7 shows that screen printing allows large scale printing (a) and can give access to both hand application and automated application and split view of the various components (b) of the thermochromic label. As can be seen, the digitally printed interface provides the reader with guidance on how the colour change should be interpreted. Furthermore, **Figure 5.8** demonstrates that the final prototype is a compact label (2 cm width, 2.1 cm length and 8 mm) that occupies minimal space as per CHARISMA proposal imposed.

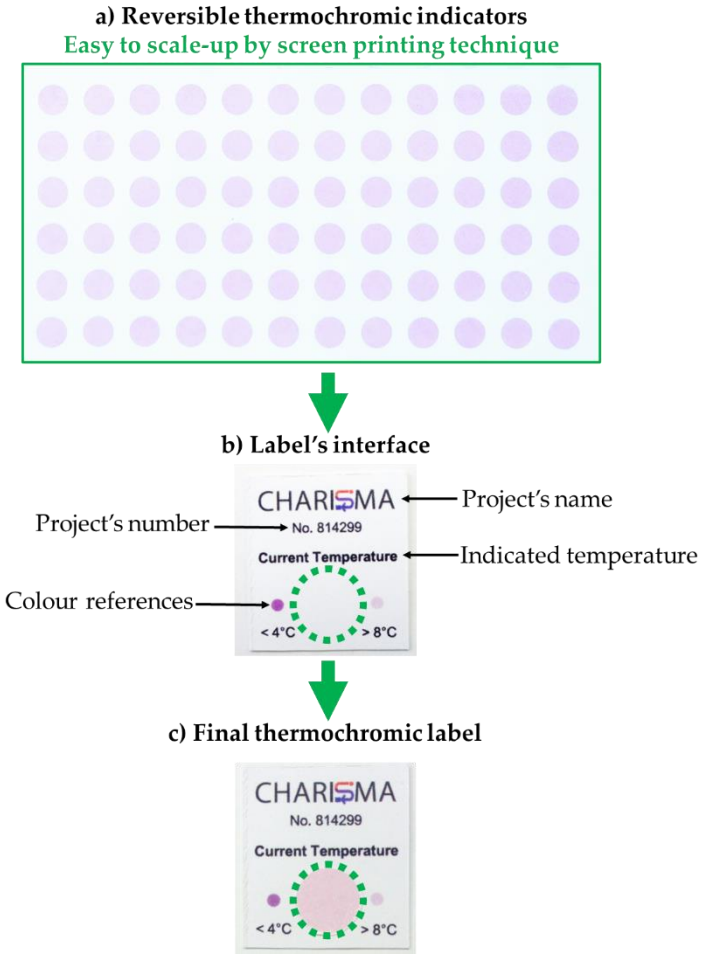

Figure 5.7 — Description of the components of the reversible thermochromic label (b). Image (a) shows a print of 72 labels on a A4 self-adhesive matte inkjet paper carried-out at 24 µm wet film (*circa* 12 µm dry film), and image (c), the final CHARISMA thermochromic label.

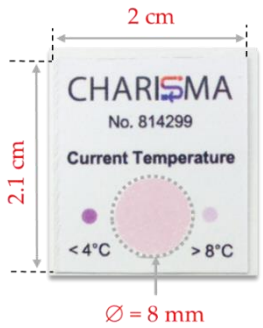

Figure 5.8 — Dimensions of reversible thermochromic smart label.

5.3.4 Cycling tests of p_8 indicator

To assess the stability of the colour, p_8 indicator was subjected to cycling tests. For these tests, we quantified the alteration in lightness (L*) across 10 consecutive heating/cooling cycles between 30 and -5°C. As depicted in **Figure 5.9**, noteworthy fluctuations in the L* values were not observed; in fact, the system exhibited a notable degree of stability.

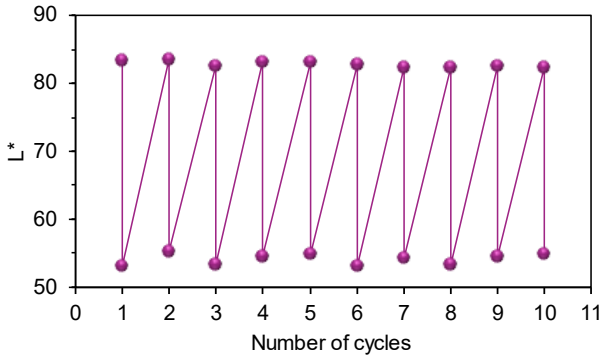

Figure 5.9 — Lightness (L*) values of p_8 thermochromic indicator recorded for 10 heating/cooling cycles to prove thermal and colour switching stability.

5.4 Combining academic and industrial expertise to reach the objectives of the CHARISMA project

Developing devices that deliver simple, reliable, and unambiguous messages is one of the challenges of sensors and was also the primary goal of the CHARISMA project. CHARISMA was an ITN European Industrial Doctorate (ITN-EID) funded by the European Union's Horizon 2020 Marie Skłodowska-Curie Actions Programme (Grant Agreement No. 814299, https://charisma.univie.ac.at/), that promoted the concept of applied chemical irreversibility to engineer displays for smart labels applications. The project brought together a unique team of leading academic groups and industry, with expertise in the fields of chemistry, physics, and materials engineering.

Through 9 Early-Stage Researchers (ESR), CHARISMA's goal was to design printable displays that combine chemical and electrical components. Constructed from chromogenic materials, the smart labels were to change colour permanently when sensing a thermal or redox stimuli. As illustrated in **Figure 5.10**, a sensing unit (red circle) detects the stimulus, which makes a chromogenic display change colour irreversibly (yellow rectangle). The sensing unit and chromogenic display are connected through a circuit (supplied by a power unit; green rectangle), which allow a response to stimulus and trigger the thermochromic/electrochromic switching. Once the signal is transmitted to the chromogenic display, the latter will undergo an irreversible colour transformation. The ideal template is thin and flexible taking virtually no space and can be manufactured at low-cost, and thus applicable in any logistics. Ultimately, the use of chromogenic display avoids additional procedures to read the alarms, making this solution easy to check by anyone at any time without any specific training.

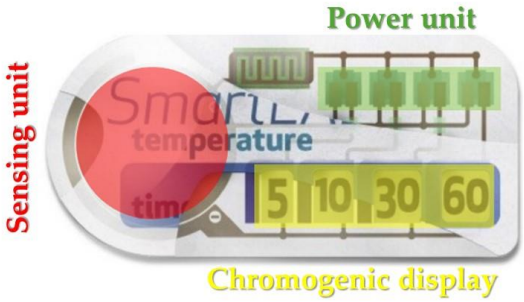

Figure 5.10 — Schematic representation of the prototype of smart label, that was the scientific and technological objective of CHARISMA. The label capitalises on a sensing unit (red circle) made up of materials changing their conduction properties after being exposed to an external stimulus or variation of temperature: thanks to a circuit and a power unit (green rectangle), the chromogenic display (yellow rectangle) will change colour permanently.

As ESR2, I was responsible for developing printed chromogenic materials able to sense a thermal stimulus. The construction of this material involved several steps and are outlined in **Scheme 5.1**. To cover step 1, two libraries of chromogenic dyes were designed, both containing 2-phenyl-1-benzopyrylium (flavylium) as structural core: (a) flavylium-based spirolactone derivatives and (b) 4-arylidene-substituted flavylium derivatives. The libraries were built by introducing donor and/or acceptor groups in different positions (e.g., position 7, 4 or 4') to cover a wide range of colours.

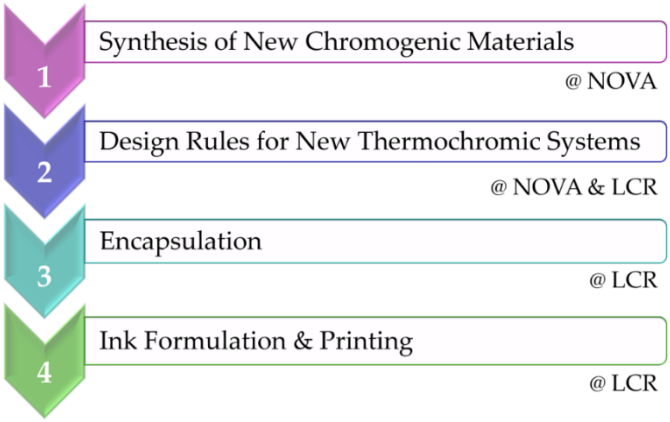

Scheme 5.1 — Steps outlining the work conducted in CHARISMA to develop printed chromogenic materials, with involvement from both academic (NOVA University) and industrial (LCR Hallcrest Company) partners.

In step 2, thermochromic systems that involve a spirolactone dye-developer-solvent or thermosensitive polymers were designed. Spirolactone dyes are known as materials with indirect thermochromism and require the design of an appropriate system to give a response to a thermal stimulus. The thermochromic system is usually composed of at least of three components: a colour former (spirolactone dye), a colour developer (weak acids or bases) and solvent (long chin alcohol or ester) that defined the sensing temperature of the system. [5,13] To achieve the desired properties, the thermochromic system first had to be microencapsulated and then mixed with a binder (to produce the ink) and screen-printed onto the selected surface (step 3 and 4).

After various tests, it was concluded that the flavylium-based spirolactone dyes can react to thermal stimuli in the presence of organic amines and polar aprotic solvents. However, the

changes were reversible, and the effect was lost when the multicomponent systems were encapsulated. It is believed that the loss of colour switching occurred due to the migration of the amine into the aqueous solution outside the capsules during encapsulation. Further isolation of *leuco* dye species and encapsulation with weak fatty acid developers resulted in thermochromic printed materials with reversible colour change. Chromogenic materials with irreversible colouration could not be achieved due to the impossibility of encapsulating Lewis acids as $FeCl_3$ (and as initially planned) because of the limitations of the used encapsulation method. *In situ* polymerisation is a water-based encapsulation method that requires the core components to be insoluble in water in order to limit their migration into the aqueous phase, which is not the case for $FeCl_3$.

Finally, it can be concluded that, although the thermochromic device engineered with flavylium-based spirolactone dyes did not show irreversible colouration after detecting the threshold temperature, it still has some important characteristics that are in line with the requirements of the CHARISMA device. For example:

- it is a tiny device (Ø×L×W=0.8×2.1×2 cm) and flexible that can be applied on various surfaces;
- the colour changes can be read with the naked eye without the need for an external reader;
- it is printable and paper-based;
- and most importantly, the printed ink is scalable.

5.5 Conclusions

In this study, eight thermochromic inks were prepared by combining microencapsulated ternary systems with a water-based acrylic binder. The developed inks were screen-printed on self-adhesive matte inkjet paper to construct indicators capable of detecting temperature functions within the surrounding environment. Scanning electron microscope (SEM) was employed to assess the quality of the printed indicators. CIELAB measurements were conducted to observe the colour change and select the optimal-performing indicator, and also to verify its colour stability through cyclic testing.

The SEM images demonstrate that the printing process does not compromise the structural integrity of the capsules, and the inks exhibit good adhesion to the paper substrate, and the resulting printed film enhances the smoothness of the paper surface. CIELAB measurements revealed that contrast increases as the systems start to freeze, and 75% colouration is achieved in a relatively short temperature range. The CIELAB data also demonstrated that the contrast increases with the concentration of the colour former and both caprylic and capric acid were observed to act as good colour developers for the novel flavylium spirolactone dye. Data fitting showed that colouration in C_{10} systems is a two-step process. The best-performing-indicator exhibited complete clearing at +10°C on the heating cycle and full recoloration at +4°C on cooling, and it also demonstrated colour switching stability.

Finally, the best-performing indicator (1.6 wt.-% leuco dye **1** and 22 wt.-% capric acid composition) was attached to an interface-based label that provided guidance on how the colour change should be interpreted by the reader. The resulting indicator (label) can be applied onto various sensitive packaging, either by hand application or by an automatic applicator to various sensitive packaging that needs storage at refrigeration temperatures. Moreover, the

manufacturing process is scalable and can also be done directly on the polypropylene-based label to avoid the use of matte self-adhesive inkjet paper.

6

CONCLUSIONS AND OUTLOOK

This thesis aimed to develop thermochromic smart labels based on novel synthesised flavylium dyes and implement them in an industrial setup.

The specific objectives were as follows:

1) synthesis of novel benzopyrylium (flavylium) spirolactone dyes, their spectroscopic and spectrophotometric characterisation and evaluation of acid-base behaviour;
2) synthesis of novel benzopyrylium dyes with a CH-acidic aryl group on the α-methylene position (4-arylidene-substituted flavylium dyes), their spectroscopic and spectrophotometric characterisation and evaluation of acid-base behaviour;
3) development of thermochromic systems using the synthesised spirolactone dyes as colour formers, organic amine as colour developers and weak/Lewis acids as colour lockers in water-insoluble solvents;
4) development of reversible thermochromic systems using benzopyrylium dyes with a CH-acidic aryl group on the α-methylene in Pluronic® F127 three-block thermoresponsive copolymer;
5) microencapsulation of multi-component systems and understanding dye-developer-solvent interactions through calorimetric measurements;
6) formulation of thermochromic inks to develop indicators that change colour reversibly at "refrigeration temperature".

6.1 Outcomes of the thesis

1) Five chromogenic dyes of spirolactone type based on flavylium backbone have been successfully synthesised. Spectroscopic characterisation was carried out by 1D and 2D NMR and HRMS analyses, and spectrophotometric characterisation involved absorption, emission and titration measurements. The influence of substituents in position 4' of the flavylium skeleton was studied in terms of colour modification, acid-basic behaviour and thermochromic properties.

The compounds displayed distinct colours in acidic methanolic solutions, going from blue (compound 1)/purple (compound 3) to various shades of magenta (compound 2, 4 and 5). The photophysical parameters show that amino group, due their electron donor properties, raise the oscillator strength and shift the absorption spectra into the red. Electron-withdrawing groups give rise to charge-transfer states, but their impact on the final colour is much smaller. Spectrophotometric studies showed that all the dyes were able to switch to the *leuco* species when acetonitrile was used as a solvent and DIPEA as a base. The results also showed the influence of substituents on the lactonisation process, since by attaching methyl groups it is much easier to reach the *leuco* species, with only 0.7 base equivalents (compound 2) required for a complete conversion process. Polar protic solvents such as water and ethanol, and acids such as gallic acid and iron(III) chloride (Lewis acid) have been tested as colour lockers, and the results showed that $FeCl_3$ is the most efficient component. Still, its high-water solubility hindered further encapsulation in multi-component systems.

2) Five chromogenic dye compounds based on 4-arylidene-substituted flavylium dyes with CH- acidic aryl group at the α-methylene position have been successfully synthesised, structurally and spectrophotometric characterised. Spectroscopic characterisation was carried out by 1D and 2D NMR and HRMS, and spectrophotometric characterisation involved absorption, emission and titration measurements. The influence of electron-donating and electron-withdrawing groups on the rigid flavylium skeleton (position 4 and 7) was studied in terms of colour modification, acid-base behaviour and thermochromic properties.
The compounds displayed shades of violet and yellow in acidic solutions of dichloromethane when going form strong to weak donating group in the 7-position. The absorption also revealed that the substituents of position-4 have little influence on the ultimate colour. Spectrophotometric studies showed that the dyes were able to change between two species by an alteration in pH, and the determined pk_a show their high stability against hydration rection that could lead to formation of various species.

3) The thermochromism of spirolactone dyes was tested in various organic solvents such as acetophenone (m.p. 20.2°C), nitrobenzene (5.7°C), acetonaphthone (55-56°C), cinnamonitrile (19-22°C) and benzoyl cyanide (28-31°C), when using N,N-dimethyldodecylamine base as both colour developer (solid state) and bleaching agent (liquid state). The result of the tests emphasised that thermochromic materials are easier to achieve in the presence of electron-withdrawing groups (push-pull effect), which favour a more labile equilibrium between leuco and coloured forms. The most balanced properties were obtained for compound **4** (with cyano group) when the ratio dye:base was 1:0.5. The colour switch of the systems was gradual and started with 2, 3°C before the full contrast was displayed.

4) The thermochromism of 4-arylidene-substituted flavylium dyes were tested in thermoresponsive Pluronic® F127. Compounds **6** and **10** were the dyes exhibiting the most noticeable thermochromism. The experiments were conducted in 20% (wt./wt.) Pluronic® F127 aqueous solutions at pH=2 for compound **6** and pH=1 for compound **10**. The defined pH ensured complete reversible colouration for compound **6** and partial colour reversibility for compound **10**.

5) The microencapsulation of the ternary thermochromic systems based on dye-developer-solvent was carried out by the *in-situ* polymerisation method. The lactone counterpart of dye **4** was used as colour former, caprylic and capric acids were selected as developers and isopropyl palmitate as the solvent component. The resulting microcapsules were characterised using dynamic light scattering (DLS), scanning electron microscopy (SEM) and differential scanning calorimetry (DSC) techniques. The data obtained from DLS and SEM demonstrated that the PI, Z-average and mean values increased in conjunction with the concentration of the colour former. The DSC analysis indicated that the crystallisation and melting processes are characterised by a multi-step mechanism, resulting from the formation of eutectic systems and the presence of polymorphic components. The DSC also showed that the transition temperatures are influenced by the polymeric wall formation and the rise in colour developer concentration.

6) Various thermochromic inks were prepared by combining microencapsulated ternary systems with a water-based acrylic binder. The developed inks were screen printed on self-adhesive matte inkjet paper to construct indicators capable of detecting temperature fluctuations. SEM and CIELAB measurements were carried out to characterise the resulting printed materials.
The SEM images demonstrate that the printing process does not compromise the structural integrity of the capsules, and the inks exhibit good adhesion to the paper substrate, and the resulting printed film enhances the smoothness of the paper surface. CIELAB measurements revealed that contrast increases as the systems start to freeze, and 75% colouration is achieved in a relatively short temperature range. The CIELAB data also demonstrated that the contrast increases with the concentration of the colour former and both caprylic and capric acid were observed to act as good colour developers for the novel flavylium spirolactone dye. Data fitting showed that colouration in C_{10} systems is a two-step process. The best-performing-indicator (indicator p_8, which was composed of 1.6 wt% leuco dye 1, 22 wt% capric acid and isopropyl palmitate solvent) exhibited complete clearing at +10°C on the heating cycle and full recoloration at +4°C on cooling, and it also demonstrated colour switching stability.

6.2 Outlook

In order for the developed thermochromic indicator to be considered for industrial use, the synthesis of the flavylium leuco dye should be further investigated on a larger scale. Other encapsulation methods for spirolactone flavylium dyes and amine developers also need to be investigated. The thermochromic properties of the remaining spirolactone dyes in microencapsulated systems also need to be evaluated. More detailed studies of dye-developer interactions are also needed, as the DSC and CIELAB data only led to some hypotheses and no clear conclusions.
The thermochromic behaviour of the 4-substituted arylidene flavylium dyes should also be investigated at different pH values and in other thermoresponsive Pluronics polymers. The Pluronics-based systems presented in this thesis should be subjected to heating-cooling-cycling tests to determine the colour resistance to fatigue.

7

BIBLIOGRAPHY

[1] Kiria P, Hyett G, Binions R. Solid State Thermochromic Materials. Adv Mater Lett 2010;1:86–105. https://doi.org/10.5185/amlett.2010.8147.

[2] Lötzsch D, Eberhardt V, Rabe C. Chromogenic Materials. In: Wiley-VCH Verlag GmbH & Co. KGaA, editor. Ullmann's Encyclopedia of Industrial Chemistry, Weinheim, Germany: Wiley-VCH Verlag GmbH & Co. KGaA; 2016, p. 1–26. https://doi.org/10.1002/14356007.t07_t01.

[3] Jesus Rosa PAV. Minimal computation structures for visual information applications based on printed electronics. Doctoral dissertation. Universidade NOVA de Lisboa, 2016.

[4] Tapuhi Y, Kalisky O, Agranat I. Thermochromism and thermal E,Z isomerizations in bianthrones. J Org Chem 1979;44:1949–52. https://doi.org/10.1021/jo01326a012.

[5] Spirache MA, Marrec P, Dias Parola AJ, Tonicha Laia CA. Reversible thermochromic systems based on a new library of flavylium spirolactone leuco dyes. Dyes and Pigments 2023;214:111208. https://doi.org/10.1016/j.dyepig.2023.111208.

[6] Cheng Y, Zhang X, Fang C, Chen J, Wang Z. Discoloration mechanism, structures and recent applications of thermochromic materials via different methods: A review. Journal of Materials Science & Technology 2018;34:2225–34. https://doi.org/10.1016/j.jmst.2018.05.016.

[7] Day JH. Thermochromism of inorganic compounds. Chem Rev 1968;68:649–57. https://doi.org/10.1021/cr60256a001.

[8] Granqvist C, Niklasson G. Thermochromic Oxide-Based Thin Films and Nanoparticle Composites for Energy-Efficient Glazings. Buildings 2016;7:3. https://doi.org/10.3390/buildings7010003.

[9] Cui Y, Ke Y, Liu C, Chen Z, Wang N, Zhang L, et al. Thermochromic VO2 for Energy-Efficient Smart Windows. Joule 2018;2:1707–46. https://doi.org/10.1016/j.joule.2018.06.018.

[10] Kahani SA, Abdevali F. Mechanochemical synthesis and characterization of a nickel(II) complex as a reversible thermochromic nanostructure. RSC Adv 2016;6:5116–22. https://doi.org/10.1039/C5RA22606F.

[11] Hakami A, Srinivasan SS, Biswas PK, Krishnegowda A, Wallen SL, Stefanakos EK. Review on thermochromic materials: development, characterization, and applications. J Coat Technol Res 2022;19:377–402. https://doi.org/10.1007/s11998-021-00558-x.

[12] Bamfield, P.,. Chromic Phenomena The Technological Applications of Colour Chemistry. Royal Society of Chemistry. 2001.

[13] Towns, A. D. Thermochromic composite materials formulated from spirolactone colour formers. ChemiChromics USA 2015;99:1171–82.
[14] Chowdhury MA, Joshi M, Butola BS. Photochromic and Thermochromic Colorants in Textile Applications. Journal of Engineered Fibers and Fabrics 2014;9:155892501400900. https://doi.org/10.1177/155892501400900113.
[15] Suleiman Abubakar Shola. Thermochromic liquid crystals as a temperature indicator. BACHELOR THESIS. Czech Technical University in Prague, Faculty of Mechanical Engineering, Department of Process Engineering, 2019.
[16] Andrienko D. Introduction to liquid crystals. Journal of Molecular Liquids 2018;267:520–41. https://doi.org/10.1016/j.molliq.2018.01.175.
[17] Jamain Z, Omar NF, Khairuddean M. Synthesis and Determination of Thermotropic Liquid Crystalline Behavior of Cinnamaldehyde-Based Molecules with Two Schiff Base Linking Units. Molecules 2020;25:3780. https://doi.org/10.3390/molecules25173780.
[18] Lagerwall Jan. Three facets of modern liquid crystal science. Halle, Univ., Faculty of Natural Sciences II, Habil.-Schr., 2010, 2011.
[19] Smith CR, Sabatino DR, Praisner TJ. Temperature sensing with thermochromic liquid crystals. Experiments in Fluids 2001;30:190–201. https://doi.org/10.1007/s003480000154.
[20] Bonnassieux Y, Brabec CJ, Cao Y, Carmichael TB, Chabinyc ML, Cheng K-T, et al. The 2021 flexible and printed electronics roadmap. Flex Print Electron 2021;6:023001. https://doi.org/10.1088/2058-8585/abf986.
[21] Kılıç M, Çınar Z. Structures and mesomorphic properties of cyano-containing calamitic liquid crystal molecules. Journal of Molecular Structure: THEOCHEM 2007;808:53–61. https://doi.org/10.1016/j.theochem.2006.12.042.
[22] Kajal Sarmah, Ankit Jain, Rahul Kumar. A review of thermochromic liquid crystal with spectrum analysis. National Journal of Multidisciplinary Research and Development 2018;3:478–82.
[23] Low-molar-mass thermotropic liquid crystals. Phil Trans R Soc Lond A 1990;330:73–94. https://doi.org/10.1098/rsta.1990.0003.
[24] Mitov M. Cholesteric liquid crystals in living matter. Soft Matter 2017;13:4176–209. https://doi.org/10.1039/C7SM00384F.
[25] Fu F, Hu L. Temperature sensitive colour-changed composites. Advanced High Strength Natural Fibre Composites in Construction, Elsevier; 2017, p. 405–23. https://doi.org/10.1016/B978-0-08-100411-1.00015-7.
[26] MacLaren DC, White MA. Design rules for reversible thermochromic mixtures. J Mater Sci 2005;40:669–76. https://doi.org/10.1007/s10853-005-6305-x.
[27] Geng X, He Y, Han N, Zhang X, Li W. Synthesis and characterization of hydrophobic reversible thermochromic MicroPCMs with amino resins shell for thermal energy storage. Energy and Buildings 2021;230:110528. https://doi.org/10.1016/j.enbuild.2020.110528.
[28] Raditoiu A, Raditoiu V, Nicolae CA, Raduly MF, Amariutei V, Wagner LE. Optical and structural dynamical behavior of Crystal Violet Lactone – Phenolphthalein binary thermochromic systems. Dyes and Pigments 2016;134:69–76. https://doi.org/10.1016/j.dyepig.2016.06.046.

[29] Li W, Yan X, Zhao W. Preparation of Crystal Violet Lactone Complex and Its Effect on Discoloration of Metal Surface Coating. Polymers 2022;14:4443. https://doi.org/10.3390/polym14204443.
[30] MacLaren DC, White MA. Dye–developer interactions in the crystal violet lactone–lauryl gallate binary system: implications for thermochromism. J Mater Chem 2003;13:1695–700. https://doi.org/10.1039/B302249H.
[31] Tang H, MacLaren DC, White MA. New insights concerning the mechanism of reversible thermochromic mixtures. Can J Chem 2010;88:1063–70. https://doi.org/10.1139/V10-069.
[32] Bourque AN, White MA. Control of thermochromic behaviour in crystal violet lactone (CVL)/alkyl gallate/alcohol ternary mixtures. Can J Chem 2015;93:22–31. https://doi.org/10.1139/cjc-2014-0251.
[33] Mizuguchi J. A low-temperature phase of the 1:1 complex of 2-(6-diethylamino-3-diethyliminio-3 *H* -xanthen-9-yl)benzoate with ethyl gallate at 93 K. Acta Crystallogr E Struct Rep Online 2008;64:o1238–9. https://doi.org/10.1107/S1600536808016528.
[34] Takahashi Y, Shirai A, Segawa T, Takahashi T, Sakakibara K. Why Does a Color-Developing Phenomenon Occur on Thermal Paper Comprising of a Fluoran Dye and a Color Developer Molecule? Bulletin of the Chemical Society of Japan 2002;75:2225–31. https://doi.org/10.1246/bcsj.75.2225.
[35] Zhu X, Liu Y, Dong N, Li Z. Fabrication and characterization of reversible thermochromic wood veneers. Sci Rep 2017;7:16933. https://doi.org/10.1038/s41598-017-17238-9.
[36] Sanjabi S, Keyvan Rad J, Salehi-Mobarakeh H, Mahdavian AR. Preparation of switchable thermo- and photo-responsive polyacrylic nanocapsules containing leuco-dye and spiropyran: Multi-level data encryption and temperature indicator. Journal of Industrial and Engineering Chemistry 2023;119:647–59. https://doi.org/10.1016/j.jiec.2022.12.011.
[37] Oh W, Angupillai S, Muthukumar P, So H-S, Son Y. Synthesis of novel tert-butyl substituted fluorans and an investigation of their thermochromic behavior. Dyes and Pigments 2016;128:235–45. https://doi.org/10.1016/j.dyepig.2016.01.036.
[38] Gavara R, Laia CAT, Parola AJ, Pina F. Formation of a *leuco* Spirolactone from 4-(2-Carboxyphenyl)-7-diethylamino-4′-dimethylamino-1-benzopyrylium: Design of a Phase-Change Thermochromic System Based on a Flavylium Dye. Chemistry A European J 2010;16:7760–6. https://doi.org/10.1002/chem.200903482.
[39] Potaniec B, Zdończyk M, Cybińska J. Controlled Synthesis of Luminescent Xanthene Dyes and Use of Ionic Liquid in Thermochromic Reaction. Molecules 2022;27:3092. https://doi.org/10.3390/molecules27103092.
[40] MacLaren DC, White MA. Dye–developer interactions in the crystal violet lactone–lauryl gallate binary system: implications for thermochromism. J Mater Chem 2003;13:1695–700. https://doi.org/10.1039/B302249H.
[41] Muthyala R, editor. Chemistry and applications of leuco dyes. New York: Plenum Press; 1997.
[42] Yang H, Wang Y, Yu Q, Cao G, Yang R, Ke J, et al. Composite phase change materials with good reversible thermochromic ability in delignified wood substrate for thermal energy storage. Applied Energy 2018;212:455–64. https://doi.org/10.1016/j.apenergy.2017.12.006.

[43] Yi S, Sun S, Deng Y, Feng S. Preparation of composite thermochromic and phase-change materials by the sol–gel method and its application in textiles. The Journal of The Textile Institute 2015;106:1071–7. https://doi.org/10.1080/00405000.2014.965501.

[44] Liu D, Zhang C, Chen S, Cui Z, Zhong Y. Reversible Thermochromic Ink based on Crystal Violet Lactone/Boric Acid/Hexadecyl Alcohol for Anti-Counterfeiting Printing. Jist 2022;66:020405-1-020405–7. https://doi.org/10.2352/J.ImagingSci.Technol.2022.66.2.020405.

[45] Liu H, Deng Y, Ye Y, Liu X. Reversible Thermochromic Microcapsules and Their Applications in Anticounterfeiting. Materials 2023;16:5150. https://doi.org/10.3390/ma16145150.

[46] Liu H, Jiao L, Lin H, Li L. Design and application research of portable reversible thermochromic patches in grid power supply systems. AIP Advances 2024;14:045322. https://doi.org/10.1063/5.0189608.

[47] Hinckley DA, Seybold PG, Borris DP. Solvatochromism and thermochromism of rhodamine solutions. Spectrochimica Acta Part A: Molecular Spectroscopy 1986;42:747–54. https://doi.org/10.1016/0584-8539(86)80095-2.

[48] Shirasaki Y, Okamoto Y, Muranaka A, Kamino S, Sawada D, Hashizume D, et al. Fused-Fluoran Leuco Dyes with Large Color-Change Derived from Two-Step Equilibrium: Iso-Aminobenzopyranoxanthenes. Journal of Organic Chemistry 2016;81:12046–51. https://doi.org/10.1021/acs.joc.6b02403.

[49] Şentürk, B. Studies on chiral spiropyran derivatives. Master's thesis. Technical University, 2021.

[50] Lukyanov BS, Lukyanova MB. Spiropyrans: Synthesis, Properties, and Application. (Review). Chem Heterocycl Compd 2005;41:281–311. https://doi.org/10.1007/s10593-005-0148-x.

[51] Kortekaas L, Browne WR. The evolution of spiropyran: fundamentals and progress of an extraordinarily versatile photochrome. Chem Soc Rev 2019;48:3406–24. https://doi.org/10.1039/C9CS00203K.

[52] Malkin YaN, Kuz'min VA, Dyadyusha GG, Boguslavskaya AN, Mikhailenko FA. The thermochromic and photochemical properties of bis-spiropyranes. Russ Chem Bull 1976;25:536–40. https://doi.org/10.1007/BF01106648.

[53] Rajimon KJ, Elangovan N, Amir Khairbek A, Thomas R. Schiff bases from chlorine substituted anilines and salicylaldehyde: Synthesis, characterization, fluorescence, thermal features, biological studies and electronic structure investigations. Journal of Molecular Liquids 2023;370:121055. https://doi.org/10.1016/j.molliq.2022.121055.

[54] El-Gammal OA, Mohamed FSh, Rezk GN, El-Bindary AA. Structural characterization and biological activity of a new metal complexes based of Schiff base. Journal of Molecular Liquids 2021;330:115522. https://doi.org/10.1016/j.molliq.2021.115522.

[55] Zbačnik M, Pičuljan K, Parlov-Vuković J, Novak P, Roodt A. Four Thermochromic o-Hydroxy Schiff Bases of α-Aminodiphenylmethane: Solution and Solid State Study. Crystals 2017;7:25. https://doi.org/10.3390/cryst7010025.

[56] Zbačnik M, Kaitner B. Ex situ and in situ monitoring of the syntheses of thermochromic Schiff bases. CrystEngComm 2014;16:4162–8. https://doi.org/10.1039/C3CE42583E.

[57] Manisha Dey, Yeasin Sikdar. Thermochromics: A Temperature Sensitive Smart Material. The Bhawanipur Education Society College 2023.

[58] Vitry J. Photochromie et Thermochromie. Chim. et Indus. Genie Chim 1969;102:1333–49.
[59] Panja SK. J-type aggregation and thermochromic behavior of a schiff base in solution: Role of keto-enol tautomerization. Spectrochimica Acta Part A: Molecular and Biomolecular Spectroscopy 2020;229:117860. https://doi.org/10.1016/j.saa.2019.117860.
[60] Hadjoudis E, Mavridis IM. Photochromism and thermochromism of Schiff bases in the solid state: structural aspects. Chem Soc Rev 2004:10.1039.b303644h. https://doi.org/10.1039/b303644h.
[61] Hadjoudis E, Rontoyianni A, Ambroziak K, Dziembowska T, Mavridis IM. Photochromism and thermochromism of solid trans-N,N′-bis-(salicylidene)-1,2-cyclohexanediamines and trans-N,N′-bis-(2-hydroxy-naphylidene)-1,2-cyclohexanediamine. Journal of Photochemistry and Photobiology A: Chemistry 2004;162:521–30. https://doi.org/10.1016/S1010-6030(03)00395-2.
[62] Hadjoudis E, Vittorakis M, Moustakali-Mavridis I. Photochromism and thermochromism of schiff bases in the solid state and in rigid glasses. Tetrahedron 1987;43:1345–60. https://doi.org/10.1016/S0040-4020(01)90255-8.
[63] A. Samat, V. Lokshin, J. C. Crano, R. J Guglielmetti. Organic Photochromic and Thermochromic Compounds. vol. 2, Chapter 10. New York: Kluwer Academic/Plenum Publishers; 1999.
[64] Pogodin S, Suissa MR, Levy A, Cohen S, Agranat I. The Tetracyanoquinodimethane Motif in Overcrowded Bistricyclic Aromatic Enes: Avoiding Thermochromism. Eur J Org Chem 2008;2008:2887–94. https://doi.org/10.1002/ejoc.200701125.
[65] Biedermann PU, Stezowski JJ, Agranat I. Polymorphism Versus Thermochromism: Interrelation of Color and Conformation in Overcrowded Bistricyclic Aromatic Enes. Chemistry A European J 2006;12:3345–54. https://doi.org/10.1002/chem.200501118.
[66] Takezawa H, Murase T, Fujita M. Temporary and Permanent Trapping of the Metastable Twisted Conformer of an Overcrowded Chromic Alkene via Encapsulation. J Am Chem Soc 2012;134:17420–3. https://doi.org/10.1021/ja308101a.
[67] Schönberg A, Mustafa A, Sobhy MEE-D. Thermochromism of Dixanthylenes [1]. J Am Chem Soc 1953;75:3377–8. https://doi.org/10.1021/ja01110a023.
[68] Bergmann, E.D. and Loewenthal, H.J.E.,. 1: 1′-Difluorodianthron-9-ylidene and an attempted synthesis of 4: 4′-dibromodianthron-9-ylidene. Journal of the Chemical Society (Resumed), 1953;523:2572-2574.
[69] Mustafa A, El-Din Sobhy ME. Thermochromism of Dixanthylenes. II [1]. J Am Chem Soc 1955;77:5124–6. https://doi.org/10.1021/ja01624a052.
[70] Mustafa A, Asker W, Sobhy MEE-D. Thermochromism of Dixanthylenes. Reactions with Substituted Xanthones. III [(1a)]. J Org Chem 1960;25:1519–25. https://doi.org/10.1021/jo01079a017.
[71] Corbet BP, Wonink MBS, Feringa BL. Fast synthesis and redox switching of di- and tetra-substituted bisthioxanthylidene overcrowded alkenes. Chem Commun 2021;57:7665–8. https://doi.org/10.1039/D1CC03098A.
[72] Gonçalves VC, Balogh DT. Synthesis and characterization of a dye-functionalized polythiophene with different chromic properties. European Polymer Journal 2006;42:3303–10. https://doi.org/10.1016/j.eurpolymj.2006.08.020.

[73] Phonchai N, Khanantong C, Kielar F, Traiphol R, Traiphol N. Low-Temperature Reversible Thermochromic Polydiacetylene/Zinc(II)/Zinc Oxide Nanocomposites for Colorimetric Sensing. ACS Appl Nano Mater 2019;2:4489–98. https://doi.org/10.1021/acsanm.9b00876.

[74] Traiphol N, Faisadcha K, Potai R, Traiphol R. Fine tuning the color-transition temperature of thermoreversible polydiacetylene/zinc oxide nanocomposites: The effect of photopolymerization time. Journal of Colloid and Interface Science 2015;439:105–11. https://doi.org/10.1016/j.jcis.2014.10.033.

[75] Yarimaga O, Im M, Choi Y-K, Kim TW, Jung YK, Park HG, et al. A color display system based on thermochromic conjugated polydiacetylene supramolecules. Macromol Res 2010;18:404–7. https://doi.org/10.1007/s13233-010-0402-7.

[76] Chance RR, Baughman RH, Müller H, Eckhardt CJ. Thermochromism in a polydiacetylene crystal. The Journal of Chemical Physics 1977;67:3616–8. https://doi.org/10.1063/1.435361.

[77] Andina RI, Kingchok S, Laohhasurayotin K, Traiphol N, Traiphol R. Multi-reversible thermochromic polydiacetylene-CuZnFe2O4 magnetic nanocomposites with tunable colorimetric response to acid-base. Colloids and Surfaces A: Physicochemical and Engineering Aspects 2022;647:129117. https://doi.org/10.1016/j.colsurfa.2022.129117.

[78] Lee S, Lee J, Lee M, Cho YK, Baek J, Kim J, et al. Construction and Molecular Understanding of an Unprecedented, Reversibly Thermochromic Bis-Polydiacetylene. Adv Funct Materials 2014;24:3699–705. https://doi.org/10.1002/adfm.201304147.

[79] Lévesque I, Leclerc M. Ionochromic and Thermochromic Phenomena in a Regioregular Polythiophene Derivative Bearing Oligo(oxyethylene) Side Chains. Chem Mater 1996;8:2843–9. https://doi.org/10.1021/cm960373s.

[80] Salaneck WR, Inganäs O, Nilsson J-O, Österholm J-E, Thémans B, Brédas J-L. Thermochromism in the poly(3-alkylthiophene)s: A study of conformational defects by photoelectron spectroscopy. Synthetic Metals 1989;28:451–60. https://doi.org/10.1016/0379-6779(89)90558-4.

[81] Wang C-C, Gao Y, Shreve AP, Zhong C, Wang L, Mudalige K, et al. Thermochromism of a Poly(phenylene vinylene): Untangling the Roles of Polymer Aggregate and Chain Conformation. J Phys Chem B 2009;113:16110–7. https://doi.org/10.1021/jp906645d.

[82] Gelinck GH, Warman JM, Staring EGJ. Polaron Pair Formation, Migration, and Decay on Photoexcited Poly(phenylenevinylene) Chains. J Phys Chem 1996;100:5485–91. https://doi.org/10.1021/jp9532071.

[83] Samat A, Lokshin V. Thermochromism of Organic Compounds. In: Crano JC, Guglielmetti RJ, editors. Organic Photochromic and Thermochromic Compounds, Boston: Kluwer Academic Publishers; 2002, p. 415–66. https://doi.org/10.1007/0-306-46912-X_11.

[84] Padwa A, Vega E. Photochromic aziridines. The photochemical valence tautomerization and cycloaddition reactions of a substituted indano[1,2-b]aziridine. J Org Chem 1975;40:175–81. https://doi.org/10.1021/jo00890a005.

[85] Padwa A, Sackman P, Shefter E, Vega E. Thermal and photochemical rearrangements, and X-ray crystal structure of a 2-benzazocine derivative. J Chem Soc, Chem Commun 1972:680. https://doi.org/10.1039/c39720000680.

[86] Lown JW. Reactive species from the electrocyclic opening of three-membered heterocycles. Reviews on Reactive Species in Chemical Reactions 1973;1:89–158. https://doi.org/10.1007/BF03155666.

[87] Mataka S, Takahashi K, Tashiro M, Lin W, Iwasaki S, Tsutsui T, et al. Color change (yellow \documentclass{article}\pagestyle{empty}\begin{document}$\rightleftharpoons$\end{document} orange) of 4,6,7-tri(alkoxy-substituted aryl)-1,2,5-thiadiazolo[3,4- *c*]pyridines in the solid phase. Journal of Heterocyclic Chem 1989;26:215–9. https://doi.org/10.1002/jhet.5570260138.

[88] Quast H, Knoll K, Peters E, Peters K, Schnering HGV. 2,4,6,8-Tetraphenylbarbaralan – ein orangeroter, thermochromer Kohlenwasserstoff ohne Chromophor [1,2]. Chem Ber 1993;126:1047–60. https://doi.org/10.1002/cber.19931260427.

[89] Quast H, Herkert T, Witzel A, Peters E, Peters K, Von Schnering HG. 2,6-Dicyano-1,5-dimethyl-4,8-diphenylsemibullvalene. — Synthesis, Structure and the Reactions with Triplet Oxygen. Chem Ber 1994;127:921–32. https://doi.org/10.1002/cber.19941270521.

[90] Quast H, Geißler E, Herkert T, Knoll K, Peters E, Peters K, et al. 2,6-Dicyan-4,8-diphenylbarbaralan. Chem Ber 1993;126:1465–75. https://doi.org/10.1002/cber.19931260630.

[91] Aldoshin SM, Filipenko OS, Novozhilova MA, Atovmyan LO, Komissarov VN, Ukhin LYu. Synthesis and crystal structure of thermochroic 2,6-di-tert-butyl-4-dimethylamino-4-(2-hydroxyphenyl) cyclohexadien-2,5-one. Russ Chem Bull 1991;40:1600–4. https://doi.org/10.1007/BF01172259.

[92] Komissarov VN, Ukhin LY, Kharlanov VA, Lokshin VA, Bulgarevich EY, Minkin VI, et al. Photo- and thermochromic mannich bases. 1. Mannich bases from 3,5-di-tert-butyl-4-hydroxybenzaldehyde and 2-naphthols. Russ Chem Bull 1992;41:1875–83. https://doi.org/10.1007/BF00863826.

[93] Komissarov VN, Ukhin LYu, Kharlanov VA, Vetoshkina LV, Konstantinovskii LE, Aldoshin SM, et al. Unusual synthesis, structure, and thermochromic properties of novel sterically hindered cyclohexadienes. Russ Chem Bull 1991;40:1003–10. https://doi.org/10.1007/BF00961363.

[94] He Y, Sun S, Han N, Zhang X, Li W. Thermal energy regulated and thermochromic composite film with temperature-sensitive "breathable" stomata. J Mater Sci 2020;55:12921–39. https://doi.org/10.1007/s10853-020-04936-5.

[95] Rosa, Paulo Alexandre Valente de Jesus. Minimal Computation Structures for Visual Information Applications based on Printed Electronics. Universidade NOVA de Lisboa (Portugal) ProQuest Dissertation & Theses, 2016.

[96] Đurđević, Stefan, Dragoljub Novaković, Gojko Vladić, Nemanja Kašiković, and Darko Avramović. The development of novel smart packaging labels and mobile application for protection, information and identification of product shelf life. Acta Graphica: Znanstveni Časopis Za Tiskarstvo i Grafičke Komunikacije 2015;26:35–41. https://actagraphica.hr/index.php/actagraphica/article/view/27.

[97] Loard, E.,. Choose marker website. 2021. https://choosemarker.com/how-do-erasable-pens-work/ (accessed October 25, 2022).

[98] Karlessi T, Santamouris M, Apostolakis K, Synnefa A, Livada I. Development and testing of thermochromic coatings for buildings and urban structures. Solar Energy 2009;83:538–51. https://doi.org/10.1016/j.solener.2008.10.005.

[99] Kulčar R, Friškovec M, Hauptman N, Vesel A, Gunde MK. Colorimetric properties of reversible thermochromic printing inks. Dyes and Pigments 2010;86:271–7. https://doi.org/10.1016/j.dyepig.2010.01.014.
[100] Aitken D, Burkinshaw SM, Griffiths J, Towns AD. Textile applications of thennochromic systems. Review of Progress in Coloration and Related Topics 1996;26:1–8. https://doi.org/10.1111/j.1478-4408.1996.tb00105.x.
[101] Rahela Kulčar, Marta Klanjšeg Gunde, Nina Knešaurek. Dynamic colour possibilities and functional properties of thermochromic printing inks. Acta Graphica: Znanstveni Časopis Za Tiskarstvo i Grafičke Komunikacije 2012;23:25–36.
[102] Aklujkar PS, Kandasubramanian B. A review of microencapsulated thermochromic coatings for sustainable building applications. J Coat Technol Res 2021;18:19–37. https://doi.org/10.1007/s11998-020-00396-3.
[103] White MA, LeBlanc M. Thermochromism in Commercial Products. J Chem Educ 1999;76:1201. https://doi.org/10.1021/ed076p1201.
[104] Pina F, Melo MJ, Laia CAT, Parola AJ, Lima JC. Chemistry and applications of flavylium compounds: a handful of colours. Chem Soc Rev 2012;41:869–908. https://doi.org/10.1039/C1CS15126F.
[105] Klaus Hunger (Editor). Industrial Dyes: Chemistry, Properties, Applications. Cambridge: Wiley-VCH, Weinheim; 2003.
[106] Czerney P, Graneß G, Birckner E, Vollmer F, Rettig W. Molecular engineering of cyanine-type fluorescent and laser dyes. Journal of Photochemistry and Photobiology A: Chemistry 1995;89:31–6. https://doi.org/10.1016/1010-6030(94)04018-W.
[107] George Wypych. Handbook of solvents. Toronto-New York: ChemTec Publishing; n.d.
[108] Pinheiro C, Parola AJ, Pina F, Laia CAT. Electrochromism of Crystal Violet Lactone in the presence of Fe(III)/Fe(II) redox pair. Electrochimica Acta 2009;54:5593–7. https://doi.org/10.1016/j.electacta.2009.04.063.
[109] Huo J, Hu Z, He G, Hong X, Yang Z, Luo S, et al. High temperature thermochromic polydiacetylenes: Design and colorimetric properties. Applied Surface Science 2017;423:951–6. https://doi.org/10.1016/j.apsusc.2017.06.198.
[110] Traiphol N, Faisadcha K, Potai R, Traiphol R. Fine tuning the color-transition temperature of thermoreversible polydiacetylene/zinc oxide nanocomposites: The effect of photopolymerization time. Journal of Colloid and Interface Science 2015;439:105–11. https://doi.org/10.1016/j.jcis.2014.10.033.
[111] Mapazi O, Matabola KP, Moutloali RM, Ngila CJ. High temperature thermochromic polydiacetylene supported on polyacrylonitrile nanofibers. Polymer 2018;149:106–16. https://doi.org/10.1016/j.polymer.2018.06.028.
[112] Naumov P, Ishizawa N, Wang J, Pejov L, Pumera M, Lee SC. On the Origin of the Solid-State Thermochromism and Thermal Fatigue of Polycyclic Overcrowded Enes. J Phys Chem A 2011;115:8563–70. https://doi.org/10.1021/jp2040339.
[113] Burkinshaw SM, Griffiths J, Towns AD. Reversibly thermochromic systems based on pH-sensitive functional dyes. J Mater Chem 1998;8:2677–83. https://doi.org/10.1039/a805994b.
[114] Roehri-Stoeckel C, Gonzalez E, Fougerousse A, Brouillard R. Synthetic dyes: simple and original ways to 4-substituted flavylium salts and their corresponding vitisin derivatives. Can J Chem 2001;79:1173–8. https://doi.org/10.1139/v01-089.

[115] João Miguel Ribeiro Avó. Síntese de sais de benzopirílio e aplicação como sensores fluorescentes e grupos protectores fotocliváveis. Dissertation. Universidade NOVA de Lisboa, Faculdade de Ciências e Tecnologia, 2009.

[116] Katritzky AR, Czerney P, Levell JR. Benzotriazole-Mediated Conversions of *para* -H-Substituted Pyrylium, Benzo[*b*]pyrylium, and Xanthylium Salts into *para* -Position Functionalized Derivatives (An Indirect Electrophilic Substitution of Electron-Deficient Heteroaromatics). J Org Chem 1997;62:8198–200. https://doi.org/10.1021/jo971174a.

[117] Katritzky AR, Czerney P, Levell JR, Du W. Molecular Engineering of Benzo[b]pyrylium Salts by Indirect Electrophilic Substitution. Eur J Org Chem 1998;1998:2623–9. https://doi.org/10.1002/(SICI)1099-0690(199811)1998:11<2623::AID-EJOC2623>3.0.CO;2-M.

[118] McClelland RA, Gedge S. Hydration of the flavylium ion. J Am Chem Soc 1980;102:5838–48. https://doi.org/10.1021/ja00538a024.

[119] Pina F, João Melo M, Maestri M, Passaniti P, Camaioni N, Balzani V. Photo- and pH-Induced Transformations of Flavylium Cation: "Write–Lock–Read–Unlock-Erase" Cycles. Eur J Org Chem 1999;1999:3199–207. https://doi.org/10.1002/(SICI)1099-0690(199911)1999:11<3199::AID-EJOC3199>3.0.CO;2-X.

[120] U.-W. Grummt, P. Czerney. 4-Alkylbenzopyrylium perchlorates as C—H Acidic compounds 2002;5:385–91. https://doi.org/10.1002/poc.515.

[121] Fernando Pina, Ana Roque, Maria João Melo, Mauro Maestri, Livia Belladelli, Vincenzo Balzani. Multistate/Multifunctional Molecular-Level Systems: Light and pH Switching between the Various Forms of a Synthetic Flavylium Salt 1998;4:1184–91. https://doi.org/10.1002/(SICI)1521-3765(19980710)4:7<1184::AID-CHEM1184>3.0.CO;2-6.

[122] Avó J, Parola AJ, Lima JC, Pina F, Cunha-Silva L. Phase transition thermochromism based on C–H acidity of 4-alkylflavylium compounds in Pluronic F-127. J Mater Chem 2011;21:16628. https://doi.org/10.1039/c1jm13348a.

[123] Schwartz M, editor. Smart Materials. 0 ed. CRC Press; 2008. https://doi.org/10.1201/9781420043730.

[124] Ritter A. Smart materials in architecture, interior architecture and design. Basel Boston: Birkhäuser; 2007.

[125] Senin S, Langebach J, Karcher Ch. Determination of Interior Surface Temperature Using Luminance Measurement of Thermochromic Liquid Crystals. Experimental Heat Transfer 2008;21:133–42. https://doi.org/10.1080/08916150701815754.

[126] Stefani FD, Kohl C, Avlasevich YS, Horn N, Vogt AK, Müllen K, et al. Thermochromic Fluorophores and Their NIR Laser Induced Transformation. Chem Mater 2006;18:6115–20. https://doi.org/10.1021/cm060665l.

[127] Ma Y, Zhu B. Research on the preparation of reversibly thermochromic cement based materials at normal temperature. Cement and Concrete Research 2009;39:90–4. https://doi.org/10.1016/j.cemconres.2008.10.006.

[128] Karlessi T, Santamouris M, Apostolakis K, Synnefa A, Livada I. Development and testing of thermochromic coatings for buildings and urban structures. Solar Energy 2009;83:538–51. https://doi.org/10.1016/j.solener.2008.10.005.

[129] Falko Doberenz, Kui Zeng, Christian Willems, Kai Zhang, Thomas Groth. Thermoresponsive polymers and their biomedical application in tissue engineering – a review. J Mater Chem B 2020;8:607–28. https://doi.org/DOI: 10.1039/C9TB02052G.
[130] Alexandra Lupu, Luiza Madalina Gradinaru, Daniela Rus, Maria Bercea. Self-Healing of Pluronic® F127 Hydrogels in the Presence of Various Polysaccharides. Gels 2023;9:719. https://doi.org/10.3390/gels9090719.
[131] Karavasili C, Fatouros DG. Smart materials: in situ gel-forming systems for nasal delivery. Drug Discovery Today 2016;21:157–66. https://doi.org/10.1016/j.drudis.2015.10.016.
[132] Anna P. Constantinou, Valeria Nele, James J. Doutch, Joana S. Correia, Roman V. Moiseev, Martina Cihova, David C. A. Gaboriau, Jonathan Krell, Vitaliy V. Khutoryanskiy, Molly M. Stevens, and Theoni K. Georgiou. Investigation of the Thermogelation of a Promising Biocompatible ABC Triblock Terpolymer and Its Comparison with Pluronic F127. Macromolecules 20222;55:1783–99. https://doi.org/10.1021/acs.macromol.1c02123.
[133] Avó J, Parola AJ, Lima JC, Pina F, Cunha-Silva L. Phase transition thermochromism based on C–H acidity of 4-alkylflavylium compounds in Pluronic F-127. J Mater Chem 2011;21:16628. https://doi.org/10.1039/c1jm13348a.
[134] Leydet Y, Gavara R, Cunha-Silva L, Parola AJ, Pina F. Phase-Dependent Photochromism of a Lactone-Stabilized Chromene from a Flavylium Reaction Network. Chemistry A European J 2011;17:3663–71. https://doi.org/10.1002/chem.201002781.
[135] Katritzky AR, Fali CN, Li J. General Synthesis of Polysubstituted Benzo[*b*]furans. J Org Chem 1997;62:8205–9. https://doi.org/10.1021/jo9710846.
[136] Lietz H, Haucke G, Czerney P, John B. Hydrolysis of Benzopyrylium Dyes - An Application of the Concept of Chemical Hardness. J Prakt Chem 1996;338:725–30. https://doi.org/10.1002/prac.199633801142.
[137] Thamrin ES, Warsiki E, Bindar Y, Kartika IA. Thermochromic ink as a smart indicator on cold product packaging - review. IOP Conf Ser: Earth Environ Sci 2022;1063:012021. https://doi.org/10.1088/1755-1315/1063/1/012021.
[138] Özkayalar S, Adıgüzel E, Alay Aksoy S, Alkan C. Reversible color-changing and thermal-energy storing nanocapsules of three-component thermochromic dyes. Materials Chemistry and Physics 2020;252:123162. https://doi.org/10.1016/j.matchemphys.2020.123162.
[139] Tözüm MS, Aksoy SA, Alkan C. Microencapsulation of Three-Component Thermochromic System for Reversible Color Change and Thermal Energy Storage. Fibers Polym 2018;19:660–9. https://doi.org/10.1007/s12221-018-7801-3.
[140] Bašnec K, Hajzeri M, Klanjšek Gunde M. Thermal and colour properties of leuco dye-based thermochromic composite with dodecanol solvent. J Therm Anal Calorim 2017;127:55–61. https://doi.org/10.1007/s10973-016-5670-9.
[141] Iqbal A, Iqbal G, Umar MN, Ur Rashid H, Khan SW. Synthesis of novel silica encapsulated spiropyran-based thermochromic materials. R Soc Open Sci 2022;9:211385. https://doi.org/10.1098/rsos.211385.
[142] Arman Kandirmaz E, Ozcan A, Er Ulusoy D. Production of thermochromic microcapsulated inks for smart packaging and examination of printability properties. PRT 2020;49:273–81. https://doi.org/10.1108/PRT-12-2019-0116.

[143] Bašnec K, Perše LS, Šumiga B, Huskić M, Meden A, Hladnik A, et al. Relation between colour- and phase changes of a leuco dye-based thermochromic composite. Sci Rep 2018;8:5511. https://doi.org/10.1038/s41598-018-23789-2.

[144] Geng X, Li W, Wang Y, Lu J, Wang J, Wang N, et al. Reversible thermochromic microencapsulated phase change materials for thermal energy storage application in thermal protective clothing. Applied Energy 2018;217:281–94. https://doi.org/10.1016/j.apenergy.2018.02.150.

[145] Geng X, Li W, Yin Q, Wang Y, Han N, Wang N, et al. Design and fabrication of reversible thermochromic microencapsulated phase change materials for thermal energy storage and its antibacterial activity. Energy 2018;159:857–69. https://doi.org/10.1016/j.energy.2018.06.218.

[146] Panák O, Držková M, Kaplanová M, Novak U, Klanjšek Gunde M. The relation between colour and structural changes in thermochromic systems comprising crystal violet lactone, bisphenol A, and tetradecanol. Dyes and Pigments 2017;136:382–9. https://doi.org/10.1016/j.dyepig.2016.08.050.

[147] Arno Seeboth, Detlef Lötzsch, Elvira Potechius, and Renate Vetter. THERMOCHROMIC EFFECTS OF LEUCO DYES STUDIED IN POLYPROPYLENE. Chinese J Polym Sci 2006;24:363. https://doi.org/10.1142/S0256767906001400.

[148] Li F, Zhao Y, Wang S, Han D, Jiang L, Song Y. Thermochromic core–shell nanofibers fabricated by melt coaxial electrospinning. J of Applied Polymer Sci 2009;112:269–74. https://doi.org/10.1002/app.29384.

[149] Luthern J, Peredes A. Determination of the stoichiometry of a thermochromic color complex via Job's method. Journal of Materials Science Letters 2000;19:185–8. https://doi.org/10.1023/A:1006790104175.

[150] Malherbe I, Sanderson RD, Smit E. Reversibly thermochromic micro-fibres by coaxial electrospinning. Polymer 2010;51:5037–43. https://doi.org/10.1016/j.polymer.2010.09.018.

[151] Panak O, Hauptman N, Klanjšek Gunde M. Colorimetric characterization of thermochromic composites with different molar ratios of components. Journa of Print and Media Technology Research 2012. https://doi.org/10.14622/JPMTR-1204.

[152] Panák O, Držková M, Svoboda R, Klanjšek Gunde M. Combined colorimetric and thermal analyses of reversible thermochromic composites using crystal violet lactone as a colour former. J Therm Anal Calorim 2017;127:633–40. https://doi.org/10.1007/s10973-016-5857-0.

[153] Panák O, Držková M, Kaplanová M. Insight into the evaluation of colour changes of leuco dye based thermochromic systems as a function of temperature. Dyes and Pigments 2015;120:279–87. https://doi.org/10.1016/j.dyepig.2015.04.022.

[154] Park S, Cho Y, Park S, Oh M, Kim D, Lim G, et al. Polyurea Microcapsules with Different Phase Change Material for Thermochromic Smart Displays. Chem Lett 2019;48:1343–6. https://doi.org/10.1246/cl.190629.

[155] Zhijia Liu, Fucheng Bao,, Feng Fu. Study of Manufacturing Thermochromic Wood. Materials Science, Environmental Science 2011;43:239–43.

[156] Ma Y, Zhu B, Wu K. Preparation of reversible thermochromic building coatings and their properties. J Coatings Tech 2000;72:67–71. https://doi.org/10.1007/BF02720527.

[157] MacLaren DC, White MA. Competition between dye–developer and solvent–developer interactions in a reversible thermochromic system. J Mater Chem 2003;13:1701–4. https://doi.org/10.1039/B302250A.
[158] Geng X, Li W, Wang Y, Lu J, Wang J, Wang N, et al. Reversible thermochromic microencapsulated phase change materials for thermal energy storage application in thermal protective clothing. Applied Energy 2018;217:281–94. https://doi.org/10.1016/j.apenergy.2018.02.150.
[159] Geng X, Li W, Yin Q, Wang Y, Han N, Wang N, et al. Design and fabrication of reversible thermochromic microencapsulated phase change materials for thermal energy storage and its antibacterial activity. Energy 2018;159:857–69. https://doi.org/10.1016/j.energy.2018.06.218.
[160] Guangjian Peng, Guijing Dou, Yahao Hu, Yiheng Sun, Zhitong Chen. Phase change material (PCM) microcapsules for thermal energy storage. Advances in polymer technology 2020:9490873. https://doi.org/10.1155/2020/9490873.
[161] Wu B, Shi L, Zhang Q, Wang W-J. Microencapsulation of 1-hexadecanol as a phase change material with reversible thermochromic properties. RSC Adv 2017;7:42129–37. https://doi.org/10.1039/C7RA06764J.
[162] Zhu X, Liu Y, Li Z, Wang W. Thermochromic microcapsules with highly transparent shells obtained through in-situ polymerization of urea formaldehyde around thermochromic cores for smart wood coatings. Sci Rep 2018;8:4015. https://doi.org/10.1038/s41598-018-22445-z.
[163] Umair MM, Zhang Y, Iqbal K, Zhang S, Tang B. Novel strategies and supporting materials applied to shape-stabilize organic phase change materials for thermal energy storage–A review. Applied Energy 2019;235:846–73. https://doi.org/10.1016/j.apenergy.2018.11.017.
[164] Campardelli R, Della Porta G, Gomez V, Irusta S, Reverchon E, Santamaria J. Encapsulation of titanium dioxide nanoparticles in PLA microspheres using supercritical emulsion extraction to produce bactericidal nanocomposites. J Nanopart Res 2013;15:1987. https://doi.org/10.1007/s11051-013-1987-5.
[165] Balaban AT, Mateescu GD, Elian M. Infra-red absorption spectra of pyrylium salts. Tetrahedron 1962;18:1083–94. https://doi.org/10.1016/S0040-4020(01)99274-9.
[166] He N, Ni Y, Teng J, Li H, Yao L, Zhao P. Identification of inorganic oxidizing salts in homemade explosives using Fourier transform infrared spectroscopy. Spectrochimica Acta Part A: Molecular and Biomolecular Spectroscopy 2019;221:117164. https://doi.org/10.1016/j.saa.2019.117164.
[167] Huang R, Li W, Wang J, Zhang X. Effects of oil-soluble etherified melamine-formaldehyde prepolymers on in situ microencapsulation and macroencapsulation of n-dodecanol. New J Chem 2017;41:9424–37. https://doi.org/10.1039/C7NJ01528C.
[168] Li C-F, Qin Z-X, Liu Y, Pan Y-D, Liu M-L. Preparation of a nano-silica modified melamine formaldehyde resin. International Journal of Adhesion and Adhesives 2022;113:103076. https://doi.org/10.1016/j.ijadhadh.2021.103076.
[169] Li D, Wang J, Wang Y, Li W, Wang X, Shi H, et al. Effect of N-isopropylacrylamide on the preparation and properties of microencapsulated phase change materials. Energy 2016;106:221–30. https://doi.org/10.1016/j.energy.2016.03.035.

[170] Zhang H, Wang X, Wu D. Silica encapsulation of n-octadecane via sol–gel process: A novel microencapsulated phase-change material with enhanced thermal conductivity and performance. Journal of Colloid and Interface Science 2010;343:246–55. https://doi.org/10.1016/j.jcis.2009.11.036.
[171] Sarier N, Onder E. Organic phase change materials and their textile applications: An overview. Thermochimica Acta 2012;540:7–60. https://doi.org/10.1016/j.tca.2012.04.013.
[172] Günther E, Huang L, Mehling H, Dötsch C. Subcooling in PCM emulsions – Part 2: Interpretation in terms of nucleation theory. Thermochimica Acta 2011;522:199–204. https://doi.org/10.1016/j.tca.2011.04.027.
[173] Prado JI, Calviño U, Lugo L. Phase change characterization of eco-friendly isopropyl palmitate-based graphene nanoplatelet nanofluid for thermal energy applications. Journal of Molecular Liquids 2022;360:119456. https://doi.org/10.1016/j.molliq.2022.119456.
[174] Onder E, Sarier N. Fatty acid alkyl ester nanowebs suitable for renewable thermal energy storage. Thermochimica Acta 2020;690:178698. https://doi.org/10.1016/j.tca.2020.178698.
[175] Alkhazaleh AH. Isopropyl palmitate integrated with plasterboard for low temperature latent heat thermal energy storage. Int J Energy Res 2021;45:10500–12. https://doi.org/10.1002/er.6537.
[176] Provost C, Herbots H, Kinget R. Transparent oil-water gels. Part II. A study of the gel structure in transparent oil-water gels by differential scanning calorimetry. International Journal of Pharmaceutics 1990;62:217–28. https://doi.org/10.1016/0378-5173(90)90235-V.
[177] Tanwar S, Kaur R. Development and investigation of microencapsulated CAPRYLIC ACID -based phase change materials for thermal energy storage applications. Intl J of Energy Research 2021;45:17302–14. https://doi.org/10.1002/er.6611.
[178] Vennapusa JR, Konala A, Dixit P, Chattopadhyay S. Caprylic acid based PCM composite with potential for thermal buffering and packaging applications. Materials Chemistry and Physics 2020;253:123453. https://doi.org/10.1016/j.matchemphys.2020.123453.
[179] Konuklu Y, Paksoy HÖ. Polystyrene-based caprylic acid microencapsulation for thermal energy storage. Solar Energy Materials and Solar Cells 2017;159:235–42. https://doi.org/10.1016/j.solmat.2016.09.016.
[180] Zhang H, Zhu J, Zhou W, Liu F, Li K. Synthesis and thermal properties of a capric acid-modified expanded vermiculite phase change material. J Mater Sci 2019;54:2231–40. https://doi.org/10.1007/s10853-018-2988-7.
[181] Kar TR, Samanta AK, Sinnur HD, Kumar M. Studies on Effect of Application of Capric Acid and Stearic Acid based Reactive Phase Change Materials (rPCM) with PHAMS Binder on Thermal Comfort of Cotton Khadi Fabric as Thermo-tropic Smart Textiles. Journal of Natural Fibers 2022;19:5504–23. https://doi.org/10.1080/15440478.2021.1880517.
[182] Zuo P, Liu Z, Zhang H, Dai D, Fu Z, Corker J, et al. Formulation and phase change mechanism of Capric acid/Octadecanol binary composite phase change materials. Energy 2023;270:126943. https://doi.org/10.1016/j.energy.2023.126943.
[183] Dunn RO. Crystallization Behavior of Fatty Acid Methyl Esters. J Americ Oil Chem Soc 2008;85:961–72. https://doi.org/10.1007/s11746-008-1279-x.

[184] Avery HE, Shaw DJ. Basic physical chemistry calculations. Repr. with corr. London: Butterworth; 1973.
[185] Cherukuvada S, Nangia A. Eutectics as improved pharmaceutical materials: design, properties and characterization. Chem Commun 2014;50:906–23. https://doi.org/10.1039/C3CC47521B.
[186] Singh P, Sharma RK, Ansu AK, Goyal R, Sarı A, Tyagi VV. A comprehensive review on development of eutectic organic phase change materials and their composites for low and medium range thermal energy storage applications. Solar Energy Materials and Solar Cells 2021;223:110955. https://doi.org/10.1016/j.solmat.2020.110955.
[187] Yanping Y, Wenquan T, Xiaoling C, Li B. Theoretic Prediction of Melting Temperature and Latent Heat for a Fatty Acid Eutectic Mixture. J Chem Eng Data 2011;56:2889–91. https://doi.org/10.1021/je200057j.
[188] Gregor-Svetec D. Intelligent Packaging. Nanomaterials for Food Packaging, Elsevier; 2018, p. 203–47. https://doi.org/10.1016/B978-0-323-51271-8.00008-5.
[189] Mueller D, Vogelsang F. Towards smart manufacturing logistics: A case study of potentials of smart label data in electronics manufacturing. Procedia CIRP 2021;104:1741–6. https://doi.org/10.1016/j.procir.2021.11.293.
[190] SKYQUEST. Global Industrial Labels Market. 2024.
[191] Ismail Sutaria. Smart Label Market. 2022.
[192] Amanda Sarley. Implications of Thermochromic Ink. BS in Graphic Communication. California Polytechnic State University - San Luis Obispo, 2011.
[193] Tran TS, Dutta NK, Choudhury NR. Graphene inks for printed flexible electronics: Graphene dispersions, ink formulations, printing techniques and applications. Advances in Colloid and Interface Science 2018;261:41–61. https://doi.org/10.1016/j.cis.2018.09.003.
[194] N. I. I. R. Board. Screen Printing Technology Hand Book. 2003.
[195] Viková M, Vik M. Transition Temperature of Color Change in Thermochromic Systems and Its Description Using Sigmoidal Models. Materials 2023;16:7478. https://doi.org/10.3390/ma16237478.

A
ANNEX A

Annex A includes supplementary materials of Chapter 2.

A.1 1D, 2D NMR and HRMS spectra, compounds 1-5

Compound 1

Table 2.5 — Assignment of ^{1}H NMR data for compound 1 (DMSO-d_6, 298.0 K) at 400 MHz.

Position	^{1}H δ /ppm (J/Hz)
2′, 6′	8.33 (2H, d, J = 8.9 Hz)
3″	8.16 (1H, d, J = 7.8 Hz)
3	7.94 (1H, s)
5″	7.84 (1H, t, J = 7.7 Hz)
4″	7.75 (1H, t, J = 7.8 Hz)
6″	7.53 (1H, d, J = 7.5 Hz)
8	7.28 (1H, d, J ~ 2 Hz)
6	7.15 (1H, dd, J = 7.2 Hz, J ~2 Hz)
5	7.10 (1H, d, J = 7.2 Hz)
3′, 5′	6.93 (2H, bt, J = 9.0 Hz)
7-N-**CH_2**-	3.56 (4H, d, J = 8.4 Hz)
4′-N-**CH_3**	3.19 (6H, s)
7-N-CH_2-**CH_2**-	1.59 (4H, m)
7-N-CH_2-CH_2-**CH_2**-	1.38 (4H, m)
7-N-CH_2-CH_2-CH_2-**CH_3**	0.94 (6H, t, J = 7.4 Hz)

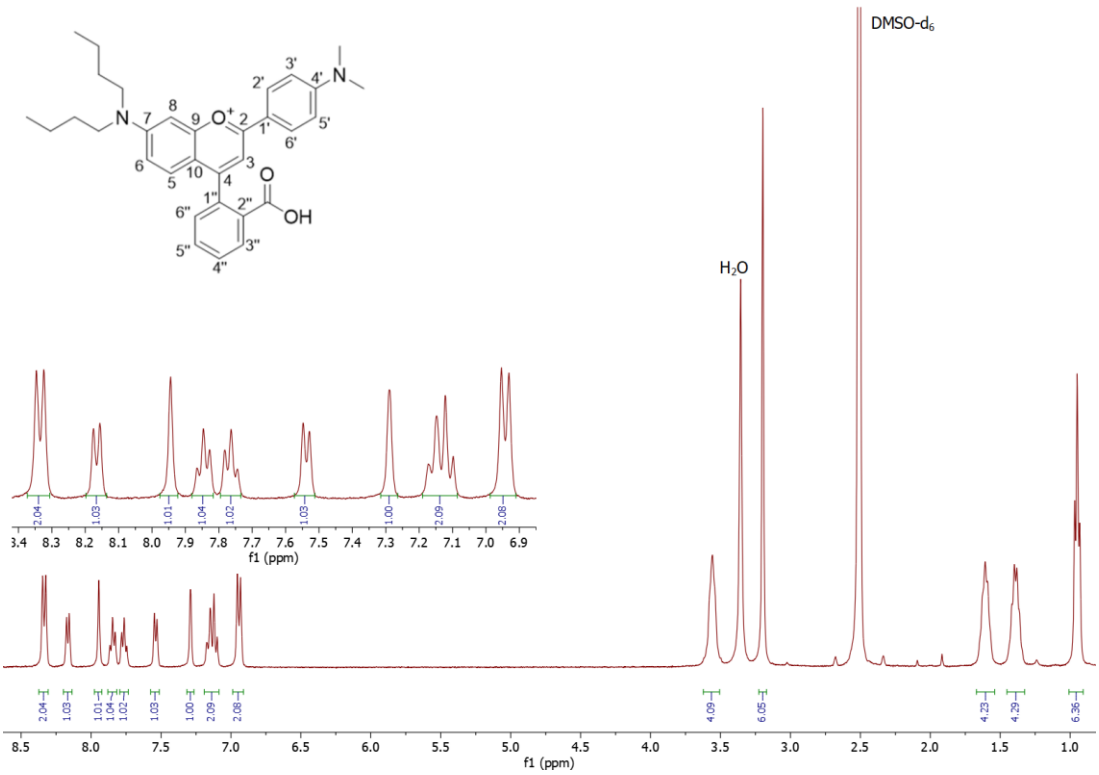

Figure 2.13 — ^{1}H NMR spectrum of compound 1 (DMSO-d_6, 298.0 K) at 400 MHz.

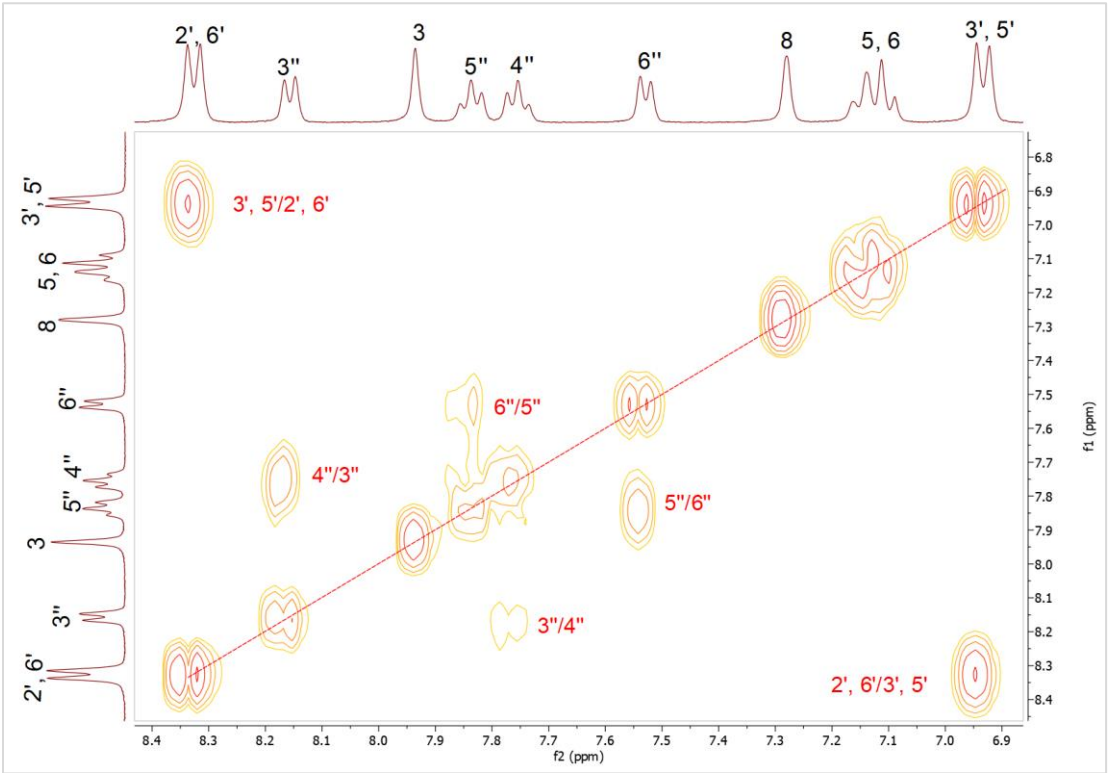

Figure 2.14 — COSY spectrum of compound 1 (DMSO-d_6, 298.0 K) at 500 MHz (lower field region).

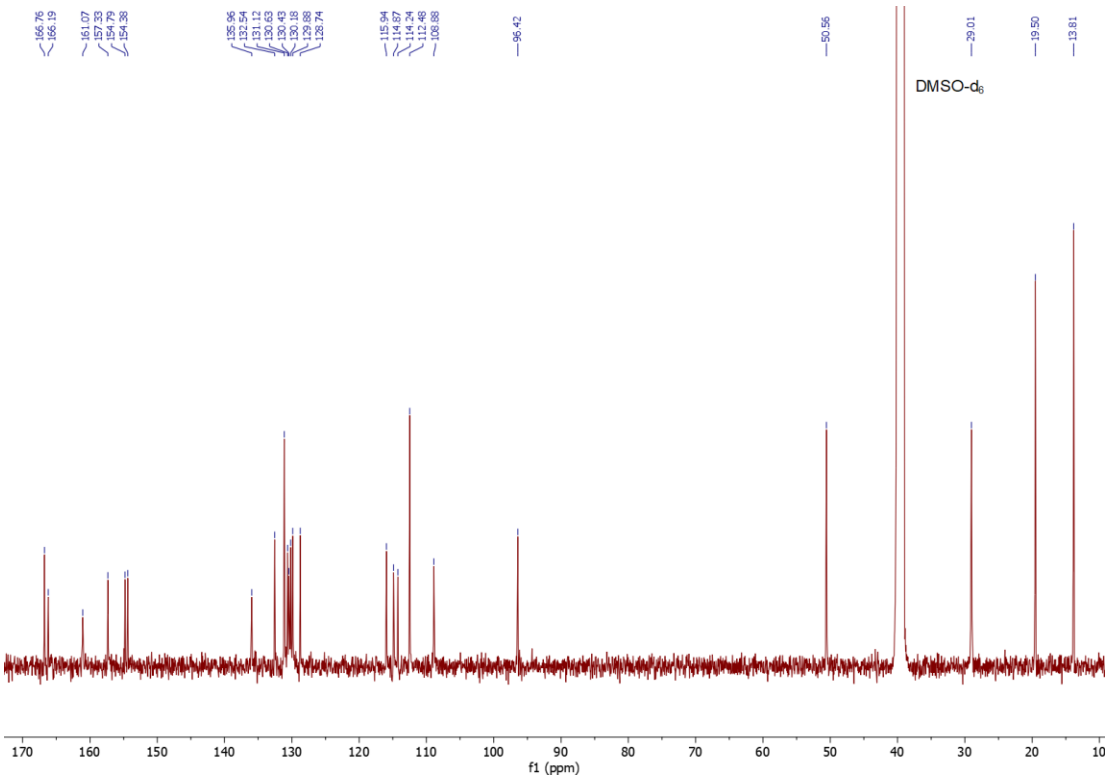

Figure 2.15 — ^{13}C NMR spectrum of compound 1 (DMSO-d_6, 298.0 K) at 126 MHz.

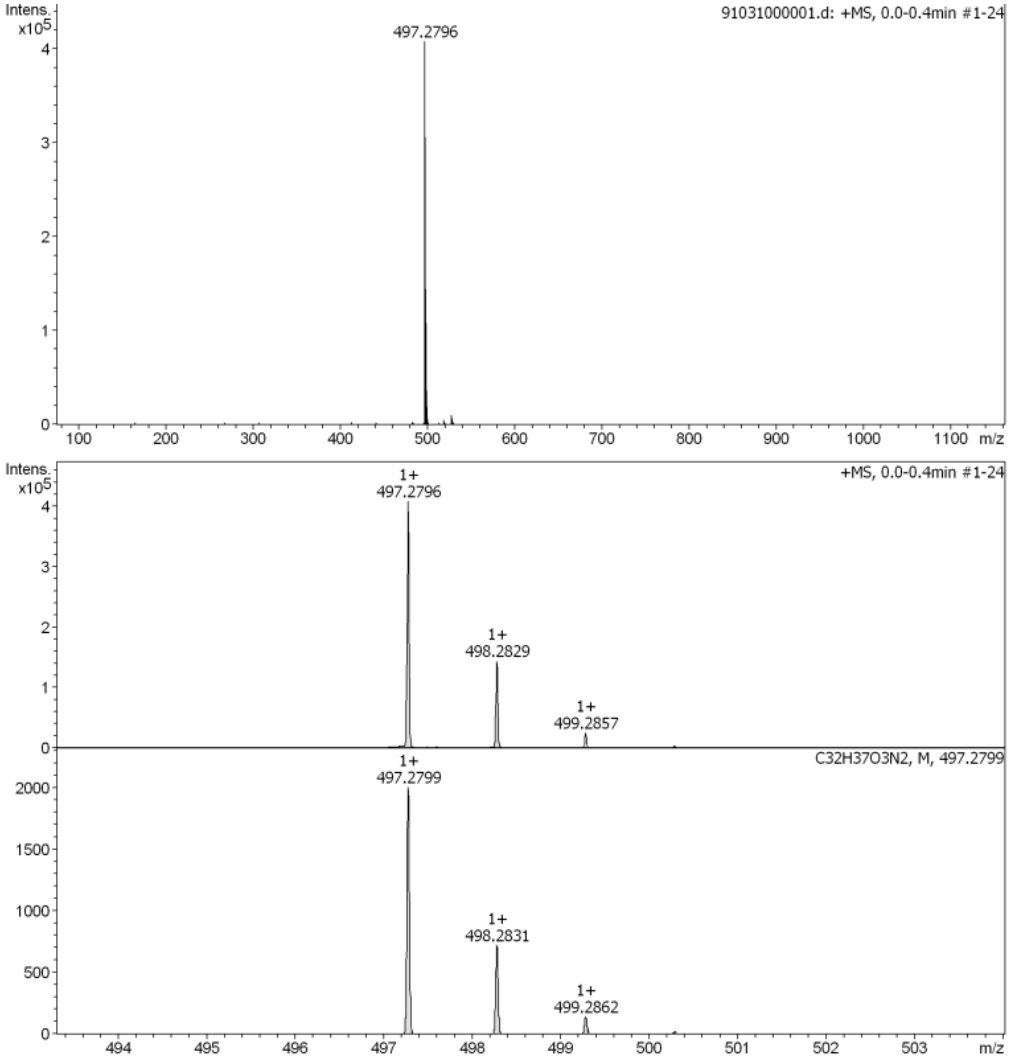

Figure 2.16 — HRMS spectrum of compound 1.

Compound 2

Table 2.6 — Assignment of ^{1}H NMR data for compound 2 (DMSO-d_6 plus DCl, 298.0 K) at 400 MHz.

Position	^{1}H δ /ppm (J/Hz)
3″	8.82 (1H, d, J = 7.7 Hz)
2′, 6′	8.71 (2H, d, J = 8.0 Hz)
5″	8.38 (1H, t, J = 7.6 Hz)
4″	8.31 (2H, t, J = 7.6 Hz)
3	8.28 (1H, s)
3′, 5′	8.04 (2H, d, J = 8.0 Hz)
6″	7.97 (1H, d, J = 7.5 Hz)
5	7.88 (1H, d, J = 9.4 Hz)
6	7.78 (1H, dd, J = 9.4 Hz, J ~2 Hz)
8	7.75 (1H, bs, J ~2 Hz)
7-N-**CH_2**-	4.15 (4H, t, J = 7.9 Hz)
4′-**CH_3**	3.02 (3H, s)
7-N-CH_2-**CH_2**-	2.31 – 2.18 (4H, m)
7-N-CH_2-CH_2-**CH_2**-	1.98 (4H, m)
7-N-CH_2-CH_2-CH_2-**CH_3**	1.53 (6H, t, J = 7.4 Hz)

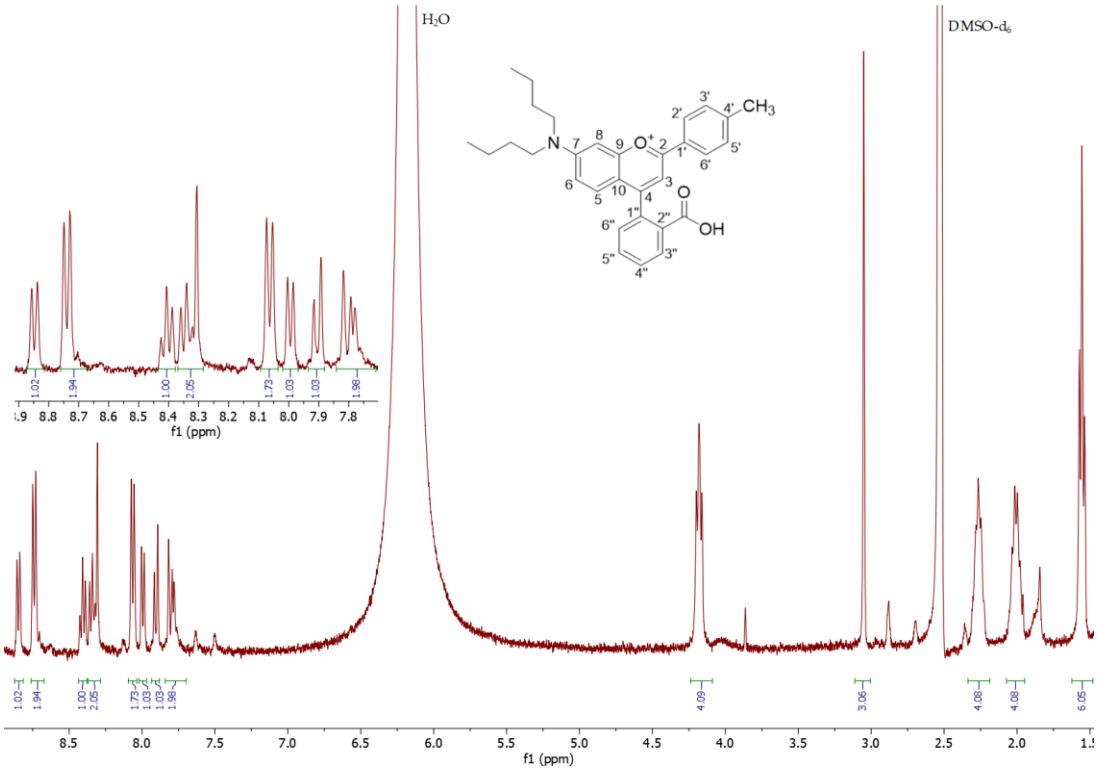

Figure 2.17 — ^{1}H NMR spectrum of compound 2 (DMSO-d_6 plus DCl, 298.0 K) at 400 MHz.

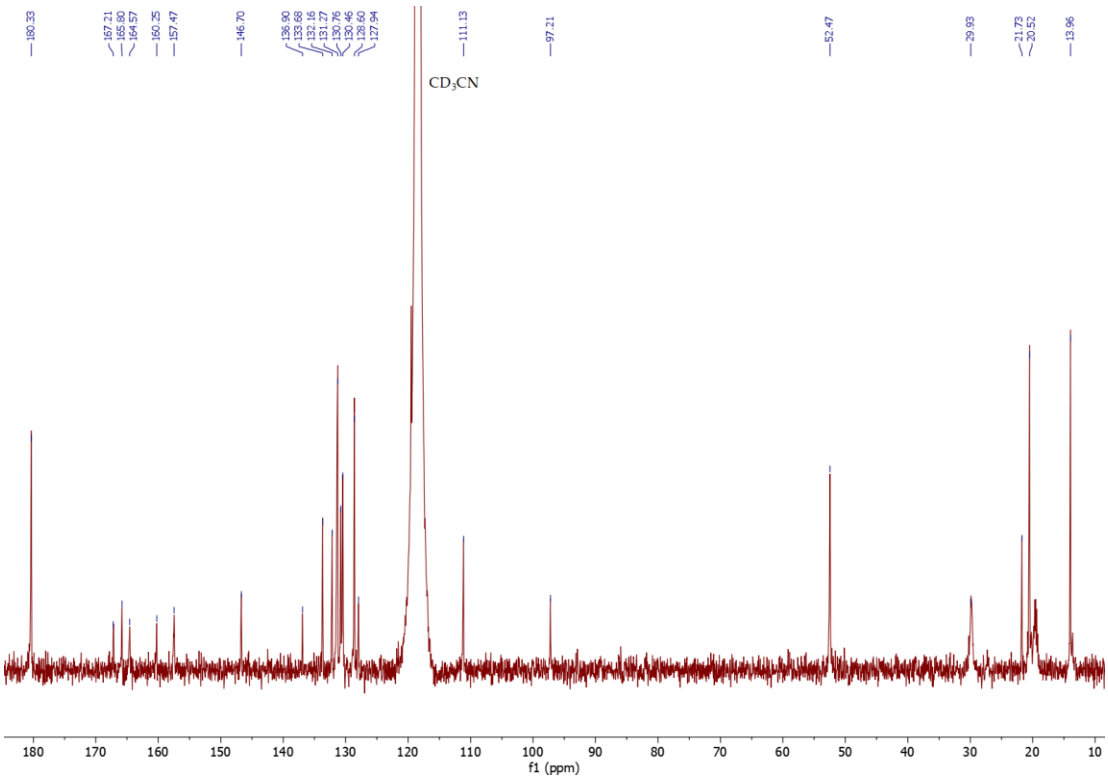

Figure 2.18 — ^{13}C NMR spectrum of compound 2 (CD_3CN plus DCl, 298.0 K) at 126 MHz.

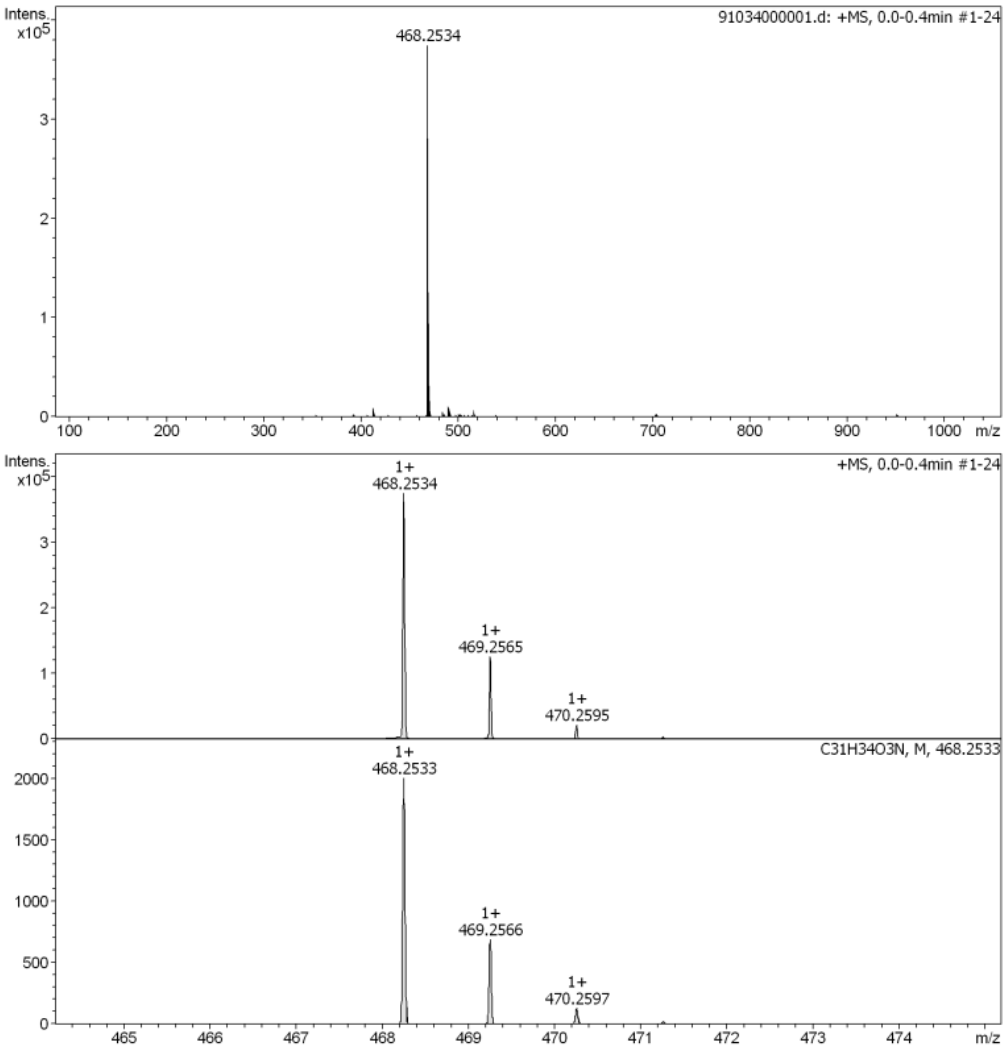

Figure 2.19 — HRMS of compound 2.

Compound 3

Table 2.7 — Assignment of ^{1}H NMR data for compound 3 (CD_3CN plus DCl, 298.0 K) at 400 MHz.

Position	^{1}H δ /ppm (J/Hz)
3′, 5′	8.44 (2H, d, J = 8.8 Hz)
2′, 6′	8.38 (2H, d, J = 8.9 Hz)
3″	8.26 (1H, d, J = 7.8 Hz)
5″	7.84 (1H, t, J = 7.5 Hz)
4″	7.77 (1H, t, J = 7.6 Hz)
3	7.71 (1H, s)
6″	7.42 (1H, d, J = 7.5 Hz)
5	7.33 (1H, d, J = 9.6 Hz)
6	7.25 (1H, dd, J = 9.5 Hz, J = 2.4 Hz)
8	7.19 (1H, d, J = 2.4 Hz)
7-N-**CH_2**-	3.62 (4H, t, J = 9.4 Hz)
7-N-CH_2-**CH_2**-	1.69 (4H, m)
7-N-CH_2-CH_2-**CH_2**-	1.44 (4H, m)
7-N-CH_2-CH_2-CH_2-**CH_3**	0.99 (6H, t, J = 7.3 Hz)

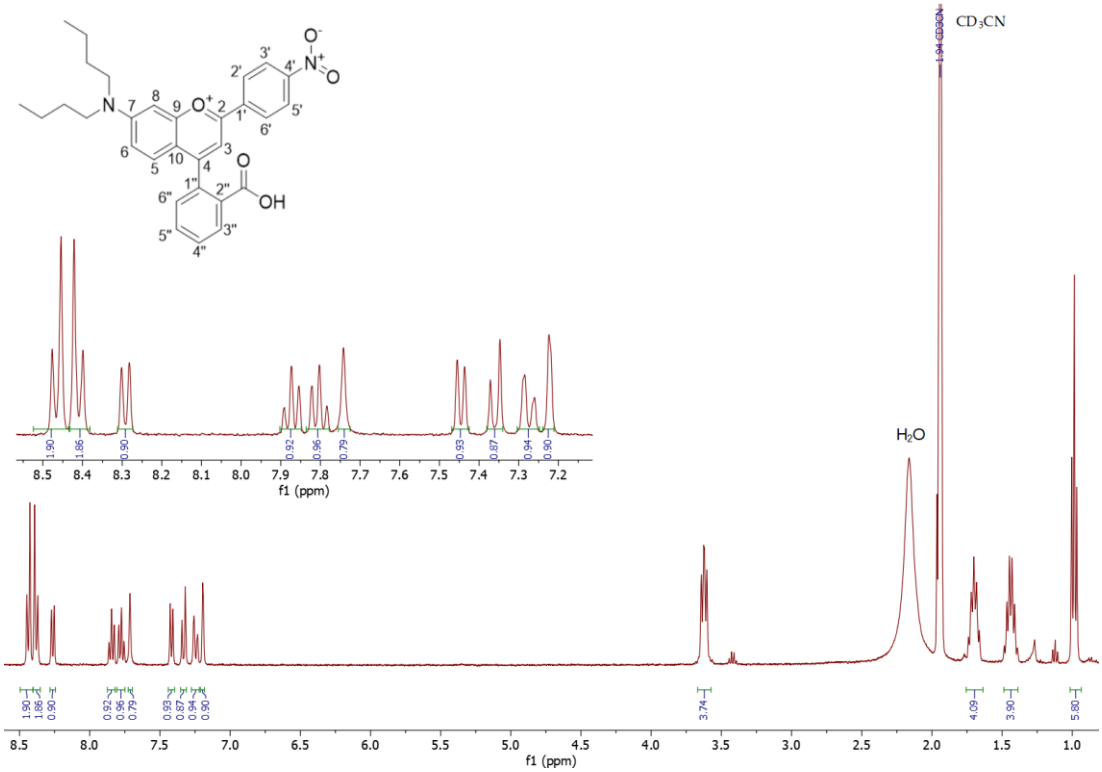

Figure 2.20 — ^{1}H NMR spectrum of compound 3 (CD_3CN plus DCl, 298.0 K) at 400 MHz.

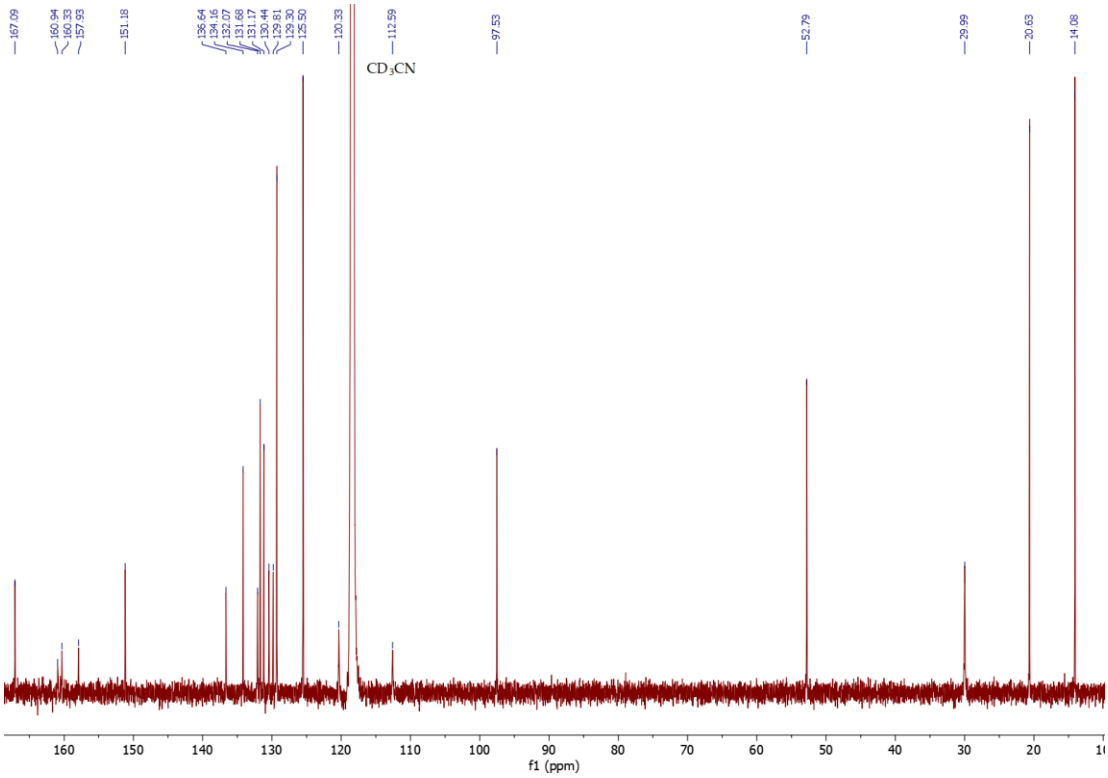

Figure 2.21 — ^{13}C NMR spectrum of compound 3 (CD_3CN plus DCl, 298.0 K) at 126 MHz.

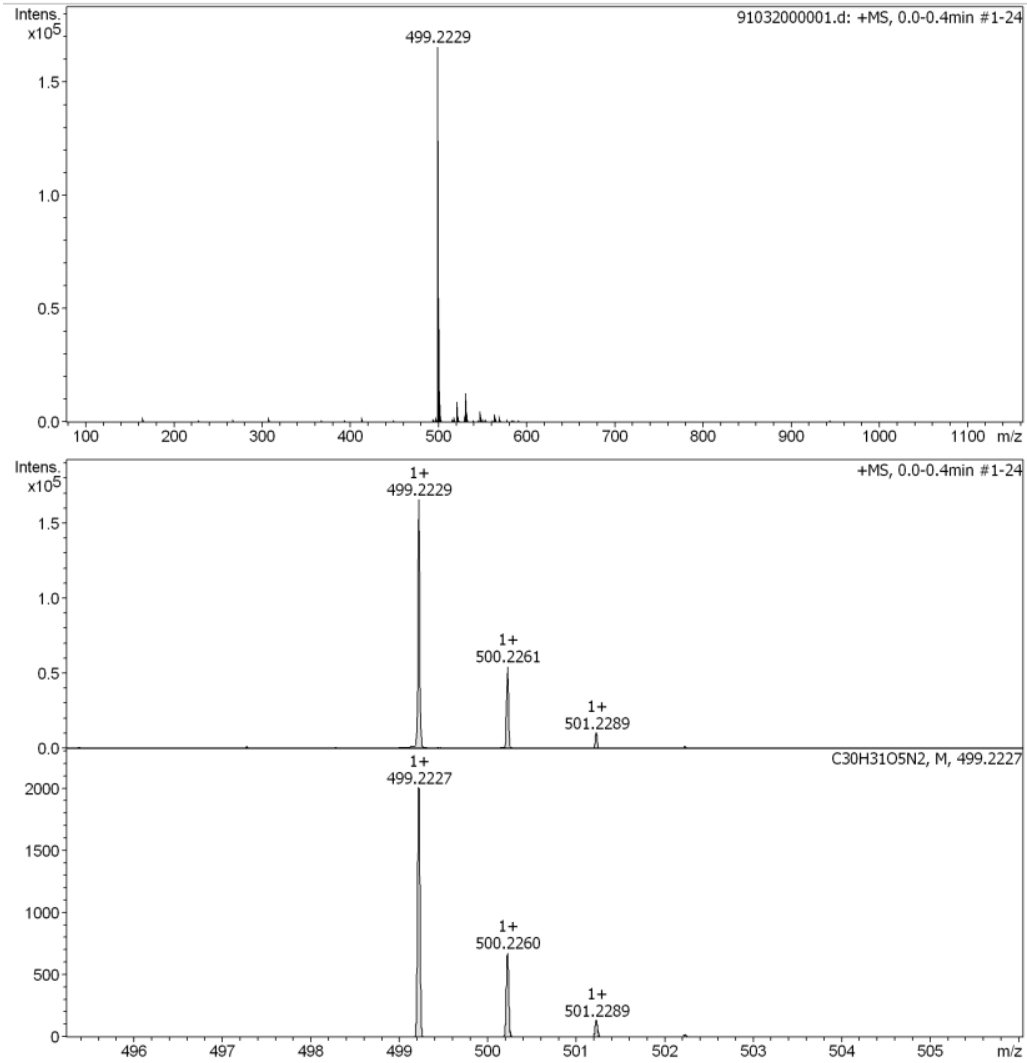

Figure 2.22 — HRMS of compound 3.

Compound 4

Table 2.8 — Assignment of ^{1}H NMR data for compound 4 (CD_3CN plus DCl, 298.0 K) at 400 MHz.

Position	^{1}H δ /ppm (J/Hz)
3′, 5′	8.29 (2H, d, J = 8.4 Hz)
3″	8.27 (2H, d, J = 7.8 Hz)
2′, 6′	8.04 (2H, d, J = 8.3 Hz)
5″	7.84 (1H, t, J = 7.6 Hz)
4″	7.77 (1H, t, J = 7.6 Hz)
3	7.74 (1H, s)
6″	7.42 (1H, d, J = 7.5 Hz)
5	7.33 (1H, d, J = 9.6 Hz)
6	7.24 (1H, dd, J = 9.5 Hz, J = 2.4 Hz)
8	7.20 (1H, d, J = 2.4 Hz)
7-N-**CH_2**-	3.62 (4H, t, J = 6.5 Hz)
7-N-CH_2-**CH_2**-	1.70 (4H, m)
7-N-CH_2-CH_2-**CH_2**-	1.44 (4H, m)
7-N-CH_2-CH_2-CH_2-**CH_3**	0.98 (6H, t, J = 7.3 Hz)

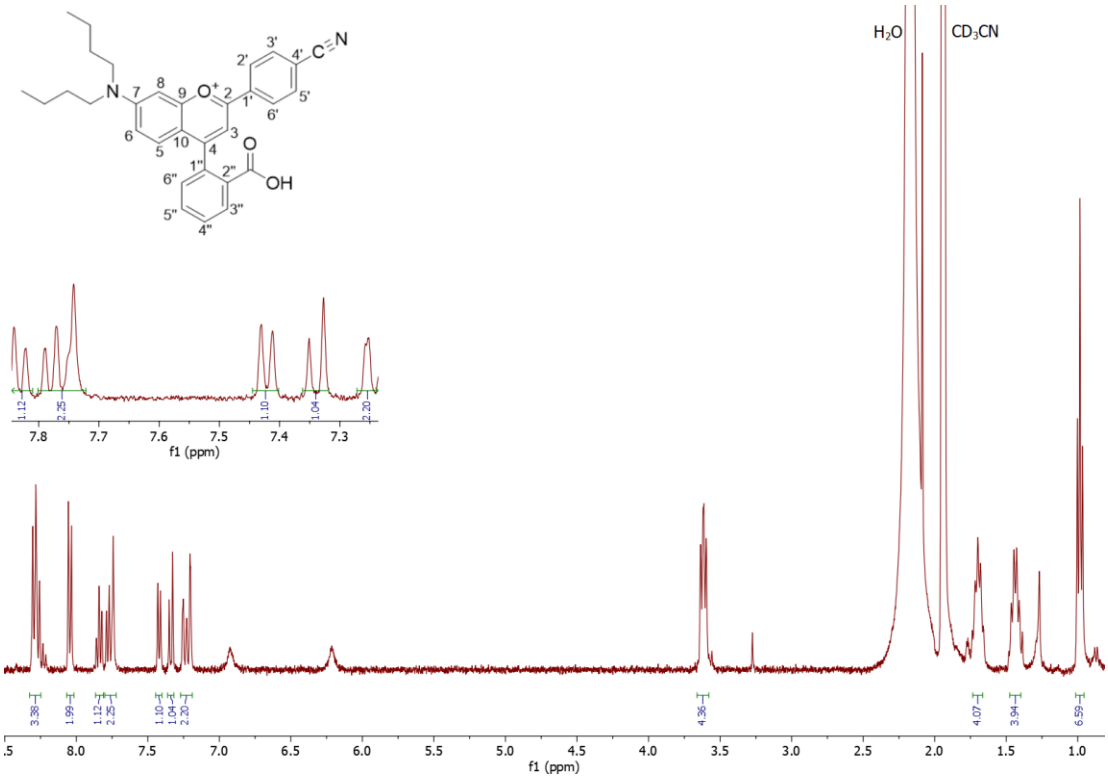

Figure 2.23 — ^{1}H NMR spectrum of compound 4 (CD_3CN, 298.0 K) at 400 MHz.

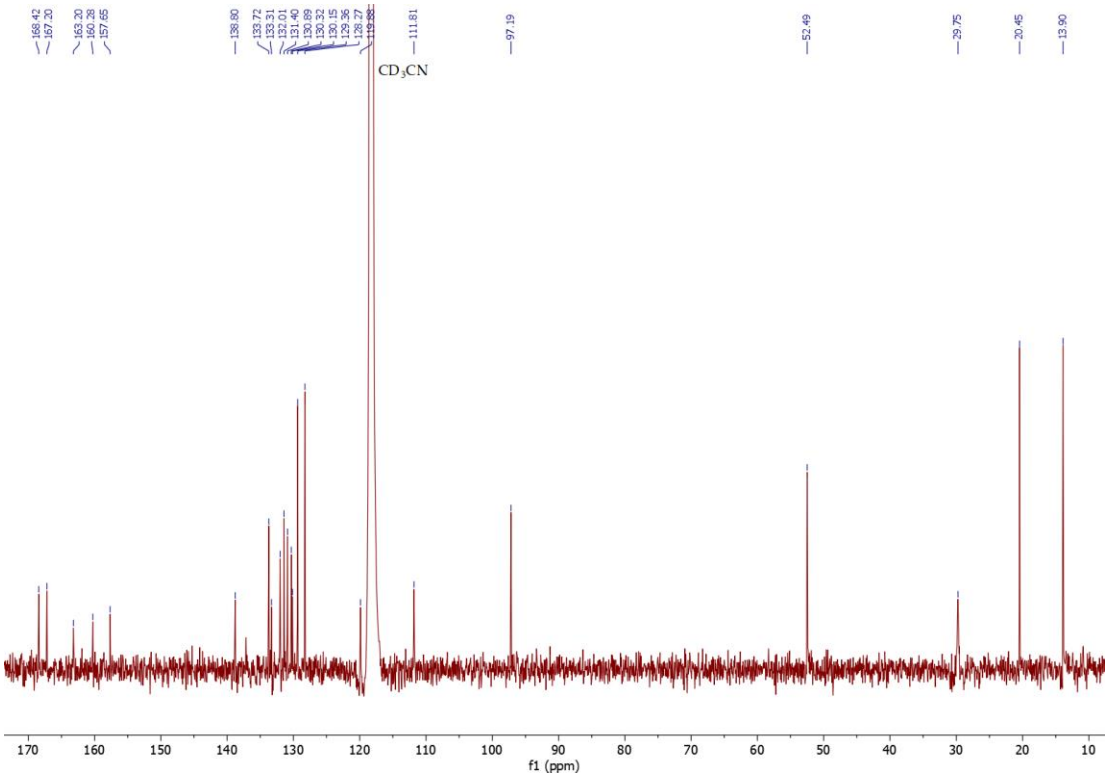

Figure 2.24 — ^{13}C NMR spectrum of compound 4 (CD_3CN plus DCl, 298.0 K) at 126 MHz.

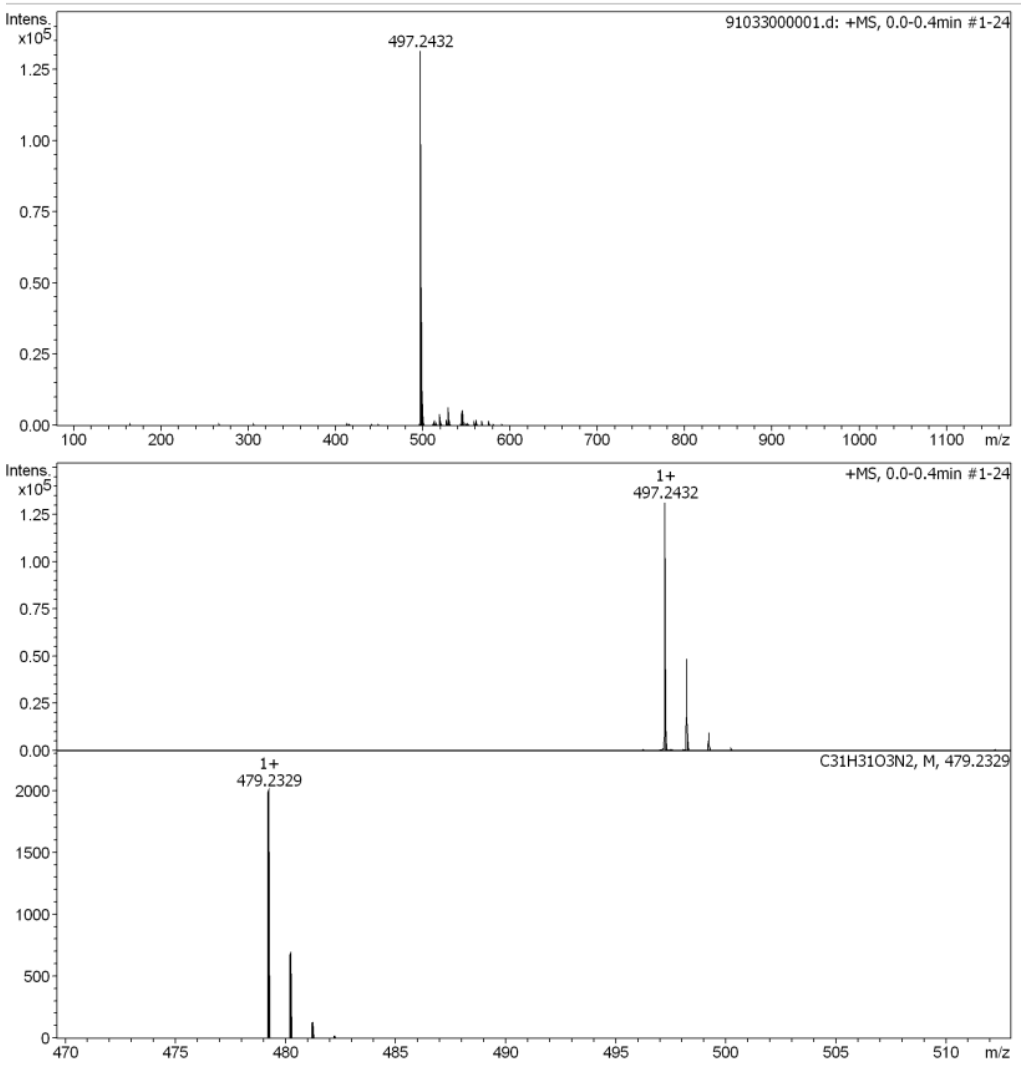

Figure 2.25 — HRMS of compound 4.

Compound 5

Table 2.9 — Assignment of ^{1}H NMR data for compound 5 (CD_3CN plus DCl, 298.0 K) at 400 MHz.

Position	^{1}H δ /ppm (J/Hz)
3′, 5′	8.30 (2H, m)
3″	8.26 (1H, d, J = 7.9 Hz)
5″	7.82 (1H, t, J = 7.6 Hz)
4″	7.76 (1H, t, J = 7.6 Hz)
3	7.71 (1H, s)
2′, 6′ and 6″	7.40 (3H, m)
5	7.33 (1H, d, J = 9.6 Hz)
6	7.23 (1H, bd, J = 9.8 Hz)
8	7.20 (1H, bs)
7-N-**CH_2**-	3.60 (4H, t, J = 8.0 Hz)
7-N-CH_2-**CH_2**-	1.68 (4H, m)
7-N-CH_2-CH_2-**CH_2**-	1.42 (4H, m)
7-N-CH_2-CH_2-CH_2-**CH_3**	0.97 (6H, t, J = 7.3 Hz)

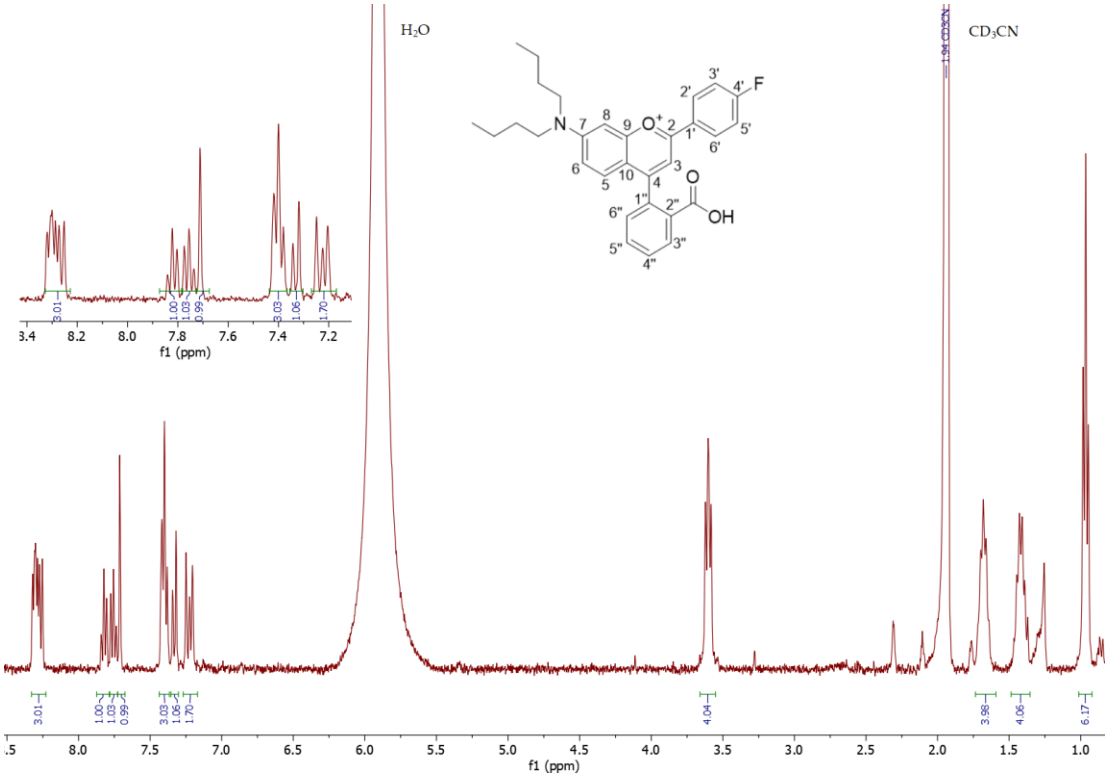

Figure 2.26 — ^{1}H NMR spectrum of compound 5 (CD_3CN plus DCl, 298.0 K) at 400 MHz.

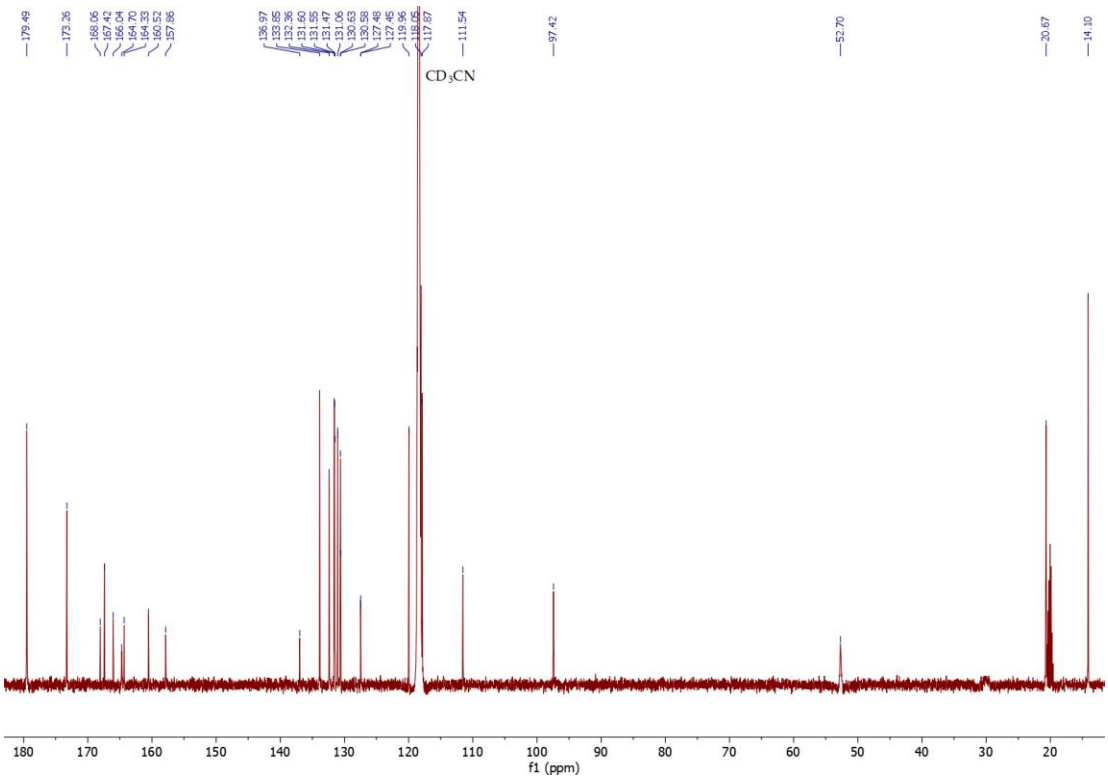

Figure 2.27 — ^{13}C NMR spectrum of compound 5 (CD_3CN plus DCl, 298.0 K) at 126 MHz.

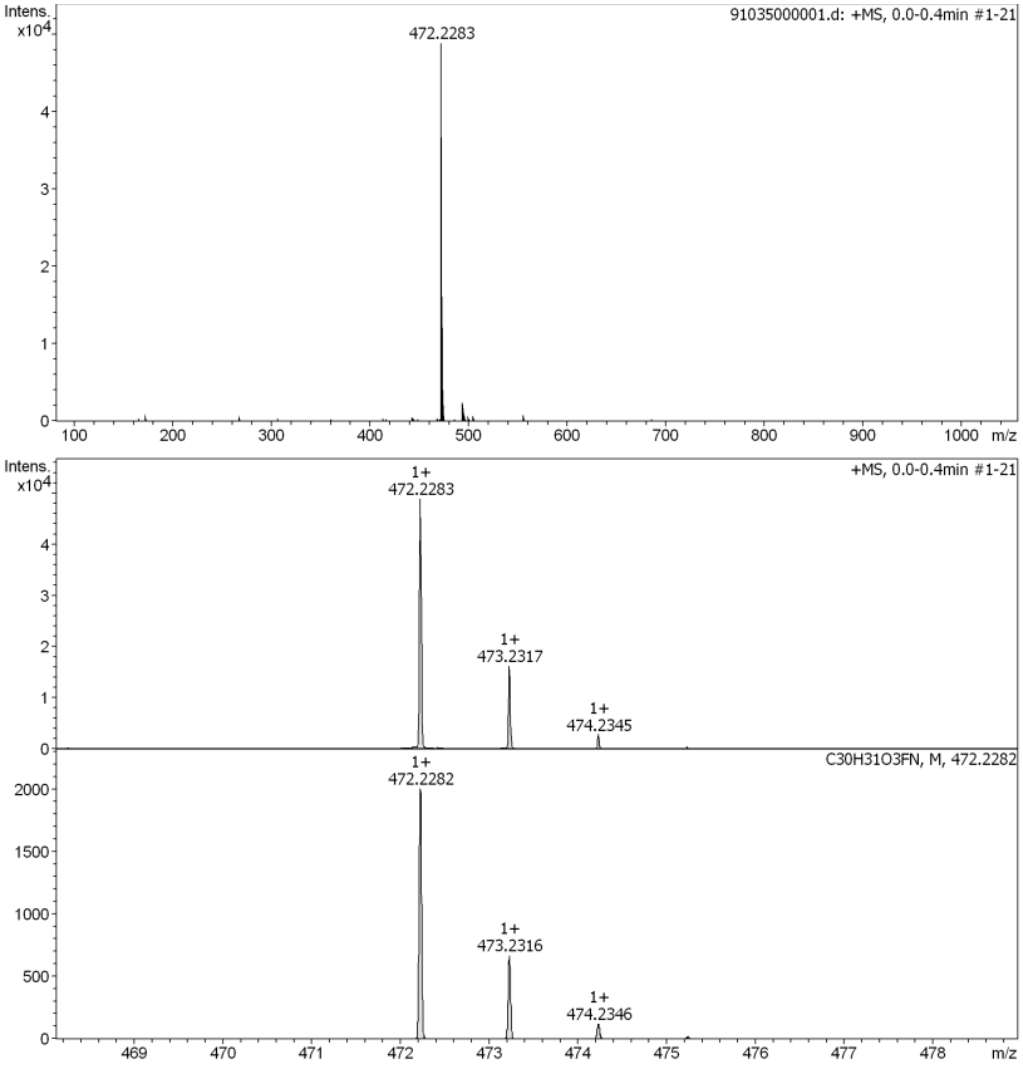

Figure 2.28 — HRMS of compound 5.

A.2 Absorption spectra in acetonitrile as a function of added DIPEA, compounds 2-5

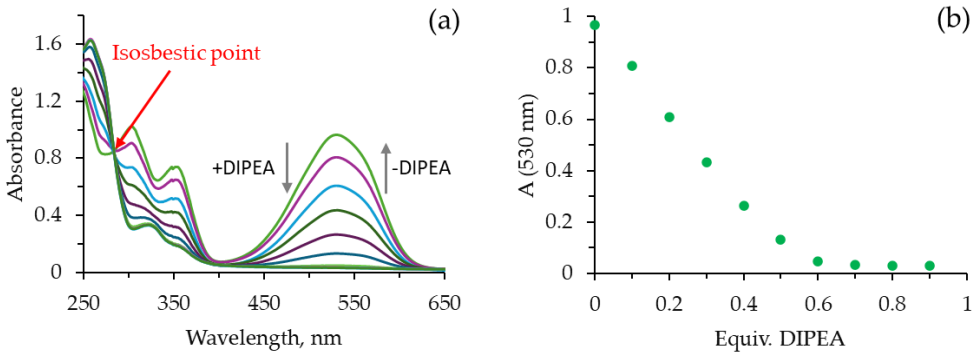

Figure 2.29 — Absorption spectra of compound 2 in acetonitrile as a function of added DIPEA (a); Absorption at λ_{max} as a function of the number of equivalents of added DIPEA (b).

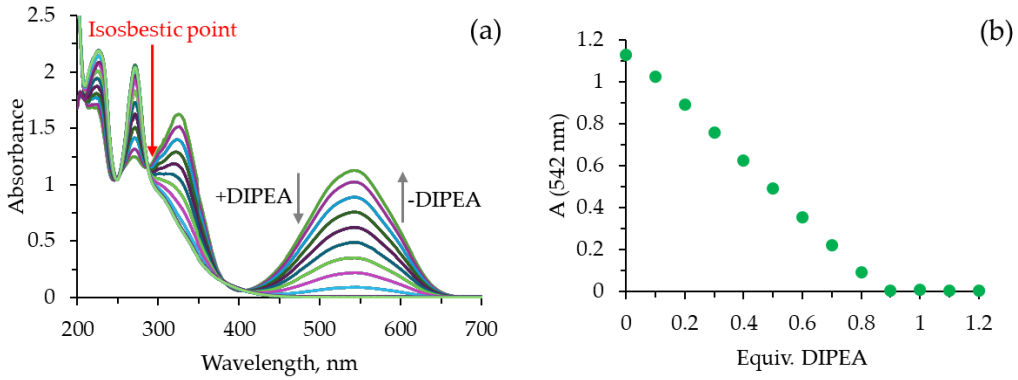

Figure 2.30 — Absorption spectra of compound 3 in acetonitrile as a function of added DIPEA (a); Absorption at λ_{max} as a function of the number of equivalents of added DIPEA (b).

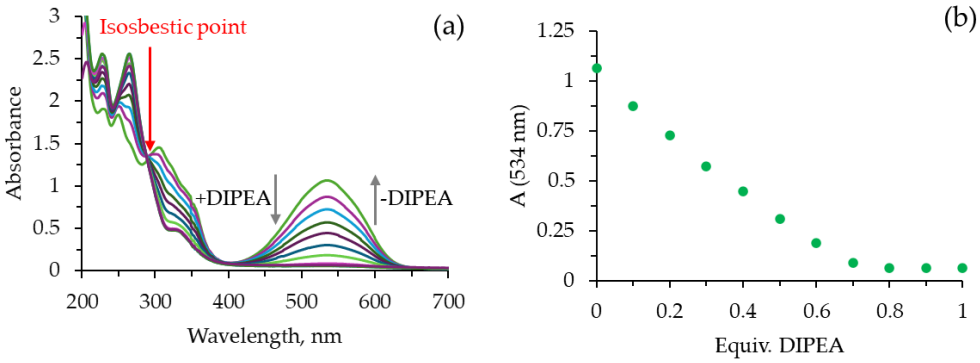

Figure 2.31 — Absorption spectra of compound 3 in acetonitrile as a function of added DIPEA (a); Absorption at λ_{max} as a function of the number of equivalents of added DIPEA (b).

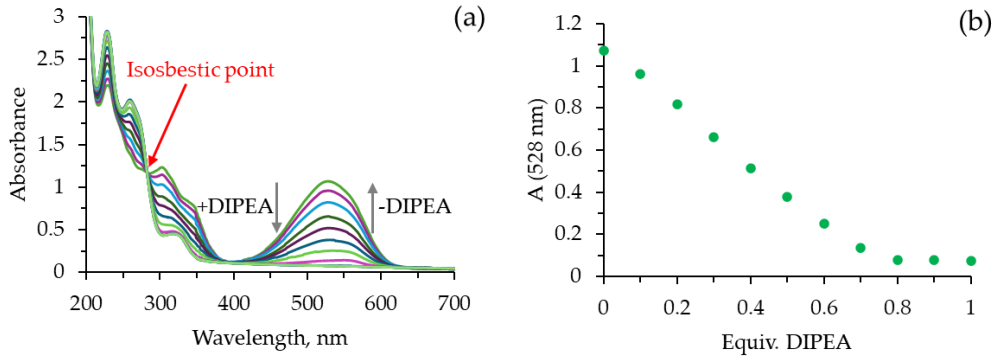

Figure 2.32 — Absorption spectra of compound 5 in acetonitrile as a function of added DIPEA (a); Absorption at λ_{max} as a function of the number of equivalents of added DIPEA (b).

A.3 Absorption spectra in acetonitrile as a function of added $FeCl_3$, compounds 2-5

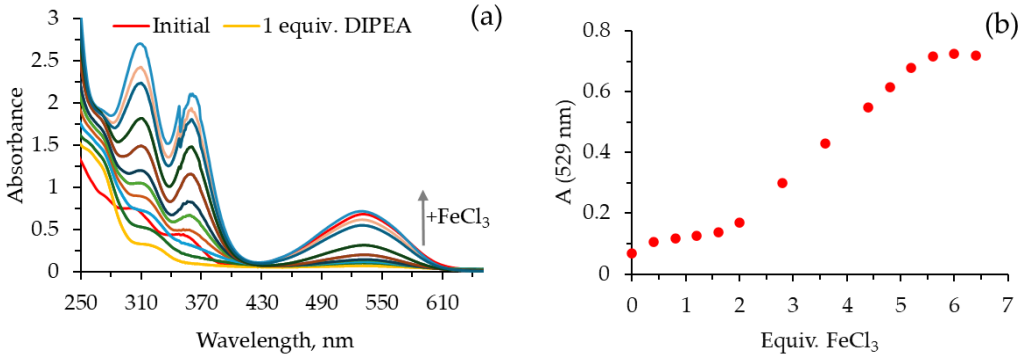

Figure 2.33 — Absorption spectra of compound 2 in acetonitrile and DIPEA (1 Equiv.), as a function of added $FeCl_3$ (a); Absorption at λ_{max} as a function of the number of equivalents of added $FeCl_3$ (b).

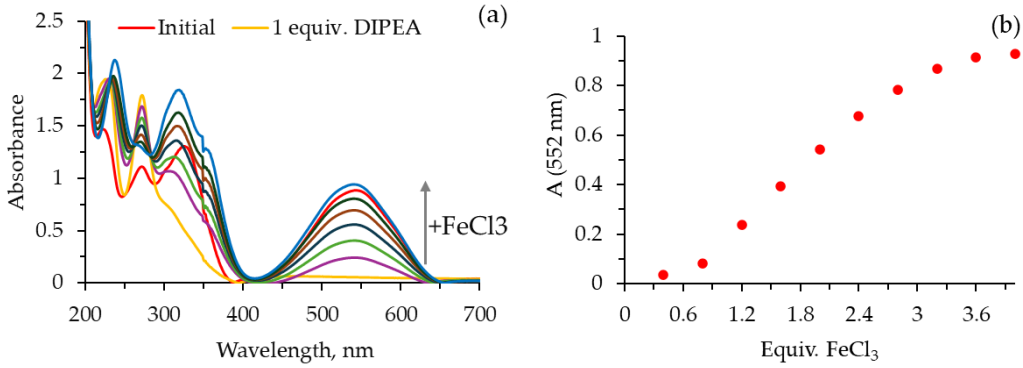

Figure 2.34 — Absorption spectra of compound 3 in acetonitrile and DIPEA (1 Equiv.), as a function of added $FeCl_3$ (a); Absorption at λ_{max} as a function of the number of equivalents of added $FeCl_3$ (b).

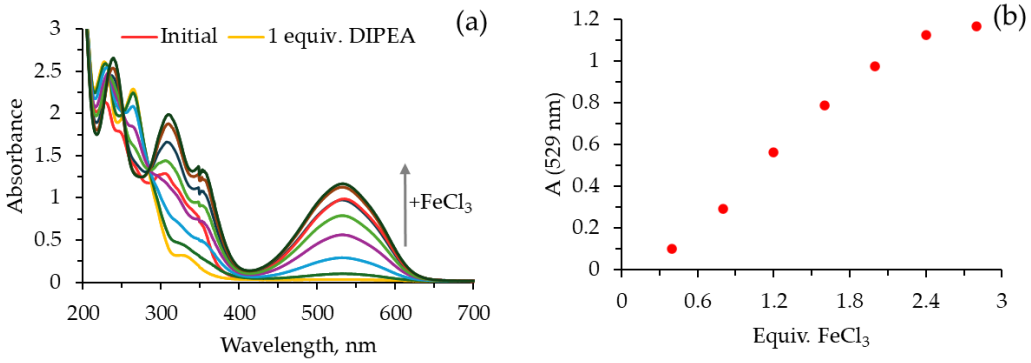

Figure 2.35 — Absorption spectra of compound 4 in acetonitrile and DIPEA (1 Equiv.), as a function of added $FeCl_3$ (a); Absorption at λ_{max} as a function of the number of equivalents of added $FeCl_3$ (b).

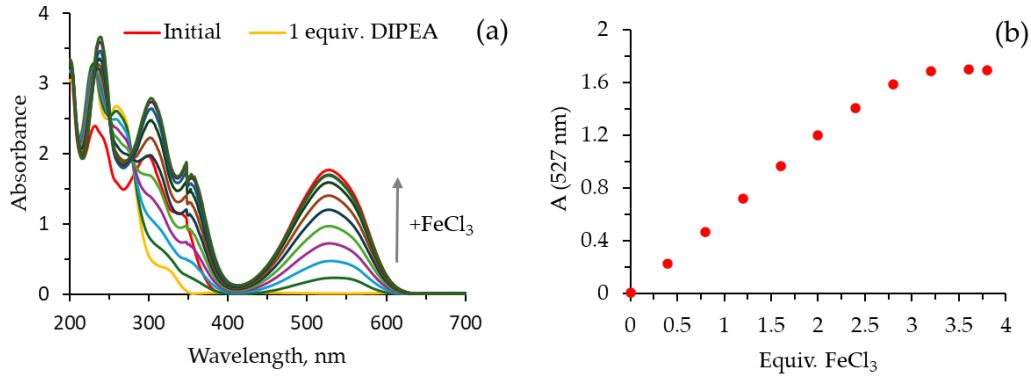

Figure 2.36 — Absorption spectra of compound 5 in acetonitrile and DIPEA (1 Equiv.), as a function of added $FeCl_3$ (a); Absorption at λ_{max} as a function of the number of equivalents of added $FeCl_3$ (b).

B

ANNEX B

Annex B includes supplementary materials of Chapter 3.

B.1 1D, 2D NMR and HRMS of compounds 6-10

Compound 6

Table 3.3 — Assignment of ^{1}H NMR data for compound 6 (CD_3CN plus DCl, 298.0 K) at 500 Hz.

Position	**^{1}H δ /ppm (J/Hz)**
5'	8.26 (1H, d, J = 7.8 Hz)
5	8.05 (1H, d, J = 9.8 Hz)
5″	7.92 (1H, s)
1″, 3″	7.75 (2H, s)
3′	7.62 (1H, t, J = 7.5 Hz)
4′	7.55 (1H, t, J = 7.6 Hz)
2′ , 6	7.45 – 7.36 (2H, m)
8	7.21 (1H, d, J = 2.6 Hz)
7′	3.01 (2H, t, J = 7.5 Hz)
8′	2.90 (2H, t, J = 7.6 Hz)
7-$NCH_2\mathbf{CH_3}$	1.30 (6H, t, J = 7.1 Hz)
7-$N\mathbf{CH_2}$-	3.69 (4H, q, J = 7.1 Hz)

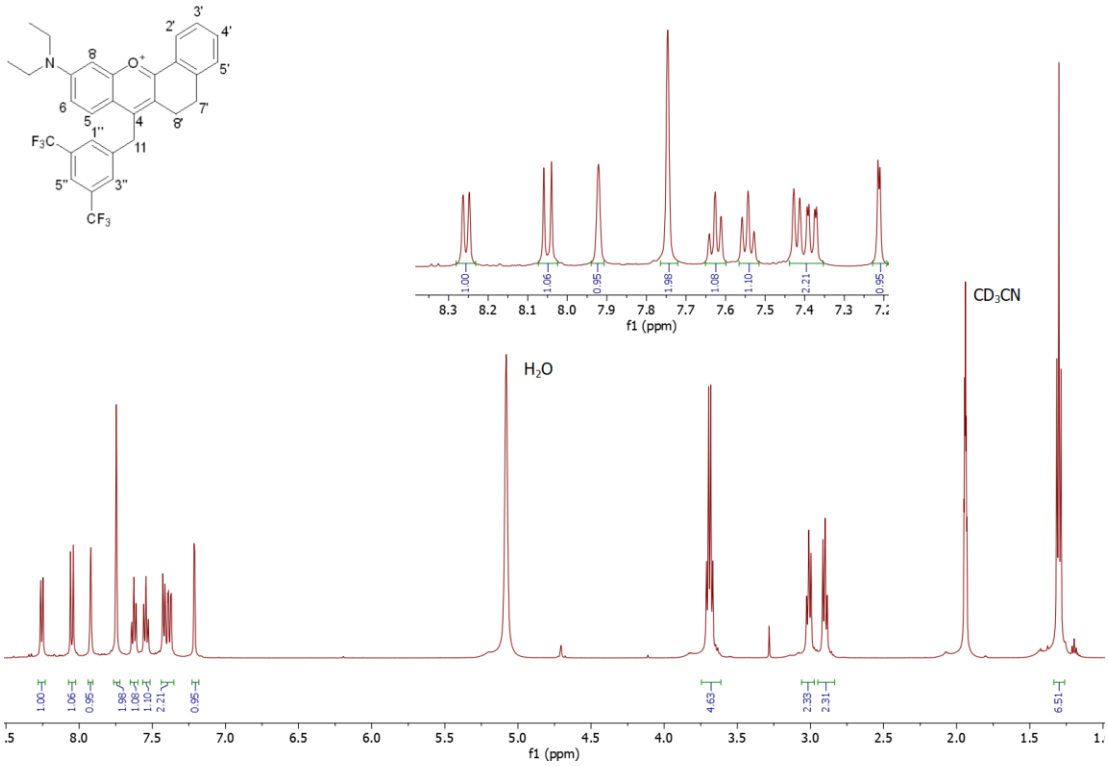

Figure 3.7 — ^{1}H NMR spectrum of compound 6 (CD_3CN plus DCl, 298.0 K) at 500 Hz.

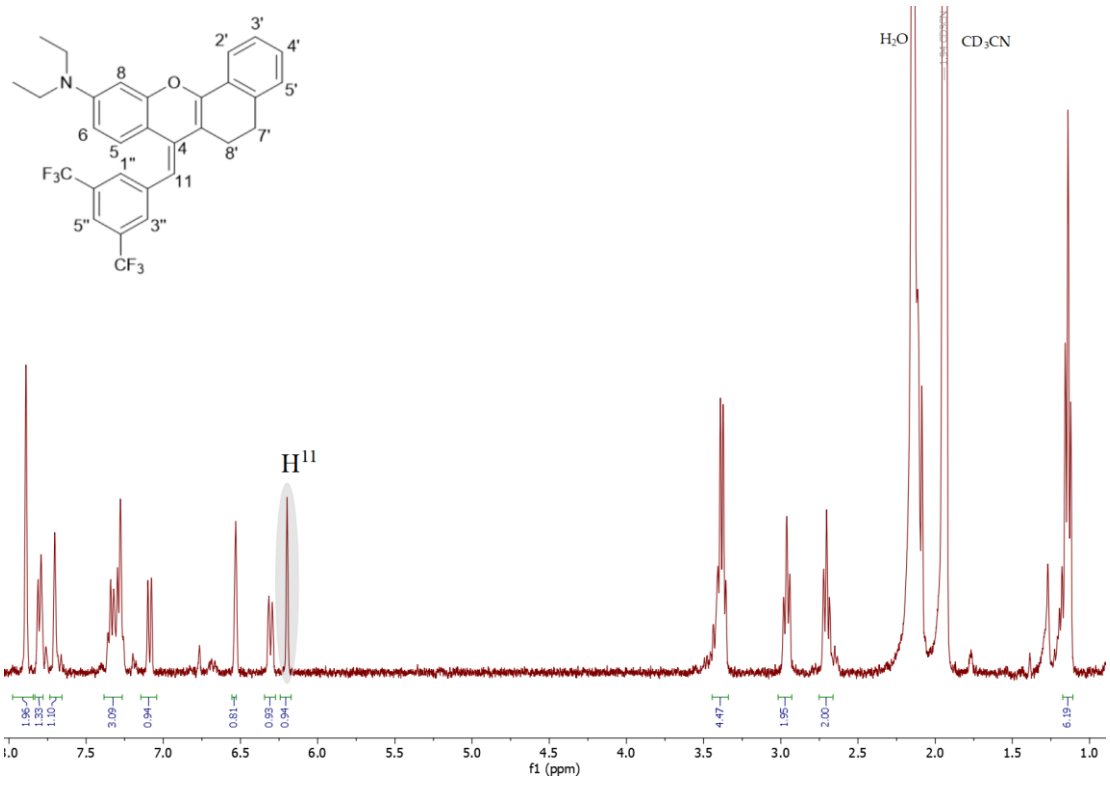

Figure 3.8 — ^{1}H NMR spectrum of compound 6 (CD_3CN, 298.0 K) at 500 Hz. The spectrum was recorded without DCl that the presence of H^{11} proton can be observed.

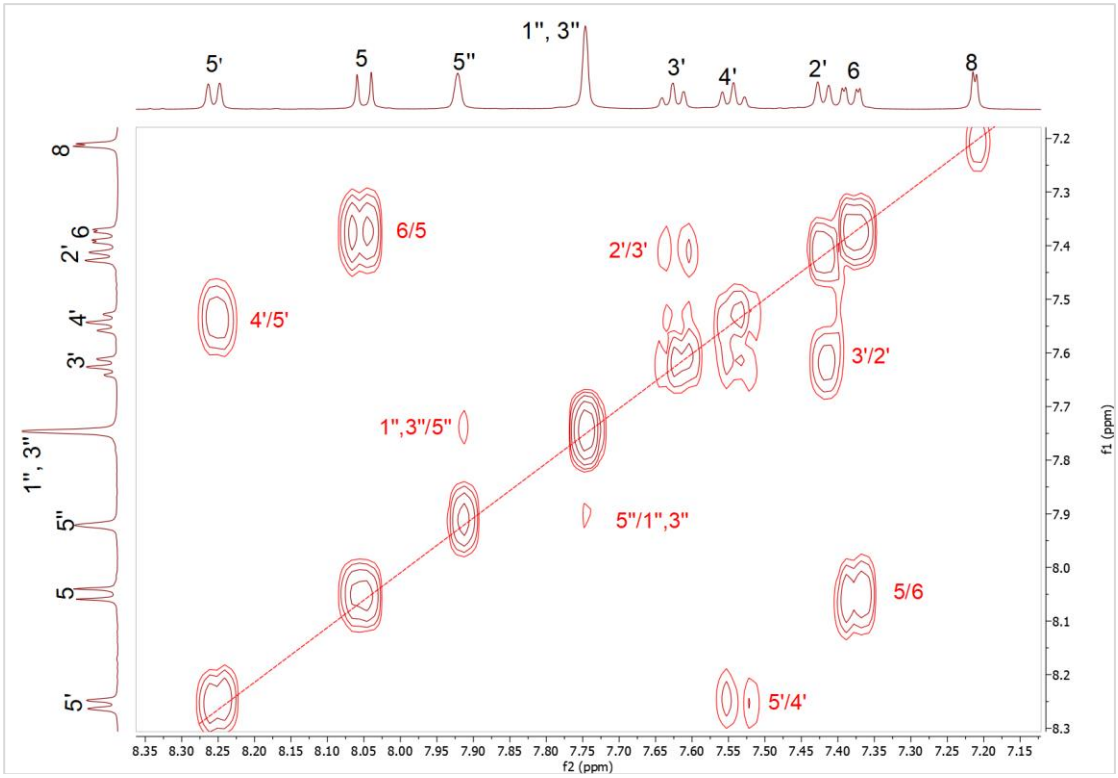

Figure 3.9 — COSY spectrum of compound 6 (CD_3CN plus DCl, 298.0 K) at 500 MHz (lower field region).

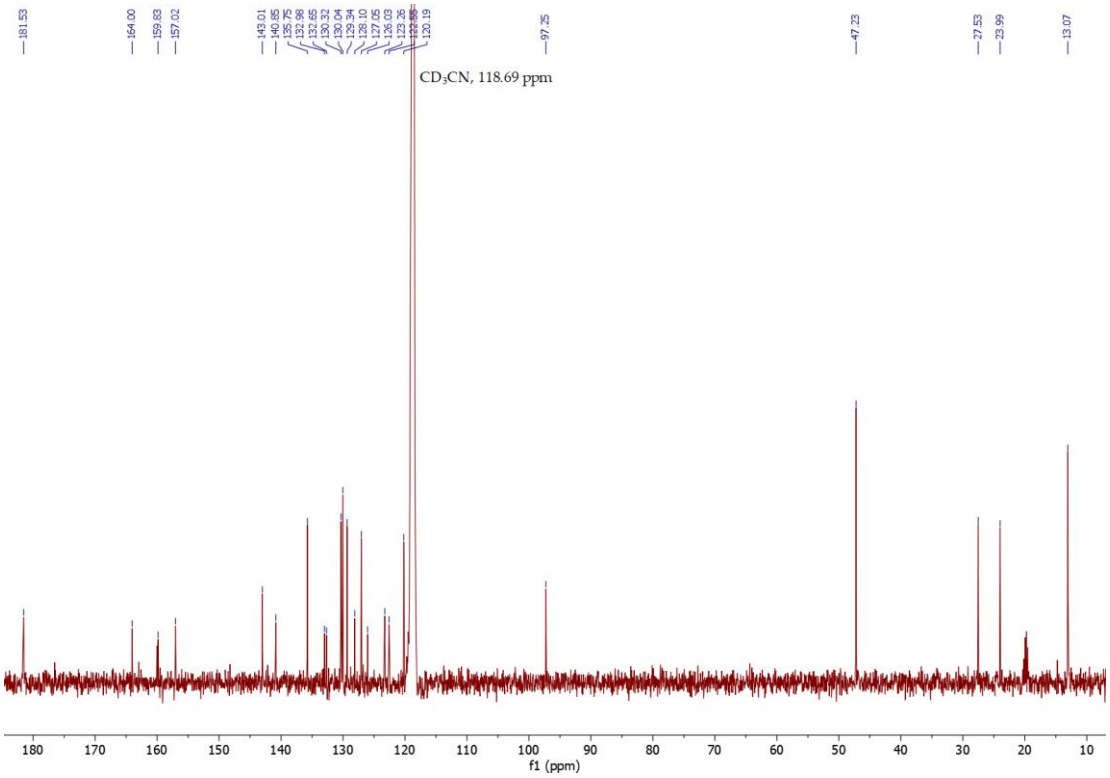

Figure 3.10 — ^{13}C NMR spectrum of compound 6 (CD_3CN plus DCl, 298.0 K) at 101 MHz.

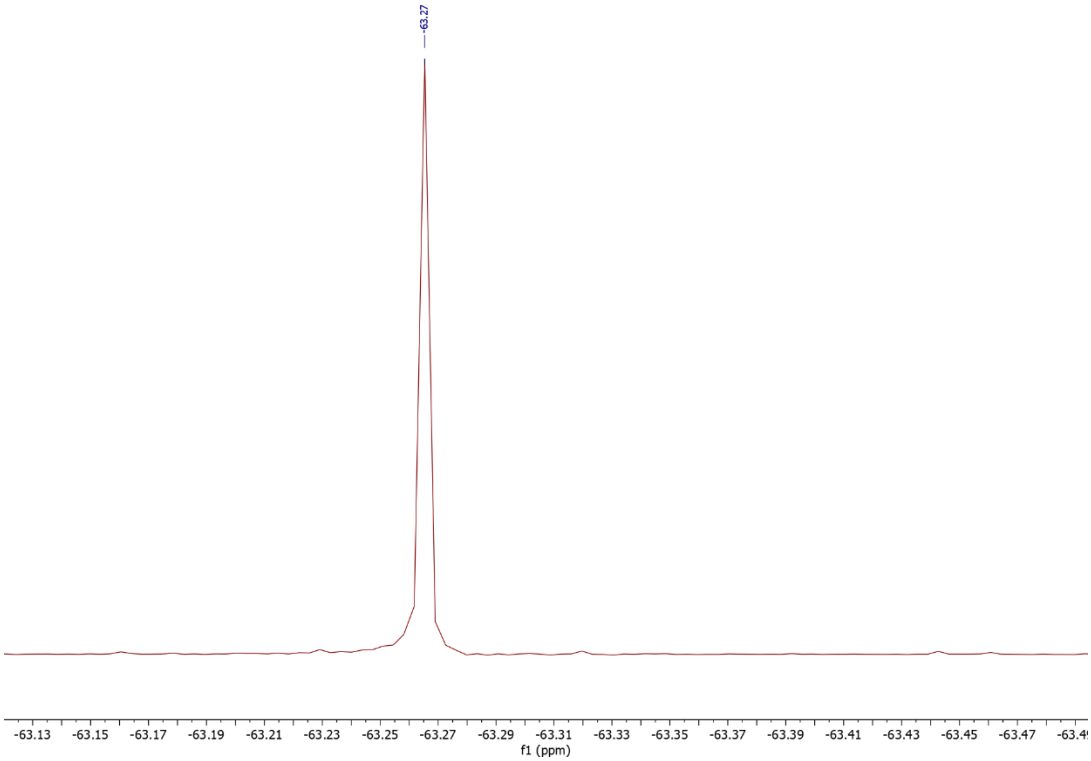

Figure 3.11 — ^{19}F NMR spectrum of compound 6 (CD_3CN plus DCl, 298.0 K) at 376 MHz.

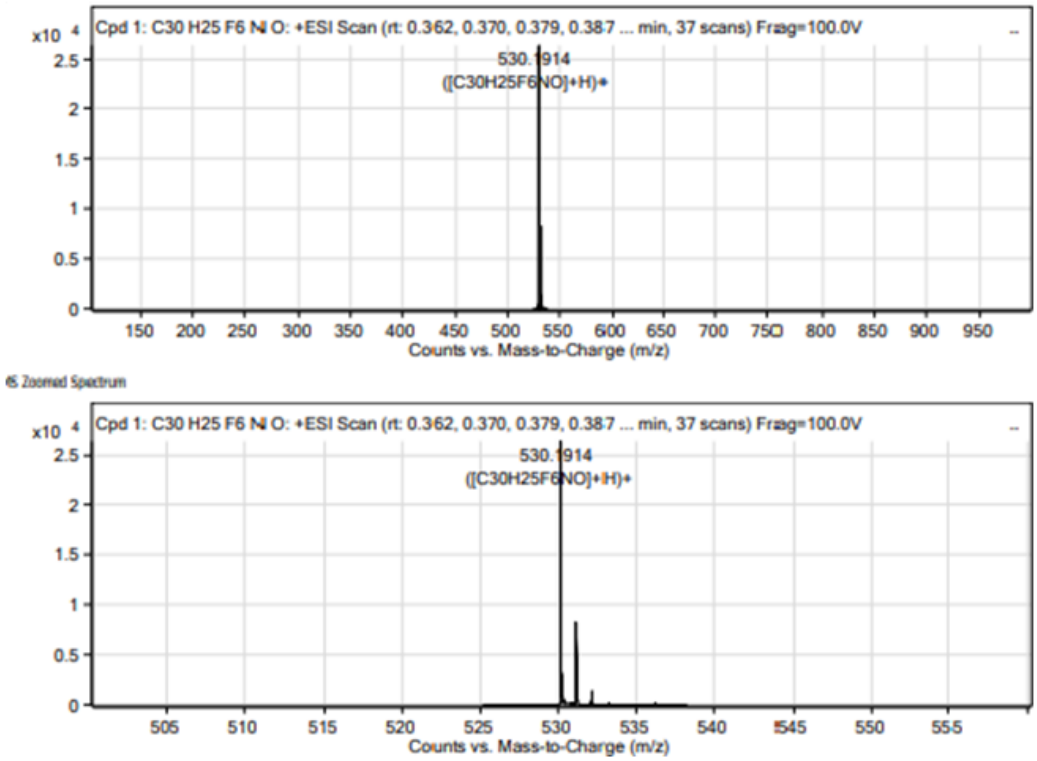

Figure 3.12 — HRMS of compound 6.

Compound 7

Table 3.4 — Assignment of ^{1}H NMR data for compound 7 (CD_3CN plus DCl, 298.0 K) at 500 Hz.

Position	^{1}H δ /ppm (J/Hz)
5'	8.44 (1H, d, *J* = 7.9 Hz)
5	8.28 (1H, d, *J* = 9.4 Hz)
8	7.92 (1H, s)
3''	7.82 (1H, d, *J* = 2.5 Hz)
3'	7.78 (1H, t, *J* = 7.5 Hz)
1″, 5″	7.74 (2H, s)
4′	7.64 (1H, t, *J* = 7.7 Hz)
2' , 6	7.56 – 7.46 (2H, m)
7′, 8′	3.13 (4H, s)
7-OCH_3	4.12 (3H, s)

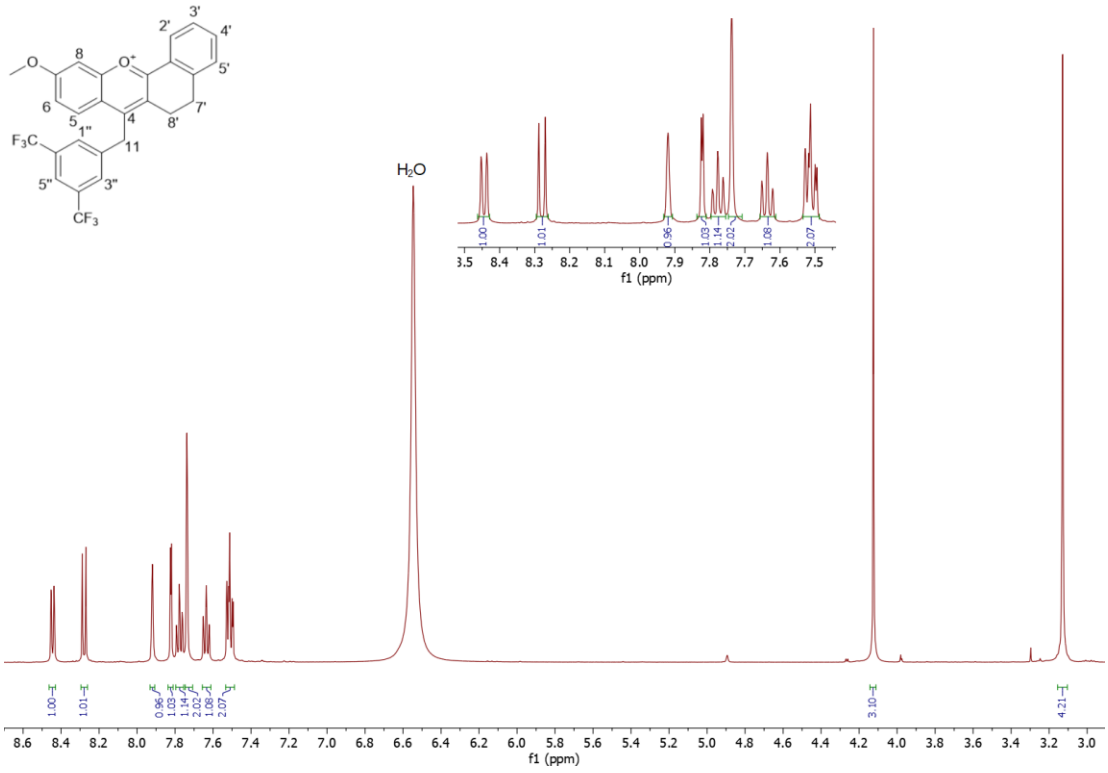

Figure 3.13 — ^{1}H NMR spectrum of compound 7 (CD_3CN plus DCl, 298.0 K) at 500 Hz.

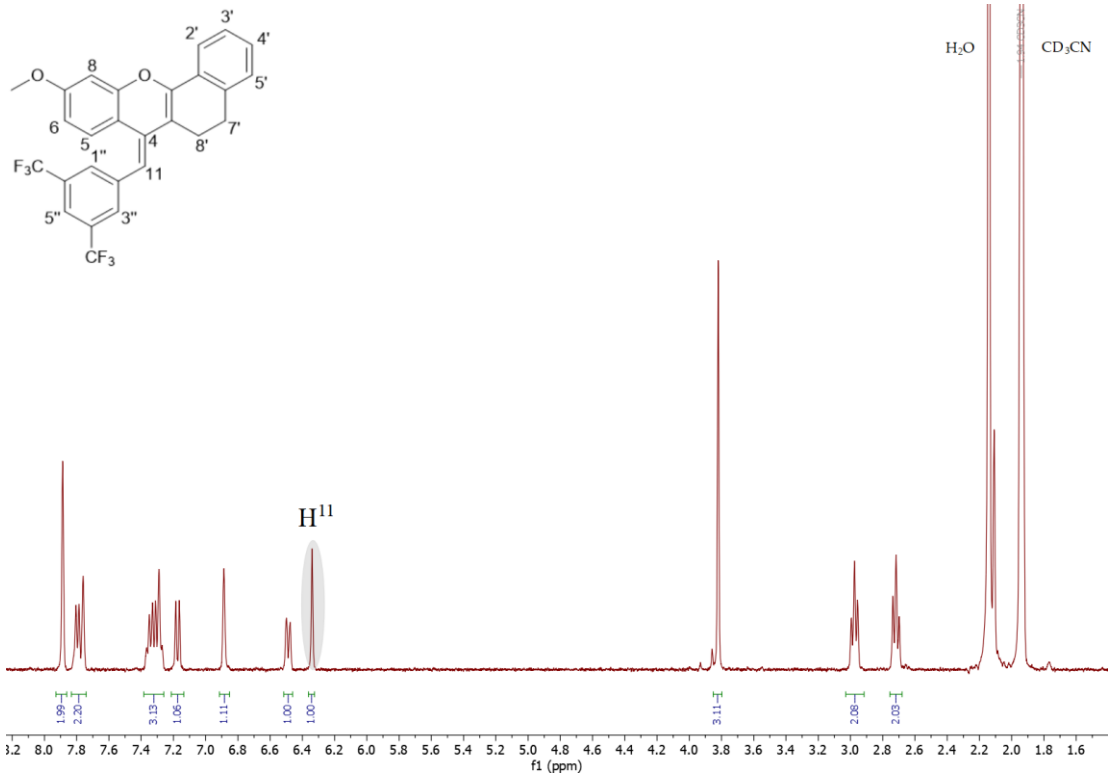

Figure 3.14 — ^{1}H NMR spectrum of compound 7 (CD_3CN, 298.0 K) at 500 Hz. The spectrum was recorded without DCl that the presence of H^{11} proton can be observed.

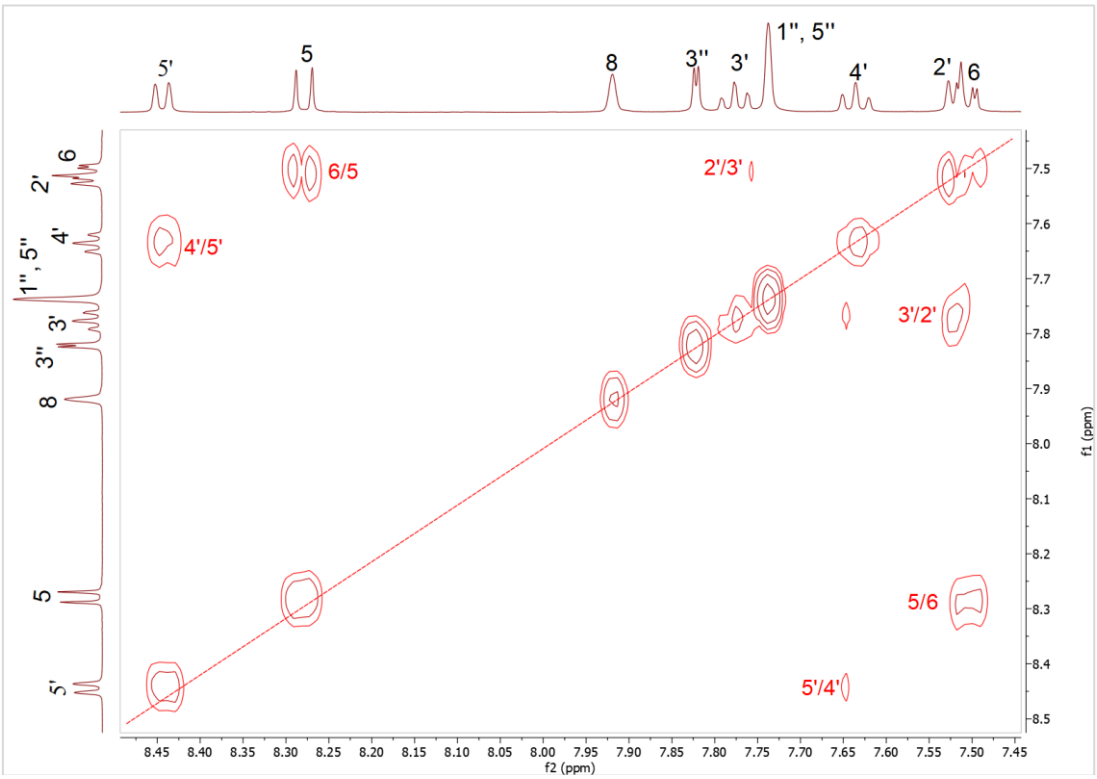

Figure 3.15 — COSY spectrum of compound 7 (CD_3CN plus DCl, 298.0 K) at 500 MHz (lower field region).

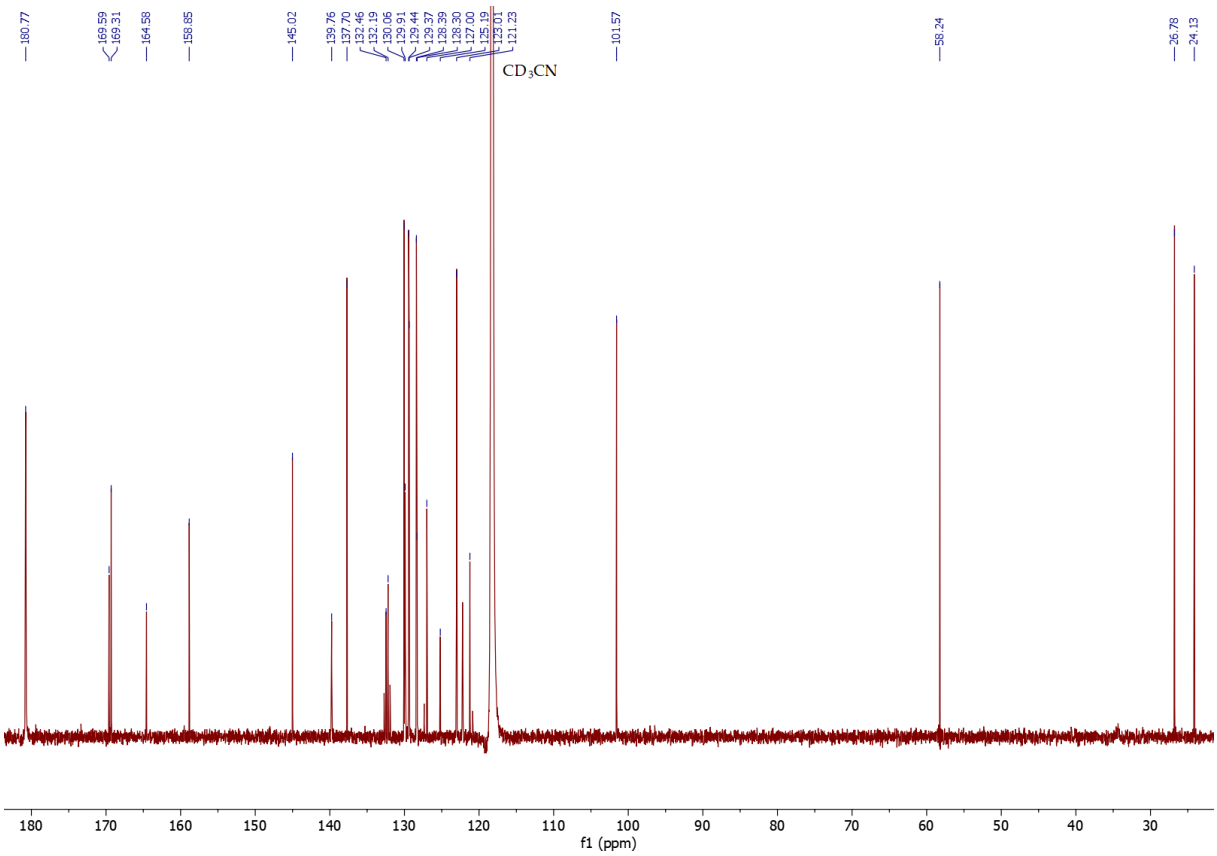

Figure 3.16 — ^{13}C NMR spectrum of compound 7 (CD_3CN plus DCl, 298.0 K) at 126 MHz.

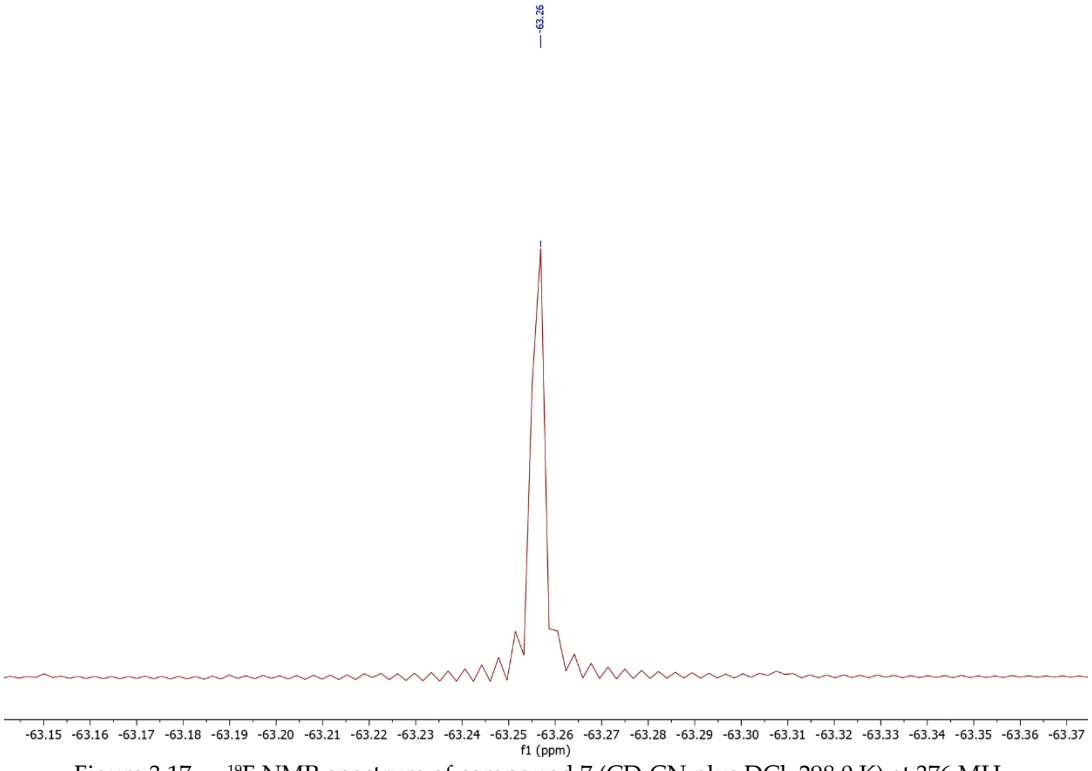

Figure 3.17 — ^{19}F NMR spectrum of compound 7 (CD_3CN plus DCl, 298.0 K) at 376 MHz.

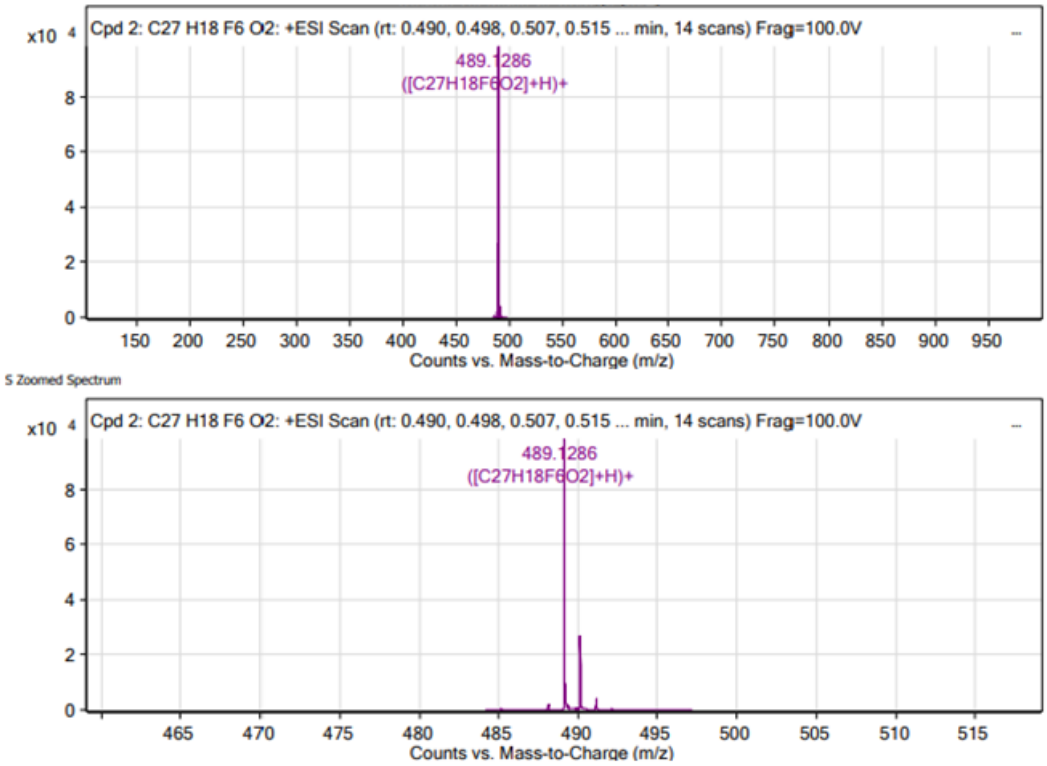

Figure 3.18 — HRMS of compound 7.

Compound 8

Table 3.5 — Assignment of ^{1}H NMR data for compound 8 (CD_3CN plus DCl, 298.0 K) at 500 MHz.

Position	**^{1}H δ /ppm (J/Hz)**
2'	8.56 (1H, d, J = 8.0 Hz)
5, 8	8.35 (2H, d, J = 8.75 Hz)
7	8.27 (1H, t, J = 7.65Hz)
6 , 3''	7.96 – 7.91 (2H, m)
4'	7.86 (1H, t, J = 7.5 Hz)
1″, 5″	7.76 (2H, s)
3′	7.68 (1H, t, J = 7.7 Hz)
5′	7.58 (1H, d, J = 7.7 Hz)
8′	3.29 – 3.24 (2H, m)
7′	3.20 (2H, m)

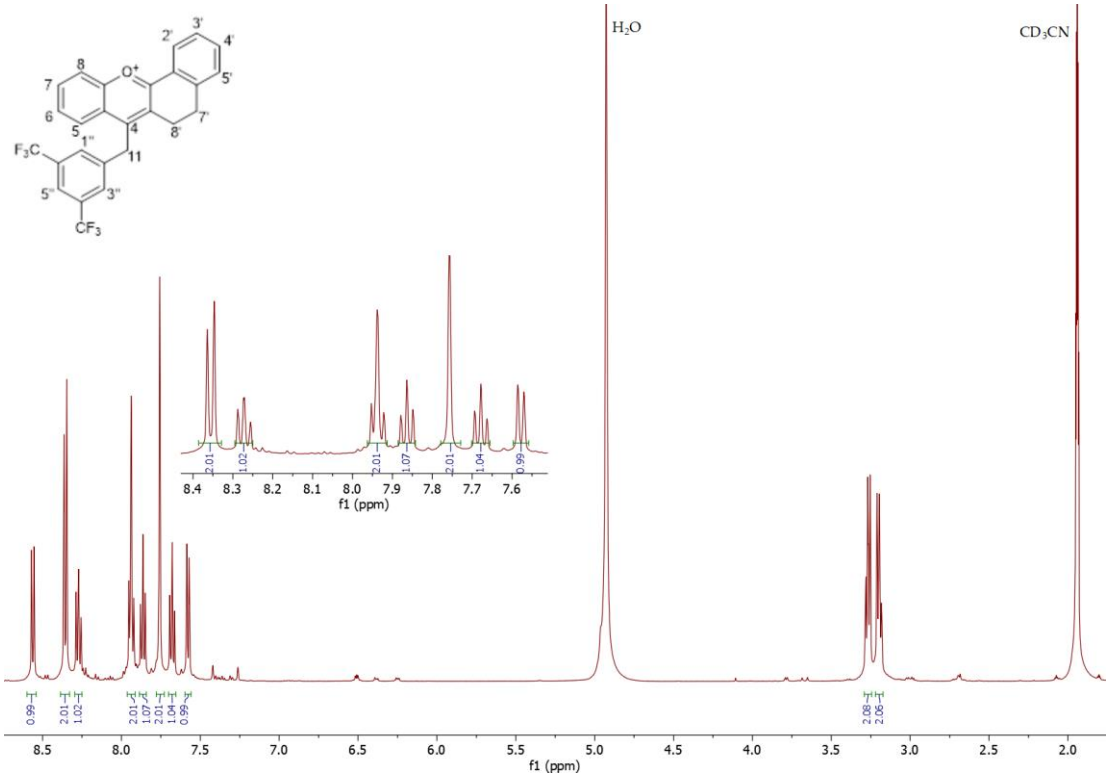

Figure 3.19 — ^{1}H NMR spectrum of compound 8 (CD_3CN plus DCl, 298.0 K) at 500 MHz.

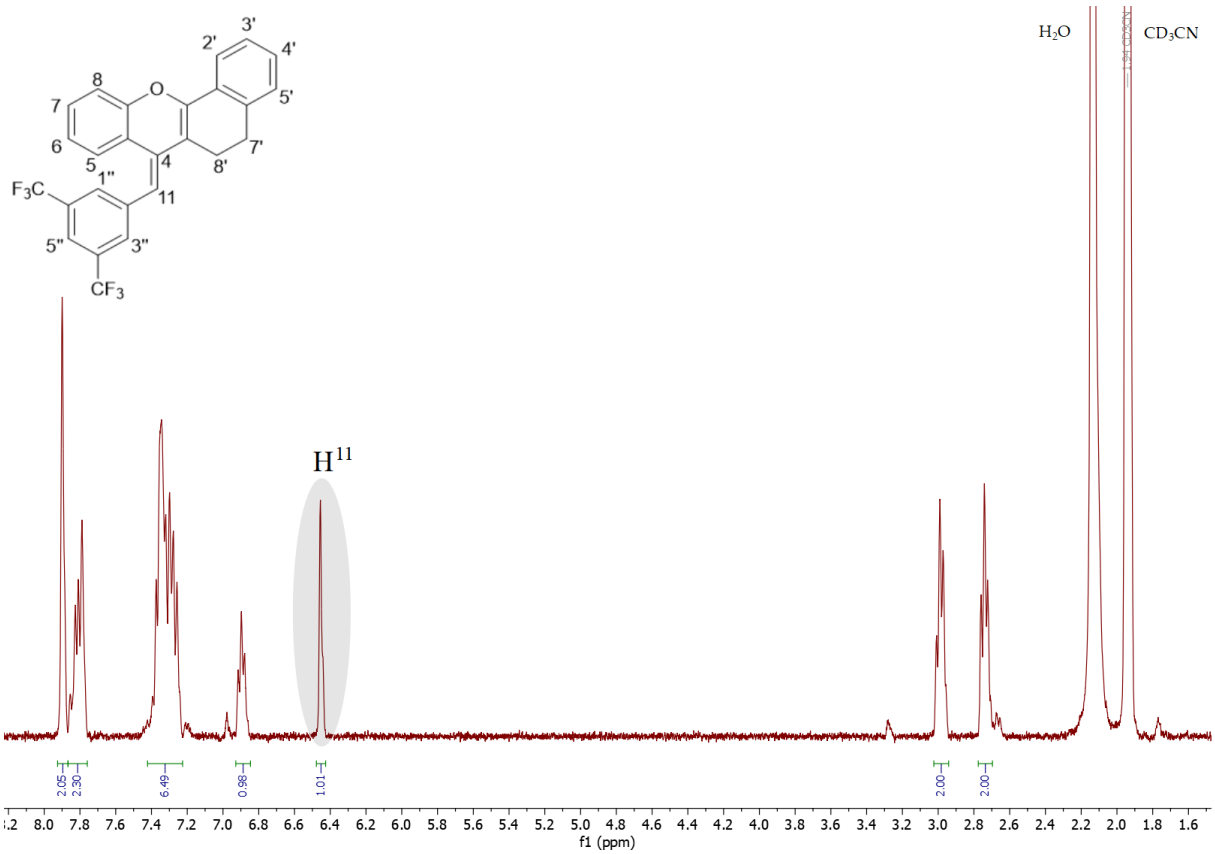

Figure 3.20 — ^{1}H NMR spectrum of compound 8 (CD_3CN, 298.0 K) at 500 MHz. The spectrum was recorded without DCl that the presence of H^{11} proton can be observed.

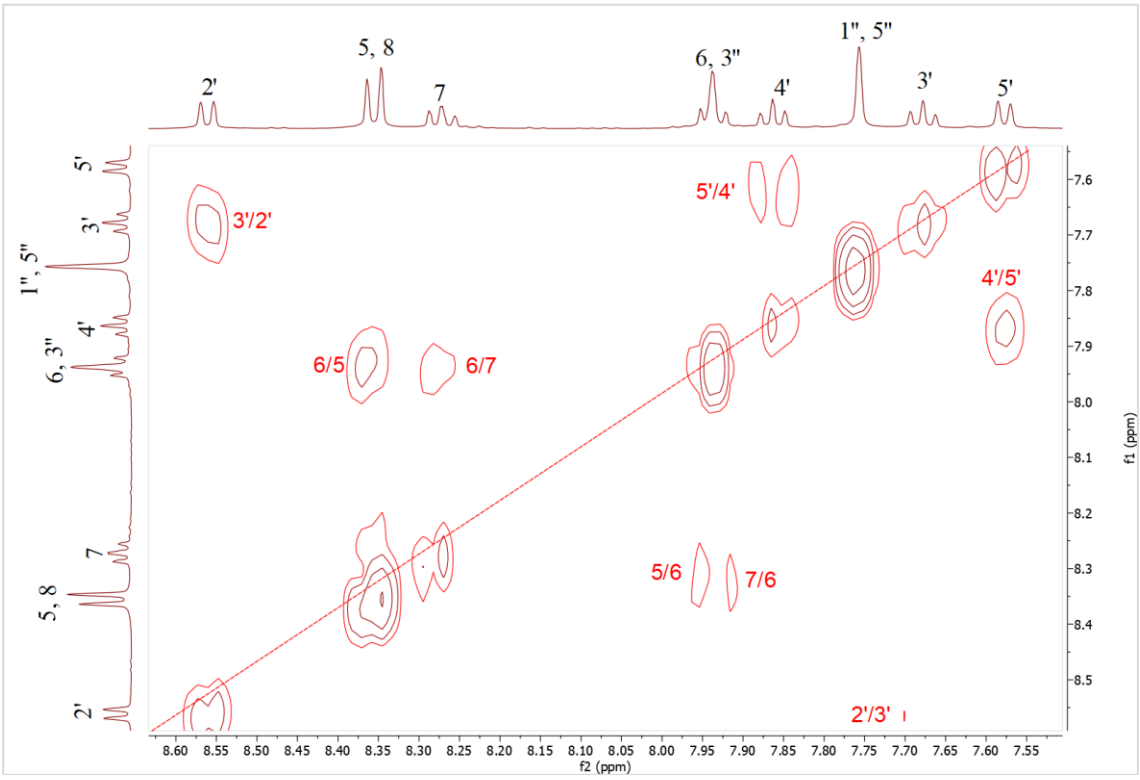

Figure 3.21 — COSY spectrum of compound 8 (CD_3CN plus DCl, 298.0 K) at 500 MHz (lower field region).

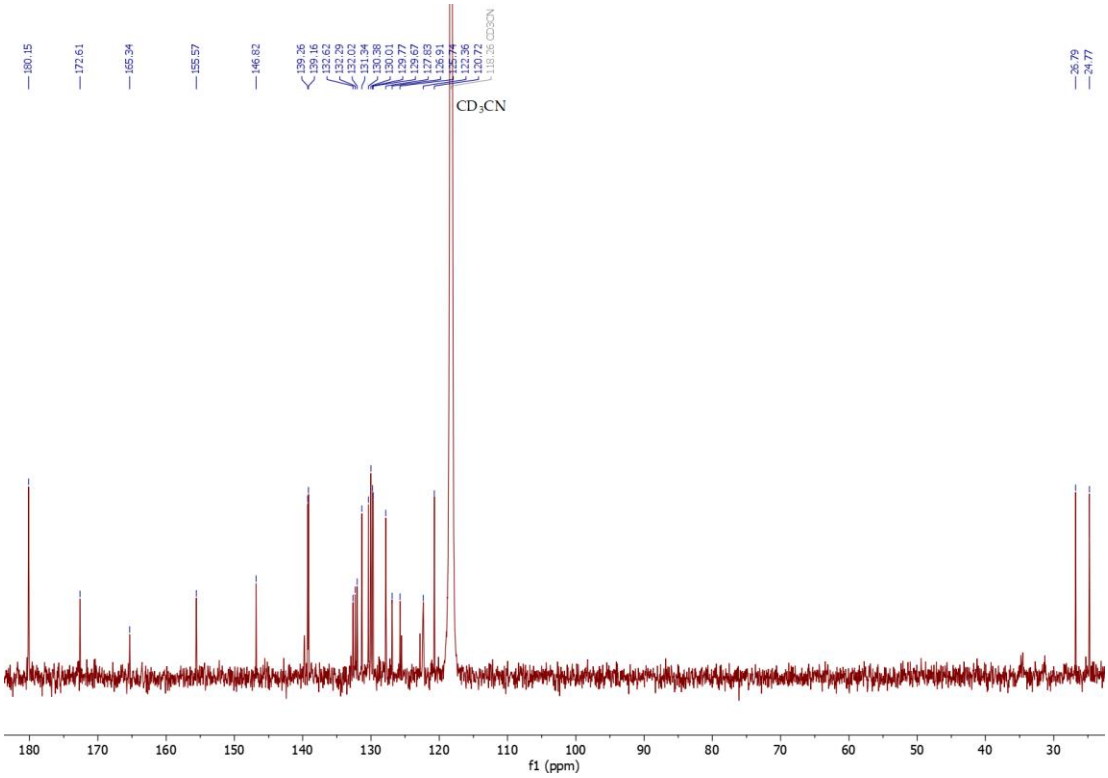

Figure 3.22 — ^{13}C NMR spectrum of compound 8 (CD_3CN plus DCl, 298.0 K) at 101 MHz.

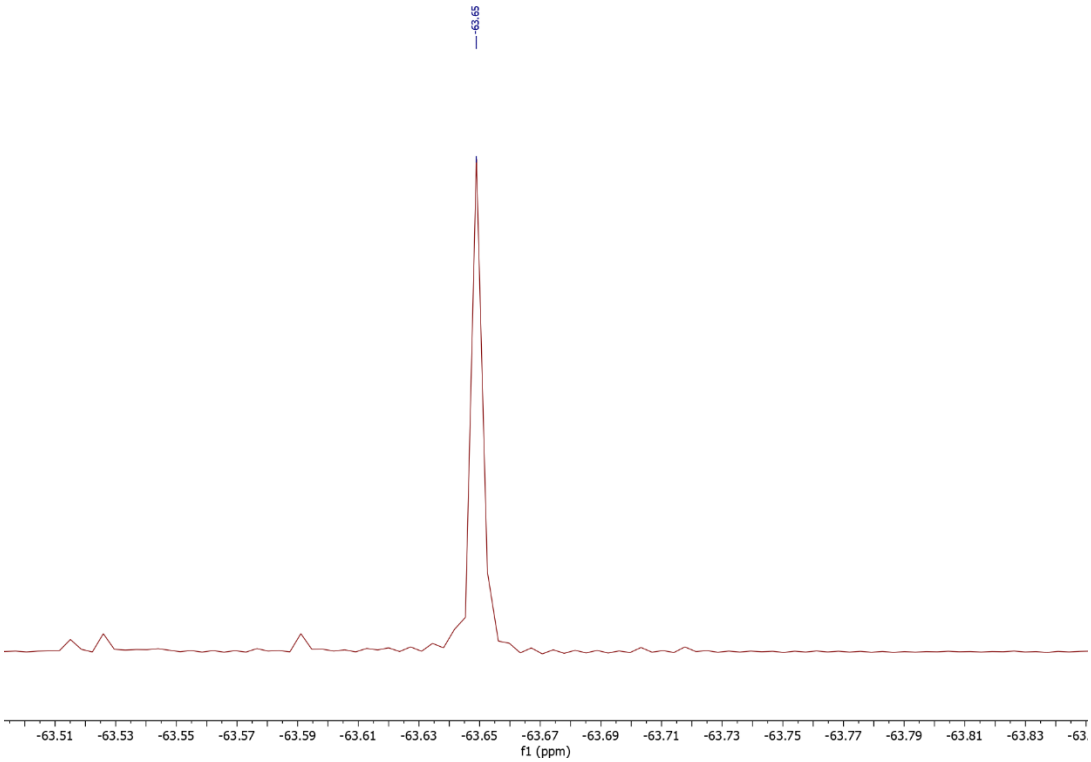

Figure 3.23 — ^{19}F NMR spectrum of compound 8 (CD_3CN plus DCl, 298.0 K) at 376 MHz.

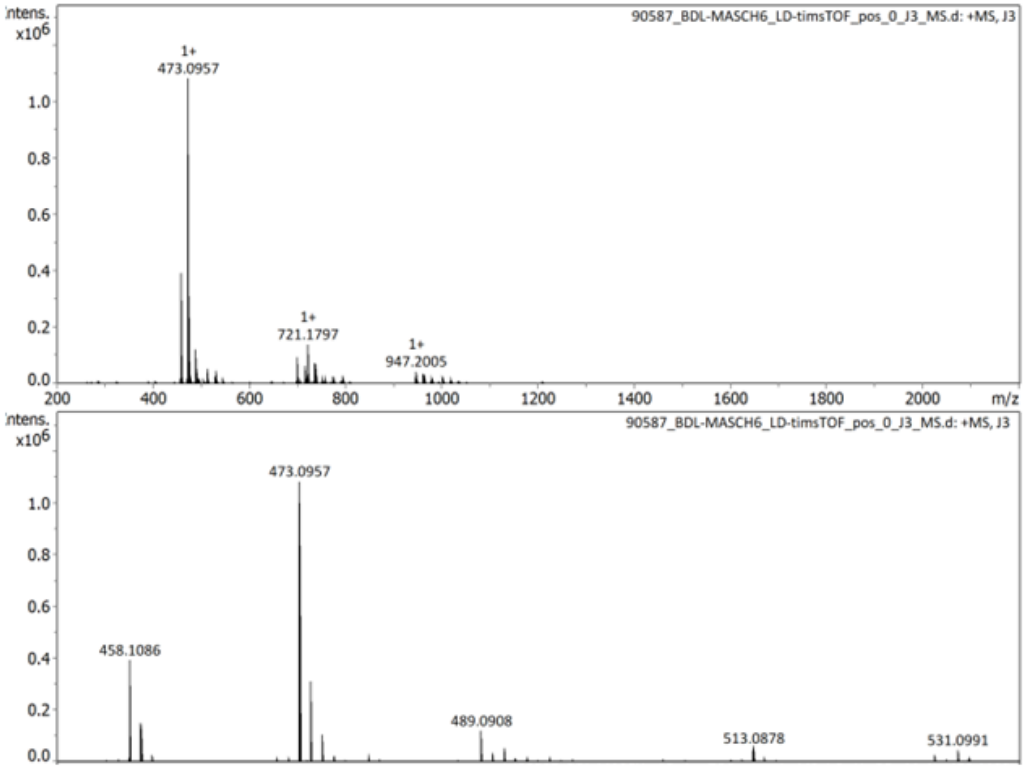

Figure 3.24 — HRMS of compound 8.

Compound 9

Table 2.10 — Assignment of ^{1}H NMR data for compound 9 (CD_3CN plus DCl, 298.0 K) at 500 Hz.

Position	**^{1}H δ /ppm (J/Hz)**
8″	8.26 (1H, d, J = 7.8 Hz)
4″	8.13 (1H, d, *J* = 9.7 Hz)
6″, 5″	7.86 (2H, m)
2'	7.74 – 7.68 (1H, m)
4'	7.61 (1H, t, *J* = 7.5 Hz)
7″, 1″	7.57 – 7.50 (2H, m)
5, 6, 8, 3', 5', 3″	7.49 – 7.33 (6H, m)
8', 7'	3.00 (4H, s)
7-$NCH_2\mathbf{CH_3}$	1.29 (6H, t, J = 7.1 Hz)
7-$N\mathbf{CH_2}$-	3.67 (4H, q, J = 7.2 Hz)

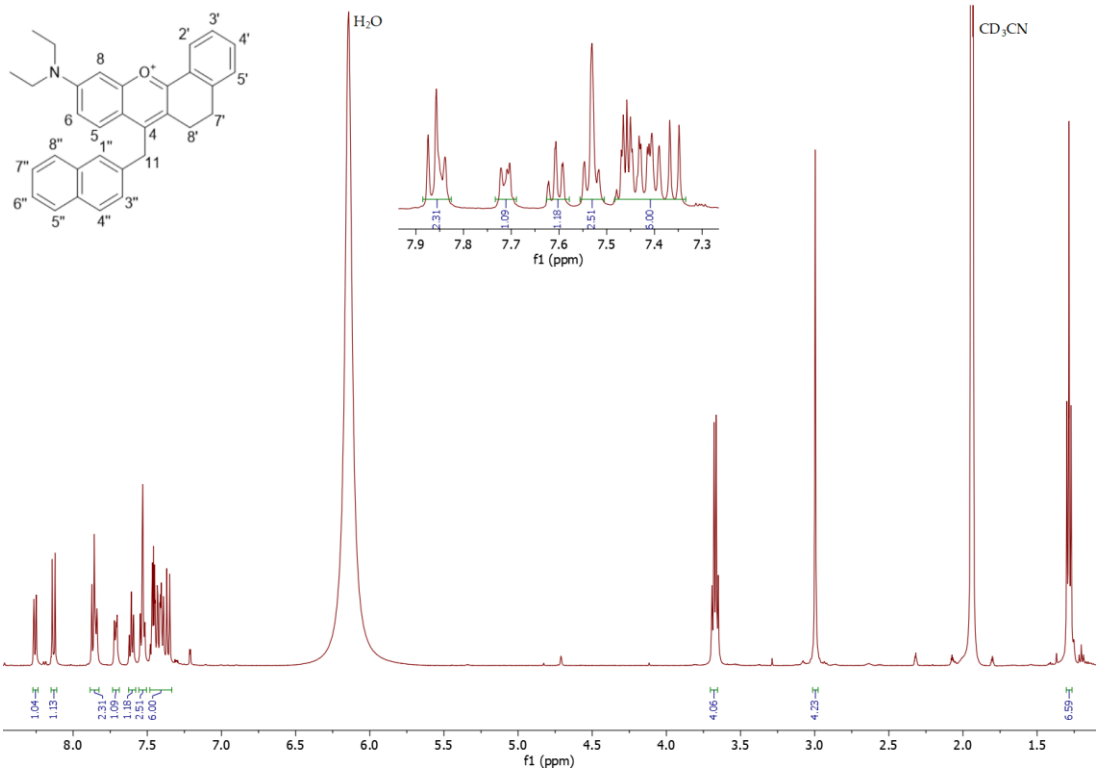

Figure 3.25 — ^{1}H NMR spectrum of compound 9 (CD_3CN plus DCl, 298.0 K) at 500 MHz.

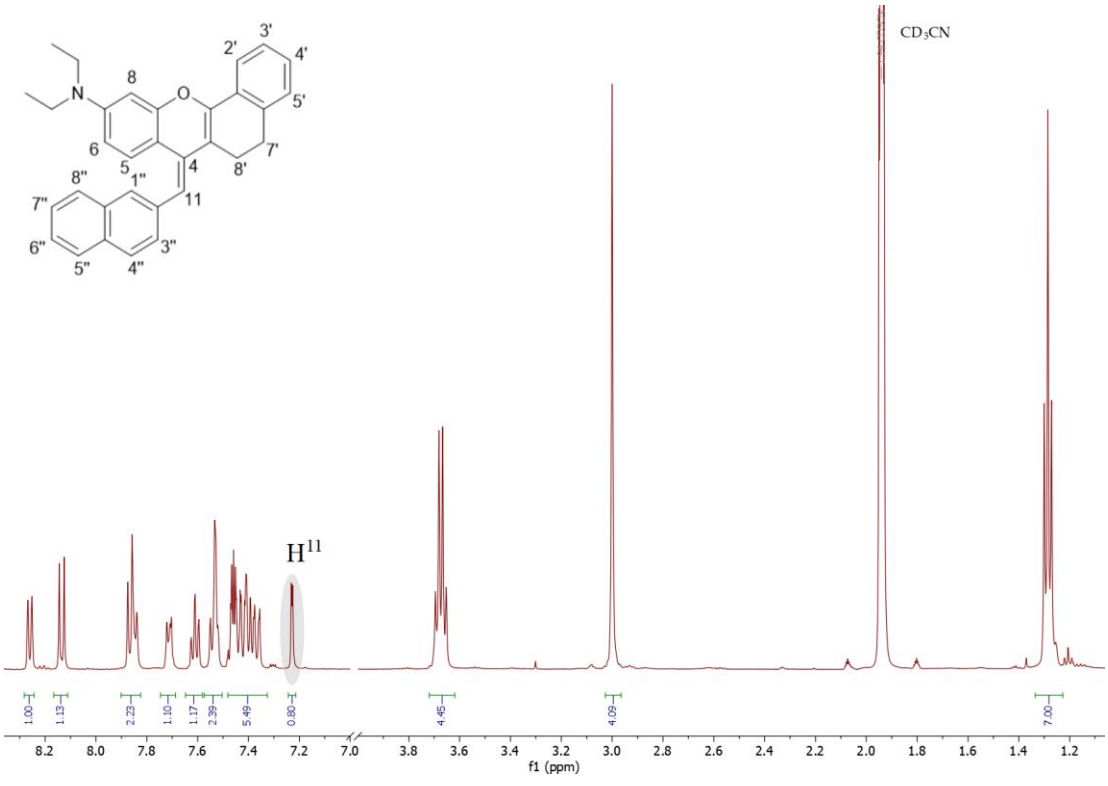

Figure 3.26 — ^{1}H NMR spectrum of compound 9 (CD_3CN, 298.0 K) at 500 MHz. The spectrum was recorded without DCl that the presence of H^{11} proton can be observed.

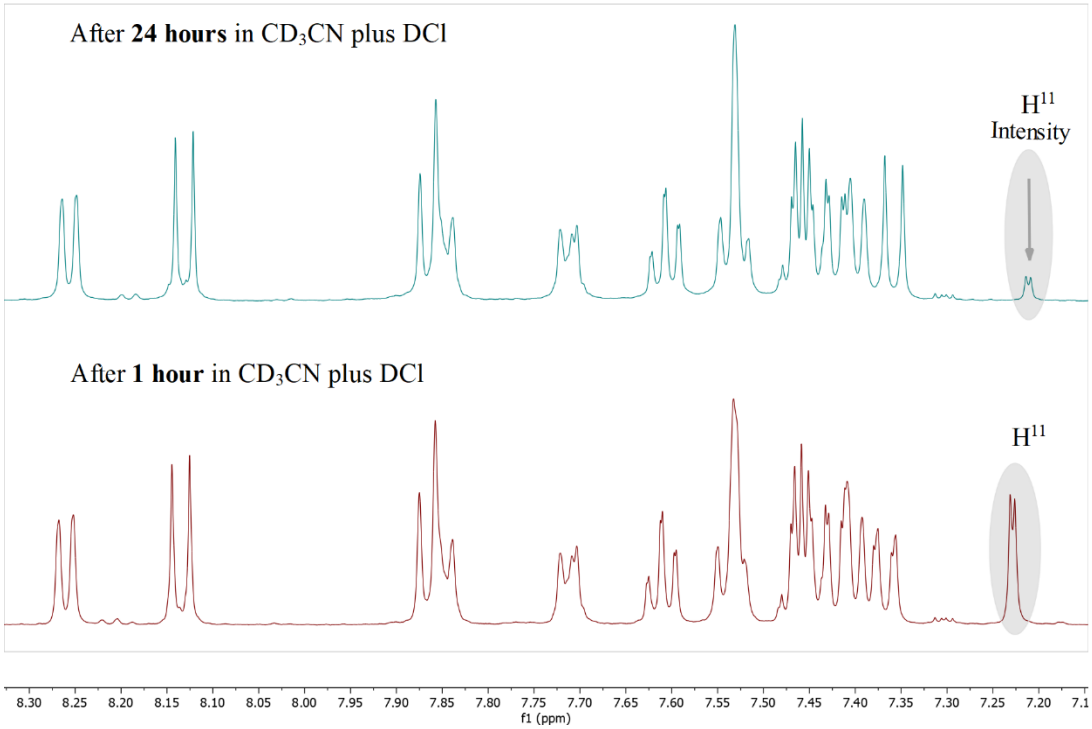

Figure 3.27 — ^{1}H NMR spectrum of compound 9 (CD_3CN plus DCl, 298.0 K) recorded overtime at 500 MHz (lower field region) to observe the replacement of H^{11} proton by DCl of deuterium.

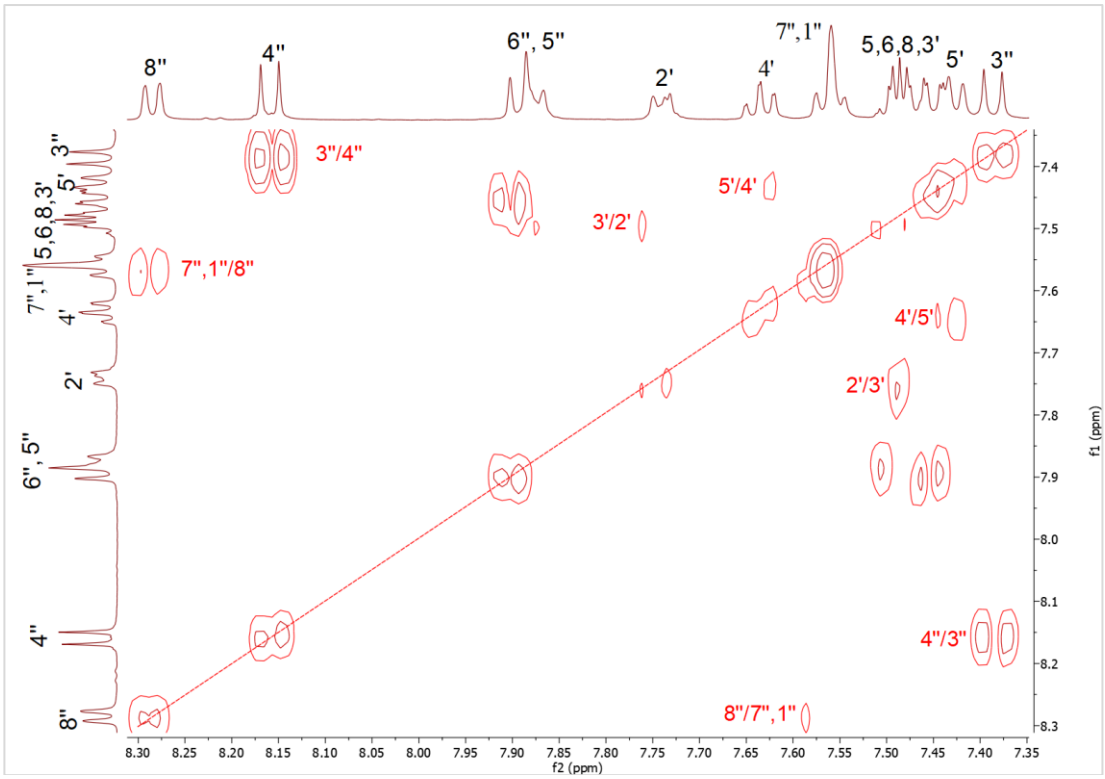

Figure 3.28 — COSY spectrum of compound 9 (CD_3CN plus DCl, 298.0 K) at 500 MHz (lower field region).

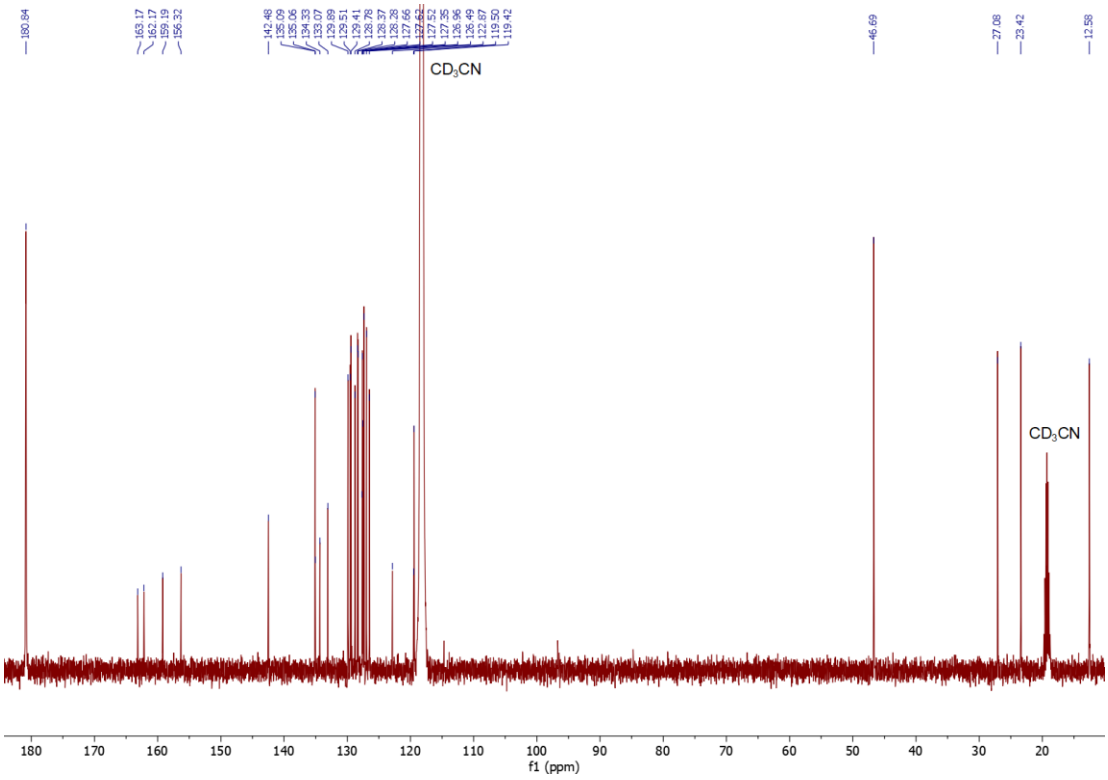

Figure 3.29 — ^{13}C NMR spectrum of compound 9 (c plus DCl, 298.0 K) at 126 MHz.

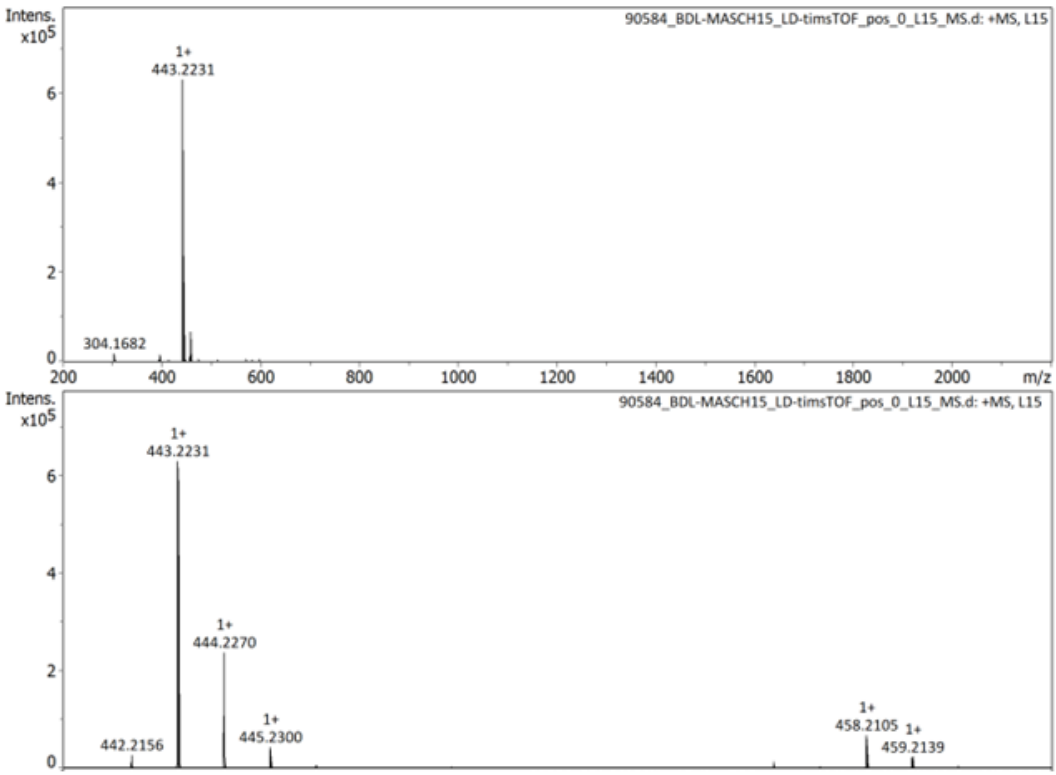

Figure 3.30 — HRMS of compound 9.

Compound 10

Table 3.6 — Assignment of ^{1}H NMR data for compound 10 (CD_3CN plus DCl, 298.0 K) at 500 MHz.

Position	^{1}H δ /ppm (J/Hz)
8''	8.52 (1H, d, J = 8.0 Hz)
1''	8.36 (1H, s)
8, 6	8.16 (2H, s)
3''	8.04 (1H, d, J = 8.3 Hz)
2', 5	7.91 (2H, d, J = 9.4 Hz)
4'	7.83 (1H, t, J = 7.6 Hz)
4″, 6″	7.76 (2H, d, J = 8.6 Hz)
7″	7.69 (1H, t, J = 7.8 Hz)
3'	7.62 (1H, t, J = 7.6 Hz)
5'	7.53 (1H, d, J = 7.9 Hz)
5″	7.42 (1H, d, J = 9.4 Hz)
8', 7'	3.17 – 3.09 (4H, m).
7-OCH_3	4.15 (3H, s)

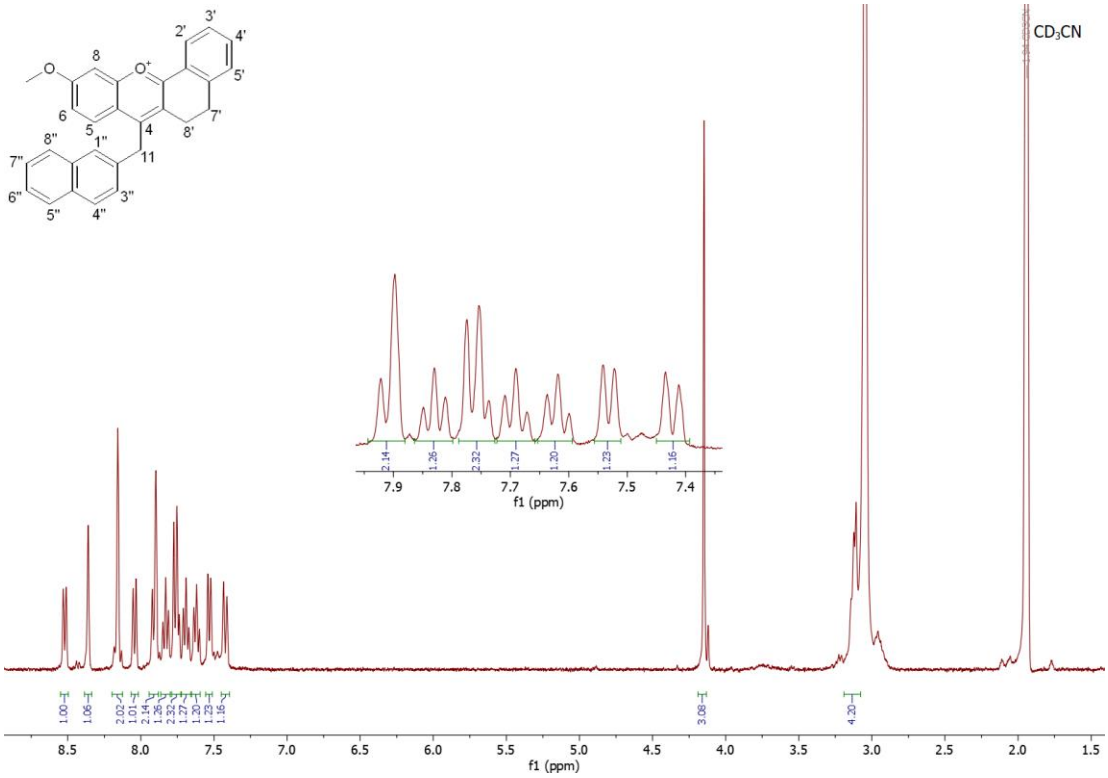

Figure 3.31 — ^{1}H NMR spectrum of compound 10 (CD_3CN plus DCl, 298.0 K) at 500 MHz.

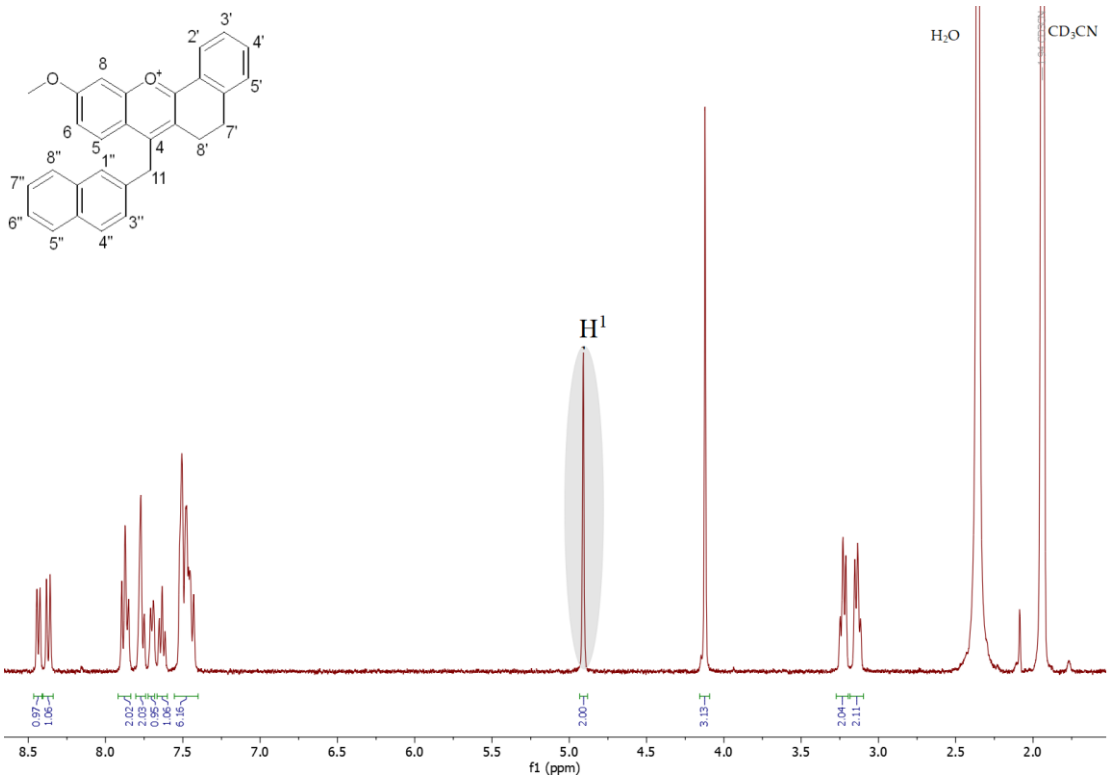

Figure 3.32 — ^{1}H NMR spectrum of compound 10 (CD_3CN, 298.0 K) at 500 MHz. The spectrum was recorded without DCl that the presence of H^{11} protons can be observed.

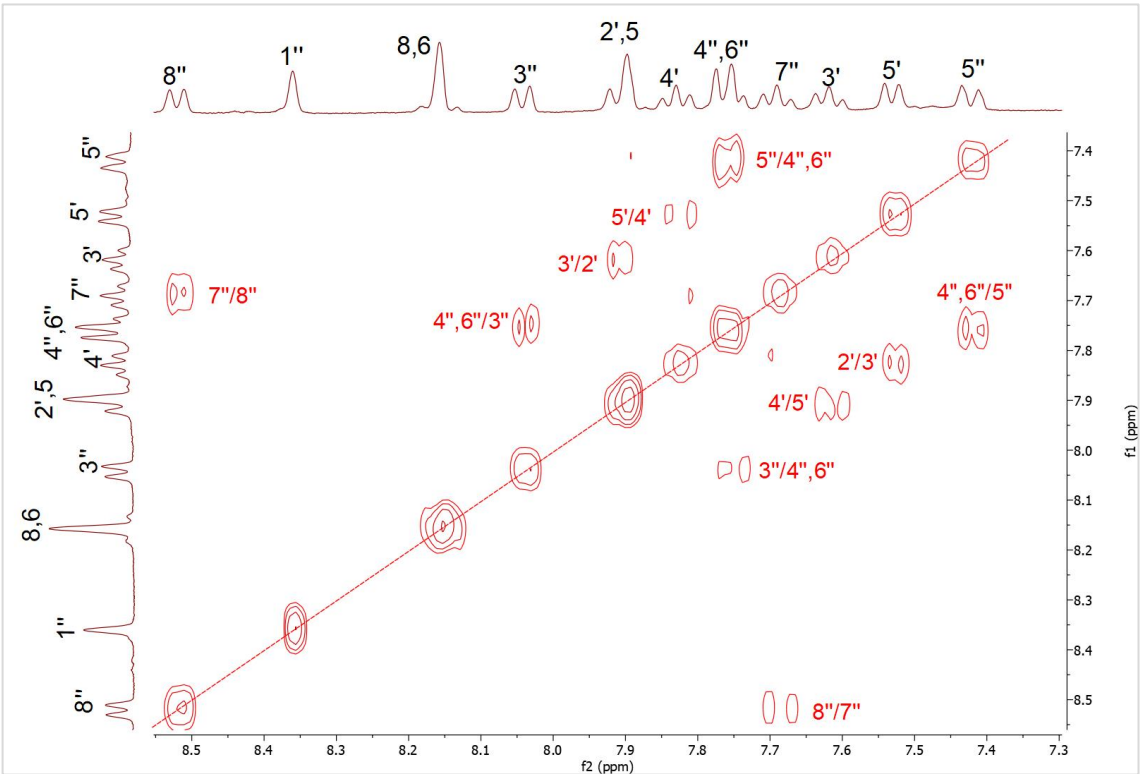

Figure 3.33 — COSY spectrum of compound 10 (CD_3CN plus DCl, 298.0 K) at 500 MHz (lower field region).

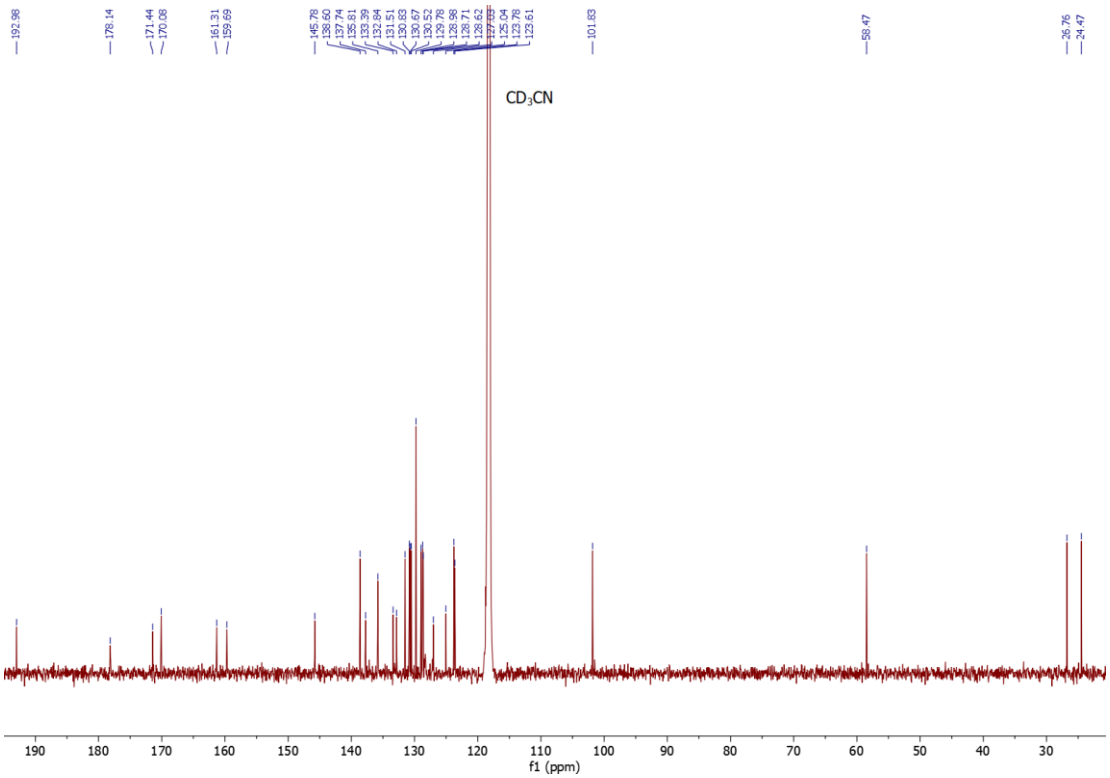

Figure 3.34 — ^{13}C NMR spectrum of compound 10 (CD_3CN plus DCl, 298.0 K) at 126 MHz. The missing carbon signal may be obscured or located beneath the solvent's signal.

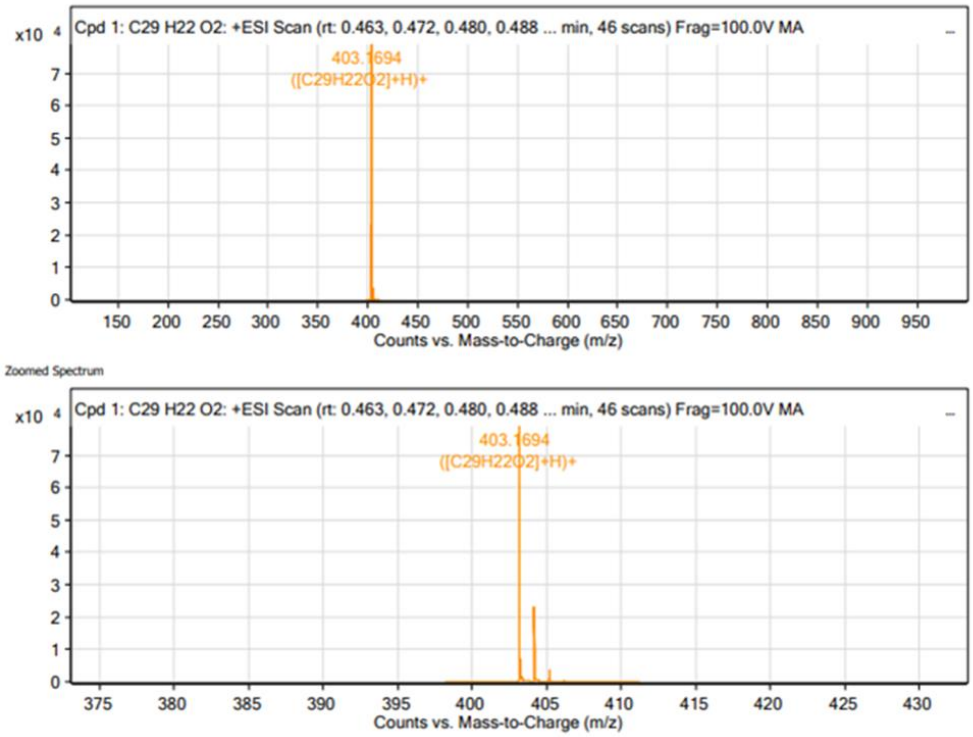

Figure 3.35 — HRMS of compound 10.

2024

MARIA ANGELA SPIRACHE

BENZOPYRYLIUM (FLAVYLIUM) BASED DYES FOR REVERSIBLE THERMOCHROMIC SMART LABELS